Multi-Shell Hybrid Nanoparticles From Controlled Polymerizations

Dissertation

zur Erlangung des akademischen Grades eines
Doktors der Naturwissenschaften (Dr. rer. nat.)

vorgelegt von

Steffen Huber

aus Friedrichshafen

an der

Universität Konstanz

Mathematisch-Naturwissenschaftliche Sektion
Fachbereich Chemie

Konstanz, 2021

Tag der mündlichen Prüfung: 22.03.2021
1. Referent: Prof. Dr. Stefan Mecking
2. Referent: Prof. Dr. Alfred Leitenstorfer

Die vorliegende Dissertation entstand in der Zeit von Juli 2016 bis Februar 2020 unter der Leitung von Prof. Dr. Stefan Mecking am Fachbereich Chemie der Universität Konstanz.

Danksagung – Acknowledgement

An erster Stelle möchte ich mich bei Prof. Dr. Stefan Mecking für die Vergabe des spannenden Themas, die freundliche Aufnahme in seine Arbeitsgruppe, die gewährten Freiheiten bei der Bearbeitung des Themas und für die hilfreichen Ideen und Diskussion bedanken.

Für die gute Zusammenarbeit, die Betreuung im Rahmen des Kooperationsprojektes, die Ratschläge zu physikalischen Fragestellungen und für die Übernahme des Zweitgutachtens möchte ich mich ganz herzlich bei Prof. Dr. Alfred Leitenstorfer bedanken.

Einen besonderen Dank möchte ich an meine Kooperationspartner Pascal Gumbsheimer und Frieder Conradt richten, die die Einzelpartikel Messungen durchgeführt haben, mir viele physikalische Fragen beantwortet haben und mit denen ich zahlreiche hilfreiche Diskussionen geführt habe. Des Weitern möchte ich Dr. Florian Werschler und allen anderen aus der AG Leitenstorfer danken, die einen Beitrag zu dieser Arbeit geleistet haben.

Ein großes Dankeschön geht an Dr. Klaus Boldt für die vielen Ratschläge, Tipps und Ideen und für die Hilfe bei der Nanopartikel Synthese, für das Erklären von theoretischen Hintergründen und für die Hilfe bei der Interpretation von Messergebnissen.

Ein weiteres großes Dankeschön geht an meine Bachelorstudenten, HIWIS und Mitarbeiterpraktikanten, die durch ihre hervorragende Arbeit viel zu der vorliegenden Arbeit beigetragen haben: Niklas Unglaube, Samuel Monter, Julian Stiegeler, Paula Wenzel, Lea Bauer, Anna Lena May, Daniel Gutzeit und Jessica Henzler.

Ulrich Haunz danke ich für seine Hilfe bei NMR Messungen, Lars Bolk für das Messen von GPC Proben und die Einweisung in die Geräte und Silke Müller für die Aufnahme von zahlreichen MALDIs. Andreas Spinnrock und Rose Rosenberg danke ich für die Durchführung der AUZ Messungen und für die Hilfe bei der Auswertung. Ein großes Dankeschön geht an Dr. Marina Krumova für die Einweisung an den TEM Geräten und besonders für die Hilfe und Geduld beim Messen der Polymerproben. Dr. Inigo Göttker gen. Schnetmann danke ich für die allgemeinen Hilfen im Labor, bei den NMR Messungen und für die unterhaltsame Zeit im Erstipraktikum. Robin Kirsten danke ich für technische Unterstützung, die Hilfe bei der Pflege der alten Glovebox und für die schöne Zeit im Erstipraktikum.

Ein großes Dankeschön geht an meinen Projektvorgänger Dr. Tjaard de Roo, der mich besonders zu Beginn dieser Arbeit unterstützt hat und mir bei vielen Fragen helfen konnte. Ferner danke ich Annika Sickinger und Dr. Julian Ruiz-Perez für die konstruktiven Diskussionen auf dem Gebiet der konjugierten Polymere.

Der gesamten AG Mecking möchte ich für jede Menge Spaß, die jederzeit gewährte Hilfe und die gesamte gemeinsam verbrachte Zeit danken. Bei Dr. Verena Goldbach, Robin Kirsten, Lars Bolk, Dr. Fei Lin und Marcel Eck bedanke ich mich für die schöne, lustige und zumeist produktive Zeit im Büro mit Fenster.

Des Weitern bedanke ich mich bei allen, die diese Arbeit oder Teile davon Korrektur gelesen haben: Pascal Gumbsheimer, Tobias Morgen, Frieder Conradt und Annika Sickinger.

Der Deutschen Forschungsgemeinschaft danke ich für die finanzielle Unterstützung der Dissertation (SFB767).

Zu guter Letzt bedanke ich mich bei meinen Freunden für die schöne Zeit in Konstanz und ganz besonders bei meiner Familie, die mich immer unterstützt hat und ohne die diese Arbeit nicht möglich gewesen wäre.

Publications & Communications

Parts of this thesis have been published.

Journal Publications

- Huber, S.; Mecking, S., Straightforward Synthesis of Conjugated Block Copolymers by Controlled Suzuki–Miyaura Cross-Coupling Polymerization Combined with ATRP. *Macromolecules* **2019,** *52*, 5917-5924.

Poster Presentations

- Steffen Huber, Tjaard de Roo, Denis Seletskiy, Alfred Leitenstorfer and Stefan Mecking at the 253rd ACS National Meeting and Exposition, San Francisco, California, USA, April 2017.
  "CdSe/CdS-Conjugated Polymer Core-Shell Hybrid Nanoparticles by a Grafting-From Approach"
- Steffen Huber and Stefan Mecking at the 258th ACS National Meeting and Exposition, San Diego, California, USA, August 2019.
  "Combining controlled Suzuki-Miyaura cross-coupling polymerization and controlled radical polymerization for the synthesis of conjugated rod-coil copolymers"
- Steffen Huber, Pascal Gumbsheimer, Philipp Henzler, Denis Seletskiy, Alfred Leitenstofer and Stefan Mecking at SFB767 Symposium on Controlled Nanosystems – Controlled Nanosystems: Interaction and Interfacing to the Macroscale, Konstanz, Germany, November 2019.
  "Ultrafast quantum control of single electrons and photons in mesoscopic systems"

Parts of this thesis have been reproduced and reprinted with permission:

Huber, S.; Mecking, S., Straightforward Synthesis of Conjugated Block Copolymers by Controlled Suzuki–Miyaura Cross-Coupling Polymerization Combined with ATRP. *Macromolecules* **2019,** *52*, 5917-5924. Copyright **2019** American Chemical Society
(*parts of chapter 4*)

Zusammenfassung – Abstract

Durch das Aufbringen konjugierter Polymerketten an halbleitende anorganische Nanokristalle entstehen hybride Nanopartikel, die für den Einsatz in optoelektronischen Geräten wie Solarzellen und lichtemittierenden Dioden sehr vielversprechend sind. Diese Partikel sind aufgrund möglicher Energie- und/oder Ladungsüberträgen zwischen den unterschiedlichen Materialien interessant. Darüber hinaus sind die Partikel ein ideales System, um die Wechselwirkung zwischen Ladungen, Photonen und Phononen in einem quantisierten System zu untersuchen. Des Weiteren sind die Partikel vielversprechend für den Einsatz als Einzelphotonenquelle für quantenoptische Studien in der Ultrakurzzeitphysik. Jedoch stellte die kontrollierte und reproduzierbare Synthese von optisch hochwertigen (hohe Quantenausbeute, stabile Emission, schmale Emissionsbanden) Hybridpartikeln mit direkt an die Oberfläche gebundenen Polymerketten eine Herausforderung dar.

Für die Darstellung hybrider Nanopartikel, bestehend aus konjugierten Polymeren und halbleitender Nanokristalle, sind optisch hochwertige Nanokristalle eine Voraussetzung. CdSe/$Cd_xZn_{1-x}S$ Quantenpunkte wurden nach einem literaturbekannten[1] Verfahren hergestellt. Die synthetisierten Quantenpunkte weisen eine Quantenausbeute von bis zu 87% auf. Bemerkenswert ist, dass schon Quantenpunkte mit einer Hülle bestehend aus 2 Monolagen CdS und 2 Monolagen ZnS diese Quantenausbeute erreichen und optisch sehr stabil sind. Eine dünne Hülle der Quantenpunkte erleichtert wahrscheinlich Ladungs- und Energieüberträge zwischen dem fluoreszenzaktiven CdSe Kern und angebundenen konjugierten Polymerketten. Des Weiteren bildet sich bei diesen Quantenpunkten eine Legierung[1] aus CdS und ZnS aus, wodurch eine Typ-1 Heterostruktur gebildet wird und nicht, wie für CdSe/CdS üblich, eine quasi Typ-2 Heterostruktur. Neben quasi-sphärischen Quantenpunkten sind auch anisotrope Nanostäbchen sehr interessant für die Untersuchung in Einzelpartikelmessungen und als Einzelphotonenquelle, da geladene Nanostäbchen eine reduzierte Auger-Rekombinationsrate aufweisen können.[2,3] CdSe/CdS Nanostäbchen mit verschiedenen Aspektverhältnissen (Länge 20–40 nm; Breite ~5 nm) wurden erfolgreich nach einem literaturbekannten[4] Verfahren synthetisiert. Durch das Abscheiden einer zusätzlichen CdS Schicht (2 Monolagen) konnten die optischen Eigenschaften der Stäbchen erheblich verbessert werden (Quantenausbeute 35–42% → 75–78%). Darüber hinaus ist die Oberfläche von

herkömmlichen CdSe/CdS Stäbchen durch eine Mischung stark bindender Phosphonsäuren abgesättigt, die sehr schwer zu verdrängen sind. Es konnte gezeigt werden, dass ein Teil der Oberfläche der CdSe/CdS/CdS Stäbchen hingegen durch Ölsäureliganden besetzt ist, die potenziell einfacher zu verdrängen sind, was einer Funktionalisierung, vor allem in der Synthese von hybriden Nanopartikeln, dienlich sein sollte.

Für die Funktionalisierung der Nanokristalle wurden konjugierte Polymere (überwiegend Polyfluorene) mit einer engen Molekulargewichtsverteilung ($M_w/M_n \leq 1{,}2$, $DP_n = 5–20$) und definierten Endgruppen unter Einsatz der kontrollierten Suzuki-Miyaura Kreuzkupplungspolymerisation synthetisiert. Die Funktionalisierung der Nanopartikel könnte durch den Einsatz mehrzähniger Polymerliganden verbessert werden. Eine Möglichkeit die nachfolgende Einbettung der Hybridpartikel in Polymernanopartikel effizienter zu machen, könnte die Verwendung von Blockcopolymeren sein, die aus einem konjugierten und einem nicht-konjugierten Segment bestehen. Deshalb wurden Copolymere bestehend aus Polyfluoren (PF8) und Polystyrol (PS), Poly(methylmethacrylat) (PMMA) bzw. Poly(2-ethylhexylmethacrylat) (PEHMA) durch einen neuen Ansatz, nämlich die Kombination aus kontrollierter Suzuki-Miyaura Kreuzkupplungspolymerisation und kontrollierter radikalischer Polymerisationen, auf einem direkten Weg dargestellt (**Abbildung 1**). Zuerst wurde ein genau definierter PF8-basierter Makroinitiator bzw. ein Makromonomer hergestellt. Die erhaltenen Polymere wurden ohne weitere Zwischenschritte direkt für die Synthese der Copolymere eingesetzt.

Eine durch den PF8 Makroinitiator initiierte Atomtransferradikalpolymerisation lieferte Diblockcopolymere mit enger Molekulargewichtsverteilung. Durch die Copolymerisation des Polyfluoren-basierten Makromonomers mit Styrol, Methylmethacrylat bzw. Ethylhexylmethacrylat wurden Kammcopolymer erhalten, wobei die Polyfluorenketten die Seitenketten bilden. Die Anzahl der Seitenkette ließ sich über das Verhältnis der verwendeten Monomere (hier: 2–15 Seitenketten pro Copolymermolekül) einstellen. Das Besondere an der verwendeten Methode ist, dass das zweite Kettenende der Polyfluoreneinheit mit einer weiteren funktionellen Gruppe funktionalisiert werden kann (hier: Diethylphenylphosphonat). Durch Entschützung des Phosphonats unter Verwendung von Brom(trimethyl)silan wurden, ohne dass dabei Nebenreaktionen beobachtet wurden, Phosphonsäure-terminierte Polymere erhalten. Die entschützten Kammcopolymere können als mehrzähnige Liganden betrachtet werden.

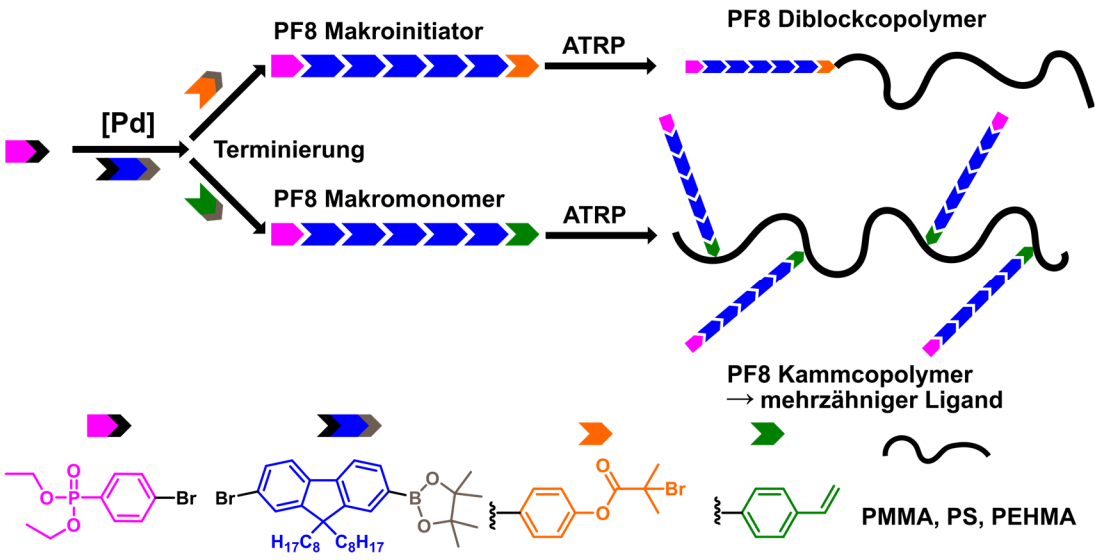

Abbildung 1. Synthese von konjugierten nicht-konjugierten Copolymeren durch die Kombination von kontrollierter Suzuki-Miyaura Kreuzkupplungspolymerisation und von kontrollierter Atomtransferradikalpolymerisation (ATRP). Basierend auf Ref.[5] Copyright **2019** American Chemical Society.

Für die Synthese hybrider Nanopartikel bestehend aus halbleitenden CdSe-basierten Nanopartikeln und Polyfluoren-basierten Polymerketten wurden verschiedene Ansätze verfolgt. CdSe/CdS Quantenpunkte wurden durch eine direkte Ligandenaustauschreaktion mit einem Phenylphosphonsäure-endfunktionalisierten Polyfluoren (DP_n = 10) funktionalisiert. Die Emission von Polyfluoren, das direkt an die Oberfläche der Quantenpunkte gebunden war, wurde vollständig gelöscht und es fand ein quantitativer Energieübertrag auf den anorganischen Emitter statt. Die erfolgreiche Anbindung konnte durch analytische Ultrazentrifugation gezeigt werden, wobei etwa 70 % des zugesetzten Polymers (zugesetzt: 175 Ketten/Partikel) an die Nanopartikel angebunden waren.

Die optisch höherwertigen CdSe/$Cd_xZn_{1-x}S$ Quantenpunkte wurden in einer Ligandenaustauschreaktion mit den neuartigen Diblockcopolymeren funktionalisiert. Die Bindungsaffinität des $PO(OH)_2$-PF8-*b*-PEHMA Copolymers war vergleichbar mit der des Phenylphosphonsäure-funktionalisierten Polyfluorens PF8-Ph-$PO(OH)_2$ und etwa 50–60 % des zugesetzten Polymers (zugesetzt ~100 Ketten/Partikel) banden an die Nanokristalle an. Bei Verwendung der mehrzähnigen Kammpolymere fiel ein Teil des Polymers und der Quantenpunkte irreversibel aus. Das in der Dispersion verbliebene Polymer war dagegen nahezu vollständig an die Quantenpunkte angebunden.

Die Zugabe des konjugierten Polymers direkt während der Synthese der Nanopartikel ermöglicht die Hybridpartikelsynthese bei einer höheren Temperatur, was die

Anbindung positiv beeinflussen könnte und zu einem Zeitpunkt, an dem die Partikelbildung noch nicht abgeschlossen ist. Darüber hinaus entfällt eine weitere, getrennte Funktionalisierungsreaktion. Benzyl- bzw. Phenylphosphonsäure-endfunktionalisiertes Polyfluoren wurde direkt bei der Synthese von $CdSe/(CdS)_2(ZnS)_2$ Quantenpunkten zugesetzt, nachdem die Abscheidung der ZnS Schale abgeschlossen war. Dadurch wurden qualitativ hochwertige hybride Quantenpunkte (Quantenausbeute 78–84%, d = 6.1 nm, relative Standardabweichung ~10%) erhalten. Eine Zugabe nach Abscheiden der CdS Hülle störte dagegen das anschließende Aufbringen der ZnS Hülle. Die Anzahl an zugesetzten Polymerketten pro Partikel wurde im Bereich 30–160 variiert und es wurde eine Anbindung zwischen 35–80 % beobachtet, wobei maximal etwa 55 Polymerketten an einen Quantenpunkt anbanden. Dabei führte die Zugabe bei einer erhöhten Temperatur (310 °C vs. 150 °C) zu einem leicht höheren Funktionalisierungsgrad. Durch Photolumineszenzanregespektroskopie konnte ein Energietransfer vom optisch angeregten Polyfluoren auf die Nanopartikel nachgewiesen werden, der qualitativ mit der Anzahl an gebundenen Polymerketten skaliert. Phenylphosphonsäure-funktionalisiertes Polyfluoren band zu einem leicht höheren Anteil als Benzylphosphonsäure-funktionalisiertes Polyfluoren an. Des Weiteren war der Energietransfer von Benzylphosphonsäure-funktionalisiertem Polyfluoren auf die Quantenpunkte um etwa 25% schwächer als für Phenylphosphonsäure-funktionalisiertes Polyfluoren, was durch die „isolierende“ CH_2 Gruppe zwischen dem konjugierten π-System und der Ankergruppe verursacht wird. Die konjugierten nicht-konjugierten Copolymere waren aufgrund ihrer Löslichkeitseigenschaften weniger gut für diesen Ansatz geeignet.

Es war nicht möglich CdSe/CdS Nanostäbchen mit einer signifikanten Anzahl an konjugierten Polymerketten zu funktionalisieren. Die Oberfläche der Stäbchen ist mit stark bindenden Phosphonsäuren abgesättigt, die nicht oder nur in einem sehr geringen Umfang durch die funktionalisierten Polymere verdrängt werden konnten.

Hybride Polyfluoren CdSe/CdS/CdS Nanostäbchen mit hervorragenden optischen Eigenschaften konnten dagegen über zwei verschiedene Ansätze hergestellt werden (**Abbildung 2**). In der ersten Methode wurde CdO mit Phenylcarbonsäure- oder Phenylphosphonsäure-endfunktionalisiertem Polyfluoren umgesetzt und in Kombination mit Cd-Oleat als Präkursor für die Abscheidung der zweiten CdS Schicht verwendet. In der zweiten Methode wurden die funktionalisierten Polymere direkt nach dem Abscheiden der zweiten CdS Schicht bei 310 °C zugegeben. Bei beiden Methoden hatte die Zugabe der

Polymere keinen negativen Einfluss auf die Partikelbildung und Nanostäbchen mit einer Quantenausbeute von 69-80 % wurden erhalten. Für die Carbonsäure-funktionalisierten Polymere wurde nur eine sehr geringe Anbindung (< 20 %) erhalten. In den Versuchen unter Verwendung der mit Phenylphosphonsäure-funktionalisierten Polymere wurde dagegen eine sehr hohe Funktionalisierung beobachtet. In Dispersionen dargestellt nach Methode 1, waren 45–65 % des Polymers angebunden und in Dispersionen dargestellt nach Methode 2, war das Polymer bis zu einer Zugabe von 300 Äquivalenten pro Stäbchen zu über 90 % angebunden. Nanostäbchen mit direkt an die Oberfläche gebundenen Polymerketten zeigten einen Energieübertrag vom angeregten PF8 auf die Stäbchen, der im untersuchten Bereich linear von der Anzahl an angebunden Polymerketten abhing. Dabei wurde die Emission von angebundenen Polymerketten gelöscht.

Für alle untersuchten Systeme konnte dieser Energieübertrag nur nachgewiesen werden, wenn die PF8-Ketten an den jeweiligen Nanokristall angebunden waren. Für Mischungen aus unfunktionalisiertem Polyfluoren und Nanokristallen wurde dieser Energieübertrag nicht beobachtet.

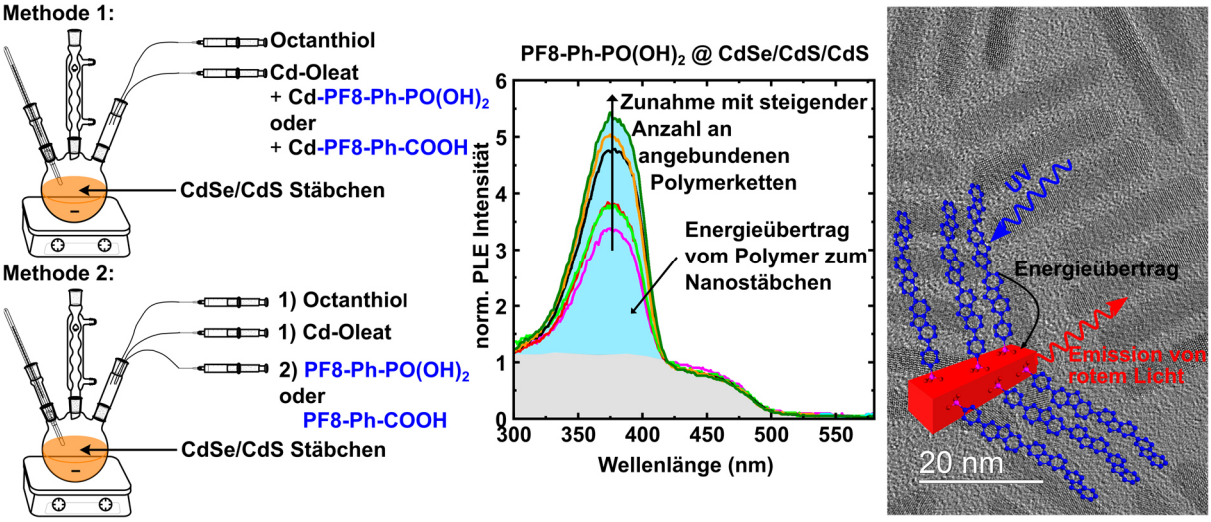

Abbildung 2. Methoden zur Synthese von Polyfluoren CdSe/CdS/CdS Nanostäbchen (links). Photolumineszenzanregespektren ($\lambda_{Detektion}$ = 605 nm) der hybriden Nanostäbchen (mittig). Beispielhaftes TEM Bild und schematische Darstellung des beobachteten Energieübertrags (rechts).

Um die optische und mechanische Stabilität der (hybriden) Nanokristalle zu erhöhen und deren Einsatz als Einzelphotonenquelle in Einzelpartikelmessungen, unter Beibehalt ihrer kolloidalen Eigenschaften, zu gewährleisten, wurden sie durch eine Miniemulsionspolymerisation in quervernetzte Polymernanopartikel eingebettet.

Die CdSe/$Cd_xZn_{1-x}S$ Quantenpunkte und hybriden Quantenpunkte konnten durch eine Miniemulsionspolymerisation erfolgreich in quervernetzte PMMA Partikel mit einer Größe im Bereich von 50–60 nm eingebettet werden. Die Quantenausbeute der CdSe/$Cd_xZn_{1-x}S$ Quantenpunkte war auch im eingekapselten Zustand signifikant höher als die der bisher verwendeten CdSe/CdS Quantenpunkte (49–64 % vs. 20–30%). Für die PF8 CdSe/$Cd_xZn_{1-x}S$ Hybridpartikel wurde eine bessere Einbettung unter Verwendung einer Mischung aus 7 : 3 vol% Methylmethacrylat und 2-Ethylhexylmethacrylat erhalten. Die eingebetteten Hybridpartikel weisen immer noch einen starken Energieübertrag vom angeregten Polyfluoren zum Nanokristall auf. Die Einbettung von Quantenpunkten, die mit konjugierten nicht-konjugierten Blockcopolymeren ($PO(OH)_2$-PF8-*b*-PMMA, $PO(OH)_2$-PF8-*b*-PS, $PO(OH)_2$-PF8-*b*-PEHMA) in einer Ligandenaustauschreaktion funktionalisiert wurden, führte zu einer (partiellen) Agglomeration der Quantenpunkte. Dadurch wurde nur ein sehr geringer Anteil an Polymerpartikel, die genau einen Quantenpunkt enthalten, erhalten und somit Einbettungsverteilungen, die weniger gut für Einzelpartikelmessungen geeignet sind.

Der Versuch Nanostäbchen unter den identischen Bedingungen wie bei der Einbettung der sphärischen Quantenpunkte in PMMA oder in PMMA-*co*-PEHMA Partikel einzukapseln, führte zu einer Clusterbildung der Stäbchen und nur ein sehr geringer Anteil an Polymerpartikel, die genau ein Stäbchen enthalten, wurde erhalten. Die Verwendung eines 1 : 1 Gemisches aus Dodecylmethacrylat und α-Methylen-γ-valerolacton führte zu einer erfolgreichen Einbettung der Nanostäbchen in die Polymerpartikel (**Abbildung 3**), wobei die Mehrzahl der Partikel leer war (~65 %), viele Partikel genau ein Stäbchen (~30 %) und sehr wenige Partikel mehr als ein Stäbchen enthielten (~5 %). Folglich wurden dadurch Einbettungsverteilungen erhalten, die sehr gut für Einzelpartikelmessungen geeignet sind. Die Stäbchen konnten auch erfolgreich in größere (D = 130 nm) Polystyrolpartikel eingebettet werden. Die Polystyrolpartikel wurden dabei mit einer zusätzlichen Hülle aus PMMA (Dicke ~13 nm) überzogen, um die optischen Eigenschaften langfristig zu bewahren. Diese beiden Methoden waren auch geeignet, um CdSe/CdS/CdS Stäbchen und Polyfluoren CdSe/CdS/CdS Hybridstäbchen erfolgreich einzukapseln. Für die eingebetteten Hybridstäbchen wurde immer noch ein starker Energieübertrag vom optisch angeregten Polyfluoren auf das anorganische Stäbchen beobachtet.

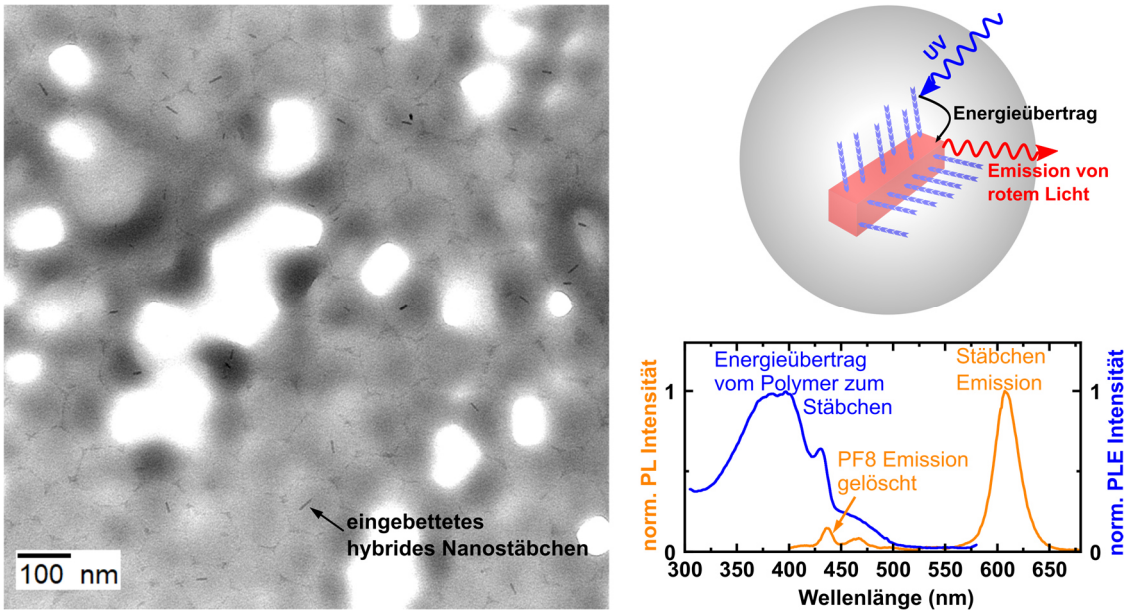

Abbildung 3. Beispielhaftes TEM Bild von in Poly(dodecylmethacrylat-*co*-α-methylen-γ-valerolacton) eingebetteten hybriden Nanostäbchen (links). Schematische Darstellung des Hybridstäbchens und des beobachteten Energieübertrags (rechts oben). Photolumineszenz- ($\lambda_{Anregung}$ = 380 nm) und Photolumineszenzanregespektren ($\lambda_{Detektion}$ = 605 nm) (rechts unten).

Ein Hauptziel dieses Projektes war es, geladene Nanokristalle durch die Wechselwirkung des anorganischen Emitters mit den angebundenen konjugierten Polymerketten zu erzeugen. In Einzelpartikel-Photolumineszenzmessungen wurden zuerst in PMMA-*co*-PEHMA Partikel eingebettete CdSe/$Cd_xZn_{1-x}S$ Quantenpunkte untersucht, die nicht mit Polyfluoren funktionalisiert waren. Diese Quantenpunkte zeigten hervorragende Emissionseigenschaften. Die Feinstruktur des Fluoreszenzspektrums besteht aus drei Emissionslinien (F1, A1, A2) und den dazugehörigen Phononrepliken, wie es für einen neutralen CdSe-basierten Emitter typisch ist. Der energetisch niedrigste Übergang vom Exzitongrundzustand in den Quantenpunktgrundzustand ist dabei „Dipol-verboten". Auch eingebettete CdSe/CdS/CdS Nanostäbchen wurden in Einzelpartikel-Photolumineszenzmessungen untersucht. Die Stäbchen zeigten gute Emissionseigenschaften und es wurde eine Exzitonfeinstruktur (3 Emissionslinien) beobachtet, die der Feinstruktur der CdSe/$Cd_xZn_{1-x}S$ Quantenpunkte ähnelt. Keiner der Polyfluoren-freien Nanokristalle (Quantenpunkte und Nanostäbchen) zeigte Fluoreszenzeigenschaften, wie sie für einen geladenen Emitter typisch wären.

Durch die Funktionalisierung der Quantenpunkte mit Polyfluoren wurden die Emissionseigenschaften stark verändert und die Bildung eines Trionzustands beobachtet (**Abbildung 4 a**). Dieser ist durch eine einzelne Emissionslinie im Fluoreszenzspektrum charakterisiert. Die strahlende Rekombination des Triongrundzustands (X^-) ist Dipol-

erlaubt, wodurch – wie erwartet – eine Erhöhung der Fluoreszenzintensität und eine kürzere Fluoreszenzlebensdauer (**Abbildung 4 b**) beobachtet wurden.

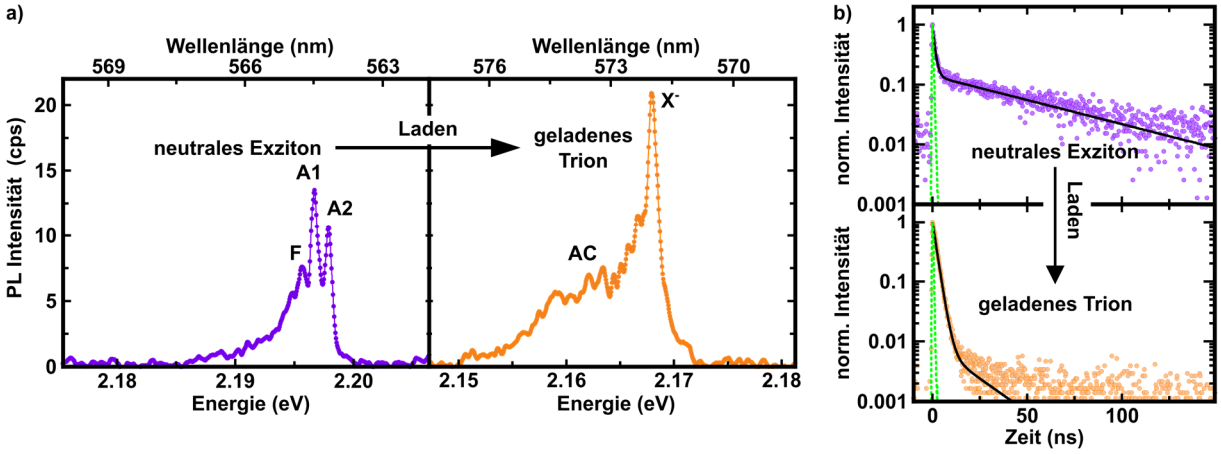

Abbildung 4. a) Hochaufgelöste Fluoreszenzspektren (T = 4.2 K, $\lambda_{Anregung}$ = 532 nm, $P_{Anregung}$= 240 nW) eines Polyfluoren CdSe/$Cd_xZn_{1-x}S$ hybriden Quantenpunktes im neutralen (links) und geladenen Zustand (rechts). Der Ladevorgang resultierte in einer Erhöhung der Emissionsintensität und Veränderung der Feinstruktur (F, A1, A2 → X^-) b) Zeitlicher Fluoreszenzabfall eines hybriden Quantenpunktes im neutralen (oben) und geladenen Zustand (unten). Ein Vergleich des ungeladenen und geladenen Quantenpunktes zeigt, dass der Ladevorgang zu einem erheblich schnelleren Fluoreszenzabfall geführt hat. AC = akustische Phononreplik; schwarze Kurven = biexponentielle Anpassung; grüne Kurven = Apparatefunktion.

Die Ladung des anorganischen Emitters konnte durch eine zusätzliche Bestrahlung mit UV-Licht (λ = 370 nm, eine Wellenlänge intensiver PF8 Absorption) induziert werden. Dabei wird wahrscheinlich ein Elektron vom Leitungsband des angeregten Polymers in das Leitungsband des CdSe-Kerns übertragen (**Abbildung 5**, links). Die Bildung eines geladenen Nanokristalls wurde auch manchmal ohne zusätzliche Bestrahlung mit UV-Licht beobachtet. Dies kann durch den Transfer eines Loches aus dem Valenzband eines angeregten Quantenpunktes auf das Valenzband eines Polyfluoren Liganden erklärt werden (**Abbildung 5**, rechts). Dieser Vorgang erfordert aber einen Tunnelprozess durch die dünne CdS/ZnS Hülle.

Einzelne Polyfluoren-funktionalisierte hybride CdSe/CdS/CdS Nanostäbchen zeigen eine einzelne Emissionslinie mit den dazugehörigen Phononrepliken im Fluoreszenzspektrum. Dies ist ein starkes Indiz für die eine Ladung des Nanokristalls. Bemerkenswert ist, dass diese hybriden Nanostäbchen ohne zusätzliche Bestrahlung mit UV-Licht schon einen geladenen CdSe-Kern aufwiesen, der eine zeitlich sehr stabile und intensive Emission zeigte. Entladungsvorgänge konnten bisher nicht beobachtet werden und alle untersuchten Polyfluoren-funktionalisierten Nanostäbchen zeigten Fluoreszenzeigenschaften, die typisch für einen geladenen Emitter sind.

Zusammenfassend kann gesagt werden, dass die Funktionalisierung von halbleitenden CdSe-basierten Nanokristallen mit Polyfluoren eine Ladung des fluoreszenzaktiven CdSe-Kerns unter kryogenen Temperaturen herbeiführen kann (**Abbildung 5**). Durch die dadurch erhaltenen Fluoreszenzeigenschaften (Dipol-erlaubter Grundübergang, hohe Emissionsintensität, eine einzelne Emissionslinie und kurze Fluoreszenzlebensdauer) stellen diese Partikel ein hoch interessantes Material für den Einsatz als Einzelphotonenquellen in sehr schnellen quantenoptischen Messungen und Anwendungen dar.

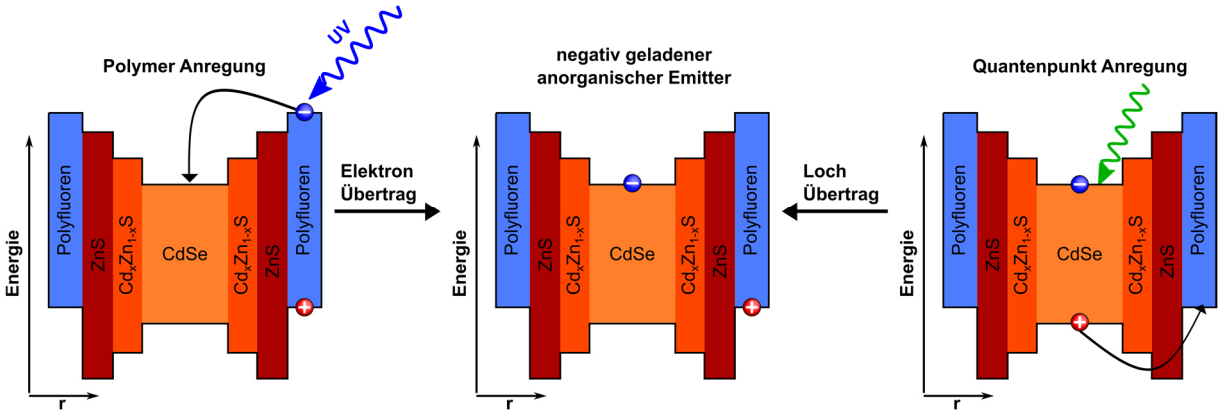

Abbildung 5. Schematische Darstellung der Energieniveaus und des angenommenen Ladungsvorgangs eines Polyfluoren CdSe/$Cd_xZn_{1-x}S$ Kern-Schale-Nanokristalls, der durch Wechselwirkung mit dem Polyfluoren Liganden geladen wird. Die gleichen Vorgänge sind auch potenziell für einen PF8 funktionalisierten CdSe/CdS Nanokristall möglich.

Table of Contents

List of Abbreviations

Abbreviations of the 'International System of Units' (SI-Units), chemical formulae, and abbreviations of chemical groups (Me, Et, etc.) according to the IUPAC (International Union of Pure and Applied Chemistry) nomenclature are not listed.

Analytical Methods:

Abs	absorbance
AFM	atomic force microscopy
DLS	dynamic light scattering
DOSY	diffusion ordered spectroscopy
FEG	field emission gun
GPC	gel permeation chromatography
NMR	nuclear magnetic resonance
MALDI-TOF MS	matrix assisted laser desorption ionization time of flight mass spectrometry
MW-AUC	multi wavelength analytical ultracentrifugation
PL	photoluminescence
PLE	photoluminescence excitation
RI	refractive index
TEM	transmission electron microscopy
UV-VIS	ultraviolet visible

Chemical Compounds

AIBN	azobis-*iso*-butyronitrile
BPin	4,4,5,5-tetramethyl-1,3,2-dioxaborolane group
DCM	dichloromethane
DPPF	1,1′-ferrocenediyl-bis(diphenylphosphine)
DMF	*N,N*-dimethylformamide
DMSO	dimethyl sulfoxide
DOMA	dodecyl methacrylate
DOPA	*n*-dodecylphosphonic acid
EHMA	2-ethylhexyl methacrylate
HPA	*n*-hexylphosphonic acid
HOAc	oleic acid

MeMBL	*α*-methylene-*γ*-valerolactone
MMA	methyl methacrylate
*n*BuLi	*n*-butyllithium
NBS	*N*-bromosuccinimide
ODE	1-octadecene
ODPA	*n*-octadecylphosphonic acid
PA	arylphosphonic acid terminus (polymer-aryl-$PO(OH)_2$)
Phos	diethyl arylphosphonate terminus (polymer-aryl-$PO(OEt)_2$)
PdG2P^{t}Bu$_3$	chloro[(tri-*tert*-butylphosphine)-2-(2-aminobiphenyl)] palladium(II)
PEHMA	poly(2-ethylhexyl methacrylate)
PF	polyfluorene
PF8	poly(9,9'-dioctylfluorene)
PMMA	poly(methyl methacrylate)
PS	polystyrene
P3HT	poly(3-hexylthiophene)
SDS	sodium dodecyl sulfate
TEOS	tetraethyl orthosilicate
THF	tetrahydrofuran
TMOS	tetramethyl orthosilicate
TMS-Br	trimethylsilyl bromide
TOP	tri-*n*-octylphosphine
TOPO	tri-*n*-octylphosphine oxide
TPMA	tris(2-pyridylmethyl)amine

Miscellaneous

ARGET	activators regenerated by electron transfer
ATRP	atom transfer radical polymerization
CRP	controlled radical polymerization
cSMCCP	controlled Suzuki-Miyaura cross-coupling polymerization
C	circularity
CB	conduction band
d	doublet
DP_n	degree of polymerization
equiv. or eq.	equivalent

ET	energy transfer
FWHM	full-width at half maximum
GS	ground state
HOMO	highest occupied molecular orbital
HWHM	half-width at half maximum
ICAR	initiators for continuous activator regeneration
KCTP	Kumada-Tamao catalyst-transfer polycondensation
L	length
LUMO	lowest unoccupied molecular orbital
m	multiplet
ML	monolayer
M_n	number average molar mass
M_w	mass average molar mass
(O)LED	(organic) light-emitting diode
NMP	nitroxide-mediated radical polymerization
NR	nanorod
$P_{exc.}$	excitation power
PDI	polydispersity index
q	quartet
QD	quantum dot
quint	quintet
QY	quantum yield
RAFT	reversible addition-fragmentation chain transfer polymerization
RCF	relative centrifugal force
ref.	reference
rpm	revolutions per minute
rt	room temperature
s	singlet
SILAR	successive ionic layer adsorption and reaction
t	triplet
T	trion
T_g	glass transition temperature
VB	valence band

W	width
X^0	exciton
$\lambda_{exc.}$	excitation wavelength
$\lambda_{emi.}$	emission wavelength
$\lambda_{det.}$	detection wavelength

1 General Introduction

Semiconducting materials are the workhorse of today's technology and the corner stone of the "Digital Age". The combination of an inorganic semiconductor and a semiconductor organic polymer is of interest due to possible charge and energy transfer processes between the two materials (**Figure 1.1**, a).[6,7,8,9] Such compounds can unlock new features excelling the properties of its single constituents. One important example would be charge separation between the two materials upon optical excitation allowing the use in photovoltaic devices.[10,11,12] Colloidal hybrid nanoparticles consisting of inorganic semiconductor nanocrystals and organic semiconductor polymers are of fundamental interest as well as for their potential use in solar cells[10,13], light-emitting devices[7,14,15,16], or flexible electronics.[7,17] Their colloidal nature allows for a more convenient processing into devices.[18,19,20]

Single-photon sources are particularly appealing for quantum-optical applications and single semiconductor (hybrid) quantum dots (QDs) are a promising material class to be employed.[21,22] The functionalization of an inorganic emitter nanocrystal with conjugated polymer chains might enable the deterministic charging of the emitter (**Figure 1.1**, b–c), which can deeply impact the emitter's properties.

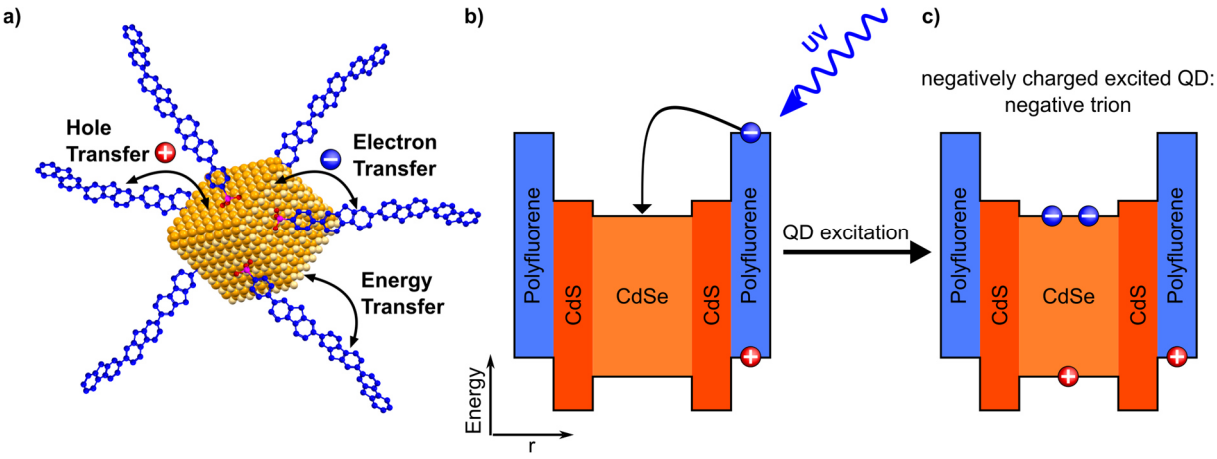

Figure 1.1. a) Schematic illustration of possible charge and energy transfer processes in a hybrid nanoparticle. b) Sketched energy level diagram based on ref.[23,24,25] of a polyfluorene CdSe/CdS hybrid nanoparticle. c) A negative trion is formed after an electron was transferred from the photoexcited conjugated polymer to the nanocrystal and excitation of the nanocrystal.

Uncharged CdSe/CdS core-shell nanocrystals feature a dipole-forbidden "dark" exciton ground state (GS) to global QD-GS recombination.[26,27] The functionalization of such nanoparticles with polyfluorene (PF) ligands aims at the deterministic charging of the inorganic emitter and the generation of a negative trion (quasi particle consisting of 2 electrons and one hole) (**Figure 1.1**,b–c). A CdSe/CdS trion (T) features a dipole-allowed transition between the T-GS and the QD-GS and thereby a fast-radiative recombination which is a prerequisite for studying and capitalizing ultrafast dynamics.[28,29]

Another requirement is an adequate colloidal and optical stability of the system which can be achieved by embedding the nanocrystals into a protective shell (silica or polymer). This encapsulation allows for long-term measurements and high excitation powers while retaining individual particles.[30,31,32,33] The size increase due to the optical transparent shell facilitates the mechanical manipulation of the nanoparticles into optical antennae or resonator systems.[34] Therefore, embedded hybrid particles — with the possibility to charge the inorganic emitter — can provide an ideal system to study and control the ultrafast dynamics and interplay of photons, phonons and charges in a fully quantized system. Such single-photon sources would be highly auspicious for the use in ultrafast photon amplifiers, for the development of efficient quantum computers or for quantum cryptography applications.[22,35,36]

1.1 Inorganic Semiconductor Colloidal Nanocrystals

1.1.1 Basics of Semiconductor Nanocrystals

Bulk semiconductor materials are the basis for the fabrication of solar cells or computer chips. If the size of a bulk semiconductor is decreased to the nanometer regime, the optical and electronic properties of the material become size dependent, termed quantum size effect.[37,38,39,40] The transition from bulk semiconductor properties to the quantum confinement regime is determined by the Bohr exciton diameter. If this diameter becomes smaller than a spatial dimension of the nanocrystal, quantum confinement effects are observed.[41,42] Regarding the spatial degree of confinement these semiconducting nanocrystals are called quantum dots (QDs) (3D confinement), nanorods (2D confinement) or nanoplatelets (1D confinement). Important materials are group II-IV semiconductors such as CdSe, CdS, PbS, ZnS, III-V semiconductors such as InP, GaAs or so-called Perovskite QDs ($CH_3NH_3PbX_3$ or $CsPbX_3$; X = Cl, Br, I). The synthesis of inorganic

nanocrystals has improved significantly over the last 25 years and today's semiconductor nanocrystals show high absorption coefficients, a size tunable emission wavelength, narrow emission line widths, high fluorescence quantum yields (QY), and very stable optical properties compared to organic emitters.[43,44] Therefore, they are perfectly suited for the use in opto-electronic devices such as solar cells[45,46], light-emitting diodes[14,47,48,49], displays [43,50] and in bio-imaging applications.[51,52,53]

Since the pioneering work by Bawendi and co-workers, the so-called hot injection reaction is the method of choice for the synthesis of narrowly distributed semiconductor colloidal nanocrystals.[54] According to this method, one organometallic precursor is heated up in a mixture of a high boiling solvent (e.g. octadecene (ODE), tri-*n*-octylphosphine oxide (TOPO), di-*n*-octylether) and coordinating ligands (e.g. oleylamine, tri-*n*-octylphosphine (TOP), oleic acid, long-chain alkylphosphonic acids). The other precursor compound is swiftly added at elevated temperatures.[55] The size of the nanocrystals can be influenced by the growth time and temperature. The coordinating ligands influence the growth kinetics of the nanocrystals, determine the morphology of the nanocrystals, and are highly important for the optical and electronic properties of the nanocrystals.[56]

1.1.2 Ligand Classification and Ligand Exchange Reactions

The optical properties of semiconductor nanocrystals are heavily influenced by the surface atoms of the nanocrystals, and thus by the stabilizing ligands.[57,58,59,60,61] Surface atoms of nanocrystals have a lower coordination number compared to bulk atoms which results in weaker bonds and dangling bonds. Thereby, undesirable electronic states within the semiconductor band gap can be created.[62,63,64] These states can trap photoexcited charges and open non-radiative relaxation pathways which lower the QY of the nanocrystals.[65] Therefore, it is crucial that these surface atoms are capped by ligands which eliminate those trap states and allow for a high fluorescence QY of the nanocrystals.[59,61,66] According to Green's formalism different ligands can be classified according to their binding behavior (**Figure 1.2**, A).[67] So-called L-type ligands (neutral Lewis bases) are datively bound, neutral two electron donors. Important examples are phosphines (tri-*n*-octylphosphine) and amines (oleylamine). Typical colloidal syntheses of nanocrystals often yield metal rich nanocrystals whose excess charges are balanced by anionic, covalently bound one electron donor X-type ligands (e.g. carboxylates, phosphonates).[58,68,69,70,71] Recent nuclear magnetic resonance (NMR) spectroscopy and

titration studies showed that the surface metal ion layer which enriches the nanocrystals formula is labile.[61,62,72] Owen et al. reported that so-called Z-type ligand complexes (e.g. $M(O_2CR)_2$ or $M(O_2P(OH)R)_2$) reversibly bind to the nanocrystals and are considered two-electron accepting Lewis acids.[61] The coverage of the surface with these Z-type ligands greatly influences the fluorescence QY of the nanocrystals which increases with increasing coverage.[61]

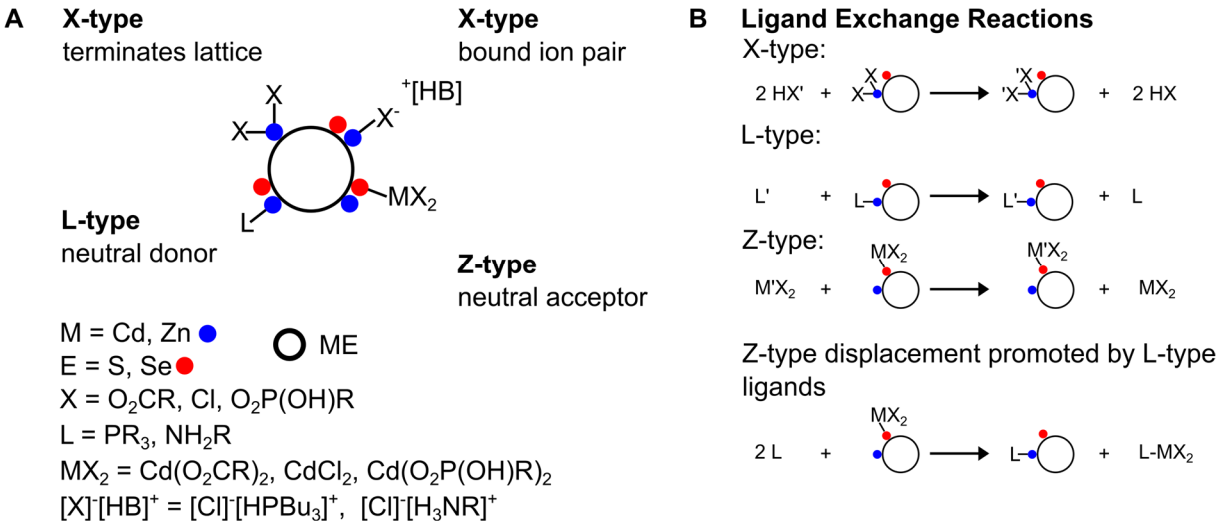

Figure 1.2. A: Illustration of ligand classification and coordination. B: Illustration of ligand exchange and displacement reactions. Figure adapted from ref.[61]

The manipulation of the nanocrystals' surface is a crucial step for the utilization of nanocrystals in opto-electronic devices and bio-imaging applications.[45,46,51,52,73,74] For the desired modification of the surface often ligand exchange or displacement reactions must be performed. They can be divided into four types: X-type, L-type, Z-type ligand exchange and Z-type ligand displacement promoted by L-type ligands (**Figure 1.2**, B). For the functionalization of nanocrystals, the direct X-type exchange is important. Mechanistically the exchange of X-type ligand exchange involves a proton or trimethylsilyl transfer.[58,69,70,75] For the surface of CdSe nanocrystals it was shown that carboxylic acid can be stoichiometrically replaced by phosphonic acids, but phosphonic acids cannot be replaced by carboxylic acids.[70,76,77] High concentrations of L-type ligands e.g. oleylamine can strip surface Cd-atoms off in a so-called Z-type displacement promoted by L-type ligands which on the one hand can have negative influences on the optical properties but on the other hand allows for the functionalization of the surface with new Z-type ligands.[61,72,78]

1.1.3 Multi-Shell Semiconductor Nanocrystals

Semiconductor nanocrystals consisting of a single material are barely used. By the combination of at least two different materials in a core-shell structure the optical and electronic properties as well as the stability of the nanocrystals can be fine-tuned.[42,79,80] The shell material efficiently saturates the surface of the core particle and improves its optical properties. Core-shell nanocrystals are normally obtained by a slow hot temperature deposition of the shell material onto a preformed seed particle. Thereby, the electronic and optical properties of the core particle can be greatly influenced. Depending on the bandgaps and the relative energy levels of the materials, the shell deposition can have different consequences (**Scheme 1.1**).[79]

Scheme 1.1. Schematic representation of the energy level alignment in different types of core-shell semiconducting nanocrystals. The preferential local distribution of the electron and hole after optical excitation is shown.

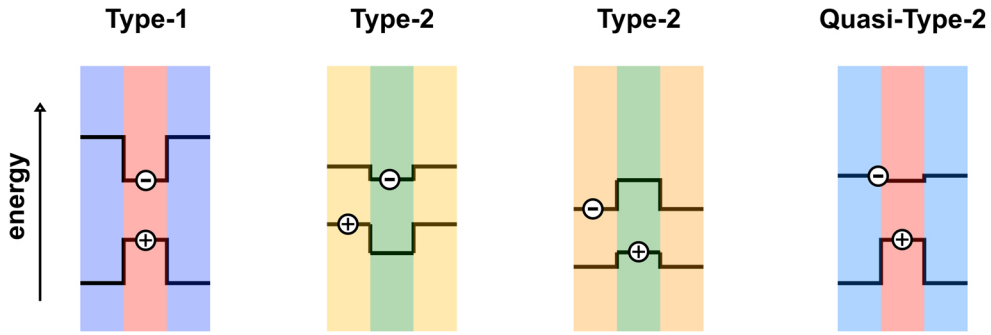

In a type-1 nanocrystal (e.g. CdSe/ZnS), the shell has a higher bandgap than the core material and the highest occupied molecular orbital (HOMO) and lowest unoccupied molecular orbital (LUMO) level of the shell are energetically lower and higher, respectively, than the HOMO and LUMO level of the core which confines the exciton to the core. Thereby, the fluorescent active core is shielded from the surrounding medium which positively influences the optical properties in terms of QY and optical stability.[79] In type-2 nanocrystals (e.g. ZnTe/CdSe) either the valence band or the conduction band of the shell lies within the bandgap of the core material, whereby the electron and hole are separated between the two materials which leads to a long fluorescence lifetime of the exciton. These materials are promising for their potential use in solar cells or as photocatalysts.[81,82,83] In a quasi-type-2 structure, one charge carrier type is confined to the core whereas the other charge carrier type is distributed over the whole core-shell structure. Important members of this material class are most CdSe/CdS nanocrystals where a red shift of the optical properties takes place during the deposition of the CdS

shell. In most CdSe/CdS core-shell particles the hole wavefunction is confined to the core whereas the electron wavefunction is spread into the shell material as well.[84,85] Also, the deposition of the CdS shell greatly improves the optical properties of the CdSe core particles.[86,87,88]

1.2 Conjugated Polymer/Inorganic Semiconductor Hybrid Nanocrystals

Conjugated polymers are an important material class for modern technology applications. Due to their conjugated π-system, they show semiconductor properties similar to inorganic semiconductors — high absorbance coefficients, strong photoluminescence, good charge carrier transport properties and upon doping electric conductivity.[89,90,91] Potential fields of applications are organic light-emitting diodes[92,93,94] (OLEDS) which are used in state-of-the-art displays, solar cells[95,96], organic transistors[97,98], and nanoparticles of conjugated polymer are studied for bio-imaging and medical applications.[90] In academic research, the synthesis of conjugated polymers is mostly based on Pd or Ni catalyzed C-C coupling reactions such as Kumada, Stille, Heck or Suzuki-Miyaura cross-coupling.[95,99] Today, methods have been developed which allow for the controlled synthesis of many different conjugated polymers in a chain growth manner with the possibility to introduce functional groups at the chain end (**Chapter 4.1.1**).[100]

Composite materials of semiconductor nanocrystals and conjugated polymers have potential application in solar cells, light-emitting diodes or flexible electronics due to possible charge and/or energy transfers between the two semiconductor materials.[6,10,17,101,102] Unfortunately, the simple mixing of separately prepared nanocrystals and conjugated polymers often results in a phase separation. [13,23,103] In the synthesis of inorganic nanocrystals long-chain aliphatic ligands are used as stabilizers which finally end up on the surface of the nanocrystals ensuring colloidal stability but also acting as insulators.[104,105,106,107] It was shown that the functionalization of the nanocrystals with conjugated polymer chains tethered directly to the surface of the nanocrystals can greatly enhance the miscibility and interaction of the two materials.[108,109,110] Additionally, such a defined combination of the two materials can emerge in different photo physics compared to the relative bulk blends.[60,111]

However, the synthesis of such defined hybrid particles is highly challenging, and often it remains unclear if the polymer is indeed bound or only loosely adsorbed to the

nanocrystals. For the functionalization of colloidal semiconductor nanocrystals different strategies have been pursued (**Scheme 1.2**): In the direct ligand exchange procedure, a polymer is functionalized with an X- or L-type functional group and an X-type or L-type ligand exchange is performed with preformed nanocrystals. Polymers can also be tethered to nanocrystals by different grafting methods. In the grafting-from approach, the nanocrystals are functionalized with ligands which are capable to initiate a polymerization from the surface of the nanocrystals. For this purpose, the surface of the nanocrystals is functionalized with a small molecule which bears two functional groups. One functional group tethers to the surface of the nanocrystals whereas the other group serves as polymerization initiator. In the grafting-onto approach, the non-binding functionality of the small molecule serves as docking point for a preformed and functionalized polymer. In the grafting-through approach, the surface of the nanocrystal is functionalized with a monomeric ligand. Afterwards, a polymerization is conducted in present of the functionalized nanocrystals and the nanocrystals are theoretically copolymerized into the polymer chain.[10,110,112]

Scheme 1.2. Methods for the functionalization of semiconductor nanocrystals with conjugated polymers. The grafting methods are adapted from Bousquet et al.[112]

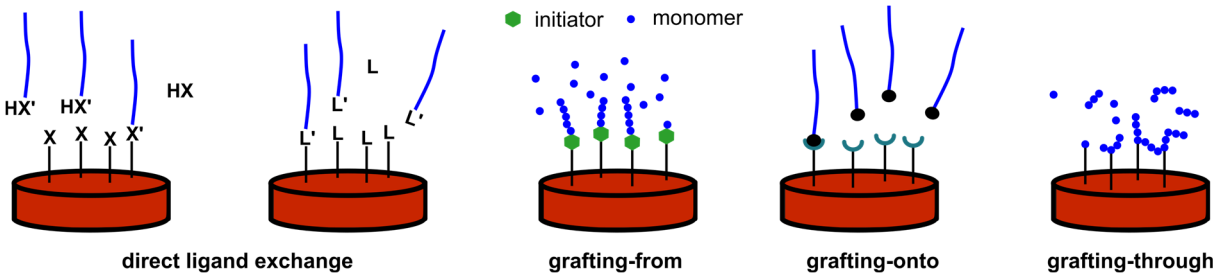

For all grafting methods, it is necessary to tether a bifunctional molecule to the nanocrystal's surface before the actual grafting step can take place. These bifunctional molecules can be introduced directly during the synthesis of the nanocrystals, partially replacing the original ligands, or they can be introduced by a ligand exchange reaction after the synthesis of the nanocrystals.

Besides these approaches also direct functionalization approaches have been developed in which the polymer serves as stabilizing ligand during the nanocrystal's synthesis or even as precursor for the formation of the nanocrystal itself.[105,113,114]

1.2.1 Hybrid Particles by a Direct Ligand Exchange

The direct replacement of the original nanocrystal's ligands by a preformed functionalized polymer seems to be the most straightforward functionalization method. Both the nanocrystal and the polymer can be synthesized separately according to known procedures and purified accordingly. Afterwards, the polymer and the nanocrystals are simply mixed and hybrid particles are theoretically obtained. The actual degree of functionalization strongly depends on the binding affinity of the functional group of the conjugated polymer compared to the binding affinity of the original ligands. In general, low molecular mass short ligands can cover the surface more densely than longer ligands due to steric repulsion between previously anchored polymer and free polymer chains. This repulsion hinders the dense functionalization of nanocrystals with conjugated polymers which are a in general much more sterically demanding compared to the original nanocrystals' ligands. One of the earliest examples for this method was reported by Fréchet and co-workers. They synthesized phosphonic acid-functionalized oligothiophenes which were mixed with CdSe QDs.[115] Also, Fréchet and co-workers synthesized amine end-functionalized poly(3-hexylthiophene) (P3HT) which was blended with CdSe nanorods (NRs).[116] This blend showed no phase separation compared to a blend of CdSe and unfunctionalized P3HT, indicating an attachment of the polymer chains to the nanocrystals. Similar hybrid particles from carbodithioic acid-terminated polythiophenes and CdSe QDs were synthesized.[117] Commonly, the photoluminescence of these hybrid systems was very weak which is attributed to an efficient charge separation between the two materials by the authors.

Mao and co-workers synthesized an amine-functionalized poly(9,9'-dihexylfluorene) (amine groups at the end of alkyl chain) which was used for the functionalization of CdSe/ZnS QDs.[23] The QDs' native ligands were supposedly first replaced by pyridine which was afterwards exchanged for the polymer. However, no direct proof of binding was reported. In films of these particles, the photoluminescence (PL) of the polymer was nearly completely quenched, the PL of the QDs increased and an energy transfer from the polymer to the nanocrystals was observed. These findings support that the polymer and the QDs were in close contact in the film which enabled the energy transfer.

1.2.2 Hybrid Particles by the Grafting-Onto Approach

Many reported examples for the functionalization of semiconductor nanocrystals with conjugated polymers utilize the grafting-onto approach. This approach offers the benefit that separately synthesized and purified nanocrystals and polymers are used Therein, a preformed functionalized polymer is coupled to a small molecule which had been tethered to the surface of the nanocrystals beforehand. These molecules bear two different functionalities: one group must be able to bind to the surface of the nanocrystal whereas the other group serves as docking point for the conjugated polymer. These molecules can be introduced to the nanocrystals' surface directly during the synthesis of the nanocrystals where they serve as additional ligand or they can be introduced to preformed nanocrystals by a ligand exchange reaction. In 2007, Lin et al. used [(4-bromophenyl)methyl]dioctylphosphine oxide as "ligand" during the synthesis of CdSe QDs.[118] Afterwards, they coupled vinyl-functionalized P3HT via a Pd catalyzed Heck coupling reaction to the QDs. Emrick et al. used a similar procedure for the functionalization of CdSe NRs.[108] The ligands of the NRs were replaced by pyridine which was then replaced by [(4-bromophenyl)methyl]dioctylphosphine oxide or by 2-(4-bromo-2,5-di-*n*-octyl-phenyl)-ethanethiol. Afterwards, vinyl-terminated P3HT was grafted by a Heck coupling reaction. Mixing these hybrid NRs with P3HT homopolymer a homogeneous distribution of the NRs in the polymer matrix was observed. However, no direct proof of binding of the conjugated polymer was presented. Regarding the functionalization with [(4-bromophenyl)methyl]dioctylphosphine oxide, it is indeed highly unlikely that the polymer is bound to the nanocrystals after the coupling as several studies have shown that phosphine oxide ligands are weak L-type ligands and the surface of nanocrystals is covered by the phosphonic acids used and not by the phosphine oxide.[68,119,120]

In 2011, Lin et al. reported about the synthesis of CdSe NRs using a mixture of 4-bromobenzylphosphonic acid and octadecylphosphonic acid.[121,122] Afterwards vinyl-terminated P3HT was tethered via a Heck coupling reaction or the bromide was transformed to an azide and then reacted in a 'Click reaction' with ethynyl-terminated P3HT (**Scheme 1.3**). A similar strategy was transferred to CdSe tetrapods.[109] In a first step, the native oleate ligands were replaced by HBF_4 which was then replaced for 4-azidobenzoic acid or 5-bromovaleric acid. Ethynyl and vinyl-terminated P3HT was grafted via a 'Click reaction' and a Heck coupling reaction, respectively. One major

drawback of the presented methods is the coupling step. Pd-catalyzed C-C couplings are not quantitative, often relative harsh reaction conditions (elevated temperatures, addition of base) must be used, and Pd and the employed ligands can partially remain in the dispersion which can all be detrimental for the optical properties. Using a catalyst free 'Click reaction' as shown in **Scheme 1.3** has the drawback that a triazole is introduced between the conjugated polymer and binding molecule, and thus the conjugated π-system is not directly bound to the surface which can hinder energy/charge transfer processes.

Scheme 1.3. Grafting of P3HT onto bromobenzylphosphonic acid-functionalized CdSe nanorods. Adapted from ref.[121] and ref.[122]

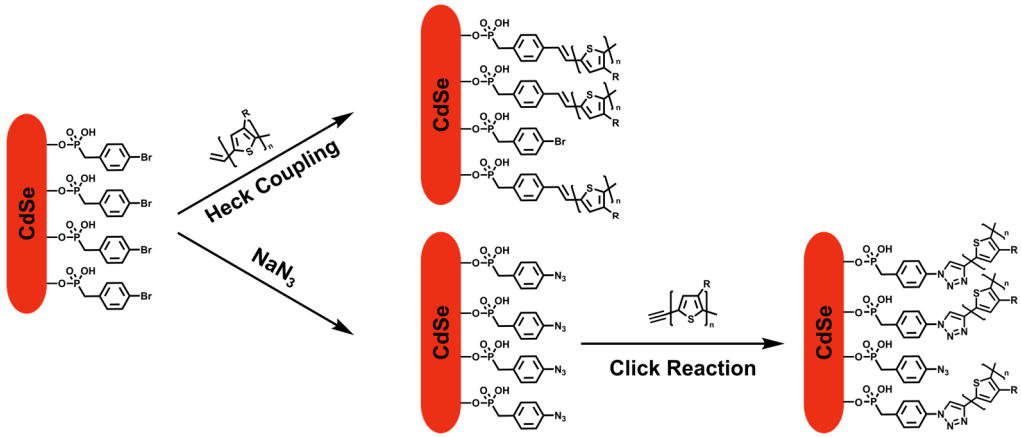

Another grafting onto approach was presented by Cotlet et al.[123] They transferred CdSe/ZnS QDs with 3-mercaptopropionic acid to water and added the oppositely charged polymer poly(9,9′-bis(6-*N*,*N*,*N*-trimethylammoniumhexyl)fluorene-*alt*-1,4-(2,5-bis(6-*N*,*N*,*N*-trimethylammoniumhexyloxy))phenylene) bromide. By exclusive excitation of the QD, they observed a hole transfer from the QD to the polymer which was exponentially depending on shell thickness. Moreover, the hole transfer rate increased with decreasing core size.[124]

1.2.3 Hybrid Particles by the Grafting-Through Approach

In the grafting-through approach, the nanocrystals are first functionalized with a small molecule which bears two functionalities: one group can bind to the nanocrystal's surface and the other group is polymerizable. Afterwards, a polymerization is conducted in the presence of the functionalized nanocrystals which will be copolymerized into the forming polymer.

In 2004, Emrick and co-workers used [(4-bromophenyl)methyl]dioctylphosphine oxide as 'ligand' during the synthesis of CdSe QDs.[125] Afterwards, a Heck-type polymerization of 1,4-di-*n*-octyl-2,5-divinylbenzene and 1,4-dibromo-2,5-di-*n*-octylbenzene was conducted

in the presence of the QDs. However, only low molecular weight polymer (tri- and tetramers) was formed and due to the step-growth nature of the polymerization polymer was also formed in solution. Holder et al. functionalized CdSe QDs with 6,6'-(2,7-dibromo-9*H*-fluorene-9,9-diyl)dihexan-1-amine which were copolymerized with 2,7-dibromo-9,9-dioctyl-9H-fluorene in a Yamamoto-type polymerization.[126] No proof of binding was shown, the emission of the QDs was completely quenched, and only broadly distributed low molecular weight polymer was obtained. The grafting-through approach is an interesting method; however, no convincing results have been achieved by this method so far due to the complexity of the system.

1.2.4 Hybrid Particles by the Grafting-From Approach – Surface Initiated Polymerizations

The grafting-from approach is also known as surface-initiated polymerization (SIP), as the nanocrystals are functionalized with an initiator molecule which is capable to start a polymerization from the surface of the nanocrystals. This procedure is the method of choice for the functionalization of nanocrystals or macroscopic surfaces with nonconjugated polymers as it allows for a controllable high grafting density and for a controlled molecular weight of the formed polymer. It is well established for the formation of nonconjugated polymer brushes by controlled radical polymerizations on the surface of many different particles e.g. silica-, polymer-, metal-, metal oxide, and semiconductor nanoparticles.[127] However, examples for the SIP of conjugated polymers are rare. Conjugated polymers are mostly synthesized by step-growth polymerizations which are not compatible with the surface confined nature. Today, the formation of conjugated polymers in a chain-growth manner by Kumada or Suzuki-Miyaura C-C cross-coupling polymerization is possible (see **Chapter 4.1.1**), which in principle enables a SIP of conjugated polymers. The surface must be functionalized with a small molecule which reacts with a metal precursor to a surface bound initiator complex. After addition of monomer, this initiator can grow the polymer from the surface. Theoretically, only surface bound polymer should be formed, the grafting density should be adjustable, and the molecular weight should be defined by the ratio of monomer to initiator. Most reported examples are restricted to the SIP from macroscopic surfaces. PF, polythiophene and poly(*p*-phenylene) were successfully grafted from functionalized gold[128], silica[129,130], silicon[131,132,133] or indium tin oxide[134] wafers.

Moreover, PF[135], polythiophene[136,137] and polythiophene-*b*-poly*para*phenylene[138] were grafted from rather large silica particles (60 nm–5 µm). However, the authors only analyzed the polymer on the surface by methods like atom force microscopy (AFM), chemical composition analysis (X-ray photoelectron spectroscopy, electron energy loss spectroscopy), small angle neutron scattering, dynamic light scattering or by scanning electron microscopy. In doing so, it is hard to distinguish between adsorbed and grafted polymer. The polymer was not detached from the particles and no polymer analysis (e.g. gel permeation chromatography (GPC), NMR, end group determination) was conducted.
In 2016, Islam et al. reported the first SIP of thiophene from semiconductor silicon nanocrystals (with a diameter of 11 nm) by a Kumada coupling polymerization.[139] They were the first who detached the polymer from the nanocrystals and analyzed the polymer end groups. However, polymer initiated in solution and detached polymer showed the same end groups and they were not able to determine the amount of polymer which was really attached to the surface. For the first time in 2016, de Roo et al. reported a SIP of fluorene and phenylene by a controlled Suzuki-Miyaura cross-coupling polymerization from the surface of CdSe/CdS QDs.[140] The QDs were functionalized in a X-type ligand exchange reaction with 4-bromophenylphosphonic acid for which a complete binding was proven by NMR spectroscopy. These QDs were reacted with a Pd/P^{t}Bu$_3$ source to form a surface confined initiator which initiated the polymerization of fluorene or phenylene from the surface (**Scheme 1.4**). Detached polymer showed mostly phenylphosphonic acid end groups which proved the polymerization from the surface. However, also a small amount of polymer was formed in solution.

Scheme 1.4. Grafting of PF8 from Pd(II)-functionalized nanocrystals by a surface initiated Suzuki-Miyaura Cross-Coupling polymerization. Reprinted with permission from ref.[140] Copyright **2016** American Chemical Society.

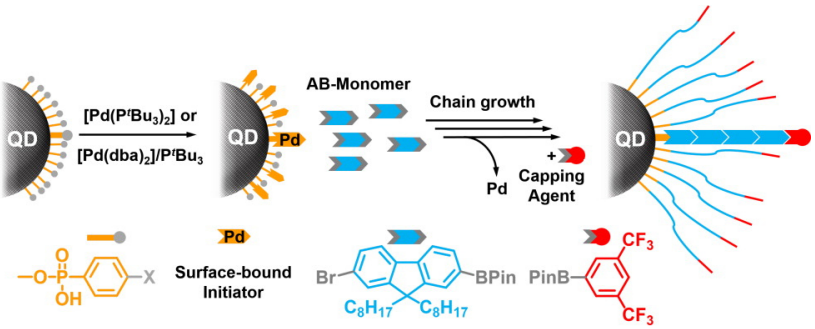

Overall, SIP approaches appear to be rather sensitive to conditions concerning their outcome, which limits their practical utility.

1.2.5 Hybrid Particles by a Direct Approach

All the methods and procedures presented so far separate the formation of the nanocrystals from the tethering of the conjugated polymer. Either ligand exchange reactions or subsequent grafting reactions are necessary which can be detrimental to the optical properties of the nanocrystals and are also time-consuming. Therefore, the use of functionalized conjugated polymers as ligand or precursor during the synthesis of the nanocrystals offers another convenient way to the formation of hybrid nanoparticles.

In 2014, de Roo et al. reported on the synthesis of phenylphosphonic acid and aniline-functionalized PF8 which was added during the synthesis of CdSe QDs. The polymer partially (10%) replaced the native ligand dodecylphosphonic acid or oleylamine, respectively.[113] Multi-wavelength analytical ultracentrifugation (MW-AUC) was used to determine the percentage of PF8 which is unambiguously tethered to the surface. The addition of an aniline-functionalized PF8 had basically no impact on the formation of the CdSe QDs, however, the polymer was also not bound to the QDs. In contrast, the addition of phenylphosphonic acid-functionalized PF8 broadened the size distribution of the QDs, but roughly 45% of the added polymer was bound to the nanocrystals. Due to solubility issues, the amount of PF8 added during the synthesis could not be increased. Moreover, in thin films quenching of the PF8 emission in the proximity of the QDs was observed – as anticipated.

Lin and co-workers synthesized a reactive P3HT Cd-precursor which was used for the synthesis of CdSe QDs.[114] CdO was complexed with 4-bromophenylphosphonic acid, and after replacing the bromide for an azide group, ethynyl-terminated P3HT was 'clicked' to the Cd salt. This polymer Cd-complex was used in a hot injection reaction as Cd-precursor. The obtained CdSe QDs P3HT hybrid material showed a strong quenching of the P3HT emission. However, the authors did not reveal how much of the polymer is indeed bound to the nanocrystals. Also, Luscombe et al. synthesized end-functionalized P3HT (**Scheme 1.5**) as reagent for the synthesis of CdSe QDs.[105] CdSe QDs were synthesized using Cd-oleate and selenium tri-*n*-butylphosphine as precursors. During the growth time of the QDs at 260 °C, various concentrations of the functionalized polymer were added, and upon reaction with Cd-oleate as displayed in **Scheme 1.5**, the formed P3HT-S-Cd species was incorporated into the CdSe nanocrystal. The binding of the polymer was elucidated by NMR and optical spectroscopy and the authors claim that around 70% of the polymer ends up on the surface of the QDs. A putative Förster resonance energy-transfer from the

polymer to QDs was observed by transient absorption spectroscopy and only takes place in these hybrid materials and not in a physical blend of its constituents.

Scheme 1.5. Reaction of end-functionalized polythiophene with a Cd-carboxylate. Adapted from ref.[105]

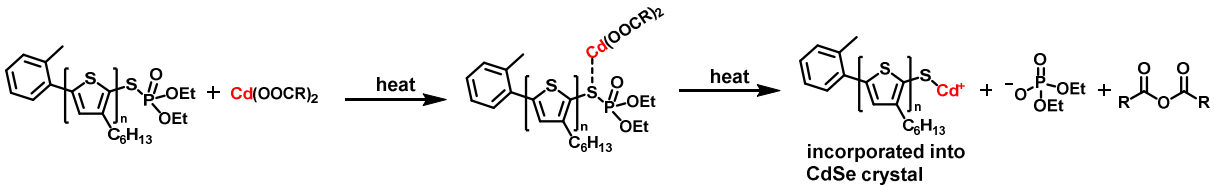

1.3 Encapsulation of Semiconductor Nanocrystals into Nanoparticles

Although the quality of semiconductor nanocrystals has significantly improved over the last years, they are still sensitive to environmental influences and against mechanical manipulation.[141,142,143] Additionally, their optical properties can suffer under ambient conditions due to photooxidation under light irradiation.[141,143] In order to prevent this, QDs are sandwiched between two high-grade oxygen/water barrier films in displays.[142] Another possible method for protection is spin-coating of a dilute QD dispersion mixed with a polymer solution.[87] Thereby, the QDs are embedded in a polymer matrix, but loose the benefits of their colloidal nature. Much effort has been taken to protect QDs in polymer or silica particles.[31,144,145] These options allow the QDs to retain their colloidal properties, their optical and mechanical stability is increased, and they become dispersible in water. For the use in single-photon sources, it is essential that only one semiconductor nanocrystal is encapsulated per polymer or silica particle. However, many reported embedding procedures result in the embedding of multiple QDs per particle.[33,146,147] For the use a single-photon sources, the shell must be of adequate thickness, density and rigidity to allow for mechanical manipulation and to ensure sufficient optical stability. On the other side, the shell should not be too thick which would be prohibitive for the positioning of the particles into plasmonic or photonic resonators.

1.3.1 Encapsulation into Polymer Nanoparticles

Heterophase polymerizations are the method of choice for the encapsulation of inorganic particles into polymer particles. Especially miniemulsion polymerizations allow for the direct encapsulation of lipophilic nanoparticles without the need for a preceding ligand

exchange to hydrophilic ligands.[148] The general procedure for such an approach is shown in **Scheme 1.6**. The QDs are mixed with a hydrophobic monomer, a hydrophobe and a radical initiator, and by applying high shear forces (e.g. by ultrasonication) this oil phase is dispersed into small droplets (50–500 nm) in which the lipophilic nanoparticles are distributed statistically. The subsequent polymerization is confined to the interior of the droplets and the nanocrystals are trapped in the forming particles because of their very low affinity towards the aqueous phase.

Scheme 1.6. Embedding of QDs into polymer nanoparticles by a miniemulsion polymerization.

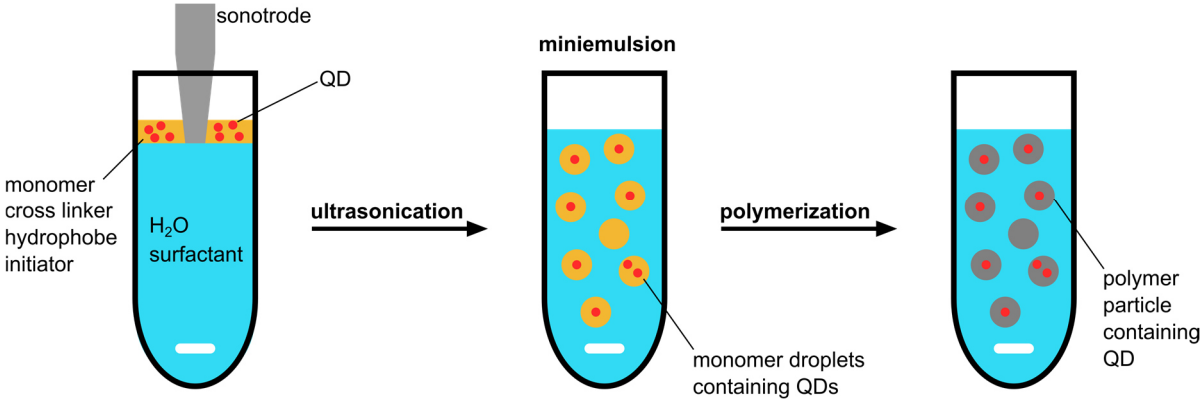

Fleischhaker et al. encapsulated CdSe/ZnS QDs into polystyrene (PS) particles by a miniemulsion polymerization.[149] They observed a tendency of the QDs to accumulate at the particle surface, therefore the PS particles were coated by an additional poly(methyl methacrylate) (PMMA) shell which confined the QDs to the PS core. Joumaa et al. also encapsulated CdSe/ZnS QDs into PS spheres; however, most PS particles contained agglomerated QDs near/at their surface.[147] Unfortunately, both reports did not provide any QYs of their dispersions. Negele et al. succeeded in encapsulating CdSe/CdS QDs into PMMA particles (**Figure 1.3**). A high QY was maintained during the embedding process while the optical stability of the QDs was significantly increased allowing for high excitation densities in single-particle PL measurements.[30]

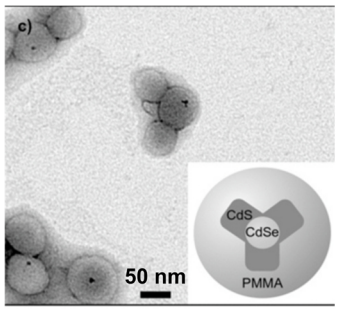

Figure 1.3. CdSe/CdS QDs embedded into poly(methyl methacrylate) nanoparticles. Reprinted with permission from ref.[30] Copyright **2013** WILEY-VCH Verlag GmbH & Co. KGaA, Weinheim.

Tjaard de Roo showed that the stability of the particles can be further increased by cross-linking the polymer shell.[150] These particles are mechanically very robust and can be moved with the tip of an atomic force microscope, and for example placed in a bulls eye resonator.[34] De San Luis et al. employed cross-linked PS particles to encapsulate CdSe/ZnS QDs and reported that the fluorescence loss over time is minimized by the deposition of an additional PMMA shell.[31] By TEM tomography, it was proven that the QDs are mostly located at the interface of both polymer materials.

QDs can also be encapsulated into polymer particles by a secondary dispersion approach. The QDs and a preformed polymer are dispersed/dissolved in a common good solvent and the solution is injected into a non-solvent containing surfactant.[150,151] Small particles can be obtained by applying high shear forces afterwards or by fast mixing under turbulent flow. However, the encapsulation by miniemulsion polymerizations has proven to be superior in terms of embedding statistics and stability. For the use as single-photon source, it is important that the particles contain exactly one emitter. Empty particles are unproblematic, however, the placement of the particles into a resonator system involves pre-selection of QD-containing particles in any case.

Besides the few reports about the encapsulation of spherical QDs into polymer particles, there a no reports describing the encapsulation of the commonly used CdSe/CdS NRs into polymer particles.

1.3.2 Encapsulation into Silica Nanoparticles

The encapsulation of semiconductor nanoparticles into silica particles has the benefit that silica materials are intrinsically compatible with biological environments which is a requirement for the use of QDs in bio-imaging applications.[33,152,153] Moreover, silica surfaces are easy to functionalize, non-toxic and silica is optical transparent and chemically inert.[154]

Monodisperse silica particles can be obtained by the “Stöber process” which is based on a sol-gel reaction.[155] This process can also be used to embed semiconductor nanocrystals.[146] However, mostly raisin-bun like particles with many QDs per silica particles were obtained, and as prerequisite the hydrophobic ligands of the nanocrystals must be exchanged to hydrophilic ones beforehand. Such a complete ligand exchange often leads to the deterioration of the optical properties.[156] Single QDs embedded in silica spheres were obtained by a reverse microemulsion process, circumventing the need for a preceding ligand exchange.[154] In most procedures, the QDs are dispersed in a mixture of

cyclohexane and a non-ionic surfactant such as Igepal CO-520 (pentaoxyethylene nonylphenyl ether). A silica precursor such as tetramethoxysilane (TMOS) or tetraethoxysilane (TEOS) is added and the microemulsion is generated by the addition of an aqueous ammonia solution. The semiconductor nanocrystals act as seeds for the silica growth and are thereby embedded into a silica shell. Its thickness can be tuned by the reaction parameters.[145,154,157,158] Using this method, it was also possible to grow silica shells around anisotropic CdSe/CdS NRs.[144,159,160,161] For the use as single-photon sources, the embedding into silica spheres is promising as the semiconductor nanocrystal multiplicity per particles can be effectively controlled so that around 99% of the silica particles contain exactly one QD (**Scheme 1.7**).

Scheme 1.7. Left and Center: Embedding of CdSe/CdS nanorods into thin silica shells by a micro-emulsion approach. Reprinted with permission from ref.[144] Copyright **2017** American Chemical Society. Right: Encapsulation of CdSe/ZnS QDs into a silica-polymer dual layer. Reprinted with permission from ref.[145] Copyright **2010** American Chemical Society.

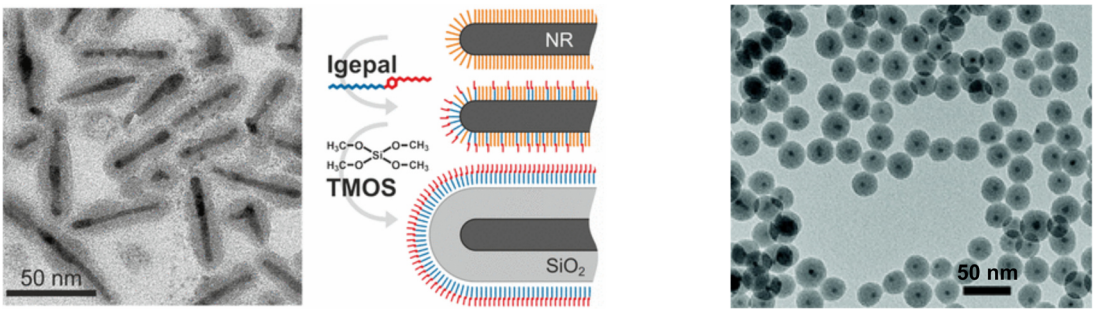

Unfortunately, CdSe/CdS QDs embedded in a silica sphere have proven to be less bright in single-particle fluorescence measurements than QDs embedded into PMMA particles. However, the maximum excitation power for QDs encapsulated into silica particles is significantly higher than for QDs embedded into PMMA particles (17 µW vs. 1.4 µW).[150]

The mechanism of the encapsulation process comprises a major barrier for the embedding of nanocrystals functionalized with conjugated polymers. The suggested mechanism how individual hydrophobic nanoparticles end up in the core of hydrophilic reverse micelles formed by Igepal in non-polar solvents is the following: The added surfactant partially replaces the native ligands. Afterwards, the hydrolysis of the tetraalkoxysilane takes place in the hydrophilic region near the nanocrystal's surface created by the surfactant. Partially hydrolyzed TMOS or TEOS replaces the ligands of the semiconductor nanocrystal and the nanocrystal acts as seed for the silica growth. After the silica growth, the native ligands of the nanocrystals — even strongly bound phosphonic acids — are completely removed from the surface of the nanocrystals

(**Scheme 1.7**, center).[144,157,160] This would also apply to bound conjugated polymers, thus reversing the tedious functionalization of the nanocrystals. The partial or complete replacement of PF8 from CdSe/CdS QDs during the embedding in silica was also observed by Tjaard de Roo.[150] Therefore, this method was not pursued for the encapsulation of hybrid nanocrystals and only the encapsulation into polymer particles was investigated in this thesis.

2 Scope of the Thesis

Hybrid particles formed by tethering organic conjugated polymers to inorganic semiconductor nanocrystals are an interesting nanomaterial due to possible charge and/or energy transfer processes between the two materials. Such particles are promising for utilization in opto-electronic devices and as single-photon sources.

In this work, synthetic routes to hybrid particles consisting of high-quality semiconductor nanocrystals and precisely functionalized conjugated polymers were evolved and further developed. For the use as single-photon source and to perform quantum-optical measurements on the single-particle level, semiconductor nanocrystals of high optical stability and quality were needed. Thus, the synthesis of CdSe-based core-shell quantum dots and anisotropic dot-in-rod nanorods of excellent optical quality and stability was pursued (**Chapter 3**). In order to enable a controlled functionalization of the nanocrystals and to facilitate the subsequent encapsulation into polymer nanoparticles, novel conjugated polymer ligands were required. To this end, the synthesis of new phosphonic acid end-functionalized conjugated nonconjugated diblock and multi-valent comb copolymers based on polyfluorene was evolved by a straightforward combination of controlled catalytic chain growth polymerization and controlled radical polymerization (**Chapter 4**). The synthesis of hybrid particles was pursued by direct ligand exchange reactions and novel direct approaches (**Chapter 5**). Therein, the binding strength of various functionalized polyfluorenes was explored.

To ensure a high optical and especially mechanical stability while maintaining their colloidal nature, encapsulation methods for the embedding of (hybrid) nanocrystals into polymer nanoparticles were elaborated (**Chapter 6**). The optical properties of the embedded (hybrid) nanocrystals were studied by ensemble photoluminescence and photoluminescence excitation measurements. The charging of the inorganic emitter by charge transfer processes between the conjugated polymer and the nanocrystal was analyzed in single-particle photoluminescence spectroscopy studies.

3 Multi-Shell Semiconductor Nanocrystals

3.1 Introduction

Amongst the range of possible applications, semiconductor nanoparticles are attractive as a fluorescent material in displays and have already been employed on the industrial scale.[48,49,50] Moreover, they can be used as efficient single-photon sources and represent a promising resource for future quantum technologies.[21,22,162,163] The prototype of these semiconductor nanoparticles are CdSe QDs and especially CdSe/CdS core-shell nanoparticles are unarguably the most studied model core-shell hetero system. The popularity of this system is based on the following features: CdSe and CdS only show a minimal crystal lattice mismatch (3.9%), which enables the synthesis of highly fluorescent core-shell heterostructure.[87,164] For this core-shell system many highly optimized and established synthetic procedures are available.[86,87,165,166] At room temperature, CdSe/CdS normally forms a quasi-type-2 band alignment (**Scheme 1.1**) with a strongly confined hole and loosely confined electron.[84,85,167] The tunable emission color of the CdSe/CdS nanoparticles covers a large portion of the visible spectrum. Additionally, CdSe/CdS QDs have proven to be well suited for single-particle micro photoluminescence (PL) studies (**Chapter 6.4.5**)[34,168], therefore the semiconductor nanoparticles employed in this thesis consist of CdSe/CdS core-shell structures.

Today, not only synthetic procedures for the synthesis of quasi-spherical CdSe/CdS QDs are available but also procedures for anisotropic CdSe/CdS nanoparticles such as nanorods (NRs) or tetrapods.[169] Compared to their spherical counterparts CdSe/CdS NRs offer some advantages: NRs have giant absorption cross sections below λ = 500 nm due to efficient light absorption by the huge CdS volume.[169] Moreover, they have recently been identified as promising single-photon emitters, which can exhibit efficient trion emission due to reduced Auger recombination.[2,170,171] Furthermore, they feature a dipole moment[172] along their long axis which can be used to align them for example in an electric

field. Aligned NRs show a polarized emission[4,173] and are interesting as optical gain medium for lasers.[174] Also in terms of charge transport NRs are superior to spherical QDs as the long axis of the NRs provides a continuous pathway for electron transport.[13,175] These benefits make NRs attractive for single-particle PL studies. Therefore, one task pursued in this thesis was to synthesize CdSe/CdS NRs according to existing procedures (**Chapter 3.2.4**), functionalize them with conjugated polymers (**Chapter 5.4.6–5.4.7**), and find a way to encapsulate them into polymer nanospheres (**Chapter 6.2.3**). A second scope of this chapter was the synthesis of CdSe/CdS QDs with improved optical properties as compared to the QDs which have already been established in the group.

3.2 Results and Discussion

In the following the synthesis of different semiconductor materials is discussed briefly. The synthesis of these materials relies on literature-known procedures; however, the reproduction of these syntheses is nevertheless challenging as the published procedures often lack details. Moreover, the synthesis of nanoparticles is highly sensitive to often unknown impurities in reagents and operational procedure.

3.2.1 Synthesis of CdSe Seed Particles by Two Different Methods

The core material of all semiconductor materials used in this thesis consists of CdSe. Semiconductor nanoparticles based on CdSe are the most studied, highly optimized procedures for their synthesis are available and their optical properties in terms of photoluminescence are unmatched. As the core-shell nanoparticles are intended for the analysis in a single-particle micro-PL set-up (**Chapter 6.4.5**), the final fluorescence wavelength of the nanoparticles has to be in the range of 580–650 nm due to set-up specifications. This requires the CdSe particles to be in a size range of roughly 3.2–4.5 nm. The synthesis of CdSe nanoparticles which are later used as seed particles for core-shell nanoparticles were synthesized by two different hot-injection reactions (**Scheme 3.1**). In method A, CdO was complexated by 6 equiv. of oleic acid. To the formed Cd-oleate, the strong X-type ligand dodecylphosphonic acid (DOPA) was added in excess (3.6 equiv.). As Se source TOP-Se in oleylamine was used.

Scheme 3.1. Synthesis of CdSe seed particles by two different methods.

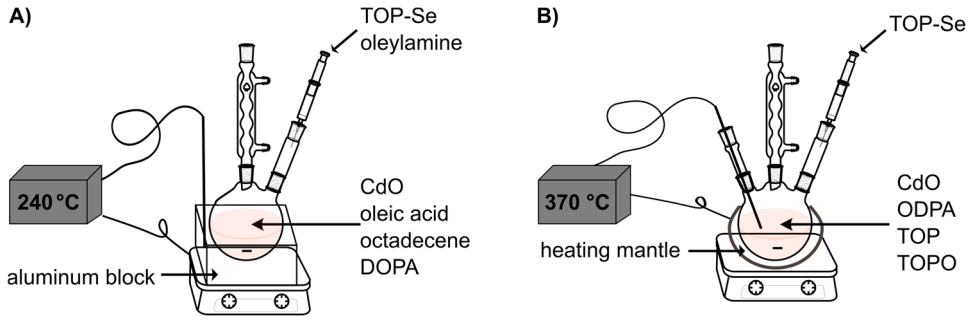

TOP: tri-*n*-octylphosphine; DOPA: 1-dodecylphosphonic acid; ODPA:1-octadecylphosphonic acid; TOPO: tri-*n*-octylphosphine oxide.

The hot-injection took place at a temperature of 240 °C and the QDs were grown at this temperature until the desired size was reached (**Figure 3.1**). The synthesis of CdSe QDs following this method was successful as the absorption spectra show well resolved and narrow transitions bands (e.g. half width at half maximum (HWHM) on the low energy side of the first exciton transition = 15 nm for 7.15 min growth time). Moreover, the photoluminescence (PL) peaks of the QDs are relatively narrow with a full width at half maximum (FWHM) between 29–30 nm.

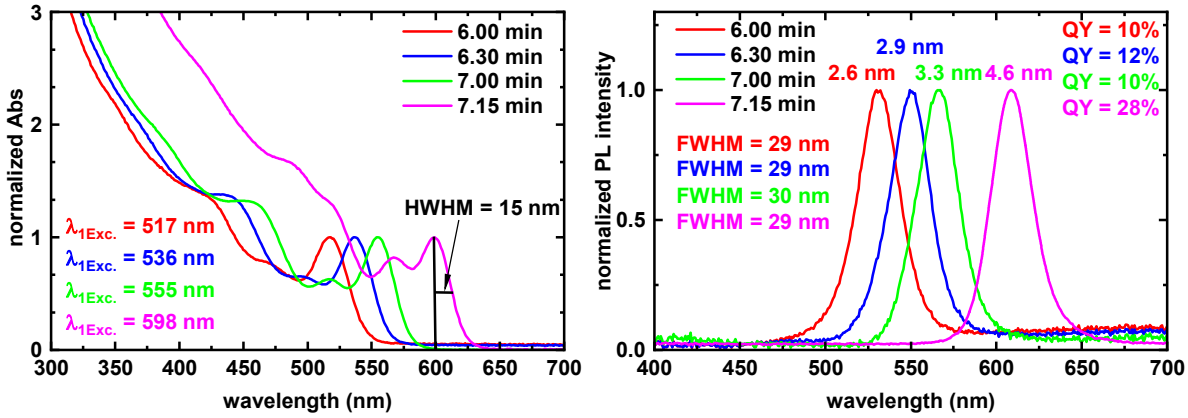

Figure 3.1. Absorption and PL spectra of CdSe QDs synthesized according to method A. λ_{exc} = 380 nm for PL and QY measurements. Sizes are diameters according to UV-VIS spectra. $\lambda_{1.Exc}$ = wavelength of the first exciton absorption peak.

For CdSe nanoparticles, these QDs show a high QY of around 10% for the smaller particle samples and even up to 28% for the largest particles. The increase in QY with size is expected as the percentage of surface atoms decreases drastically with increasing size. Moreover, the homogeneity and crystallinity of the QDs can be seen in the TEM images (**Figure 3.2**). The obtained QDs are not perfectly spherical but slightly anisotropic with a circularity (C) of 0.8 (**Chapter 3.4.2**). In general, the size of the nanoparticles as

determined by UV-VIS spectroscopy using the position of the first exciton absorption peak[176] and the size as measured by TEM matched well. Therefore, in terms of simplicity the size of CdSe-seed particles for the synthesis of core-shell nanoparticles was determined by UV-VIS spectroscopy throughout this thesis.

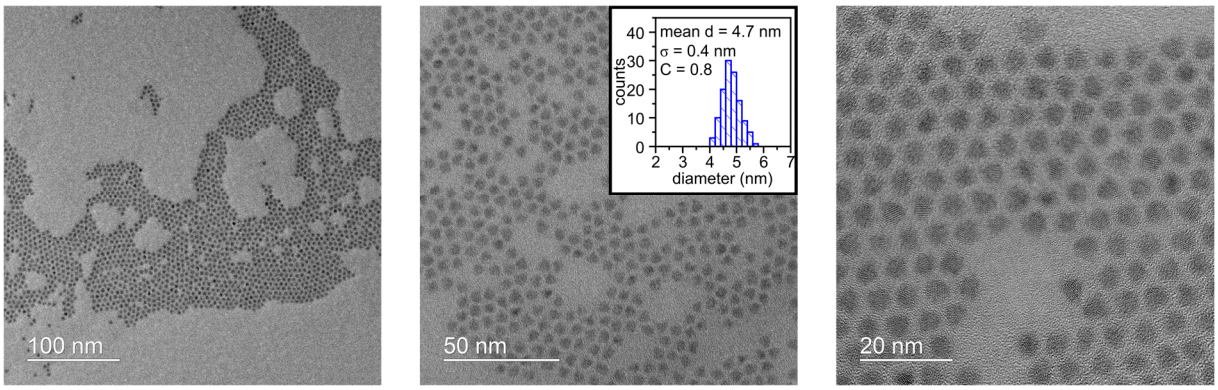

Figure 3.2. Exemplary TEM images of CdSe seed particles synthesized according to method A with a growth time of 7.15 min. The mean diameter (d), the standard deviation (σ), and the circularity (C, see **Chapter 3.4.2** for definition) are given in the size histogram inset.

Most reported procedures for the synthesis of high-quality CdSe-based core-shell nanoparticles employ Wurtzite-type CdSe QDs synthesized according to a procedure which was developed by Manna and co-workers.[4] In this procedure (method B in **Scheme 3.1**), CdO was complexated with only 1.8 equiv. of octadecylphosphonic acid (ODPA) employing TOPO as coordinating solvent. After complexation, TOP was added, and water was liberated. As Se source TOP-Se was used, but no oleylamine was employed. The hot-injection was performed at 370 °C which led to a very fast growth of the CdSe nanoparticles. According to Manna and co-workers a growth time of 3 min leads to QDs emitting in the red regime. We observed that a significantly shorter growth time in the range of 25 s to 40 s was sufficient to yield QDs in the desired size range of 3.5 nm to 4 nm (**Figure 3.3**). The QDs in this size range feature very narrow emission linewidths with a FWHM of 23–25 nm and sharp absorptions bands (HWHM on the low energy side of the first exciton transition 10–12 nm).

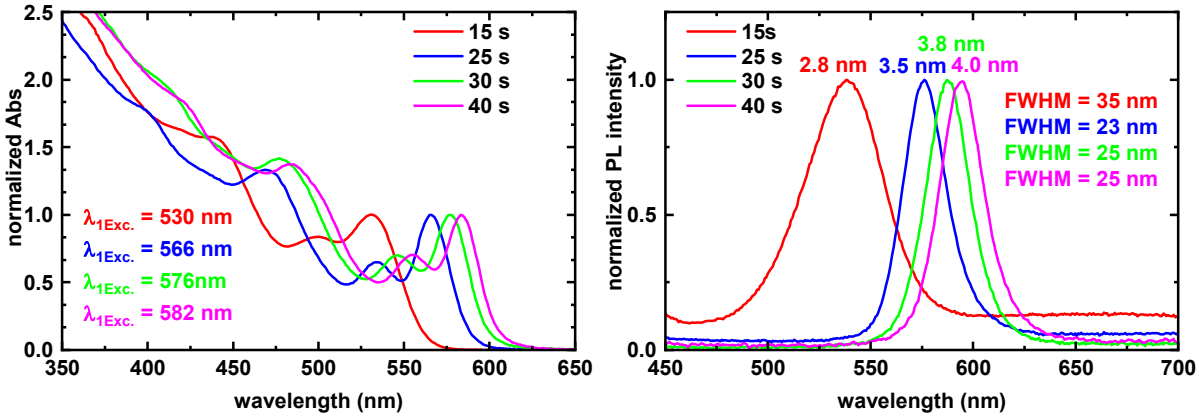

Figure 3.3. Absorption and PL spectra of CdSe QDs synthesized according to method B. $\lambda_{exc.}$ = 380 nm for PL and QY measurements. Sizes are diameters according to UV-VIS spectra. QYs are below 5% for these QDs.

Also, TEM (**Figure 3.4**) measurements confirmed the formation of very uniform nanoparticles with a narrow size distribution (6% relative standard deviation). Also, these QDs showed a slight anisotropy (C = ~0.8). The fluorescence properties of these QDs were poor and the QY was normally below 5%. In the synthesis of CdSe QDs according to method A, oleic acid (6 equiv. vs. Cd), DOPA (3.6 equiv. vs. Cd) and oleylamine (4 equiv. vs. Cd) are used as stabilizing ligands. Here, only 1.8 equiv. of ODPA is used and the surface of the QDs is not fully saturated by ligands which explains the low QY. The difference in growth kinetics as compared to the literature was most probably caused by the amount of water present in the system. Kirkwood et al. recently reported that even small amounts of protic additives drastically affect the pathway and growth kinetics of CdSe nanoparticles.[177]

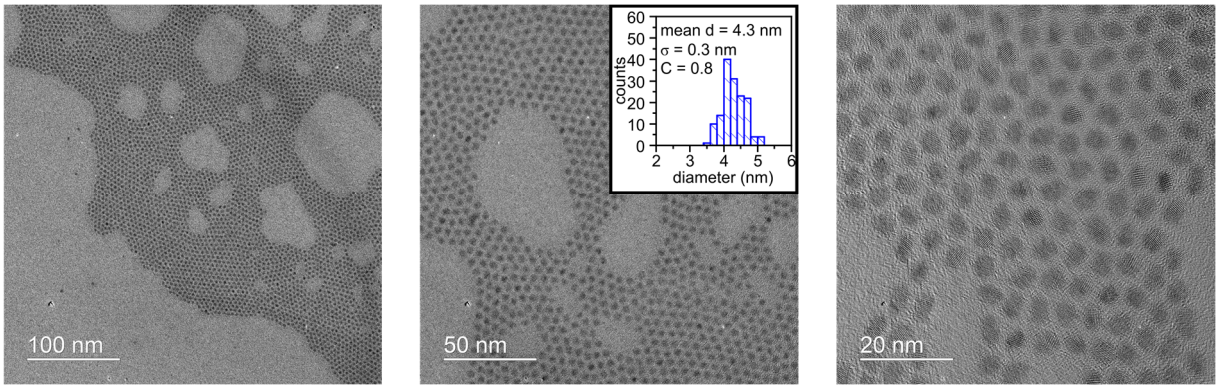

Figure 3.4. TEM images of an exemplary batch of CdSe seeds synthesized according to method B at different magnifications.

The drawback of such a short growth time is that it becomes practically very difficult to synthesize two batches of CdSe QDs with exactly the same size. Therefore, the water, which is released during the complexation of CdO, was removed by applying vacuum for 30 min after TOP had been added to the reaction mixture. Thereby, the growth of the nanoparticles was slowed down significantly (**Figure 8.1**, e.g. 140 s growth time for red fluorescent QDs). However, in general particles with a much broader size distribution (HWHM of the first absorption peak 17–25 nm) were obtained by this approach. As CdSe seed batches with unsuitable broad size distributions cannot be used for further studies and had to be discarded, the water removal step was omitted during the syntheses of these CdSe seed particles.

3.2.2 CdSe/CdS Core-Shell Quantum Dots

The optical properties of CdSe QDs can be greatly improved in terms of QY as well as concerning optical and chemical stability by the deposition of a CdS shell. CdSe/CdS QDs are by far the most studied core-shell QD system. CdSe/CdS QDs synthesized by a successive ionic layer adsorption and reaction (SILAR) process have proven to be well suited for single-particle PL studies in the group of Professor Alfred Leitenstorfer in the Department of Physics at the University of Konstanz.[34,168] The synthesis used here is based on a synthesis by Dubertret and co-workers which was optimized by Carla Negele and Tjaard de Roo during their dissertations,[86,150,178] the main difference being the use of dodecylphosphonic acid (DOPA) instead of tetradecylphosphonic acid in the synthesis of the CdSe seeds. CdSe QDs (synthesized according to method A) were used as seed particles and sulfur and Cd-oleate were used as CdS precursors (**Scheme 3.2**). At 240 °C the precursors were sequentially added to the seed particles (1 mono layer per addition cycle, 6 cycles), the last injection consisting of Cd-oleate in order to achieve a Cd-rich surface to which X-type ligands such as phosphonic acids can bind more strongly.

Scheme 3.2. Schematic illustration of the SILAR process used for the synthesis of CdSe/CdS QDs.

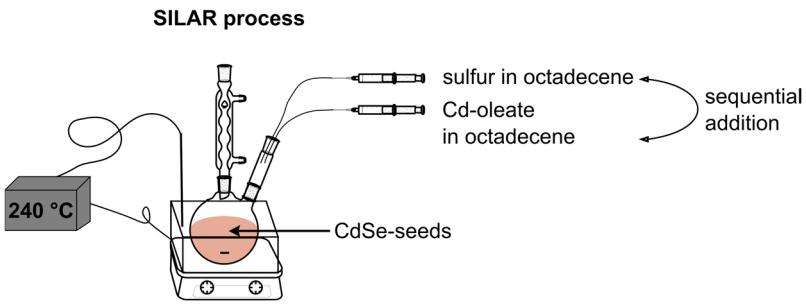

The synthesis showed a good reproducibility in terms of size, size distribution and absence of secondary nucleation. However, a significant fluctuation of the QY of the CdSe/CdS QDs synthesized by this SILAR process was observed (ranging from 30% up to 61%, 11 successful syntheses) and the average QY of these QDs was only 42%. The obtained QDs were not spherical (circularity of 0.8) and exhibited a nonuniform distribution of shapes, e.g. pyramids, spheres, prism, cubic structures and tripods (**Figure 3.5**). The growth of the CdS shell caused a significant red shift of the PL maximum in the range of 35 nm which is due to the formation of quasi-type-2 heterostructure at room temperature where the electron wave function is partially spread into the shell.

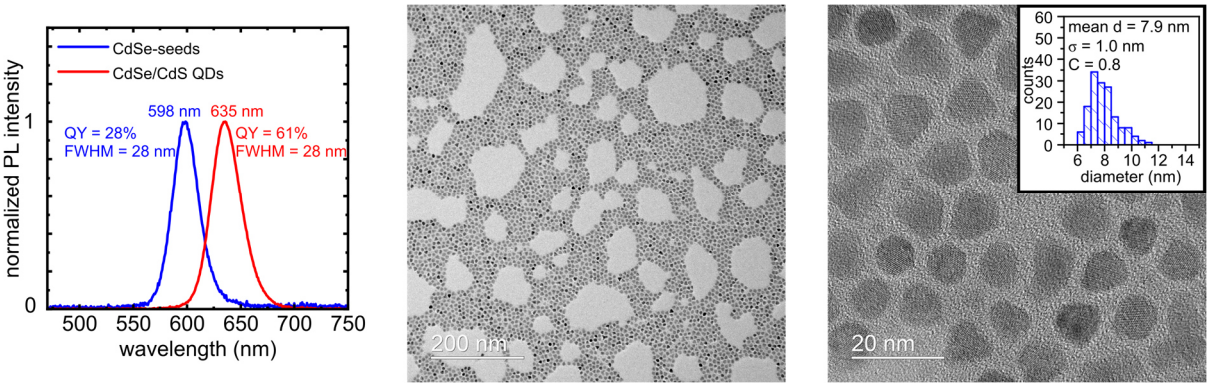

Figure 3.5. PL spectra ($\lambda_{exc.}$ = 380 nm) and TEM images of CdSe/CdS QDs synthesized according to a SILAR process.

3.2.3 Graded-Shell CdSe/$Cd_xZn_{1-x}S$ Quantum Dots

The CdSe/CdS synthesized according to the SILAR process (**Chapter 3.2.2**) are of good quality, however, nowadays procedures are available which yield better QDs in terms of QY, optical stability and blinking behavior. In 2013, Bawendi and co-workers showed that CdSe/CdS QDs synthesized by using Cd-oleate and octanethiol as CdS precursors which are slowly and simultaneously added to CdSe seeds at a high temperature of 310 °C outperform CdSe/CdS QDs synthesized by a conventional SILAR process in every aspect.[87] Independently, Boldt et al. reported a similar procedure (**Scheme 3.3**) for the synthesis of highly stable graded-shell CdSe/$(CdS)_x(ZnS)_y$ (x,y: number of monolayers; the formula is also written as CdSe/$Cd_xZn_{1-x}S$ to account for the graded-shell) QDs.[1]

Scheme 3.3. Synthesis of graded-shell CdSe/$(CdS)_x(ZnS)_y$ QDs.

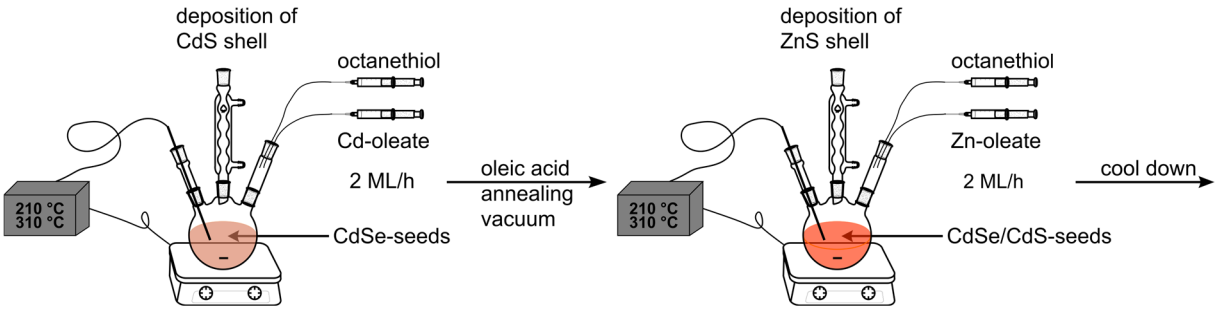

At the deposition temperature of 310 °C, an alloying between the CdS and ZnS shell takes place, which allows switching between quasi-type-2 and type-1 band alignment depending on the amount of precursors used. In PL measurements, the graded-shell particles were reported to possess a higher stability in terms of photobleaching, against quenching agents and less blinking as compared to CdSe/CdS QDs. Remarkably, already 2–4 monolayers (ML) of CdS in combination with 2–4 ML of ZnS are sufficient to yield very stable and robust particles. In the case of CdSe/CdS QDs thicker shells (> 6 ML) are necessary due to lack of electron confinement. Regarding the envisioned charging of QDs by a charge transfer with a conjugated polymer Cotlet and co-workers reported that a thinner shell facilitates charge transfer processes.[123] Therefore, one aim of this thesis was to reproduce the synthesis of these graded-shell QDs and functionalize them with polyfluorene (**Chapter 5.2.2**).

Four different combinations of graded-shell nanoparticles were synthesized (2 ML CdS, 2 ML ZnS; 2 ML CdS, 4 ML ZnS; 4 ML CdS, 2 ML ZnS; 4 ML CdS, 4 ML ZnS). The amount of precursor solution was calculated from the CdSe seed size and desired shell thickness (thickness of 1 ML CdS = 0.337 nm; thickness of 1 ML ZnS = 0.312 nm) assuming a quantitative conversion of Cd and Zn precursor, respectively. The precursor solutions were added with a syringe pump adding the equivalent of 2 MLs per hour.

In all four experiments, highly fluorescent dispersions were obtained (**Figure 3.6**). The QYs ranged from 67% up to 87% and were much higher than for CdSe/CdS QDs synthesized according to the SILAR process (average QY 42%). Only the sample CdSe/$(CdS)_2(ZnS)_4$ had a QY below 80%, which is likely due to the high amount of ZnS compared to CdSe and CdS which induces strain on the nanoparticle due to the lattice mismatch between the materials.

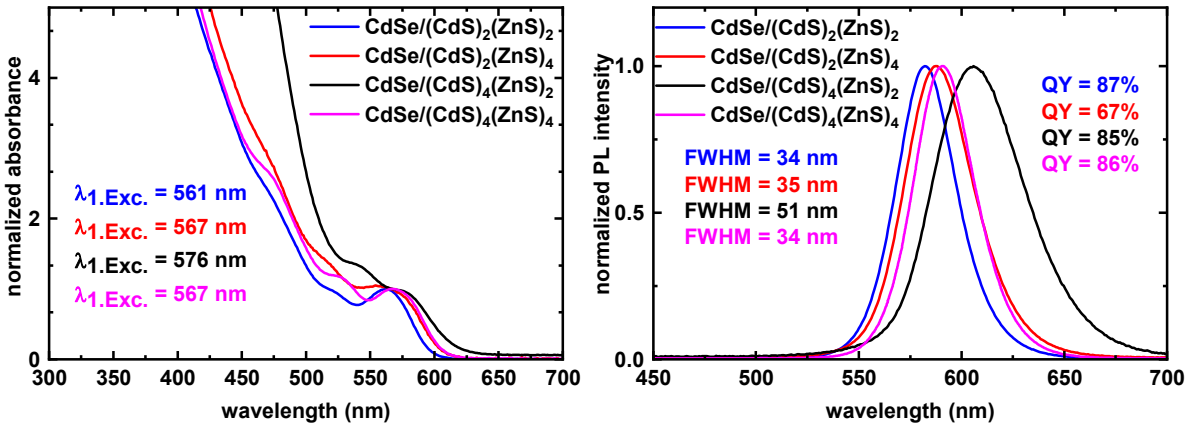

Figure 3.6. Absorption and photoluminescence spectra of $CdSe/(CdS)_x(ZnS)_y$ QDs. All four batches were synthesized using the same batch of CdSe seeds with a size of 3.3 nm. $\lambda_{exc.}$ = 380 nm for PL and QY measurements.

The FWHM of the emission peak is in the range of 35 nm, only for the sample consisting of 4 ML of CdS and 2 ML of ZnS a very broad emission peak (FWHM of 51 nm) was observed. However, the sample still showed a high QY of 85%. Relatively broad emission peaks were also reported occasionally in literature upon deposition of the ZnS shell.

The crystallinity and uniformity of the nanoparticles can also be seen in the TEM pictures (**Figure 3.7**). The particles possess a narrow size distribution (~10%) and form superlattices on the TEM grid upon drying which also indicates the high quality of the particles.

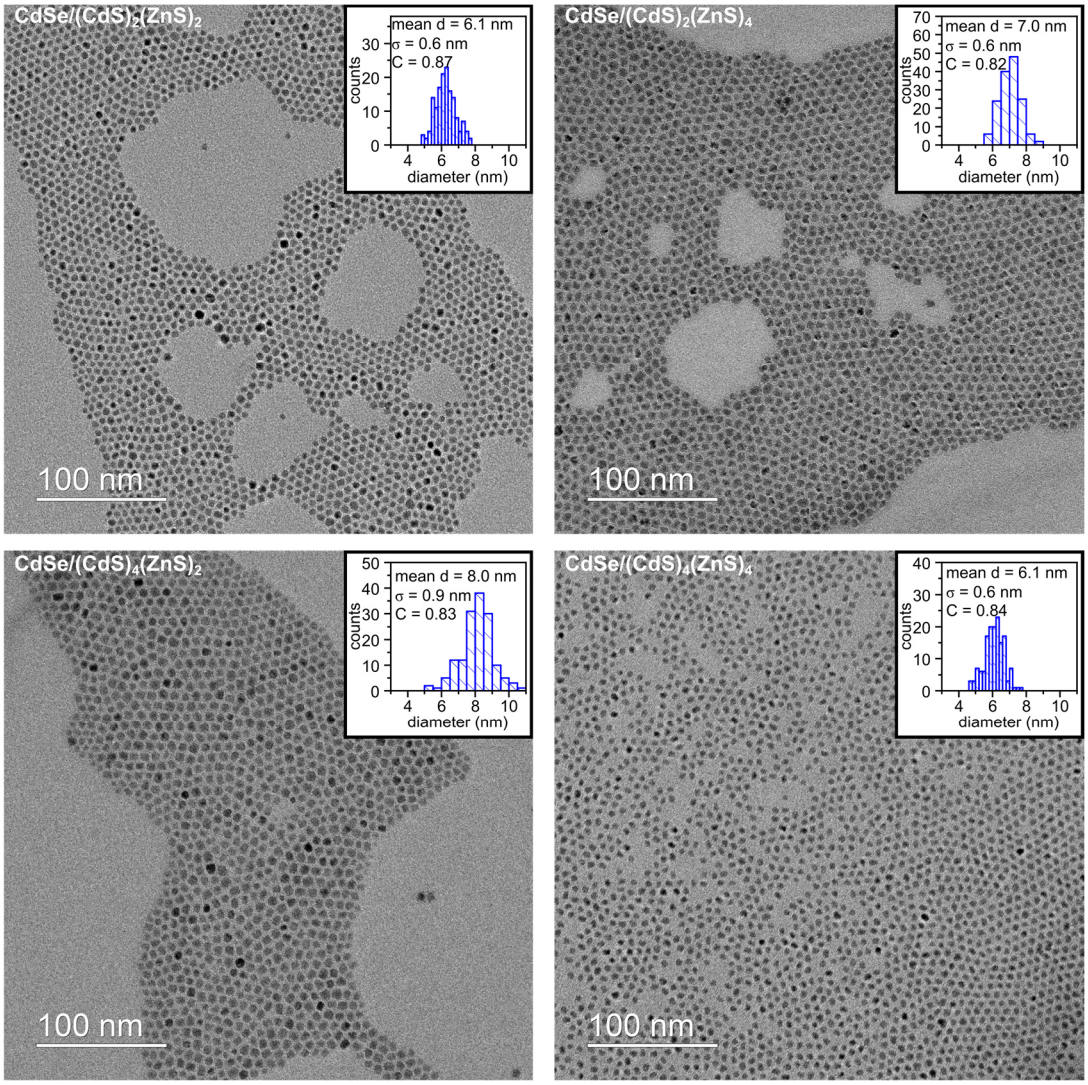

Figure 3.7. TEM images of CdSe/$(CdS)_x(ZnS)_y$ QDs. Additional high-magnification TEM images of the four different CdSe/$(CdS)_x(ZnS)_y$ QD batches are shown in the appendix (**Figure 8.2**).

The size of the QDs (according to TEM) 6.1 nm (theoretically 5.9 nm), 7.0 nm (theoretically 7.2 nm), 8.0 nm (theoretically 7.3 nm) and 6.1 nm (theoretically 8.5 nm) fit well to their theoretical size (calculated from the size of the CdSe seed particles and the added amount of CdS-precursor and ZnS-precursor), only for the sample consisting of 4 ML of CdS and 4 ML of ZnS the particles are significantly smaller than expected.

For the functionalization with PF8 by a direct approach (directly during the synthesis), particles with 2 ML of CdS and 2 ML of ZnS were considered most suited because of their thin shell which might facilitate a charge transfer process between the polymer and the inorganic emitter. For this shell composition, an analysis was performed whether indeed a confinement of the electron wave function to the core takes places (**Figure 3.8**). The deposition of the CdS shell onto the CdSe core caused a red shift of 26 nm of the PL maximum and a red shift of 23 nm of the 1S transition in the absorption spectra. This red

shift was nearly compensated by the addition of a 2 ML thick shell of ZnS. The 1S absorption was blue shifted by 17 nm and the PL maximum by 11 nm. The addition of the ZnS indeed led to a confinement of the electron wavefunction to the core which might be beneficial for the intended optical applications.

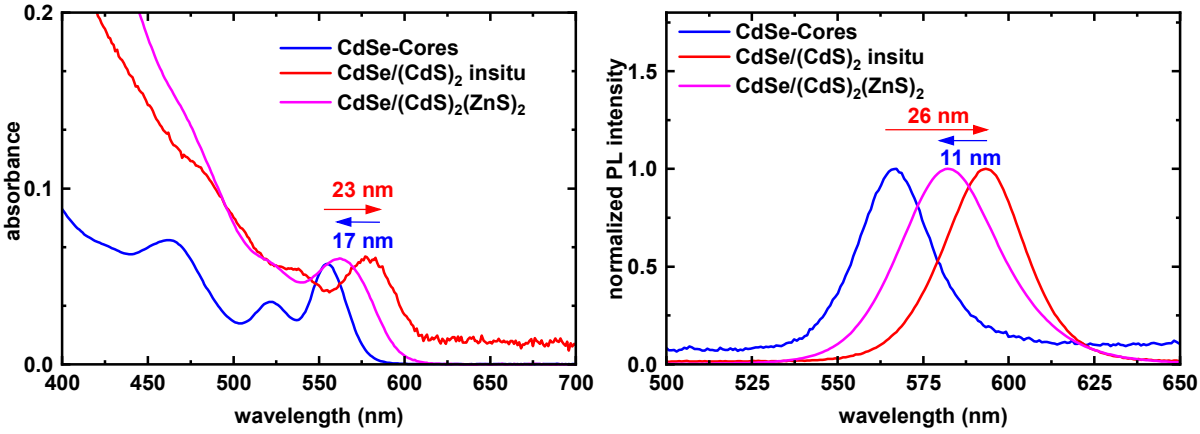

Figure 3.8. Absorption (left) and PL spectra (right) of CdSe seed particles, *in situ* formed $CdSe/(CdS)_2$ particles and the final graded-shell $CdSe/(CdS)_2(ZnS)_2$ QDs. $\lambda_{exc.}$ = 380 nm for PL measurements.

3.2.4 CdSe/CdS and CdSe/CdS/CdS Nanorods

The state of the art synthesis of uniform and high-quality CdSe/CdS NRs was developed by Manna and co-workers in 2007.[4] The synthesis is based on a seeded growth method. CdSe QDs act as seed particles for a homogeneous nucleation of CdS and a so called "dot-in-rod structure" is formed (**Scheme 3.4**). The aspect ratio of the rods can be adjusted by the amount of CdO and sulfur used. However, mainly the length of the NRs is changed, whereas the diameter stays nearly constant for different aspect ratios. The NRs are elongated along the unique c-axis of the wurtzite crystal structure. The anisotropic growth of the NRs in the [0001] and [000$\bar{1}$] direction of the wurtzite crystal structure is caused by employing a precise mixture of octadecylphosphonic and hexylphosphonic acid and a certain precursor concentration.[179,180] As anion-rich (000$\bar{1}$) planes exhibit a higher growth rate as compared to cation-rich (0001) planes in this electron donating ligand mixture, the seed dot is not located in the center of the rod.[180]

Scheme 3.4. Synthesis of CdSe/CdS nanorods by the seeded growth method. Depending on the amount of CdS precursors used, nanorods of different aspect ratios are yielded.

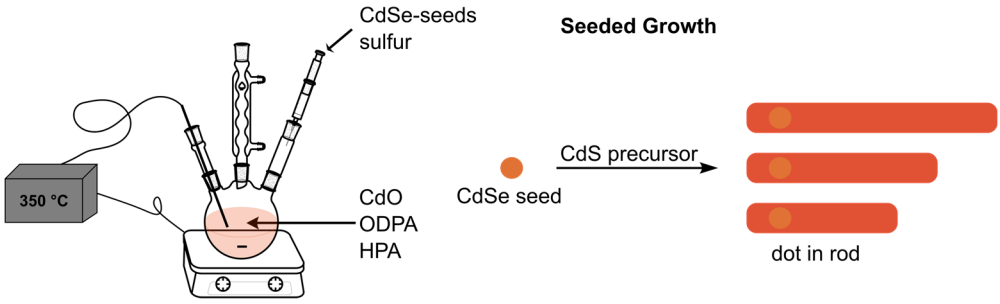

For the synthesis of CdSe/CdS NRs, CdSe seeds synthesized according to method B were employed. Following the protocol by Manna and co-workers, high-quality CdSe/CdS NRs were obtained (**Figure 3.9**). NRs with a length between 20 nm and 38 nm were synthesized. Longer NRs were not synthesized as the QY of the NRs decreased with increasing length (QY (20 nm) = 52%; QY (38 nm) = 26%). However, the QYs were lower as compared to literature values reporting a QY of up to 70% for the short NRs. The deposition of the CdS caused a red shift of the first exciton transition (30–33 nm) in the absorption spectra and of the PL maximum (24–26 nm). As in the case of CdSe/CdS QDs a quasi-type-2 heterostructure was presumably formed. The PL peaks stayed narrow (FWHM of 25–27 nm) during the rod formation and were comparable with the width of the PL peak of the seed particles (FWHM 25 nm). The absorption spectra feature well-resolved first exciton transitions and below λ = 500 nm, the absorption is dominated by the CdS shell. The strong interaction between the NRs and their tendency to form superstructures can be seen in the TEM images, where densely packed rows of rods formed during deposition on the TEM grid. Compared to the procedure reported in literature, it was also possible to up-scale the reaction by a factor of 1.5 without detrimental effects on the properties of the NRs.

In the past, CdSe/CdS QDs with a core synthesized according to method A, have proven to be well suited for single-particles PL studies. Therefore, it was also probed if NRs can be synthesized employing those seed particles. However, using the same conditions as before for the synthesis of rods with an expected length of 20 nm, elongated particles (**Figure 8.3**) showing different shapes were formed and the FWHM of the PL peak broadened to 38 nm. Presumably, no defined rods were formed, as the two different types of seed particles have a totally different surface chemistry and even small changes in the composition and concentration of the ligands can have a tremendous impact on the

formation of nanoparticles. As high-quality NRs were obtained following the literature-known procedure, the second method was not further investigated.

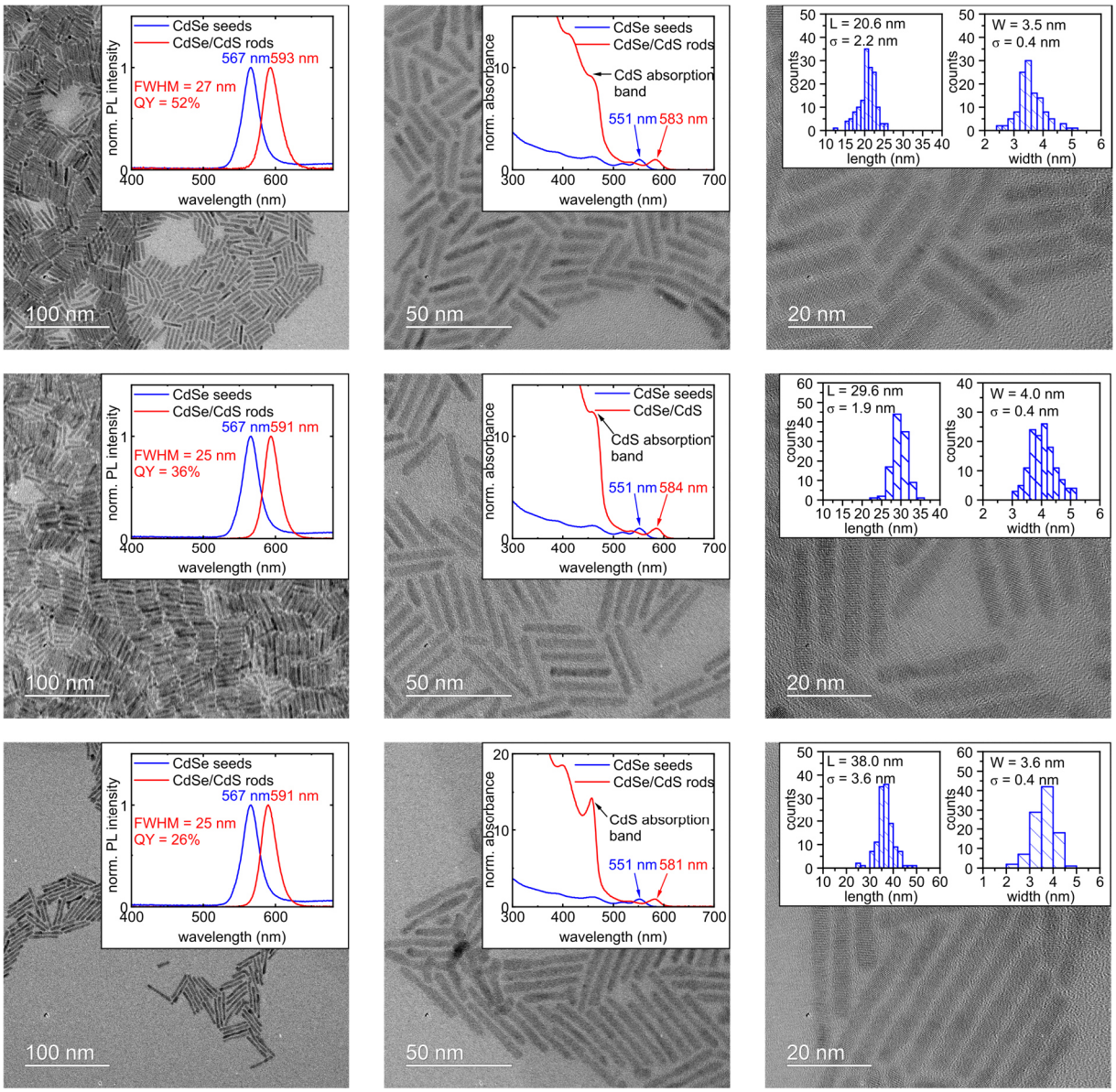

Figure 3.9. TEM images, PL ($\lambda_{exc.}$ = 380 nm) and absorption spectra of CdSe/CdS NRs of different sizes. All three CdSe/CdS rod batches were synthesized starting from the same batch of CdSe seeds.

Regarding the functionalization of CdSe/CdS NRs, one major obstacle will be that the surface of these rods is mostly covered by strongly binding phosphonic acids as X-type ligands which are difficult to replace. Bawendi and co-workers showed that the optical properties of CdSe/CdS NRs can be greatly improved by the slow deposition of an additional CdS shell.[181] Similar to the synthesis of high-quality CdSe/CdS or CdSe/$Cd_xZn_{1-x}S$ QDs, Cd-oleate and octanethiol are used as precursors (**Scheme 3.5**).

Scheme 3.5. Synthesis of CdSe/CdS/CdS NRs by slow deposition of CdS on CdSe/CdS NRs.

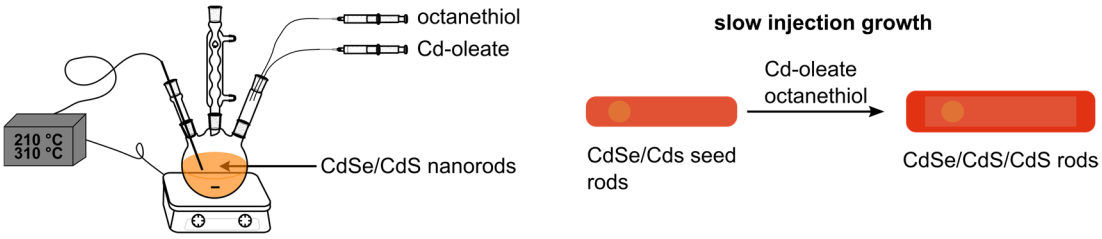

However, the authors did not state how they prepare their Cd-oleate, and neither the composition of the Cd-oleate regarding the amount of oleic acid, is given. Therefore, we employed the same Cd-oleate solution (ratio Cd to oleic acid of 1 to 3) as used in the synthesis of CdSe/$(CdS)_x(ZnS)_y$ QDs (**Chapter 3.4.4**). The amount of precursor solution was calculated based on the desired shell thickness. Bawendi and co-workers saw the best improvement in the optical properties of the NRs upon deposition of 2 ML of CdS. In **Figure 3.10**, the results for the deposition of a theoretical 2 ML thick CdS layer on short CdSe/CdS NRs (top, L = 20 nm) and long NRs (bottom, L = 30 nm) are shown. As injection rate, a deposition of 1 ML/h was chosen. In both experiments, highly fluorescent dispersions were obtained and a significant increase in QY was observed (42% → 78% respect. 36% → 75%). For both samples, a red shift (absorption 13–14 nm; PL maxima 12–14 nm) of the optical properties occurred which indicates that the width of the NRs (confined dimension) increased. Upon deposition of the CdS shell, no secondary nucleation occurred, and the NRs kept their defined rod form. Moreover, also the new NRs feature a strong tendency to align upon solvent evaporation. The red shift of the optical properties was reflected in an increase in width by 1.4 nm for the short rods and 1 nm for the long rods.

The theoretical increase in width based on the amount of precursors added is 1.3 nm which fits well to the measured values. However, for both batches a decrease in length of 3 nm and 2 nm, respectively, was observed. In literature, a slight decrease in length was also reported. Shim and co-workers showed that metal carboxylates (e.g. Cd-oleate) can induce etching of nanocrystals which happens in the case of CdSe/CdS NRs preferentially along the c-direction.[182]

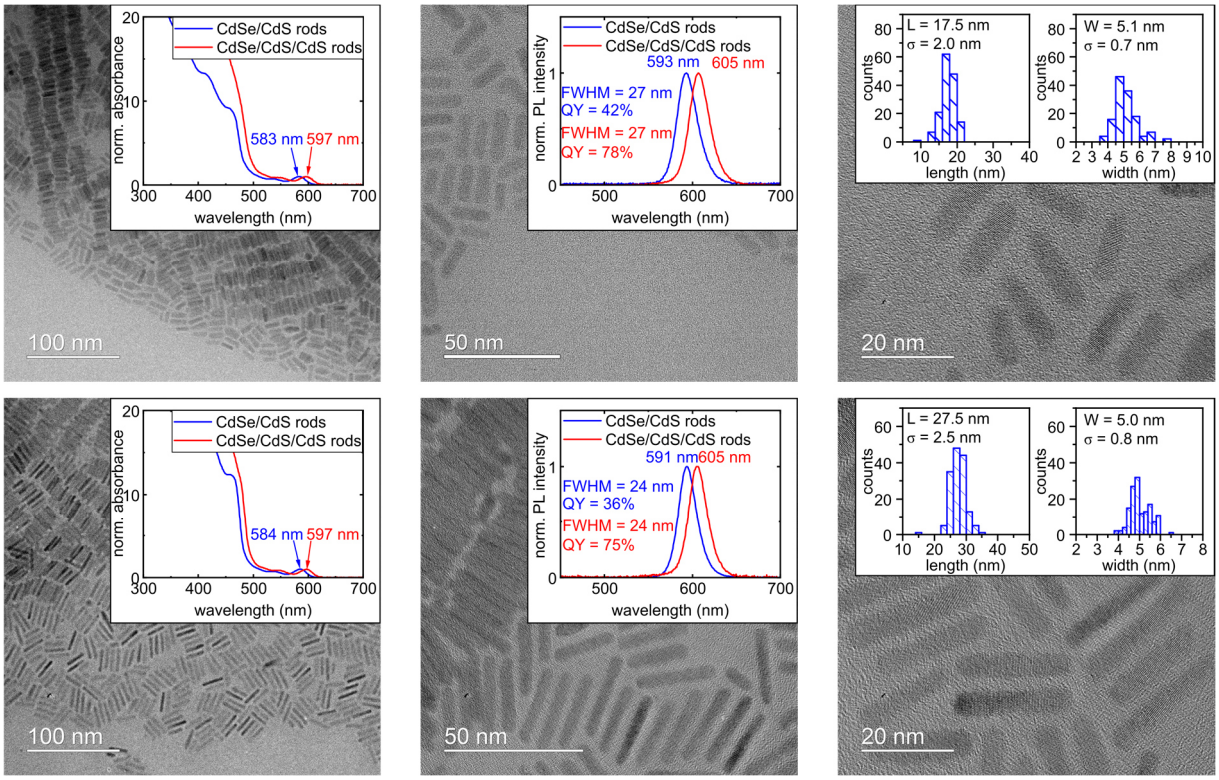

Figure 3.10. TEM images, absorption and PL ($\lambda_{exc.}$ = 380 nm) spectra of CdSe/CdS/CdS NRs which were synthesized from CdSe/CdS seed rods with a length of 20.5 nm and a width of 3.7 nm (top) and a length of 29.6 nm and a width of 4.0 nm (bottom), respectively. Both CdSe/CdS seed rod batches were synthesized from the same CdSe seed particles.

In a dispersion of purified CdSe/CdS NRs no unbound phosphonic acids could be detected by NMR spectroscopy (**Figure 8.4**). As the surface of the NRs upon deposition of the additional CdS shell increased (factor ~1.16), a part of the surface has to be passivated by oleic acid which is a weaker binding X-type ligand as compared to ODPA or HPA. A small amount of oleic acid was indeed bound to the NRs which could be elucidated by proton NMR spectroscopy (**Figure 8.5**) where a downfield shift of the signal of the olefinic protons and a disappearance of the triplet signal of the α-protons of oleic acid were observed which is typical for bound oleic acid.[119] Thus, these CdSe/CdS/CdS NR not only show improved optical properties but should also be more accessible to functionalization.

3.3 Summary and Conclusion

For the subsequent functionalization with conjugated polymers by a ligand exchange reaction and to have a suitable reference material in hand, high-quality core-shell semiconductor nanocrystals were synthesized. As core material CdSe QDs were successfully synthesized by two different methods. CdSe/CdS QDs were generated by a SILAR process. These QDs possessed different forms and they only showed an average QY of 42% (ranging from 30–61%). These QDs are a typical example for a quasi-type-2 heterostructure, where the electron wavefunction is partially spread into the shell. Graded-shell CdSe/$Cd_xZn_{1-x}S$ QDs were successfully synthesized based on a literature-known procedure[1] as an alternative with a higher optical quality as compared to the previously employed CdSe/CdS QDs. The graded-shell QDs featured a narrow size distribution (~10%) and QYs above 80%. Especially thin-shelled CdSe/$(CdS)_2(ZnS)_2$ QDs (**Figure 3.11**) are promising for the functionalization with conjugated polymers, as the thin shell should facilitate energy and charge transfer processes. Moreover, the deposition of the ZnS shell leads to an increased confinement of the electron wavefunction to the core and the formation of a type-1 heterostructure which is beneficial for the optical stability of the QDs.

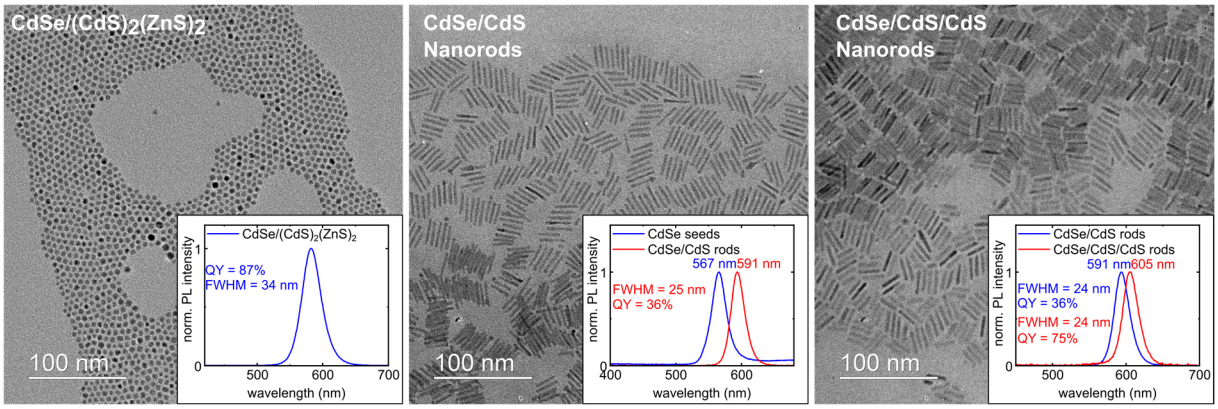

Figure 3.11. Overview over the synthesized high-quality semiconductor nanocrystals. Left: CdSe/$(CdS)_2(ZnS)_2$ QDs. Center: CdSe/CdS NRs. Right: CdSe/CdS/CdS NRs.

High-quality CdSe/CdS NRs (length 20–40 nm, width ~5 nm) were successfully synthesized based on a literature known procedure.[4] Adapted from a procedure developed by Bawendi and co-workers[181], an additional CdS shell (2 monolayers) was deposited on these NRs. This deposition resulted in a significant increase in the QY of the NRs (35–42% → 75–78%). Moreover, the surface of NRs became partially covered by oleic acid, which should be beneficial for the functionalization of these NRs.

3.4 Experimental Section

3.4.1 Materials and General Considerations

All manipulations of air- and/or water sensitive compounds were carried out under inert atmosphere using standard glove box and Schlenk techniques.

Cadmium oxide (> 99.99%-Cd, lot MKBT7524V), hexylphosphonic acid (HPA; 95%, lot MKBX1133V), oleylamine (70%), oleic acid (90%), octanethiol (> 98.5%), tri-*n*-octylphosphine (TOP; 99%), tri-*n*-octylphosphine oxide (TOPO; 99%), zinc acetate (99.99%, lot MKCC8484), and octadecene (90%) were purchased from Sigma-Aldrich. *n*-Octadecylphosphonic (ODPA, 98%, lot 807601N16) acid was obtained from PCI. 1-Dodecylphosphonic acid (95%, lot 1343062) and CdO (99.999%-Cd, lot 1364353) were purchased from ABCR (annotation: the CdO by ABCR was not suited for the synthesis of CdSe-seed particles).

Octadecene, oleic acid and oleylamine were degassed by purging with nitrogen for two hours and by applying vacuum at 80 °C for 20 h.

3.4.2 Analytical Methods

Absorption spectroscopy (UV-VIS spectroscopy):

Absorption spectra were recorded on a Varian Cary 100 scan spectrometer with the neat solvent (mostly toluene or *n*-hexane) as reference.

Photoluminescence Measurements and Quantum Yield Determination:

Ensemble emission spectra and quantum yields were measured using a Hamamatsu Absolute PL Quantum Yield Measurement System C9920-02 equipped with an integrating sphere.

Transmission Electron Microscopy (TEM):

TEM micrographs were aquired using a Jeol JEM-2200FS transmission electron microscope using a FEG with 200 kV acceleration voltage or using a Zeiss Libra120 employing a LaB_6 emitter with 120 kV acceleration voltage. Samples were prepared by drop casting 2 µL of a diluted particle dispersion on a TEM grid (Quantifoil S 7/2 + 2 nm C, Cu 400).

Particle size and distributions of QDs were obtained by measuring the area of at least 150 particles in TEM images at a magnification of 200000. From the area, the diameter of the

particles was calculated by assuming the particles to be circular. The circularity C of the particles was determined with the help of ImageJ and is defined as followed:

$$C = \frac{4 \cdot \pi \cdot \ area}{parimeter^2}$$

A circularity value of 1.0 indicates a perfect circle. As the value approaches 0.0, it indicates an increasingly elongated polygon. The size and size distribution of rods was obtained by measuring the length and width of at least 150 particles. All size measurements were performed at images taken at a magnification of 200000.

Determination of CdSe Concentration:

The size, molar extinction coefficients and concentration of CdSe seed particles were determined by using the sizing curve established by Jasieniak et al.[176] Briefly, 3.0 mL of *n*-hexane or toluene were placed in a sealable UV-VIS cuvette. 10 µL of the seed particle dispersion was added and an UV-VIS spectrum was recorded. This procedure was repeated until a total volume of 40 µl was added. The wavelength of the first absorption maximum λ_{1S} and the half width at half maximum on the low energy side of the absorption peak was determined. With these values the concentration and size of the particles was calculated using the formulas given by Jasieniak et al. and the average value from four measurements was calculated.

3.4.3 Synthesis of CdSe Seed Particles

CdSe Seeds from Cd-Oleate Precursor (Method A)

In a 50 mL Schlenk flask, 145 mg (1.1 mmol, 1 equiv.) of CdO and 2 mL (6.3 mmol, 5.7 equiv.) of oleic acid were mixed and heated up to 170 °C until a clear solution was obtained (for experimental set-up see **Figure 3.12**). After cooling to 70 °C, 3 mL of 1-octadecene and 1 g of 1-dodecylphosphonic acid (4 mmol, 3.6 equiv.) were added. The yellow solid was degassed at 80 °C for 2 h. In another 50 mL Schlenk tube, 117 mg (1.5 mmol, 1.3 equiv.) of selenium was dissolved in 1.5 mL (3.4 mmol) of tri-*n*-octylphosphine by sonication. 1.5 mL (4.5 mmol, 4.1 equiv.) of oleylamine was added and the solution was degassed for 2 h at 80 °C. The Cd-precursor solution was heated up to 240 °C and the Se-precursor solution was quickly injected via syringe. After stirring for 6.5 min, the heating block was removed, and the reaction mixture was cooled with compressed air followed by cooling in a water bath. The intensively red-colored dispersion was diluted with tetrahydrofuran (THF). The QDs were precipitated by the addition of 30 mL of methanol and collected by centrifugation. The precipitated QDs were

redispersed in 4 mL of *n*-hexane and centrifuged to precipitate the excess of phosphonic acid as a slightly red gel. The QDs were precipitated from methanol, collected by centrifugation and redispersed in toluene. The QDs were precipitated from methanol, collected by centrifugation and the obtained pellet was dried in a nitrogen stream and dispersed in 10.0 mL of toluene and stored at 6 °C under exclusion of light.

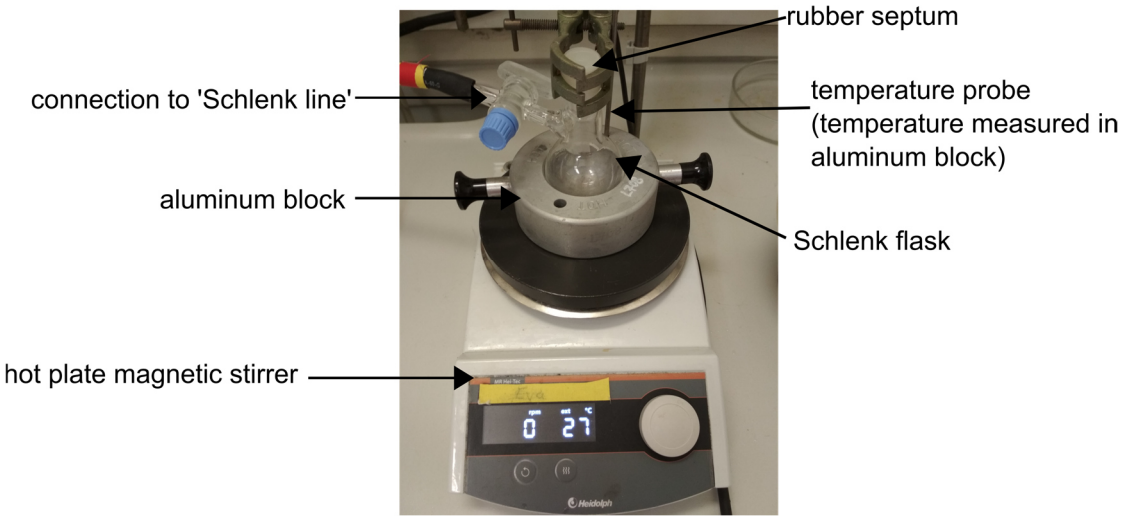

Figure 3.12. Exemplary photo of the set-up used for the synthesis of nanoparticles using an aluminum block, Schlenk flask and measuring the temperature in the aluminum block.

CdSe Seeds from Cd-Octadecylphosphonic Acid Precursor (Method B)

The synthesis of CdSe followed a modified protocol by Carbone et al.[4] Briefly, 60 mg (0.467 mmol, 1 equiv.) of CdO, 280 mg of octadecylphosphonic acid (0.837 mmol, 1.8 equiv.) and 3.00 g of tri-*n*-octylphosphine oxide (TOPO, 7.759 mmol) were mixed in a 25 mL three neck flask. The flask was equipped with a reflux condenser, rubber septum and a heating mantle with a thermo couple device (temperature measured in the reaction mixture, **Figure 3.13**). The reagents were degassed at 150 °C under vacuum for 1 h. Under nitrogen, the temperature was increased to 330 °C and the reaction was stirred until it turned clear, indicating the entire complexation of the Cd^{2+} ions. Typically, this takes around 2 hours. During the complexation, the flask had to be carefully shaken several times to wash down CdO from the flask's side. 1.8 mL of tri-*n*-octylphosphine was added and the mixture was heated to 370 °C. A TOP-Se solution (prepared by stirring 57 mg of Se and 360 mg of tri-*n*-octylphosphine in a glovebox for 1 hour at room temperature) was injected swiftly and the reaction was cooled down quickly by removing the heating mantle and by cooling with compressed air after the desired size of CdSe seed had been reached. Typically, the growth time was between 30 s and 60 s. At 100 °C, 3 mL of toluene was added. The CdSe cores were purified by precipitation in methanol, centrifugation (5000 g,

5 min), discarding the supernatant and redispersion in toluene for three times. The cores were finally precipitated from MeOH, collected by centrifugation, dried in a stream of nitrogen gas and redispersed in 4.0 mL of *n*-hexane, filtered through a syringe filter and stored in a refrigerator under exclusion of light.

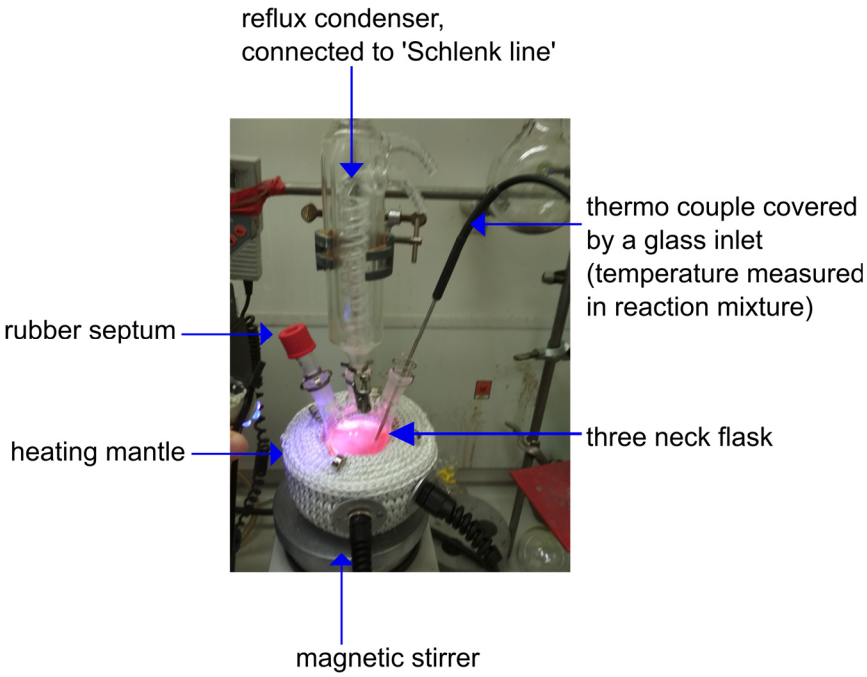

Figure 3.13. Exemplary photo of the set-up used for the synthesis of nanoparticles using a heating mantle and measuring the temperature directly in the reaction mixture.

3.4.4 Synthesis of Precursors

Synthesis of Cd-Oleate

In a 100 mL three neck flask, equipped with a septum, thermo couple and reflux condenser (set-up as shown in **Figure 3.13**), CdO (512 mg, 4 mmol, 1 equiv.), oleic acid (3.388 g, 12 mmol, 3 equiv.) and 40.4 mL of octadecene were degassed by applying vacuum for 30 min at room temperature and for 1 h at 80 °C. Under nitrogen, the mixture was heated to 300 °C and kept at this temperature until the solution turned clear, indicating the complete complexation of CdO. The mixture was cooled down to 100 °C and oleylamine (2.136 g, 8 mmol, 2 equiv.) was added to prevent gelation during cooling. The mixture was placed under vacuum for 1 h at 100 °C, placed under nitrogen, cooled down and stored in a nitrogen-filled glovebox.

Final concentration: c(Cd) = 0.0854 mol/L

Synthesis of Zinc-Oleate

In a 100 mL three neck flask, equipped with a septum, thermo couple and reflux condenser (set-up as shown in **Figure 3.13**), zinc acetate (1.467 g, 8 mmol, 1 equiv.), oleic acid (4.519 g, 16 mmol, 2 equiv.) and 28 mL of octadecene were degassed by applying vacuum for 30 min at room temperature and for 1 h at 80 °C. Under a nitrogen atmosphere the temperature was increased to 280 °C and the mixture was stirred until a clear and colourless solution was obtained (takes normally between 1 and 2 hours). The mixture was cooled down to 150 °C and 4.279 g (16 mmol, 2 equiv.) of oleylamine was added. The solution was degassed by applying vacuum for 1 hour at 100 °C, and finally stored inside a nitrogen-filled glovebox.

Final concentration: c(Zn) = 0.208 mol/L

3.4.5 Synthesis of Core-Shell Nanoparticles

Synthesis of CdSe/CdS Core-Shell Quantum Dots

In a 50 mL Schlenk flask, 436 mg (3.4 mmol) of cadmium oxide and 6 mL (18.9 mmol) of oleic acid were mixed and heated to 170 °C until a clear solution was obtained (set-up as shown in **Figure 3.12**). The solution was cooled to 80 °C and 24 mL of 1-octadecene was added. In another 50 mL Schlenk tube, 96 mg (3.0 mmol) of sulfur was dissolved in 30 mL of 1-octadecene by sonication. Both solutions were degassed at 80 °C for 1 h. In a 250 mL Schlenk flask, 9 mL of CdSe QDs (seeds from Cd-Oleate precursor) in toluene were mixed with 12 mL of oleylamine and 24 mL of 1-octadecene. Toluene was removed by applying vacuum at rt and the solution was degassed at 80 °C for 1 h. 1.7 mL of the Cd-precursor solution was added to the QD seed mixture, which was then heated to 240 °C (temperature of aluminum block). At 240 °C the following amounts of precursor solutions were consecutively added in periods of 10 min via a syringe pump. 1.7 mL of S-, 2.8 mL of Cd-, 2.8 mL of S-, 3.9 mL of Cd-, 3.9 mL of S-, 5.2 mL of Cd-, 5.2 mL of S-, 6.8 mL of Cd- and 6.8 mL of S-precursor solution. Finally, 8.5 mL of the Cd-precursor solution was added. The reaction solution was stirred at 240 °C for 20 min before the heating mantle was removed and the reaction mixture was cooled with compressed air and in a water bath. The QDs were diluted with THF, precipitated by the addition of methanol and collected by centrifugation. The QDs were redispersed in a minimal amount of toluene, precipitated from methanol and collected by centrifugation. This procedure was repeated one more

time. The QDs were dried in a nitrogen stream and redispersed in 10.0 mL of toluene and stored at 6 °C under exclusion of light.

Synthesis of CdSe/$Cd_xZn_{1-x}S$ Graded-Shell Quantum Dots

The synthesis of CdSe/$Cd_xZn_{1-x}S$ QDs (also written as CdSe/$(CdS)_x(ZnS)_y$ to indicate the shell thicknesses) QDs followed a slightly modified protocol published by Boldt et al.[1] Briefly, 1.5 mL of octadecene, 1.5 mL of oleyl amine and 50 nmol of CdSe seed particles were placed in a 25 mL three neck flask equipped with a rubber septum, thermo couple and reflux condenser (set-up as shown in **Figure 3.13**). The mixture was placed under vacuum and degassed for 45 min at 50 °C and for 20 min at 105 °C. Under a nitrogen atmosphere the temperature was raised to 310 °C. Starting at 210 °C, Cd and S precursor solutions were added via separate syringes controlled by a syringe pump. The precursors solutions were prepared by diluting the required amount of Cd-oleate and 1-octanethiol respectively with octadecene to a final injection volume of 1.5 mL. The required precursor amount was calculated from the size of the CdSe seed particles and the desired number of added monolayers of CdS (thickness of 1 ML CdS = 0.337 nm). A complete conversion of Cd-oleate was assumed, and a ratio of octanethiol to Cd-oleate of 1.2 : 1 was used. The injection rate was adjusted to ensure the addition of the amount equivalent to 2 ML of CdS per hour. After the addition of the precursors had been completed, the temperature was lowered to 200 °C and 0.5 mL of oleic acid was added dropwise. Noteworthy, due to the occasional occurrence of strong boiling retardance, this step requires particular attention. Afterwards, the reaction mixture was annealed at 200 °C for 1 hour. For the synthesis of CdSe/$Cd_xZn_{x-1}S$ graded-shell QDs, the temperature was decreased to 120 °C and the mixture was degassed by applying vacuum for 30 min. The reaction mixture was again heated to 310 °C and starting at 230 °C, precursor solutions of zinc-oleate and octanethiol, each diluted in octadecene to a final injection volume of 1.5 mL were added via separate syringes controlled by a syringe pump. The addition rate was set that the equivalent of 2 ML of ZnS was added per hour. The required precursor amount was calculated from the calculated size of the intermediately formed CdSe/CdS seed particles and the desired number of added monolayers of ZnS (thickness of 1 ML ZnS = 0.312 nm). A complete conversion of Zn-oleate was assumed, and a ratio of octanethiol to Zn-oleate of 2 : 1 was used. After the precursor addition had been completed, the mixture was cooled to room temperature by removing the heating mantle and cooling with compressed air. The particles were precipitated by the addition of an 8 : 1 v/v mixture of acetone and methanol

and by cooling in liquid nitrogen for a few seconds. The particles were collected by centrifugation (5 min at 3500 g) and redispersed in a minimal amount of chloroform. This procedure was repeated two times. In the final round, the precipitated particles were dried to a powder under a stream of nitrogen and dispersed in 4 mL of toluene, filtered through a syringe filter, and stored at 6 °C under exclusion of light.

Synthesis of CdSe/CdS Nanorods

The synthesis of CdSe/CdS NRs followed the protocol published by Carbone et al.[4], but was up-scaled by a factor of 1.5.

Briefly, TOPO (4.5 g), ODPA (435 mg, 1.3 mmol), HPA (120 mg, 0.72 mmol) and CdO (for a rod length of 20 nm: 86 mg, 0.66 mmol; for a rod length of 35 nm: 129 mg, 1 mmol) were degassed in a 25 mL three neck flask, equipped with a septum, thermo couple and reflux condenser (set-up as shown in **Figure 3.13**) for 1 hour at 150 °C and then heated to 330 °C under a nitrogen atmosphere. The mixture was kept at this temperature until it turned clear indicating the complexation of Cd. At this step, 3 mL of TOP is slowly added, and the temperature is increased to the injection temperature of 350 °C. Simultaneously, a mixture consisting of 180 mg (5.6 mmol) of S, 2.7 mL of TOP and 120 nmol of CdSe seed cores in hexane was prepared and the hexane was removed in vacuum at 80 °C over a period of 1 hour. When the temperature of the CdO reaction mixture had reached 350 °C, the core precursor solution was rapidly injected. After stirring the mixture for 8 min at 350 °C, it was cooled down by removing the heating mantle and cooling with compressed air. The NRs were purified by three rounds of precipitation by the addition of methanol, centrifugation and discarding the supernatant and redispersion in toluene. Finally, the NRs were precipitated from methanol, collected by centrifugation, dried in a stream of nitrogen gas and redispersed in 4 mL of *n*-hexane, filtered through a syringe filter and stored in a dark refrigerator.

Synthesis of CdSe/CdS/CdS Nanorods

The synthesis of CdSe/CdS/CdS NRs was performed by a modified version of the procedure published by Bawendi et al.[181]

A mixture of 20 nmol of CdSe/CdS rods in hexane with 1.5 mL of octadecene, 1.5 mL of oleylamine and 1.5 mL of oleic acid was prepared in a 25 mL three neck flask equipped with a thermo couple, rubber septum and reflux condenser (set-up as shown in **Figure 3.13**), and hexane and water residues were removed at 50 °C in vacuum for 45 min and another 15 min at 105 °C. Under nitrogen, the temperature of the reaction mixture was

raised to the final reaction temperature of 310 °C. Already when the temperature reached 210 °C during the heating process, the injection of the precursor solutions was started. Solutions of Cd-oleate and 1-octanethiol, each diluted with octadecene to give a final injection volume of 3 mL, were injected from separated syringes using a syringe pump (injection rate 1.5 mL/h). The octanethiol precursor solution was degassed by applying vacuum for 45 min at 60 °C before use. The amounts of precursor were calculated from the size of the initial CdSe/CdS NRs and the desired shell thickness (number of monolayers, thickness of 1 ML of CdS = 0.337 nm). A complete conversion of Cd-oleate was assumed and a ratio of octanethiol to Cd of 1.2 : 1 was used. After the precursor addition was completed, the reaction mixture was cooled down and precipitated in an acetone/MeOH mixture (70/30). The mixture was centrifuged at 5000 g for 5 min, the supernatant was discarded and the pellet redispersed in a minimal amount of toluene. The procedure was repeated three times and afterwards the rods were dried in a stream of nitrogen, redispersed in toluene, filtered through a syringe filter and stored in a refrigerator under the exclusion of light.

4 Functional Conjugated Polymers and Conjugated Nonconjugated Block Copolymers by Controlled Polymerizations

4.1 Introduction

Poly(fluorene)s (PFs) are important semiconducting materials for light-emitting devices because of their wide band gap and thereby blue-light-emitting character, high photoluminescence quantum yield, good charge transport properties, great thermal stability and good solubility in organic solvents.[183,184,185,186,187,188,189]

In the course of his dissertation Tjaard deRoo showed that phenylphosphonic acid-functionalized poly(9,9'-dioctylfluorene) (PF8) can bind strongly to CdSe or CdSe/CdS QDs (QDs) whereas aniline-functionalized PF8 binds only rather weakly.[113,150] Moreover, for some of his systems observations hint at an energy transfer (ET) from the polymer to the QDs. Guo et al. could reveal a strong ET from PF to CdSe/ZnS QDs.[23] Given the energy levels of PF8 and CdSe/CdS nanocrystals, an electron transfer from photoexcited polymer to the nanocrystal resulting in the desired charged nanoparticles should be possible in principle (see **Chapters 1, 5.1** and **6.1** for details). Therefore, the synthesis of conjugated polymers was mainly focused on PF8. For single-particle spectroscopy measurements, the functionalized nanocrystals are encapsulated into a larger polymer particle by a miniemulsion polymerization (**Chapter 6**). The embedding process might be facilitated by employing nanocrystals which are functionalized with PF8 bearing a radically polymerizable end group (PF8 macromonomer, **Scheme 4.1**). As second method to improve the embedding, the introduction of a nonconjugated polymer block to the PF8 chain was pursued (PF8 diblock copolymer, **Scheme 4.1**). Regarding the functionalization of the QDs with PF8 itself, the binding affinity of PF8 might be improved by employing a

multi-valent ligand. This multi-valent polymer ligand could be synthesized by the radical copolymerization of the PF8 macromonomer with a radically polymerizable monomer (PF8 comb copolymer, **Scheme 4.1**). Therefore, the following heterodifunctionalized PF8s were targeted:

- A PF8 macromonomer bearing a phenylphoshonic acid and a radically polymerizable end group.
- A PF8 macroinitiator bearing a phenylphosphonic acid end group and an end group capable to initiate a controlled radical polymerization.

Further, conditions had to be found to convert the macromonomer/macroinitiator to the respective comb copolymer or diblock copolymer in a controlled manner.

Scheme 4.1. Synthesis of conjugated nonconjugated copolymers by combining controlled Suzuki-Miyaura cross coupling polymerization (cSMCCP) and controlled radical polymerization (CRP). Reprinted with permission from ref.[5] Copyright **2019** American Chemical Society.

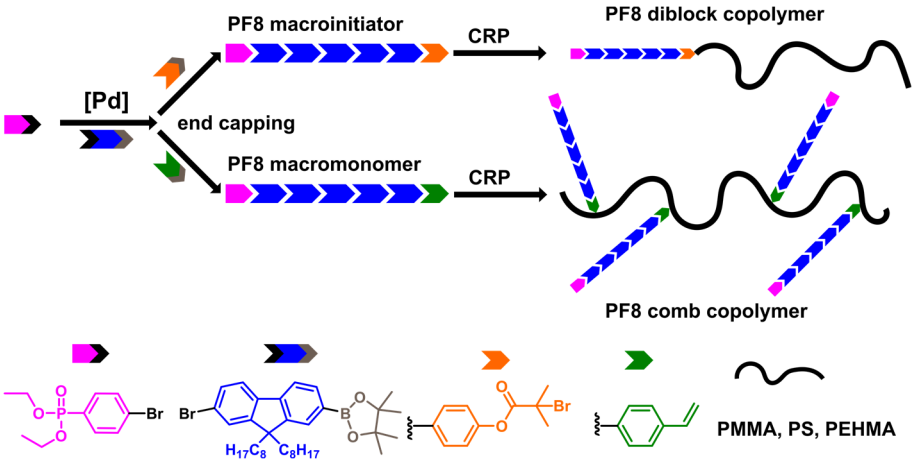

4.1.1 Controlled Synthesis of Conjugated Polymers – Suzuki-Miyaura Cross-Coupling Polymerization

The development of metal catalyzed C-C coupling reactions enabled the polymerization of nearly all aromatic monomers to conjugated polymers in a step growth manner.[95] However, such polymerization techniques only allowed for a low control of molecular weight and the quantitative introduction of functional groups at the chain ends was practically not possible. In 2004, Yokozawa[190] and McCullough[191] independently reported on the first controlled nickel-catalyzed Kumada-Tamao coupling polymerization of 2-bromo-5-chloromagnesio-3-hexylthiophene. Their procedure enabled the syntheses of polythiophenes with defined chain length, narrow molecular weight distribution and end

group functionalization.[100] As highly reactive Grignard-type monomers are used, the direct introduction of functional end groups is limited. Moreover, the introduction of two different functionalities at both ends is quite difficult.[192]

In 2007, Yokozawa and co-workers reported the first Suzuki-Miyaura cross-coupling polymerization (SMCCP) of bromofluoreneboronic acid ester employing [PdBr(Ph)(P^{t}Bu$_3$)] as initiator proceeding in a chain growth manner with each polymer chain functionalized with the phenyl group from the initiator.[193] Using SMCCP many monomers such as fluorenes[193], thiophenes, phenylenes[194,195], phenanthrenes[196] and fluorene-benzothiadiazoles[197] can be polymerized in a controlled manner. The controlled SMCCP (cSMCCP) allows for the synthesis of hetero end-functionalized π-conjugated polymers which can be understood by the mechanism of the polymerization (**Scheme 4.2**). The polymerization is initiated by the transmetalation reaction (**1**) between monomer and the three-coordinate Pd(II) complex, resulting in complex **I** which undergoes successive reductive elimination (**2**). The Pd(P^{t}Bu$_3$) moiety does not leave the molecule but forms a π-complex (**II**) with the conjugated system of the molecule and then undergoes intramolecular oxidative addition (**3**), resulting in complex (**III**). This step is responsible for the chain growth characteristic of the polymerization.[193,198,199] Successive transmetalation (**4**) of the monomer followed by reductive elimination (**5**), and intramolecular oxidative addition leads to the polymer complex (**IV**). The polymerization can be terminated either by the addition of an acid such as HCl (**6**) resulting in the hydrogen-terminated polymer (**V**) or by the addition of a functionalized arylboronic acid (ester) in excess (**7**), yielding the hetero difunctionalized polymer (**VI**). This procedure allows for precise polymer end group functionalization by introducing functional groups through the aryl moiety of the initiator complex[113,200,201] and the aryl moiety of the boronic acid (ester) used for quenching.[198,200,202]

As initiators three-coordinate Pd(II) complexes such as [PdBr(Ph)(P^{t}Bu$_3$)] are commonly employed, which can be synthesized by the reaction of an arylbromide with [Pd(P^{t}Bu$_3$)$_2$]. However, the isolation of these complexes is tedious, and the complexes are prone to decomposition which leads to fluctuations in the polydispersity index of the obtained polymers. [Pd(Aryl)(P^{t}Bu$_3$)X] complexes (X= Br, I) can also be generated *in situ* by the combination of [Pd$_2$(dba)$_3$], P^{t}Bu$_3$ and ArylX.[203,204]

Scheme 4.2. Proposed mechanism of the controlled Suzuki-Miyaura cross-coupling polymerization employing an isolated three-coordinate Pd(II) initiator.[193,198,199,205]

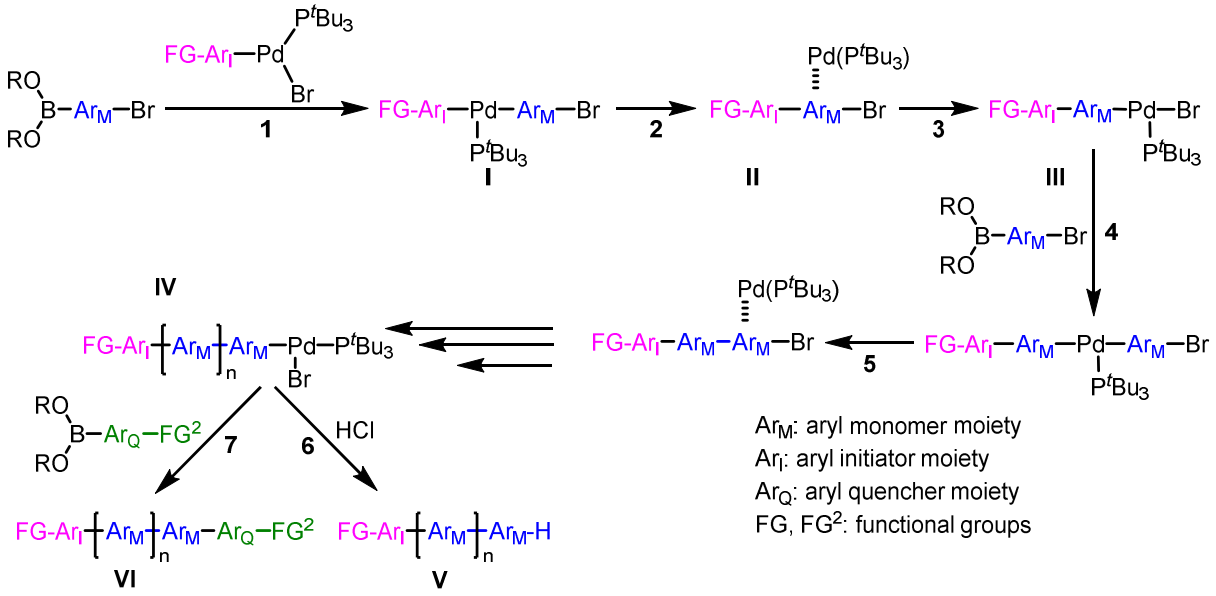

Thereby, the time-consuming isolation step is omitted, and narrow polydispersity indices are obtained reproducibly. However, the combination of typical Pd(0) complexes such as [Pd$_2$(dba)$_3$] and P^{t}Bu$_3$ only forms robust initiators with a very limited scope of ArylX.[203,204] In 2016, Hu and co-workers introduced chloro[(tri-*tert*-butylphosphine)-2-(2-aminobiphenyl)] palladium(II) (PdG2P^{t}Bu$_3$) as Pd source.[202] Under basic conditions PdG2P^{t}Bu$_3$ is reported to be a source of a highly reactive 12-electron [(P^{t}Bu$_3$)Pd(0)] species which forms effective initiator systems with various aryl bromides (**Scheme 4.3**).[202,206]

Scheme 4.3. Formation of the three-coordinate Pd(II) initiator complex using PdG2P^{t}Bu$_3$ as Pd precursor and an Aryl-X (X= Br, I). Mechanism adapted from ref.[202]

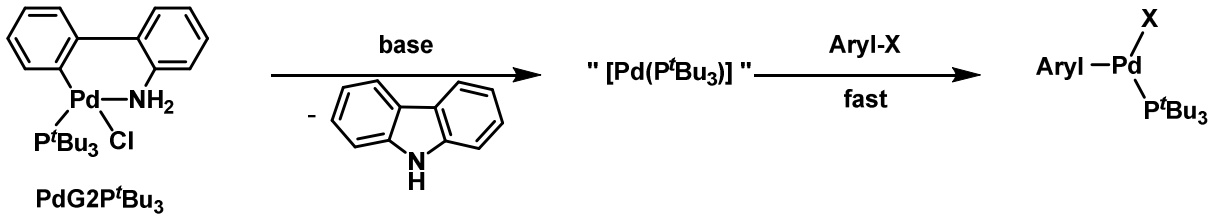

4.1.2 Reversible-Deactivation Radical Polymerizations

Starting in the 1990s, polymerization methods were developed which allow for the control of molecular weight, narrow molecular weight distribution and chain end functionalization during radical polymerizations.[207] These reversible-deactivation radical polymerizations methods, also known as living/controlled radical polymerizations[208],

enable the syntheses of multiblock copolymers and complex polymer topologies such as stars, combs or brushes. The most prominent techniques are nitroxide-mediated polymerization (NMP), atom transfer radical polymerization (ATRP) and reversible addition-fragmentation chain transfer (RAFT) polymerization.[209] In all of these methods, a dynamic equilibrium between the propagating radicals and a dormant species (**Scheme 4.4**) is established.[209] Thereby, irreversible termination reactions are suppressed to a great extent which enables control of the polymerization.

Scheme 4.4. Equilibrium reactions in reversible-deactivation radical polymerizations which are responsible for the controlled manner of the reactions.

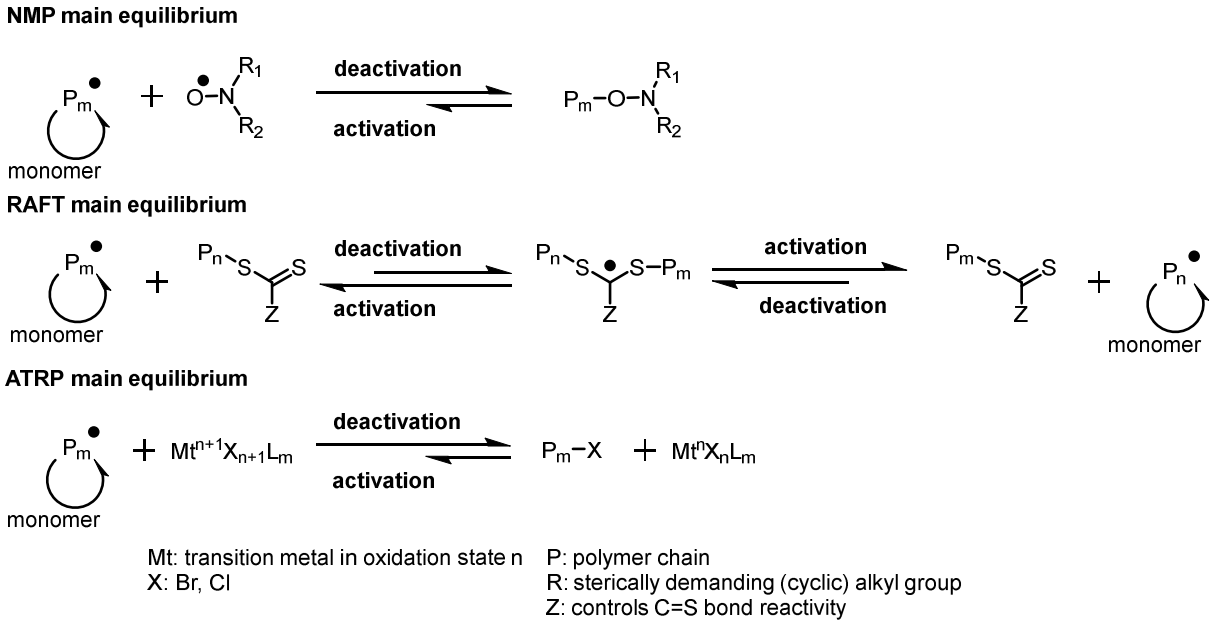

In NMP and RAFT polymerizations the equilibrium is adjusted using organic species whereas in an ATRP transition metal complexes – mainly Cu complexes – are used. ATRP is the most versatile technique and by choosing the proper initiator and metal complex many monomers can be polymerized in a controlled manner.[210] The drawback of the classical ATRP method is the requirement of a comparatively large amount of metal catalyst (1000-10000 ppm). Remaining transition metal impurities can be detrimental for the use of the polymer in biomedical, food packaging or optical applications. In recent years, methods such as ARGET (activators regenerated by electron transfer) ATRP[211,212] or ICAR (initiators for continuous activator regeneration) ATRP[213] have been developed, enabling to reduce the amount of metal complex down to 5-200 ppm. Therefore, only a minimal subsequent purification for catalyst removal is needed.

Using NMP as method, the controlled polymerization of methacrylates and particularly methyl methacrylate is difficult as it requires sophisticated nitroxides or the

copolymerization with another monomer.[209,214] Therefore, ARGET ATRP and RAFT were chosen as method to synthesize conjugated nonconjugated copolymers. However, as the synthesis of a RAFT macroinitiator by cSMCCP failed (**Chapter 4.2.1**), only ARGET ATRP was employed.

4.1.3 Conjugated Nonconjugated Block Copolymers

The combination of a rod-like conjugated polymer with a coil-like polymer can significantly influence the opto-electronic properties of the conjugated polymer by changing its solubility, crystallization behavior, morphology, aggregation, self-assembly, and conductivity properties.[215,216,217,218,219] Today, it is possible to synthesize various conjugated polymers with narrow molecular weight distributions and well-defined end groups. However, regarding the synthesis of conjugated nonconjugated copolymers based on PF, the PF part is predominantly synthesized under harsh reaction conditions using step growth polymerizations (Suzuki[220] or Yamamoto[221] type coupling) without precise control of molecular weight and end groups. The attachment point for the nonconjugated (coil) block(s) is laboriously introduced in several steps after the polymerization.[221,222,223,224]

Various rod-coil copolymers of poly(3-alkylthiophenes) have been synthesized by the combination of controlled Kumada-Tamao catalyst transfer polycondensation (KCTP)[192,225] and CRP. A comprehensive review on this topic was published by Magurudeniya *et al.* in 2012.[226] Most procedures rely on the synthesis of vinyl- or allyl-terminated poly(3-alkylthiophenes) by KCTP and *in situ* end-capping using the corresponding Grignard reagents.[227,228,229] This is followed by hydroboration/oxidation to generate a hydroxyl-terminated polymer which can be functionalized by esterification.[230,231] The nonconjugated block can be attached by a controlled radical polymerization starting from a P3HT macroinitiator[230,232,233,234] or synthesized separately and subsequently tethered to the P3HT part.[235,236] All approaches have in common, that they are based on multi-step procedures. Moreover, only one terminus of the conjugated polymer is functionalized, with the second block, while the other chain end does not feature an additional functional group.

A more straightforward approach was applied here by using cSMCCP instead of KCTP including the benefit that both polymer chain ends can be functionalized – one with the second polymer and one with an additional functional group amenable to Suzuki-Miyaura cross-coupling conditions (**Scheme 4.1**).

4.2 Results and Discussion

4.2.1 Heterodifunctional Polyfluorenes by Controlled Suzuki-Miyaura Cross-Coupling Polymerization

The PF8 macromonomer and PF8 macroinitiator were synthesized by cSMCCP. As initiator the isolated Pd(II) complex bromo(4-diethoxyphosphoryl-phenyl)(tri-*tert*-butylphosphine)palladium (II) (**Scheme 4.5**, **Ini1**) was compared to the *in situ* system consisting of diethyl-(4-bromophenyl)phosphonate and chloro[(tri-*tert*-butylphosphine)-2-(2-aminobiphenyl)] palladium(II) (PdG2P^{t}Bu$_3$) (**Ini2**). The diethyl phenylphosphonate moiety is introduced to the PF8 chain via these Pd initiators and can be deprotected in a second step yielding the phenylphosphonic acid moiety. To generate a radically polymerizable PF8 macromonomer, the polymerization was end-capped with 4-vinylphenylboronic acid pinacol ester (**1**) or with 4-(4,4,5,5-tetramethyl-1,3,2-dioxaborolan-2-yl)phenyl methacrylate (**2**) (**Table 4.1**, entries 1–3).

Scheme 4.5. Synthesis of hetero difunctional polyfluorenes by cSMCCP.

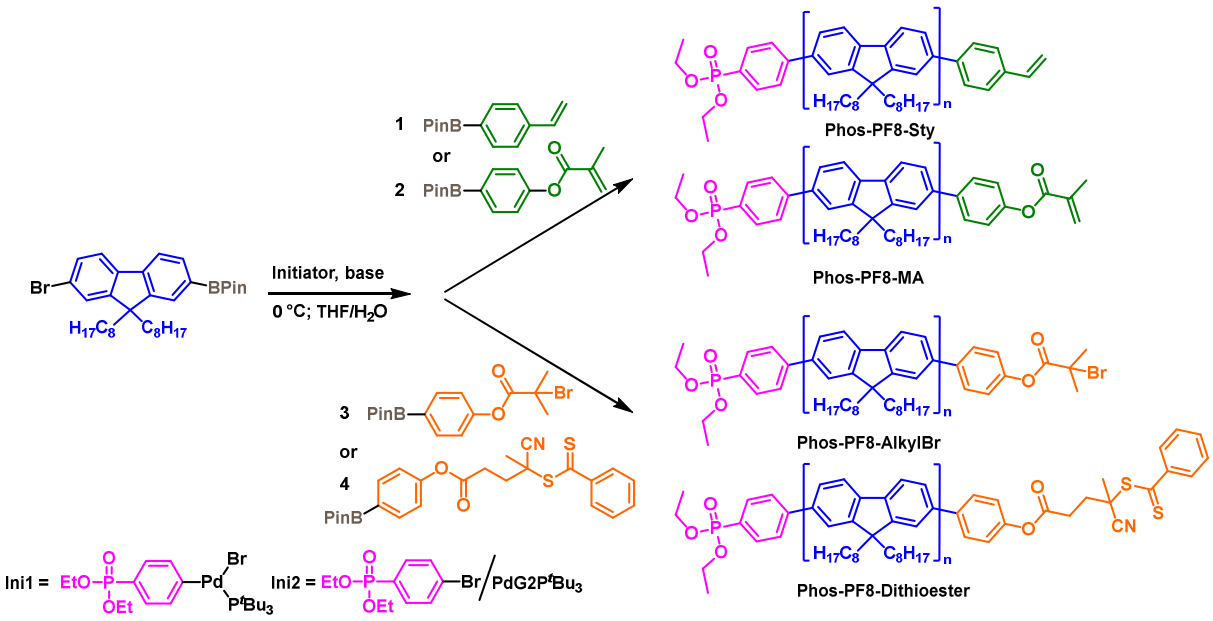

The polymerization with the isolated initiator **Ini1** afforded perfectly initiated and end-capped polyfluorene Phos-PF8-Sty with a narrow molecular weight distribution of $M_w/M_n = 1.16$. The matrix assisted laser desorption ionization time of flight mass spectrum (MALDI-TOF MS) (**Figure 4.1**) is characterized by only one series of signals, which differ in the molecular weight of one fluorene repeat unit, corresponding to polymer chains with initiator- and end-capper-derived chain ends. The quantitative

double functionalization is also proven by ^{1}H nuclear magnetic resonance (NMR) spectroscopy (**Figure 4.1**), which also allows to determine the degree of polymerization (DP_n) by NMR spectroscopy. The obtained DP_n agrees well (9 vs. 10) with the DP_n expected from the monomer-to-Pd ratio.

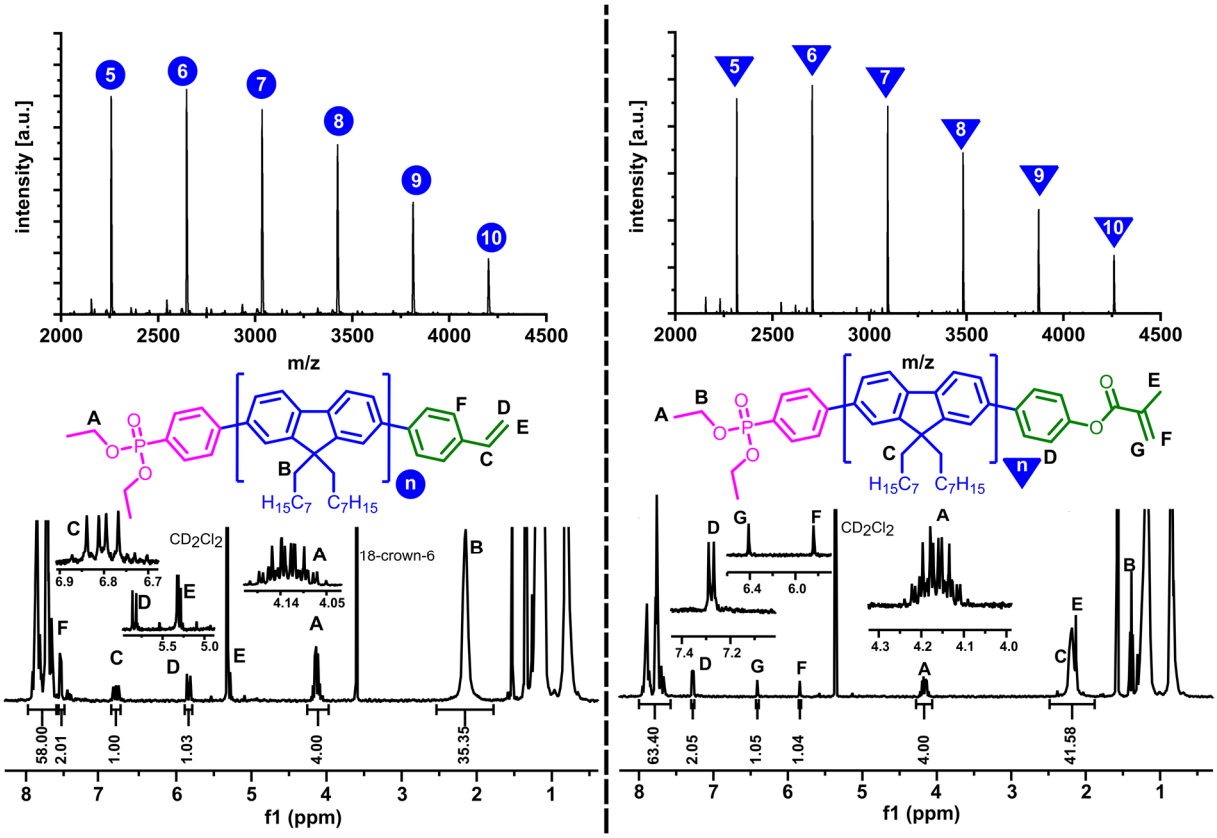

Figure 4.1. MALDI-TOF mass spectra (top) and ^{1}H NMR spectra (bottom) of the polyfluorenes Phos-PF8-Sty (left) and Phos-PF8-MA (right) which were synthesized by cSMCCP. Left: Reprinted with permission from ref.[5] Copyright **2019** American Chemical Society.

The synthesis of these isolated three-coordinate Pd(II) initiators is tedious, and additionally they are sensitive towards decomposition. Therefore, the use of an *in situ* system employing a commercial Pd(II) precursor such as PdG2P^{t}Bu$_3$ is desirable. Under basic conditions PdG2P^{t}Bu$_3$ is a source of a highly reactive 12-electron "(P^{t}Bu$_3$)Pd(0)" species which forms effective initiator systems with various aryl bromides (**Scheme 4.3**).[202,206] Also polymerization with the *in situ* system (**Ini2**) consisting of diethyl-(4-bromophenyl)phosphonate and PdG2P^{t}Bu$_3$ in combination with K_2CO_3 as base afforded quantitatively functionalized PF8 (**Figure 8.6**) with a narrow M_w/M_n of 1.18 (entry 2). Also, the polymerization using **Ini2** and end-capping with **2** (entry 3) yielded perfectly hetero difunctionalized Phos-PF8-MA (**Figure 4.1**) with a narrow molecular weight distribution of M_w/M_n = 1.15 and a DP_n of 10 as expected from the monomer-to-

Pd ratio. Remarkably, side products are virtually absent in these polymerizations, although potentially reactive styrene or phenyl methacrylate end groups were attached.

Table 4.1. Synthesis of hetero difunctional polyfluorenes by controlled Suzuki-Miyaura cross-coupling polymerization.

#	initiator	base	end-capping agent	DP_n (theo.)[c]	DP_n (NMR)[d]	M_n (GPC)[e] [g mol^{-1}]	M_w/M_n
1	**Ini1**	CsF/18-6	**1**[a]	10	9	5067	1.16
2	**Ini2**	K_2CO_3	**1**[a]	10	9	4371	1.18
3	**Ini2**	K_2CO_3	**2**[a]	10	10	6200	1.15
4	**Ini1**	CsF/18-6	**4**[a]	10	n.d	5540	1.15
5	**Ini2**	K_2CO_3	**4**[a]	10	n.d	5650	1.17
6	**Ini1**	CsF/18-6	**3**[a]	10	10	6196	1.15
7	**Ini2**	CsF/18-6	**3**[a]	10	n.d.	17000	1.63
8	**Ini2**	K_2CO_3	**3**[a]	10	8	6310	1.18
9	**Ini2**	K_2CO_3	**3**[b]	10	10	5441	1.16
10	**Ini2**	K_2CO_3	**3**[b]	5	5	2346	1.16
11	**Ini2**	K_2CO_3	**3**[b]	15	15	7928	1.17
12	**Ini2**	K_2CO_3	**3**[b]	20	20	11450	1.20

a) End-capping reaction time over night. b) End-capping reaction time 2 h at 0 °C. c) Ratio of monomer to Pd(II) initiator. d) DP_n was determined by comparison of end group to backbone signals by ^{1}H NMR spectroscopy. e) Determined by gel permeation chromatography (GPC) (tetrahydrofuran, 35 °C, vs. polystyrene standards, RI detection).

For the synthesis of conjugated nonconjugated diblock copolymers by CRP, a functional group capable of initiating a CRP is required on the PF8 chain. First, the attachment of a group, capable to control a RAFT polymerization, to the Phos-PF8 chain was approached by end-capping with the newly synthesized end-capping agent 4-(4,4,5,5-tetramethyl-1,3,2-dioxaborolan-2-yl)phenyl 4-cyano-4-((phenylcarbonothioyl)thio)pentanoate (**4**) (entries 4–5). However, using the isolated initiator **Ini1** as well as the *in situ* system **Ini2**, no single defined PF8 species was obtained (**Figure 8.7**) and the Phos-PF8-Dithioester was only obtained in a moderate amount. As all assignable species bear the diethyl phenylphosphonate moiety (initiator-derived group), and the molecular weight and molecular weight distribution are comparable to successful polymerizations, the difficulty of synthesis presumably is based on the end-capping reaction. Tjaard de Roo

also observed, while trying to synthesize thiol-functionalized PF8, that end-capping or initiation with sulfur containing compounds often leads to a variety of end groups.[150] It is known in literature, that Suzuki coupling involving protected thiols and dithioesters can lead to a diversity of products, especially under aqueous basic conditions.[237,238]

Therefore, the synthesis of a PF8 macroinitiator capable to initiate an ATRP was pursued. 2-Bromo-2-methylpropanoates are capable to initiate the controlled polymerization of various monomers.[212,213,230] Thus, the end-capping agent 4-(4,4,5,5-tetramethyl-1,3,2-dioxaborolan-2-yl)phenyl 2-bromo-2-methylpropanoate (**3**) was synthesized and used in the synthesis of heterodifunctional PF8s (entry 6–12). Using the isolated initiator **Ini1** (entry 6), perfectly initiated and end-capped polyfluorene Phos-PF8-AlkylBr (**Figure 4.2**) was obtained. The isolated initiator is usually used employing CsF as mild base instead of carbonates or phosphonates as CsF is compatible with many base sensitive groups (e.g. end-capping agent **3**). However, employing PdG2P^{t}Bu$_3$ in combination with CsF/18-crown 6 as an initiator system (entry 7), no single defined PF8 species was obtained (**Figure 8.8**) and only a small portion of chains featured initiator-derived end groups. Apparently, the Pd initiator precursor PdG2P^{t}Bu$_3$ cannot be activated by the mild base CsF but a strong base such as K_2CO_3 is required. In order to ensure a quantitative end-capping, the end-capping reaction was usually performed overnight, which unfortunately led to a partial degradation of the Br-moiety intended as an ATRP initiator (entry 8, **Figure 8.9**) using K_2CO_3 as base. Reducing the end-capping reaction time to 2 h at 0 °C (entry 9) was sufficient to obtain a perfectly initiated and end-capped polyfluorene Phos-PF8-AlkylBr using the *in situ* initiator system. The controlled manner of the Suzuki-Miyaura cross-coupling polymerization was demonstrated by experiments 9–12 (**Table 4.1**) where degree of polymerizations of 5, 10 ,15 and 20 were obtained by adjusting the ratio of Pd initiator to monomer accordingly while maintaining a narrow PDI (≤ 1.2; see **Figure 8.10** for GPC traces).

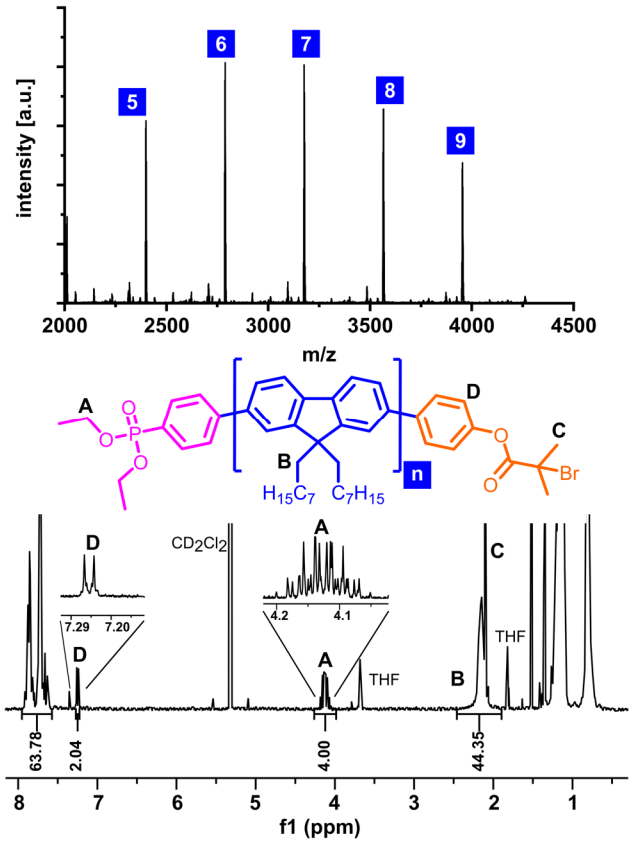

Figure 4.2. MALDI-TOF mass spectrum (top) and ^{1}H NMR spectrum (bottom) of the polyfluorene Phos-PF8-AlkylBr synthesized by cSMCCP. Reprinted with permission from ref.[5] Copyright **2019** American Chemical Society.

Besides using the PF8 macromonomers for the synthesis of conjugated nonconjugated copolymers, also the direct functionalization of QDs with these macromonomers was intended. Prior to the application as ligand, the diethyl phenylphosphonate group has to be deprotected to the free phosphonic acid as only those are strongly binding to chalcogenide surfaces.[239] The mildest deprotection method for phosphonate esters is the 'McKenna reaction' (**Scheme 4.6**) using trimethylsilyl bromide (TMS-Br) as cleavage agent.[240]

Scheme 4.6. 'McKenna reaction': Dealkylation of phosphonic acid dialkyl esters by TMS-Br.

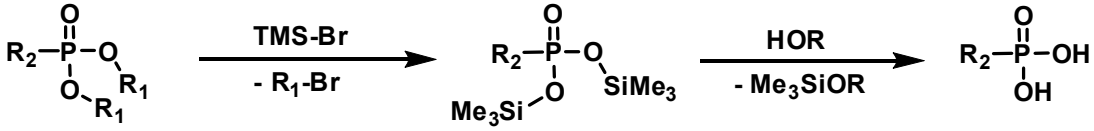

Tjaard de Roo successfully used this reaction for the deprotection of diethyl phenylphosphonate-functionalized PF8, however, this polymer did not have a potentially labile second functional group.[150] Regarding the deprotection of Phos-PF8-MA, the carboxylic acid ester could be cleaved, or the olefin group could be saturated during the

deprotection. The silylation was performed under optimized conditions in dichloromethane (DCM) using 10 equiv. of TMS-Br and a reaction time of 4 h at room temperature. The following alcoholysis was performed in a mixture of DCM and methanol over 16 hours. The deprotection of Phos-PF8-MA was successful (**Figure 4.3**), as the diethyl phenylphosphonate moiety was completely deprotected and no carboxylic acid ester cleavage or reaction of the olefin group was observed.

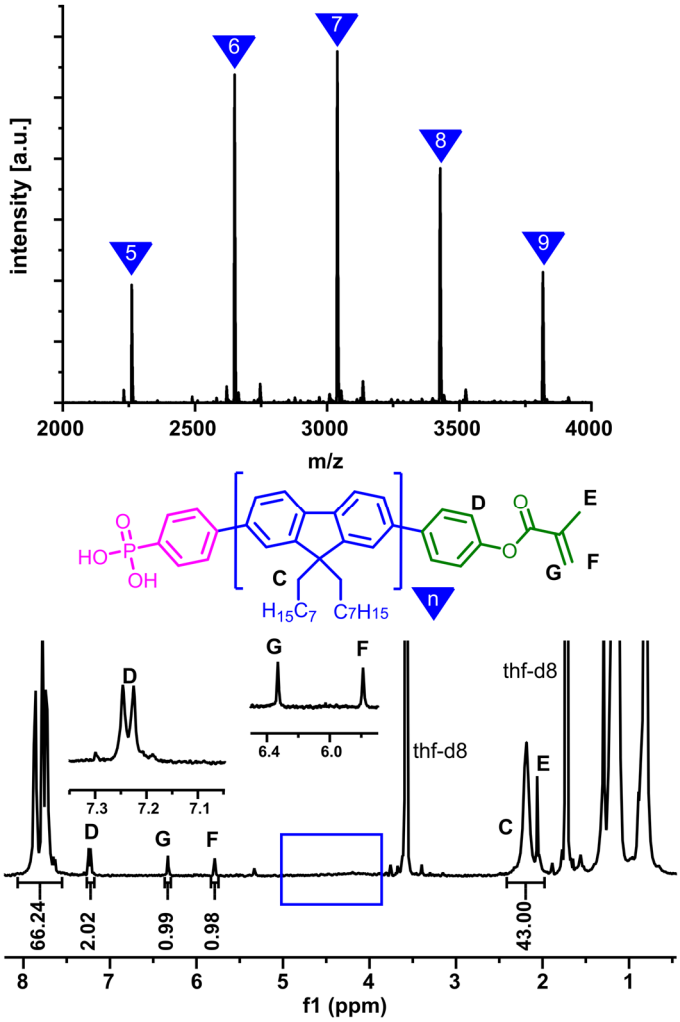

Figure 4.3. MALDI-TOF mass spectrum (top) and ^{1}H NMR spectrum (bottom) of the deprotected polymer PA-PF8-MA. The quantitative dealkylation of the diethyl phenylphosphonate group is visible by the complete disappearance of the signals of the P-O-**CH_2**-CH_3 groups (blue rectangle).

However, during the deprotection of the Phos-PF8-Sty macromonomer under the same conditions, the diethyl phenylphosphonate group was completely deprotected, but also the olefin group was deteriorated (**Figure 8.11**). Changing the solvent from DCM to tetrahydrofuran had no positive effect. Also, reducing the amount of TMS-Br down to 2.2 equivalents and a reduction of the reaction time to only 2 h for each silylation and alcoholysis at room temperature did not improve the outcome. Therefore, Phos-PF8-Sty

was first copolymerized with a comonomer and the resulting conjugated nonconjugated comb polymer was deprotected afterwards (**Chapter 4.2.4**).

4.2.2 Functional Conjugated Polymers for the Functionalization of Semiconductor Nanocrystals

Besides the heterodifunctional PF8 macromonomer and macroinitiator (**Chapter 4.2.1**) additional functional conjugated polymers for the functionalization of semiconductor nanocrystals were synthesized by cSMCCP (**Scheme 4.7**). Three different PF8s (PA-Ph-PF8, PA-Bn-PF8 and COOH-Ph-PF8) were synthesized to explore the binding behavior of different functional groups (**Chapter 5**) towards semiconducting CdSe/CdS nanocrystals. The two thiophene macromonomers (Phos-Ph-P3HT-MA and Phos-Ph-P3HT-Sty) were synthesized as low-band gap polymers as alternative to the high-band gap polymer PF8. The polymers were synthesized using the respective arylbromides in combination with PdG2P^{t}Bu$_3$ and K_2CO_3 as base and the respective arylboronic acid pinacol ester as end-capping agent. All polymers were obtained with the desired end groups, DP_n values consistent with the of Pd-to-monomer ratio and a narrow molecular weight distribution of $M_w/M_n < 1.2$. Selected NMR and MALDI-TOF mass spectra of the polymers are shown in the appendix (**Figure 8.12** – **Figure 8.19**). For the synthesis of Phos-Bn-PF8 and COO^{t}Bu-Ph-PF8, the reaction time between the respective arylbromide and PdG2^{t}Bu$_3$ had to be increased from 60 min at room temperature to 90 min at room temperature to ensure a complete conversion of the Pd precursor and thereby a complete functionalization. For the synthesis of polythiophenes the polymerization time had to be decreased to 15 min. The deprotection of the respective diethyl phosphonate esters or carboxylic esters to the corresponding acids was successful, however, in the case of Phos-Ph-P3HT-Sty the olefin group was destroyed during the deprotection as observed before for the case of Phos-PF8-Sty. Therefore, the polymer Phos-Ph-P3HT-Sty was not utilized further.

Scheme 4.7. Functional conjugated polymers for the functionalization of semiconductor nanocrystals. For the fluorene-based polymers a DP_n of 10 was targeted, for the thiophene-based polymers a DP_n of 15.

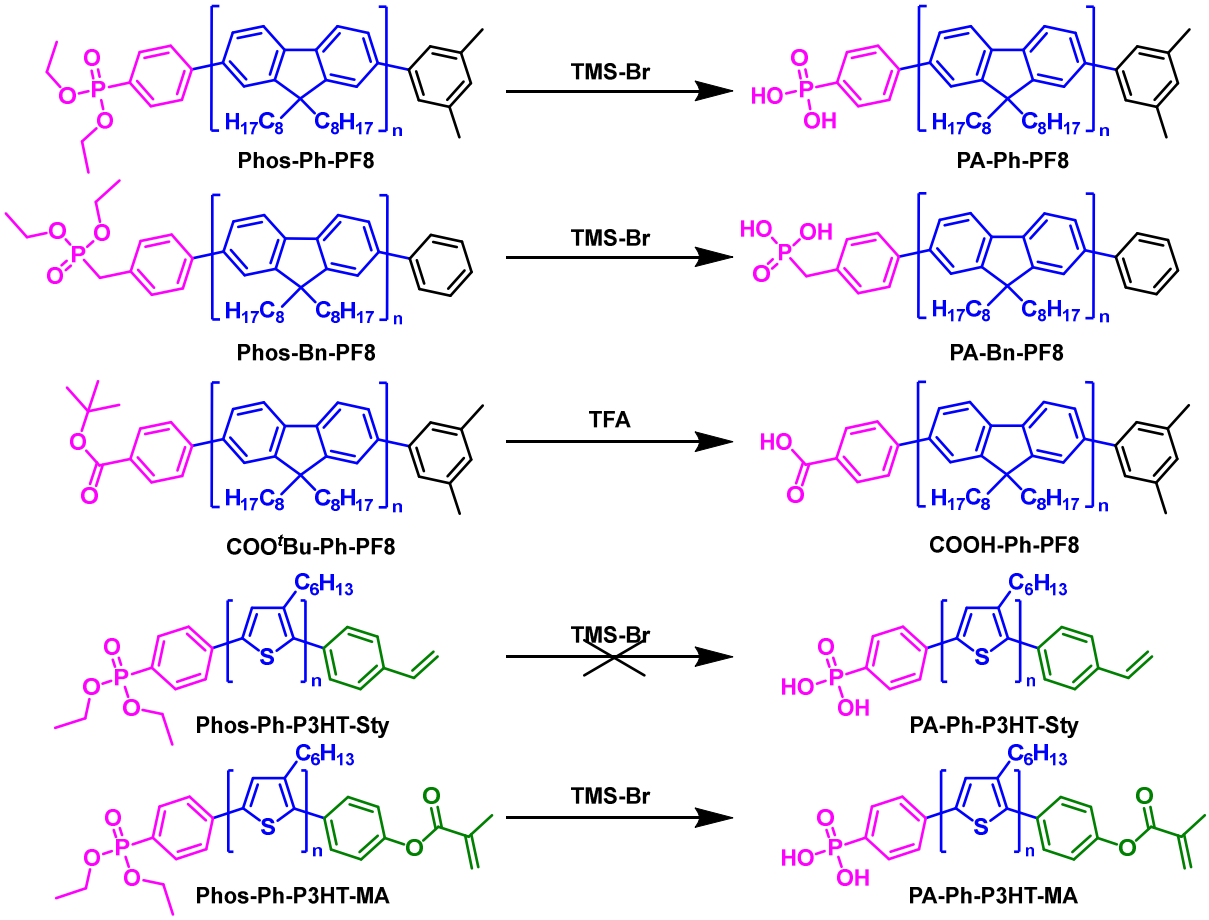

4.2.3 Functional Conjugated Nonconjugated Block Copolymers

The heterodifunctional polymer Phos-PF8-AlkylBr was used as macroinitiator in an ATRP for the synthesis of diblock copolymers. We chose an activators regenerated by electron transfer (ARGET)[212] ATRP approach in order to minimize the amount of copper catalyst present in the system. As comonomer methyl methacrylate (MMA), styrene (Sty) and 2-ethylhexyl methacrylate (EHMA) were used as they have been successfully applied for the embedding of semiconductor nanocrystals (**Chapter 6**). A PMMA block was grown from the PF8 macroinitiator (**Table 4.2**, entry 1). The polymerization was stopped at an MMA conversion of 52%. The molecular weight distribution stayed narrow during the polymerization (**Figure 4.4**). GPC measurements were performed using simultaneous detection by RI and UV (370 nm). By comparison with the GPC trace of the macroinitiator, it is apparent that all macroinitiator was converted. Homo-PMMA is not detected by the UV detector at a wavelength of 370 nm. Therefore, it can be concluded that indeed a block

copolymer was formed, and as the signal of the RI detector and the UV detector match well, no additional 'sacrificial' homo-PMMA was formed.

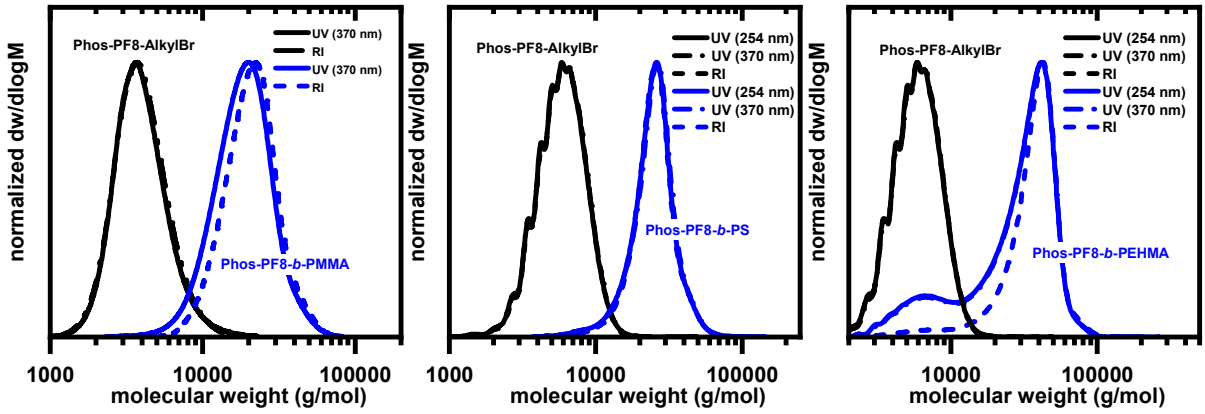

Figure 4.4. Molecular weight distribution (GPC) of the respective PF8 macroinitiator Phos-PF8-AlkylBr (black) and the Phos-PF8-*b*-PMMA diblock copolymer (left, blue, **Table 4.2**, entry 1), the Phos-PF8-*b*-PS block copolymer (center, blue, **Table 4.2**, entry 7) and the Phos-PF8-*b*-PEHMA block copolymer (right, blue, **Table 4.2** entry 11). Reprinted with permission from ref.[5] Copyright **2019** American Chemical Society.

The successful formation of a block copolymer is further confirmed by diffusion ordered (DOSY) NMR spectroscopy (**Figure 8.20**) as all parts of the polymer have the same diffusion coefficient. The theoretical number of MMA units per PF8 is given by the conversion of the monomer and the ratio of monomer to macroinitiator. According to ^{1}H NMR analysis of the block copolymer 152 MMA units were attached to one PF8 chain (**Figure 4.5**) which fits perfectly to the theoretical value of 150. Additionally, the quantitative conversion of the macroinitiator is supported by ^{1}H NMR spectroscopy as the singlet of the methyl protons of the 2-bromo-2-methylpropanoate is shifted upfield (**Figure 8.21**).

In entries 2–5, Phos-PF8-AlkylBr with different chain lengths (DP_n = 5, 10, 15 and 20) were used as macroinitiators generating Phos-PF8-*b*-PMMA block copolymers with similar total molecular weight.

Table 4.2. Synthesis of PF8 conjugated nonconjugated diblock copolymers by ARGET ATRP.

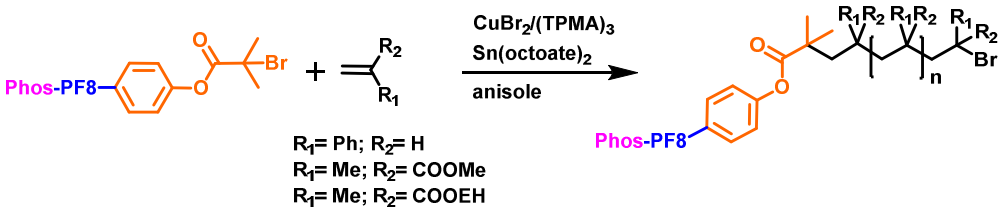

#	macroinitiator M_n[a] [g mol^{-1}] (M_w/M_n)	monomer	n[mon]/ n[ini]	time [h]	p [%][d]	M_n (GPC)[e] [kg mol^{-1}]	M_w/M_n	monomer units/chain[f]
1	3953 (1.16)	MMA[b]	300	10	52	23	1.23	152
2	2398 (1.16)	MMA[b]	200	20	88	19	1.23	200
3	4341 (1.16)	MMA[b]	200	20	85	18	1.20	180
4	6284 (1.17)	MMA[b]	200	20	76	19	1.60	100
5	11450 (1.20)	MMA[b]	200	18	64	19	1.18	80
6	4341 (1.20)	Sty[c]	185	2	45	18	1.40	90
7	4341 (1.18)	Sty[c]	185	3	55	19	1.10	130
8	4341 (1.18)	Sty[c]	185	16	75	23	1.14	180
9	4341 (1.16	Sty[c]	100	20	74	17	1.15	85
10	4341 (1.16)	Sty[c]	280	21	72	36	1.50	210
11	4341 (1.16)	EHMA[b]	200	3	85	24	1.30	218

General polymerization conditions: 200 ppm of $CuBr_2$/(tris(2-pyridylmethyl)amine (TPMA))$_3$ vs. amount of monomer, 12 equiv. of Sn(octoate)$_2$ vs. Cu. a) M_n was determined by ^{1}H NMR spectroscopy. b) Polymerization at 90 °C. c) Polymerization at 110 °C. d) The conversion of the monomer was determined by ^{1}H NMR spectroscopy. e) Determined by GPC (tetrahydrofuran, 35 °C, vs. polystyrene standards, RI detection. f) Determined by ^{1}H NMR spectroscopy.

To demonstrate the scope of Phos-PF8-AlkylBr as a macroinitiator and to obtain block copolymers compatible with polystyrene (PS) or poly(2-ethylhexyl methacrylate) (PEHMA), also hard PS and soft and hydrophobic PEHMA blocks were grown from the macroinitiator. For the synthesis of polystyrene diblock copolymers only the reaction temperature had to be raised to 110 °C (**Table 4.2**, entries 6–10). Block copolymers with narrow molecular weight distributions consisting of a Phos-PF8 block with a DP_n of 10 and 90, respectively, 130 and 180 styrene-derived repeat units were successfully synthesized (**Table 4.2**, entries 6–8) by increasing the polymerization time from 2 to 3 or 16 h. A complete conversion of the macroinitiator to the block copolymer without formation of PS homo-polymer is evidenced by GPC measurements (**Figure 4.4**) using

three-fold detection (RI, UV 254 nm, UV 370 nm). The length of the PS block was adjusted by changing the ratio of monomer to macroinitiator. Setting the ratio to 100, a short PS block consisting of 85 styrene units was grown from the macroinitiator while maintaining a narrow M_w/M_n of 1.15. The polymerization was stopped at a conversion of 74% and the chain length of the styrene-block matches well to the expected length. By increasing the monomer-to-macroinitiator ratio to 280 (entry 10), a longer PS block consisting of 210 styrene units was attached.

The same ARGET ATRP system was used to attach a soft and hydrophobic PEHMA block to the Phos-PF8-AlkylBr macroinitiator. The formation of a block copolymer was proven by GPC measurement (**Figure 4.4**) and DOSY NMR spectroscopy (**Figure 8.24**). The number of EHMA units per PF8 as determined by NMR (**Figure 8.25**) fits well to the theoretical value. A small amount of macroinitiator (< 6%) was not converted to a block copolymer which is demonstrated by GPC analysis using UV detection.

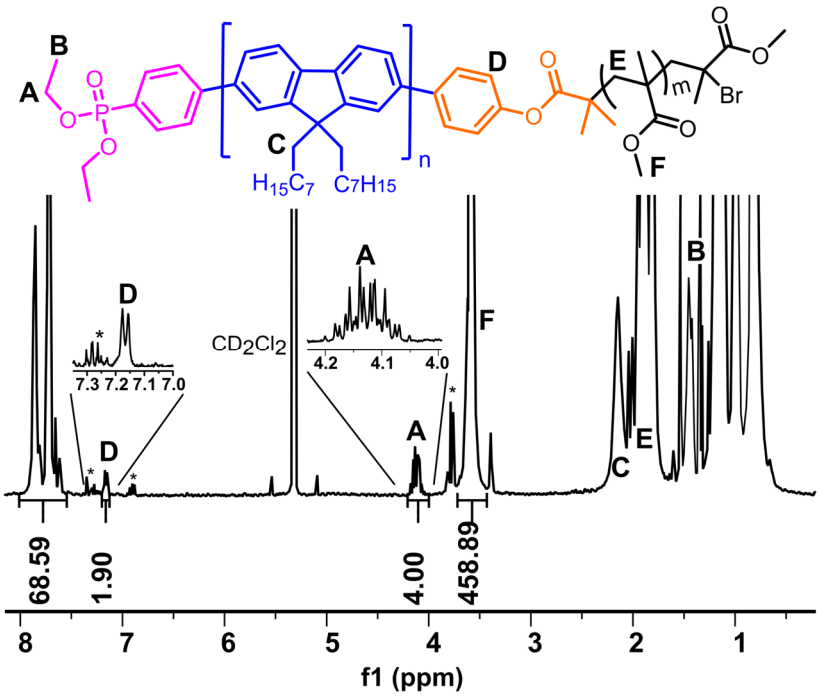

Figure 4.5. ^{1}H NMR spectrum of the Phos-PF8-*b*-PMMA block copolymer from entry 1, **Table 4.2**. Residual anisole is marked with an asterisk**.** Reprinted with permission from ref.[5] Copyright **2019** American Chemical Society.

For the use of these polymers in the functionalization of semiconductor nanocrystals the transformation of the diethyl phenylphosphonate group to the phenylphosphonic acid was necessary. Therefore, selected polymers were deprotected by the 'McKenna reaction' (**Scheme 4.6**). The deprotection of the diblock copolymers proceeded smoothly and no cleavage of the connecting carboxylic ester or of the ester groups in the methacrylate

polymers was observed (see **Figure 4.6** for the NMR spectra of an exemplary deprotection of a Phos-PF8-*b*-PMMA diblock copolymer).

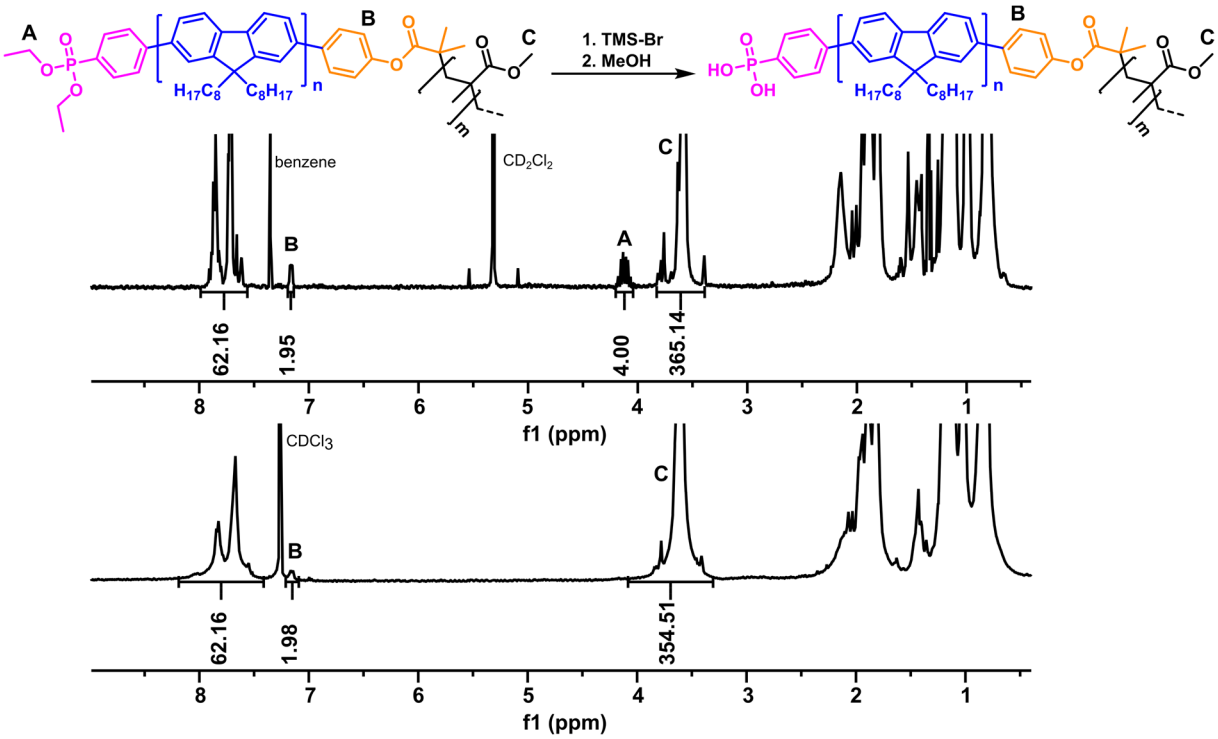

Figure 4.6. ^{1}H NMR spectra of a Phos-PF8-*b*-PMMA diblock copolymer (top) and the respective deprotected diblock copolymer PA-PF8-*b*-PMMA (bottom). As no significant change in the ratio of the integrals of the aromatic protons and the 0-C**H**$_3$ (labeled with C) protons was observed, ester hydrolysis can be excluded. A complete deprotection of the diethyl phenylphosphonate moiety is proven by the disappearance of the signals of the P-O-**CH**$_2$-CH$_3$ group (labeled with A).

GPC analysis was not possible due to interaction of the polymers with the columns, however, the integrity of the diblock copolymers was additionally confirmed by DOSY NMR spectroscopy (**Figure 8.26**).

4.2.4 Functional Conjugated Nonconjugated Comb Polymers

Comb polymers consisting of a nonconjugated backbone and phosphonic acid-functionalized PF8 side groups could serve as multi-dentate ligands for the functionalization of semiconductor nanocrystals. For the synthesis of such unprecedented comb polymers (**Scheme 4.1**), the conjugated polymer Phos-PF8-Sty was used as macromonomer and copolymerized with nonconjugated monomers (Sty, MMA, EHMA) generating comb copolymers. Phos-PF8-Sty was copolymerized with Sty in ratios of Sty to macromonomer of 170, 85, 50 and 20 using an ARGET ATRP approach (**Table 4.3**, entries 1–4). In all experiments, random comb copolymers of macromonomer and Sty were formed, as evidenced by GPC measurements (**Figure 4.7**).

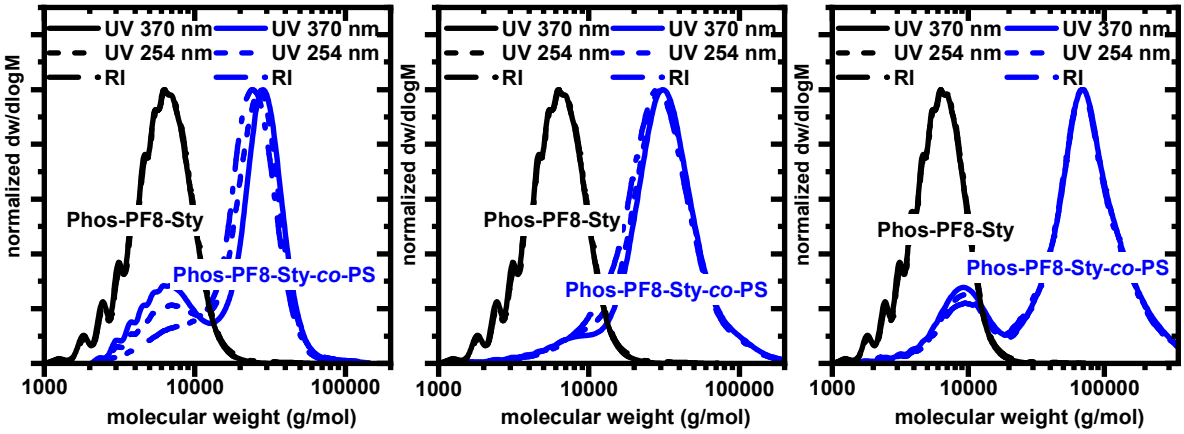

Figure 4.7. Molecular weight distributions (GPC) of random copolymers of Phos-PF8-Sty and Sty. Left: Ratio of Sty to Phos-PF8-Sty is 124/1 (**Table 4.3**, entry 1). Center: Ratio of Sty to Phos-PF8-Sty is 45/1 (entry 3). Right: Ratio of Sty to Phos-PF8-Sty is 20/1 (entry 4). Reprinted with permission from ref.[5]. Copyright **2019** American Chemical Society.

As the conversion of Sty reached only around 70% (the reaction was stopped as this point as the mixture was highly viscous, also impeding further reaction), it is not surprising that a small amount of macromonomer was also not consumed as the macromonomer should show a reactivity similar to styrene. The composition of the copolymers as determined by NMR spectroscopy (**Figure 8.27** for an exemplary spectrum) agrees well with the monomer-to-macromonomer ratio in the initial reaction mixture.

We chose a diethyl phenylphosphonate group as functional moiety for the second PF8 terminus as it can be used to tether the polymer to a surface. By changing the ratio of macromonomer to comonomer, the amount of phosphonate groups per chain was increased from around only two to up to twelve groups. Therefore, the comb polymers

with a high content of phosphonate groups per chain can be regarded as multivalent ligands.

Table 4.3. Synthesis of comb polymers by copolymerization of Phos-PF8-Sty and olefins by atom transfer radical polymerization.

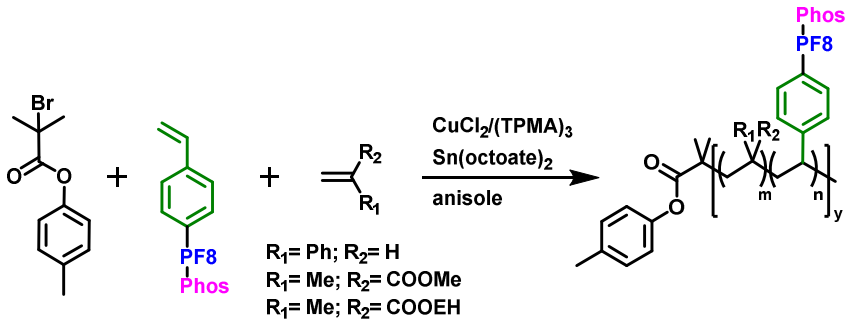

#	co-monomer	ratio n[comonomer] /n[Phos-PF8-Sty]	v(solvent)/ v(monomer)	time [h]	temp [°C]	p[c] [%]	M_n[d] [kg mol^{-1}]	M_w/M_n	incorporated ratio [comonomer]/ [Phos-PF8-Sty][f]	PF8 side chains/ comb polymer chain[g]
1[a]	Sty	170	1:1	25	110	68	25[e]	1.1[e]	124	2
2[a]	Sty	85	1:1	25	110	65	36[e]	1.2[e]	74	3
3[b]	Sty	50	2:1	20	110	63	29	1.5	45	4
4[b]	Sty	20	2:1	20	110	68	68[e]	1.4[e]	20	12
5[a]	MMA	185	2:1	17	90	75	39	1.6	140	2
6[b]	MMA	50	2:1	17	90	76	40	1.4	65	4
7[b]	MMA	20	2:1	17	90	81	95	1.7	24	15
8[b]	EHMA	50	1:1	16	90	97	52[e]	1.2	49	4
9[b]	EHMA	20	2:1	16	90	96	100[e]	1.6	16	15

General polymerization conditions: 200 ppm of $CuCl_2/(TPMA)_3$ vs. total amount of monomer, 12 equiv. of $Sn(octoate)_2$ vs. Cu, 200 equiv. of monomer vs. initiator. a) 0.015 mmol of Phos-PF8-Sty with M_n 3814 g mol^{-1} (NMR) and a M_w/M_n of 1.17 (GPC) used. b) 0.029 mmol of Phos-PF8-Sty with M_n 3814 g mol^{-1} (NMR) and M_w/M_n of 1.19 (GPC) used. c) Conversion of the comonomer as determined by ^{1}H NMR spectroscopy. d) Determined by GPC (tetrahydrofuran, 35 °C, vs. polystyrene standards, RI detection). e) Bimodal molecular weight distribution, only the major peak was analyzed. f) Molar ratio of the two monomers incorporated in the comb polymer as determined by ^{1}H NMR spectroscopy. g) The absolute number of side chains (Phos-PF8) per comb polymer chain was determined by division of M_n(GPC) by the molar mass of one theoretical repeat unit, calculated by using the molar ratio of the incorporated monomers.

The macromonomer Phos-PF8-Sty can also be copolymerized with a more polar monomer such as MMA (**Table 4.3**, entries 5–7) using the same reaction conditions as for the copolymerization with Sty. Assuming the macromonomer to have a copolymerization parameter comparable to styrene, the consumption of Phos-PF8-Sty should be slightly favored in the copolymerization with MMA given the copolymerization parameters of

r_{Sty} = 0.52 and r_{MMA} = 0.42.[241] Indeed, well defined copolymers of Phos-PF8-Sty and MMA were formed with complete conversion of the macromonomer (**Figure 4.8**).

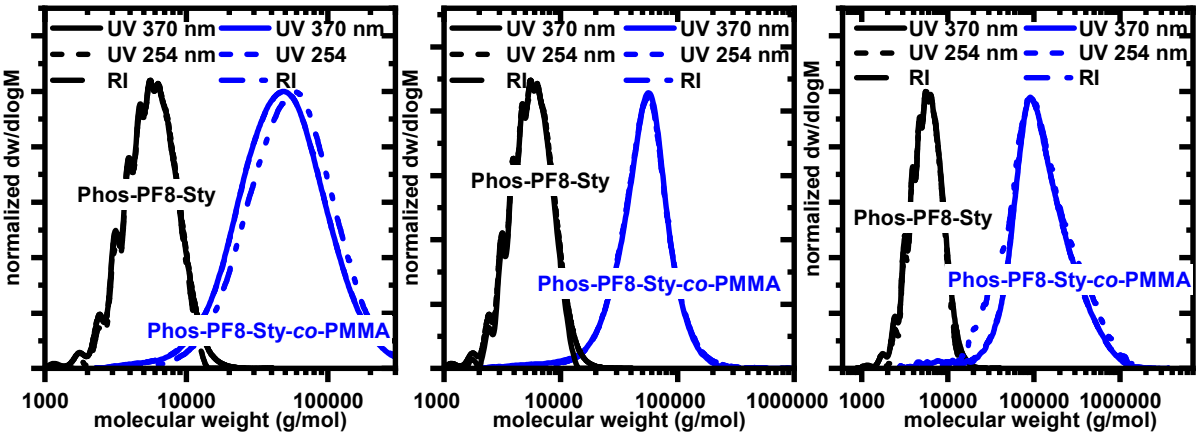

Figure 4.8. Molecular weight distributions (GPC) of random copolymers of Phos-PF8-Sty and MMA. Left: Ratio of MMA to PF8-Sty is 140/1 (entry 5). Center: Ratio of MMA to PF8-Sty is 65/1 (entry 6). Right: Ratio of MMA to PF8-Sty is 24/1 (entry 7). Reprinted with permission from ref.[5] Copyright **2019** American Chemical Society.

The NMR spectrum (**Figure 4.9**) of the polymer obtained in experiment 7, **Table 4.3** displays PS-like aromatic signals (marked with D) in a ratio of 1:1 to the phosphonate moiety, which additionally evidences a quantitative polymerization of the styrene-type end group.

Comb polymers showing ratios of MMA to PF8 of 140, 65 and 25 were obtained, which corresponds to 2, 4, 15 phosphonate groups per polymer chain.

In order to generate a soft, hydrophobic comb polymer which should feature a good solubility in nonpolar solvents (as normally used for the synthesis or functionalization of semiconductor nanocrystals), copolymers of the macromonomer Phos-PF8-Sty and the hydrophobic monomer EHMA were produced (**Table 4.3**, entries 8–9) using the same ARGET ATRP system. Comb copolymers (**Figure 8.30 – Figure 8.32**) with 4–15 phosphonate groups per chain were obtained.

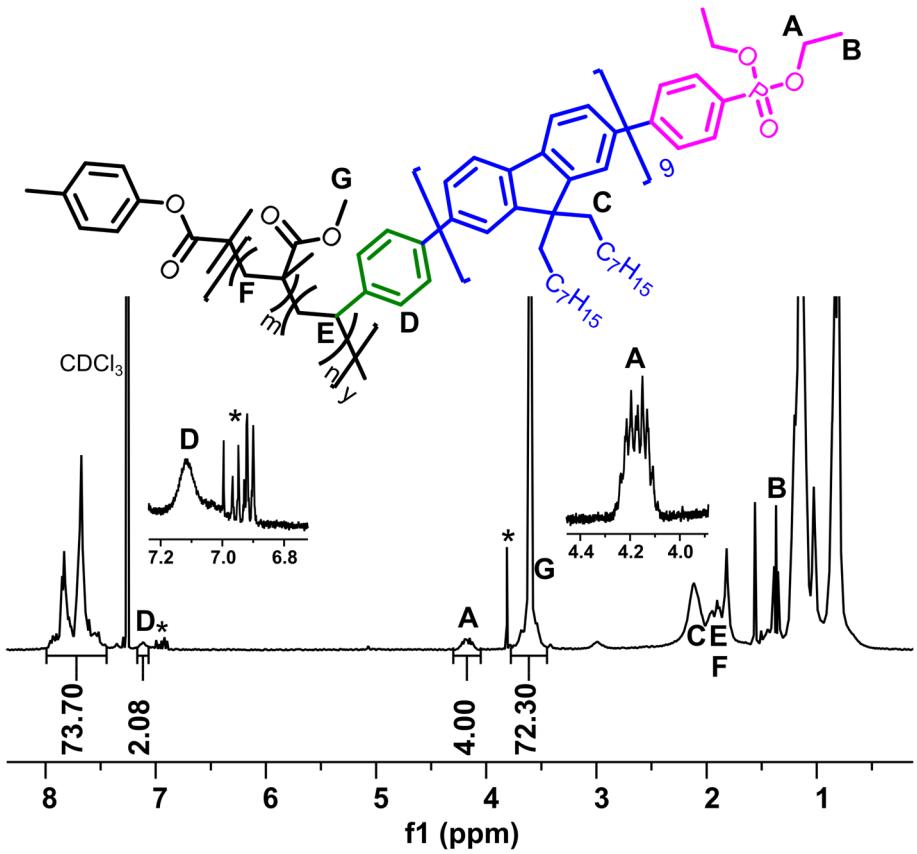

Figure 4.9. Exemplary ^{1}H-NMR spectrum of the comb polymer Phos-PF8-Sty-*co*-PMMA obtained in experiment 7, **Table 4.3**. Residual anisole is marked with an asterisk. Reprinted with permission from ref.[5] Copyright **2019** American Chemical Society.

For the functionalization of semiconductor nanocrystals with these conjugated nonconjugated comb copolymers, the diethyl phenylphosphonate group had to be transformed into the free phenylphosphonic acid. The deprotection was performed as described in the previous chapters (**Chapters 4.2.1** and **4.2.3**) using the 'McKenna reaction'. **Figure 4.10** depicts the NMR spectra of an exemplary Phos-PF8-*co*-PEHMA copolymer before and after deprotection. The diethyl phenylphosphonate groups were completely dealkylated (signal A vanished) and as the ratio between the integral of the aromatic protons (C) and the carboxylic ester protons (B) remained constant, no carboxylic acid ester cleavage occurred. Also, for the other comb polymers, the diethyl phenylphosphonate group was successfully dealkylated to yield the corresponding phenylphosphonic acid-type end groups, and in case of polymers with a polymethacrylate (MMA or EHMA) backbone, no cleavage of the carboxylic esters was observed. However, the solubility of polymers bearing several PF8 side chains changed substantially during the deprotection. While the protected polymers are all well soluble in solvents such as $CHCl_3$, CH_2Cl_2 or toluene, the deprotected polymers PA-PF8-Sty-*co*-PMMA and PA-PF8-

Sty-*co*-PS are hardly soluble in those solvents but can be dissolved in tetrahydrofuran or dimethyl sulfoxide. PA-PF8-Sty-*co*-PEHMA, as the most lipophilic comb copolymer, still shows a decent solubility in warm toluene. The solubility of the deprotected comb copolymers is improved by the addition of a small amount of oleic acid (~5 vol%). During the deprotection, the polarity of the polymer is increased which agrees with the improved solubility in more polar solvents. Additionally, alkylphosphonic acids can form inter- and intramolecular superstructures and anhydrides that are probably badly soluble in the case of high molecular weight polymeric phosphonic acids. These formations are probably suppressed by the addition of an acidic solvent.

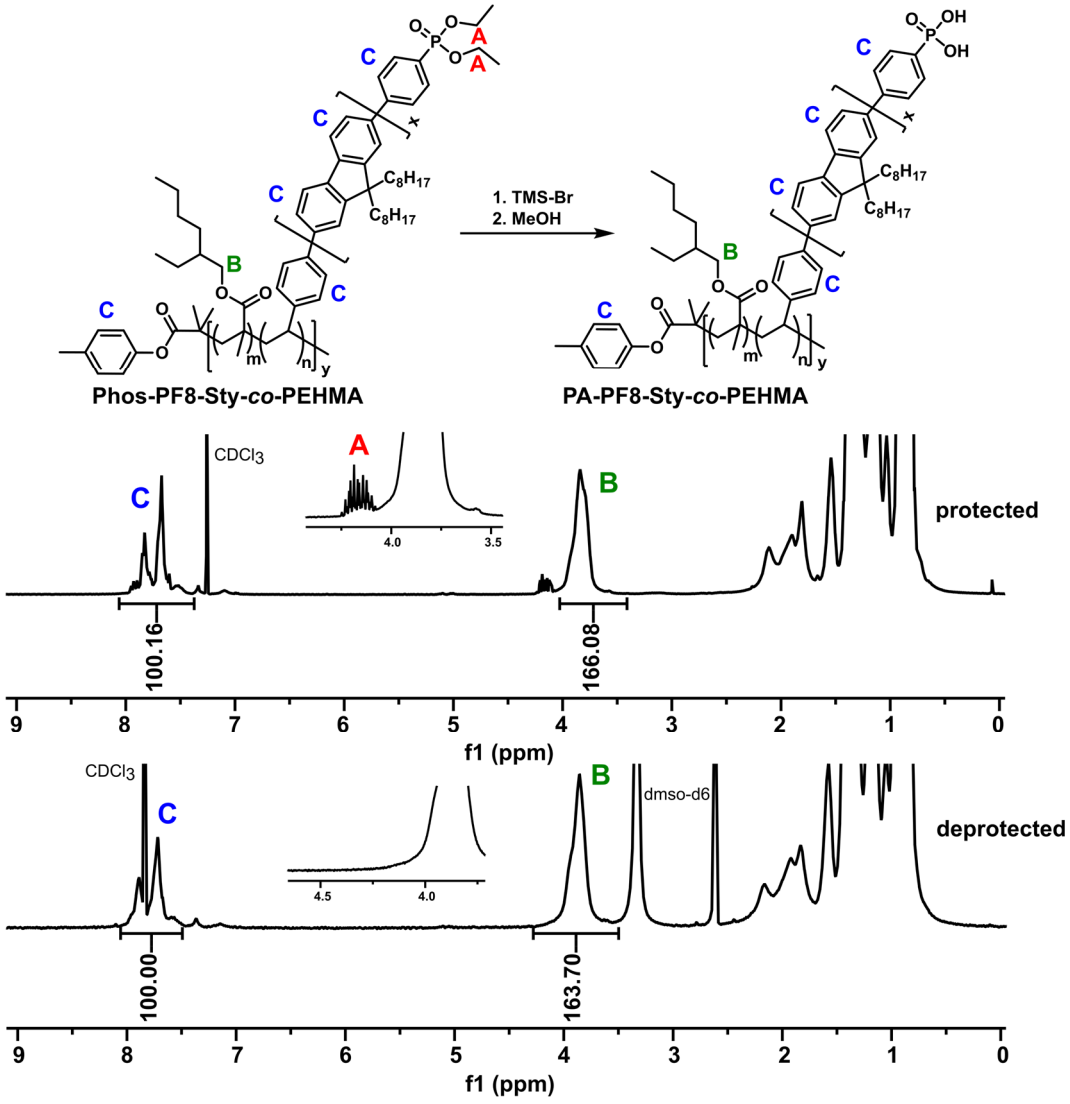

Figure 4.10. ^{1}H NMR spectra of the deprotection of an exemplary Phos-PF8-Sty-*co*-PEHMA (top) comb copolymer to the corresponding free phenylphosphonic acid-functionalized PA-PF8-Sty-*co*-PEHMA (bottom) copolymer.

4.3 Summary and Conclusion

The controlled Suzuki-Miyaura cross-coupling polymerization (cSMCCP) is a powerful tool for the synthesis of heterodifunctional polymers. A novel and straightforward approach to the synthesis of conjugated nonconjugated copolymers by sequential cSMCCP and controlled radical polymerization was developed. As a first step, well-defined heterodifunctional PF8s featuring a phosphonate group (initiating chain end) and a radically polymerizable or ATRP-initiating group (terminating chain end) were generated by catalytic chain growth (**Scheme 4.8**).

Scheme 4.8. Heterodifunctional PF8s obtained by cSMCCP.

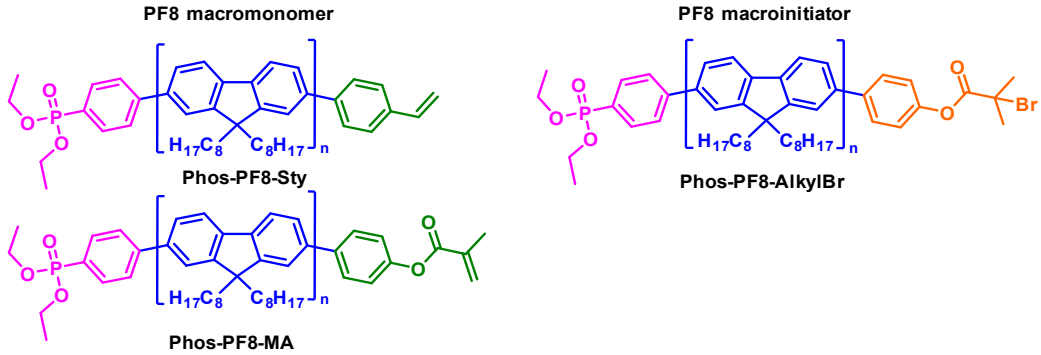

Three-coordinate Pd(II) initiators generated *in situ* from the respective arylbromide and PdG2P^{t}Bu$_3$ were found to perform equally well as compared to the corresponding tediously isolated Pd(II) complexes. The resulting polymers were directly employed for the growth of a second nonconjugated block without further intermediate conversion steps (**Scheme 4.9**). ARGET ATRP of styrene or methacrylates, respectively, from PF8 macroinitiators under appropriate conditions afforded narrowly distributed diblock copolymers free of homo-polymers.

Scheme 4.9. Straightforward synthesis of conjugated nonconjugated block copolymers by sequential cSMCCP and ARGET ATRP. Reprinted with permission from ref.[5] Copyright **2019** American Chemical Society.

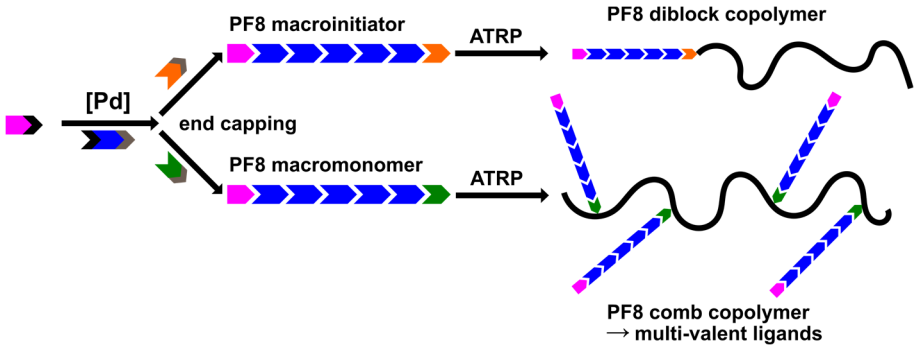

The diethyl phenylphosphonate group of these polymers could selectively be transformed to the corresponding phosphonic acid without cleavage of any carboxylic acid esters present in the polymers.

Controlled radical copolymerization of PF8 macromonomers bearing a styrene-type end group with styrene or methacrylates, respectively, opens access to conjugated nonconjugated comb polymers. The number of PF8 side chains per backbone chain can be tuned by the ratio of the two monomers employed. Notably, this approach allows the incorporation of functional end groups, as demonstrated here for phosphonates. The latter are relevant for binding to nanoparticle and macroscopic surfaces. The multivalent character of the comb polymers is of particular interest as it may allow for an efficient and strong attachment to nanoparticles. For the intended functionalization of CdSe/CdS nanoparticles, the diethyl phenylphosphonate groups of these comb polymers were selectively transformed to the corresponding phosphonic acids. However, the deprotected comb polymers showed a reduced solubility as compared to their protected counterparts which can potentially limit their application as nanoparticle ligands.

Nevertheless, two novel species of conjugated nonconjugated copolymers (block and comb) were synthesized in an unprecedented straightforward way.

4.4 Experimental Section

4.4.1 Materials and General Considerations

All chemicals were used as received unless stated otherwise. Standard organic solvents and chemicals were obtained from various commercial suppliers such as Sigma-Aldrich, ABCR, VWR and Roth. Tris(2-pyridylmethyl)amine (TPMA, > 98%), 2-ethylhexyl methacrylate (EHMA) (> 99%, stabilized with MEHQ), diethyl (4-bromobenzyl)phosphonate (> 98%), 2-(3,5-dimethylphenyl)-4,4,5,5-tetramethyl-1,3,2-dioxaborolane (> 97%) and 4-vinylphenylboronic acid were acquired from TCI. 4-Hydroxyphenylboronic acid pinacol ester, 1-bromo-4-iodobenzene (97%), tin(II) 2-ethylhexanoate (Sn(octoate)$_2$), fluorene, 1-bromooctane, 1-bromohexane, *tert*-butyl 4-bromobenzoate, tri-*iso*-propyl borate and 2-bromo-2-methylpropionyl bromide (97%) were supplied by ABCR. Pinacol (98%), CsF (99%), 18-crown-6 (> 99%), anisole (> 99%), chloro[(tri-*tert*-butylphosphine)-2-(2-aminobiphenyl)] palladium(II) (> 98%), methyl methacrylate (MMA) (99%, contains < 30 ppm MEHQ as inhibitor), styrene (> 99%, contains 4-*tert*-butylcatechol as stabilizer), 1,1′-ferrocenediyl-bis(diphenylphosphine), phenylboronic acid pinacol ester (> 98%), 3-bromothiophene, bis(dibenzylideneacetone)palladium(0), palladium(II) acetate, 4-cyano-4-((phenylcarbonothioyl)thio)pentanoic acid, bis(pinacolato)diboron, 2-butanone, diethyl phosphite (98%), [1,3-dis(diphenylphosphino)propane]-dichloronickel(II), 4,4′-di-*tert*-butyl-2,2′-dipyridyl, tri-*tert*-butylphosphine solution (1M in toluene), bis(1,5-cyclooctadiene)diiridium(I) dichloride, copper(II) bromide (99%) and copper(II) chloride (99%) were purchased from Sigma-Aldrich.

Deionized water was distilled under a nitrogen atmosphere, and THF was distilled from sodium/benzophenone ketyl under a nitrogen atmosphere. *N,N*-Dimethylformamid (DMF) was distilled over CaH_2 and triethylamine was distilled over KOH under a nitrogen atmosphere. Dichloromethane, toluene and *n*-pentane were dried and degassed on a commercial MBraun solvent purification system (BASF PuriStar® R3-11G / 4 Å molecular sieves). Anisole (Sigma-Aldrich, > 99%) was dried over 4 Å molecular sieves and degassed by sparging with nitrogen for 1 h. Methacrylate monomers were filtered over basic aluminum oxide, dried over 4 Å molecular sieves, degassed by three freeze-pump-thaw cycles and stored inside a glovebox at -30 °C. Styrene was vacuum transferred, degassed by three freeze-pump-thaw cycles and stored inside a glovebox at -30 °C.

All manipulations of air- and /or water sensitive compounds were carried out under inert atmosphere using standard glove box and Schlenk techniques.

4.4.2 Analytical Methods

Nuclear Magnetic Resonance (NMR) Spectroscopy

NMR spectra were recorded on a Bruker Avance III 400 and on a Bruker Avance III HD 400 spectrometer (^{1}H: 400 MHz, ^{13}C: 101 MHz, ^{19}F: 376 MHz, ^{31}P: 162 MHz). ^{1}H-NMR and ^{13}C-NMR chemical shifts were referenced to the residual signal of the deuterated solvent. Multiplicities are given as follows: s: singlet, d: doublet, t: triplet, q: quartet, p: quintet, m: multiplet.

Diffusion Ordered NMR Spectroscopy (DOSY NMR)

DOSY NMR spectra were measured on a Bruker Avance III HD 400 at 300 K running TopSpin3 using the pulse sequence ledbpgp2s. The diffusion parameters, consisting of the gradient pulse length δ/2 (0.1 s to 0.2 s) and the diffusion delay Δ (700 µs to 5000 µs) were chosen such that a signal decay of roughly 90 – 95% was obtained at a gradient strength of 95%. The gradient strength was linearly (16 or 32 increments) varied from 2 to 98% of the maximum strength. DOSY workup and processing was performed using the GNAT software tool by Nilsson et al.[242] or the TopSpin3 software package.

Gel permeation chromatography (GPC)

GPC measurements were carried out on a Polymer Laboratories PL-GPC 50 with two PLgel 5 µm MIXED-C columns in THF at 50 °C with RI and UV (370 nm) detection against polystyrene standards or on a PSS Agilent 1260 Infinity II equipped with two PSS SDV LinearM analytical columns at 35 °C using refractive index and UV detection (254 nm and simultaneously 370 nm) and linear calibration vs. polystyrene standards.

Matrix Assisted Laser Desorption Ionization Time of Flight Mass Spectrometry (MALDI-TOF MS)

MALDI-TOF MS measurements were carried out on a Bruker Microflex MALDI-TOF using tetrahydrofuran as solvent and *trans*-2-[3-(4-*tert*-butylphenyl)-2-methyl-2-propenylidene]malononitrile (DCTB) or α-cyano-4-hydroxycinnamic acid (HCCA) as matrix.

4.4.3 Syntheses of Monomers, Initiators and End-Capping Agents

Synthesis of 2,7-dibromofluorene[243]

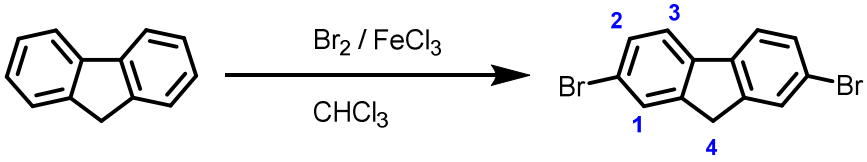

To a solution of 56.5 g of fluorene (339.9 mmol, 1 equiv.) in 500 mL of $CHCl_3$, 1.4 g of $FeCl_3 \cdot 6\ H_2O$ (5.1 mmol, 0.015 equiv.) was added. The mixture was cooled to -10 °C and 115 g of bromine (719.9 mmol, 2.12 equiv.) was added dropwise over a period of 2 h under exclusion of light. The mixture was stirred for 3 h and allowed to warm to room temperature. 100 mL of an aqueous $Na_2S_2O_5$ solution was added and the mixture was vigorously stirred for 30 min until the brown color disappeared. The organic layer was separated, and the water layer was extracted with 200 mL of CH_3Cl. The combined organic layers were washed with water, dried over $MgSO_4$ and the solvent was removed under reduced pressure. The crude product was recrystallized from ethanol yielding 100 g (308 mmol, 90%) of white crystals.

^{1}H-NMR (400 MHz, $CDCl_3$, 25 °C): δ = 7.62 (m, 2H, H_3), 7.53 (m, 2H, H_1), 7.47 (m, 2H, H_2), 3.78 (s, 2H, H_4) ppm.

Synthesis of 2,7-dibromo-9,9-dioctylfluorene[244]

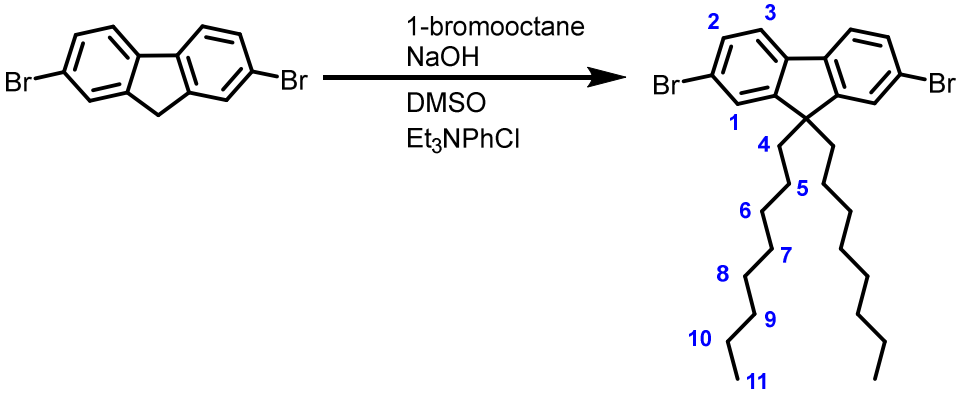

To a solution of 50 g (154 mmol, 1 equiv.) of 2,7-dibromofluorene in 250 mL of degassed dimethyl sulfoxide, benzyltriethylammonium chloride (1.76 g, 7.71 mmol, 0.05 equiv.) was added. 70 g (854 mmol, 5.5 equiv.) of an aqueous NaOH solution (50 w%) was added and the resulting suspension was thoroughly degassed. 1-Bromooctane (71.5 g, 370 mmol, 2.4 equiv.) was added and the mixture was shaken overnight on a lab shaker at room temperature. After addition of diethyl ether (500 mL), the organic phase was

separated, sequentially washed with water, 2 M HCl and brine and dried over $MgSO_4$. The solvent was removed under reduced pressure and the residue was recrystallized from ethanol yielding 73 g (133 mmol, 87%) of white crystals.

^{1}H NMR (400 MHz, $CDCl_3$, 25 °C): δ = 7.52 (m, 2H, H_3), 7.45 (m, 4H, H_{1-2}), 1.95-1.86 (m, 4H, H_4), 1.27-1.00 (m, 20H, H_{6-10}), 0.83 (t, $^3J_{HH}$ = 7.1 Hz, 6H, H_{11}), 0.59 (m, 4H, H_5) ppm.

Synthesis of (7-bromo-9,9-dioctyl-9H-fluoren-2-yl)boronic acid[220]

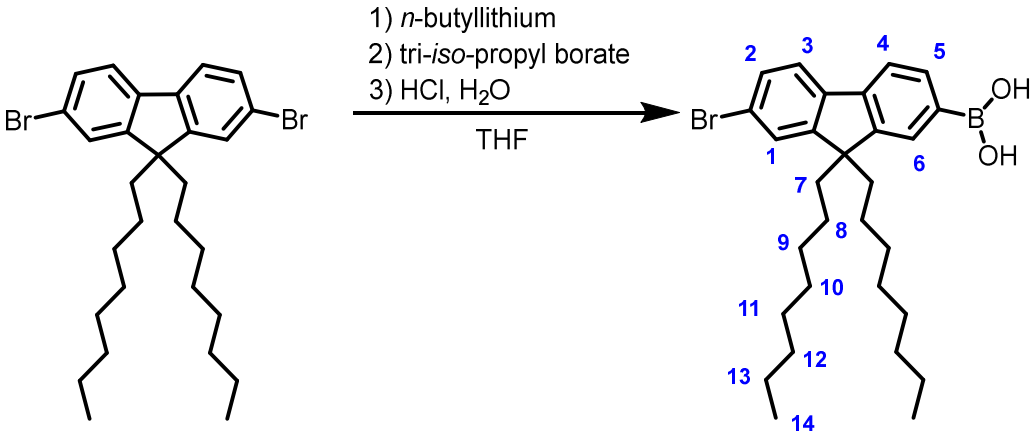

In a 500 mL Schlenk flask, 20 g (36.4 mmol, 1 equiv.) of 2,7-dibromo-9,9-dioctyl-9H-fluorene was dissolved in 200 mL of dry and degassed THF. The colorless solution was cooled to -78 °C and 25.1 mL (40.1 mmol, 1.1 equiv.) of a 1.6 M solution of *n*-butyllithium in *n*-hexane was continuously added by syringe within 15 min. After stirring for 90 min at -78 °C, 11.7 mL (51.05 mmol, 1.4 equiv.) of tri-*iso*-propyl borate was added. The reaction mixture was stirred overnight and allowed to warm up to rt. 10 mL of 2 M HCl and 100 mL of H_2O were added, and the product was extracted with 100 mL of petrol ether and the aqueous phase was extracted two more times with 100 mL of petrol ether. The combined organic phases were dried over $MgSO_4$ and the solvent was removed in vacuo. A yellow oil was obtained, which was purified by column chromatography (12 : 1 petrol ether : ethyl acetate to 6 : 1 PE: ethyl acetate) over silica gel. 7.865 g (15.3 mmol, 42%) of the product were obtained as a colorless oil.

^{1}H NMR (400 MHz, dmso-d6 / D_2O, 25 °C): δ = 8.00 (s, 1H, H_6), 7.82 (s, 1H, H_1), 7.79 – 7.71 (m, 2H, H_{2-3}), 7.64 (m, 1H, H_4), 7.48 (m,1H, H_5), 2.20-1.95 (m, 4H, H_7), 1.35 – 0.88 (m, 20H, H_{9-13}), 0.76 (t, $^3J_{HH}$ = 7.1 Hz, 6H, H_{14}), 0.55 – 0.34 (m, 4H, H_8) ppm.

Synthesis of 2-(7-bromo-9,9-dioctyl-*9H*-fluoren-2-yl)-4,4,5,5-tetramethyl-1,3,2-dioxaborolane[245]

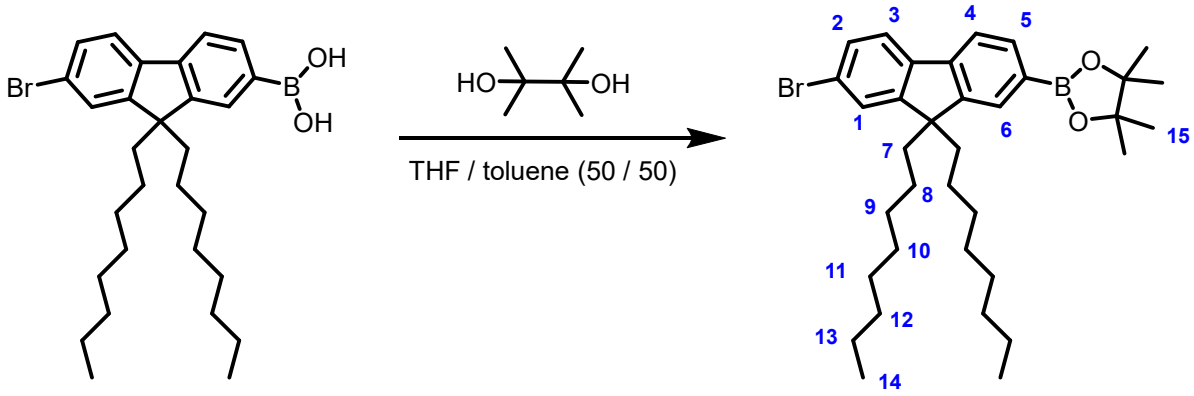

In a 250 mL flask, 7.865 g (15.3 mmol, 1 equiv.) of (7-bromo-9,9-dioctyl-9H-fluoren-2-yl)boronic acid and 2.172 g (18.3, 1.2 equiv.) of pinacol were dissolved in 100 mL of an 1 : 1 mixture of THF and toluene. At complete dissolution, the solvent was removed at 40 °C by a rotary evaporator. The procedure of dissolving and evaporation was repeated for three more times. At the last time, the solvent was removed completely in vacuo. The obtained colorless oil was recrystallized three times from ethanol. 3.911 g (6.6 mmol, 41%) of 2-(7-bromo-9,9-dioctyl-9H-fluoren-2-yl)-4,4,5,5-tetramethyl-1,3,2-dioxaborolane were obtained as colorless crystals in high purity.

^{1}H NMR (400 MHz, $CDCl_3$, 25 °C): δ = 7.81 (m, 1H, H_4), 7.73 (m, 1H, H_3), 7.66 (m, 1H, H_1), 7.57 (m, 1H, H_5), 7.46 (m, 2H, H_2, H_6), 2.06-1.88 (m, 4H, H_7), 1.39 (s, 12H, H_{15}), 1.27-1.04 (m, 20H, $H_{9\text{-}13}$), 0.82 (t, $^3J_{HH}$ = 7.1 Hz, 6H, H_{14}), 0.59 (m, 4H, H_8) ppm.

Synthesis of 3-hexylthiophene[246]

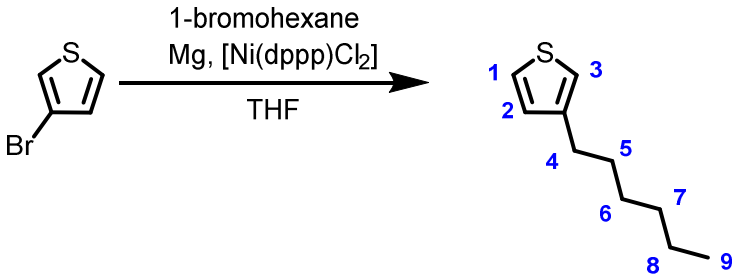

31.64 g (191.7 mmol, 1.25 equiv.) of 1-bromohexane was diluted in 150 mL of dry and degassed THF. This mixture was slowly added to a flask containing 4.82 g (198.4 mmol, 1.29 equiv.) of magnesium turnings and 50 mL of THF. The addition rate was adjusted to maintain a gentle reflux of THF. After complete addition, the mixture was stirred for additional 2 hours until all magnesium was consumed. This mixture was slowly added to another flask containing a solution of 3-bromothiophene (25 g, 153.3 mmol, 1 equiv.) and

415 mg (0.76 mmol, 0.005 equiv.) of [Ni(dppp)Cl_2] in 50 mL of THF at 0 °C. After stirring for 3 hours, the mixture was allowed to warm to room temperature and stirred for additional 24 hours. The mixture was quenched by pouring into a mixture of HCl (2M) and ice water. The aqueous phase was extracted with diethyl ether (1*150 mL, 1*50 mL) and the combined organic phases were washed with a saturated $NaHCO_3$ solution, and two times with water. The organic phases were dried over $MgSO_4$ and the solvent removed in vacuo. The crude product was purified by distillation at 55 °C and 0.55 mbar, resulting in a colorless oil with a yield of 70% (107 mmol,18 g).

^{1}H-NMR (400 MHz, $CDCl_3$, 25 °C): δ = 7.23 (m, 1H, H_1), 6.98-6.89 (m, 2H, H_{2-3}), 2.63 (t, $^3J_{HH}$ = 7.9 Hz, 2H, H_4), 1.63 (m, 2H, H_5), 1.40-1.27 (m, 6H, H_{6-8}), 0.90 (t, $^3J_{HH}$ = 7.6 Hz, 3H, H_9) ppm.

Synthesis of 2-bromo-3-hexylthiophene[246]

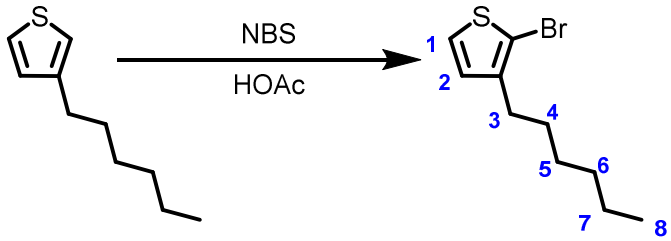

13.4 g (79.8 mmol, 1 equiv.) of 3-hexylthiophene was dissolved in 80 mL of nitrogen purged acetic acid, and under light exclusion 14.2 g (79.8 mmol, 1 equiv.) of *N*-bromosuccinimide (NBS) was slowly added. The mixture was stirred under a nitrogen atmosphere overnight, and then poured into a mixture of water (200 mL) and diethyl ether (200 mL). After phase separation, the water phase was additionally extracted with 100 mL of diethyl ether, and the combined organic phases were washed with 2M NaOH until a pH of 6-7 was reached. The combined organic phases were dried over $MgSO_4$ and the solvent removed under reduced pressure. Purification of the crude product was performed by distillation at 44 °C at 1.2 mbar, yielding a colorless oil in a yield of 65% (51 mmol, 12.8 g).

^{1}H-NMR (400 MHz, $CDCl_3$, 25 °C): δ = 7.19 (d, $^3J_{HH}$ = 5.6 Hz, 1H, H_1), 6.80 (d, $^3J_{HH}$ = 5.6 Hz, 1H, H_2), 2.59 (t, $^3J_{HH}$ = 7.7 Hz, 2H, H_3), 1.58-1.49 (m, 2H, H_4), 1.40-1.26 (m, 6H, H_{5-7}), 0.91 (t, $^3J_{HH}$ = 6.7 Hz, 3H, H_8) ppm.

Synthesis of 2-(5-bromo-4-hexylthiophen-2-yl)-4,4,5,5-tetramethyl-1,3,2-dioxaborolane[246]

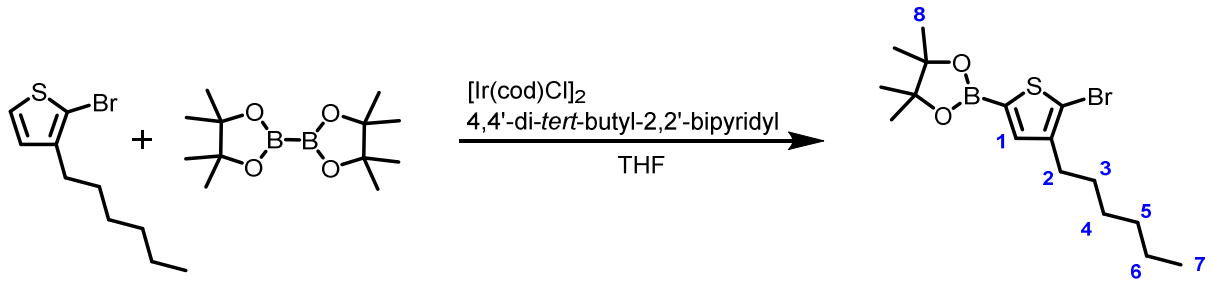

5.0 g (20.2 mmol, 1 equiv.) of 2-bromo-3-hexylthiophene, 5.2 g (20.4 mmol, 1.01 equiv.) of bis(pinacolato)diboron, 54 mg (0.2 mmol, 0.001 equiv.) of 4,4'-di-*tert*-butyl-2,2'-dipyridyl and 67 mg (0.1 mmol, 0.0005 equiv.) of bis(1,5-cyclooctadiene)diiridium(I) dichloride were dissolved in 75 mL of dry and degassed THF and stirred for 24 hours at 65 °C. The mixture was poured onto water (100 mL) and extracted with diethyl ether (1*150 mL, 1*50 mL). The combined organic phases were washed with brine, water, and dried over magnesium sulfate. The solvent was removed in vacuo and the obtained red oil was purified by column chromatography (pure petrol ether → petrol ether : ethyl acetate 50 : 50). A colorless oil was obtained in a yield of 50% (11 mmol, 4.1 g).

^{1}H-NMR (400 MHz, $CDCl_3$, 25 °C): δ = 7.32 (s, 1H, H_1), 2.56 (t, $^3J_{HH}$ = 7.8 Hz, 2H, H_2), 1.58 (m, 2H, H_3), 1.33 (s, 12H, H_8), 1.34-1.24 (m, 6H, H_{4-6}), 0.91 (t, $^3J_{HH}$ = 6.9 Hz, 3H, H_7) ppm.

Synthesis of diethyl (4-bromophenyl)phosphonate[247]

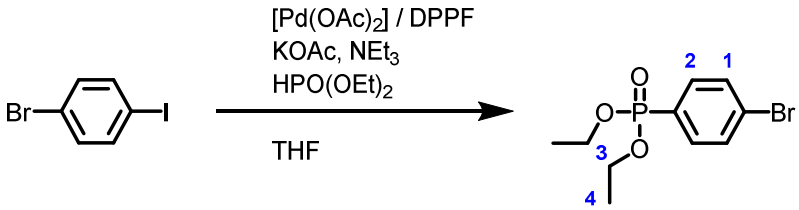

4 g (14.1 mmol, 1 equiv.) of 1-bromo-4-iodobenzene, 140 mg (1.41 mmol, 0.1 equiv.) of potassium acetate and 390 mg (0.705 mmol, 0.05 equiv.) of 1,1′-ferrocenediyl-bis(diphenylphosphine) (dppf) and 80 mg (0.35 mmol, 0.025 equiv.) of palladium (II) acetate were placed in 200 mL Schlenk tube and degassed by applying vacuum for 10 min and purging with nitrogen (3 times). 100 mL of dry and degassed THF and 2.4 mL (17.62 mmol, 1.25 equiv.) of NEt_3 were added. The mixture was heated to 60 °C, stirred for 45 min, and 2.18 mL (16.9 mmol, 1.2 equiv.) of degassed diethyl phosphite was added over a period of 15 min. The mixture was stirred for 12 hours at 60 °C, filtered, and the solvent of the filtrate was removed under reduced pressure. A brown oil was obtained

which was purified by column chromatography (PE : EA 70 : 30 to PE : EA 0 : 100) yielding 2.5 g (8.5 mmol, 60%) of the desired product as slightly brown oil.

^{1}H-NMR (400 MHz, $CDCl_3$, 25 °C) δ = 7.63 (m, 4 H, $H_{1\text{-}2}$), 4.10 (m, 4 H, H_3), 1.31 (t, 6 H, $^3J_{HH}$ = 7.05 Hz, H_4) ppm.

^{31}P{^{1}*H*}-NMR (162 MHz, $CDCl_3$, 25 °C) δ = 17.7 ppm.

Synthesis of bis(tri-*tert*-butylphosphine)palladium(0)[248]

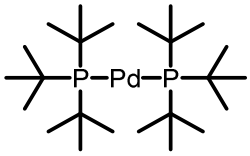

7.3 mL (7.3 mmol, 2.1 equiv.) of a 1 M solution of P^{t}Bu$_3$ in toluene was concentrated to dryness and 7 mL of degassed and dry DMF was added. 2 g (3.47 mmol, 1 equiv.) of bis(dibenzylideneacetone)palladium(0) dispersed in 8 mL of DMF was added and the mixture was stirred for 4.5 hours at room temperature. The formed white precipitate was filtered off, washed with the filtrate (4 times) and with 5 mL of DMF (2 times). The solid was dissolved in 5 mL of pentane, the solvent was evaporated, and the obtained white crystals were dried under reduced pressure to obtain the desired product (1.4 g, 2.7 mmol, 77%).

^{1}H-NMR (400 MHz, C_6D_6, 25 °C) δ = 1.52 (dd, $^3J_{PH}$ = 7.0 Hz, $^5J_{PH}$ = 5.6 Hz, 54 H) ppm.

^{31}P{^{1}*H*}-NMR (162 MHz, C_6D_6, 25 °C) δ = 85.06 ppm.

Synthesis of bromo(4-diethoxyphosphoryl-phenyl)(tri-*tert*-butylphosphine) palladium[113]

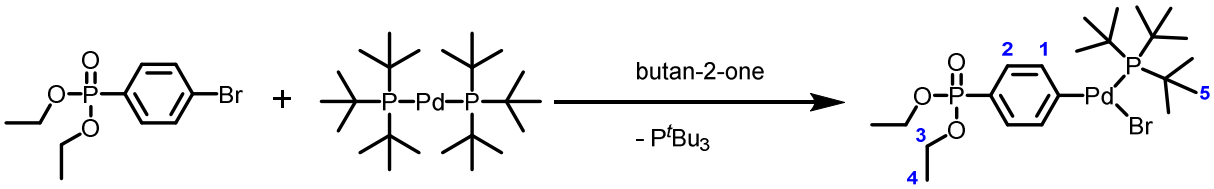

300 mg (0.587 mmol, 1 equiv.) of bis(tri-*tert*-butylphosphine)palladium(0) and 258 mg (0.88 mmol, 1.5 equiv.) of diethyl (4-bromophenyl)phosphonate were dissolved in 30 mL of dry and degassed butan-2-one. The mixture was stirred for 3 hours at 75 °C, afterwards the solvent was removed in vacuo. 15 mL of dry and degassed pentane was added, and the mixture was sonicated for 30 min in an ultrasonic bath. The yellow suspension was transferred to a centrifugation flask, centrifuged, and the supernatant discarded. The product was washed two times with 8 mL of pentane and dried under reduced pressure

yielding 120 mg (0.199 mmol, 34%) of a yellow powder. The product was stored inside a nitrogen-filled glovebox at –25 °C.

^{1}H-NMR (400 MHz, C_6D_6, 25 °C) δ = 7.73 – 7.40 (m, 4H, $H_{1\text{-}2}$), 4.12 – 3.61 (m, 4H, H_3), 1.02 (t, $^{3}J_{HH}$ = 7.1 Hz, 6H, H_4), 0.97 (d, $^{3}J_{HP}$ = 12.6 Hz, 27H, H_5) ppm.

^{31}P{*^{1}H*}-NMR (162 MHz, C_6D_6, 25 °C) δ = 62.9 (**P**^{t}Bu$_3$), 19.3 (**P**(OEt)$_2$) ppm.

Synthesis of 4-vinylphenylboronic acid pinacol ester[249]

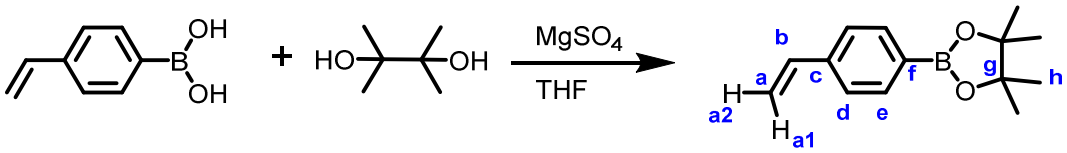

1 g (6.8 mmol, 1 equiv.) of 4-vinylphenylboronic acid and 0.8 g (6.8 mmol, 1 equiv.) of pinacol were dissolved in 50 mL of anhydrous THF and two spatula tips of magnesium sulfate were added. The mixture was stirred at rt for 3 h and filtered. The solvent was removed under reduced pressure, yielding a colorless powder (1.4 g,6.1 mmol, 90%).

^{1}H-NMR (400 MHz, $CDCl_3$, 300 K) δ = 7.78 (d, $^{3}J_{HH}$ = 8.1 Hz, 2H, H_e), 7.41 (d, $^{3}J_{HH}$ = 8.1 Hz, 2H, H_d), 6.73 (dd, $^{3}J_{HH}$ = 17.6, 10.9 Hz, 1H, H_b), 5.82 (dd, $^{3}J_{HH}$ = 17.6 Hz, $^{2}J_{HH}$ = 1.0 Hz, 1H, H_{a1}), 5.30 (dd, $^{3}J_{HH}$ = 10.9 Hz, $^{2}J_{HH}$ = 1.0 Hz, 1H, H_{a2}), 1.35 (s, 12H, H_h) ppm.

^{13}C{*^{1}H*}-NMR (151 MHz, $CDCl_3$, 300 K) δ = 140.36 (C_c), 137.04 (C_b), 135.16 (C_e), 125.66 (C_d), 114.99 (C_a), 83.92 (C_g), 25.02 (C_h). C_f not visible.

Synthesis of 4-(4,4,5,5-tetramethyl-1,3,2-dioxaborolan-2-yl)phenyl methacrylate

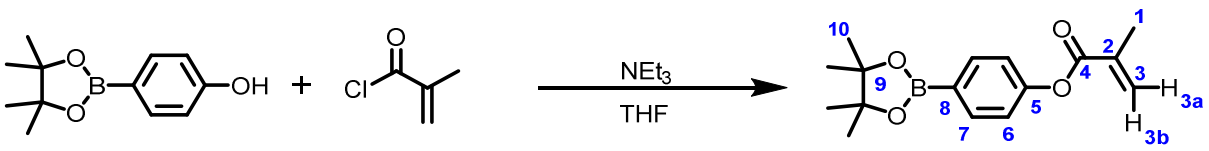

In a 250 mL Schlenk flask, 2 g (9.1 mmol, 1 equiv.) of 4-hydroxyphenylboronic acid pinacol ester was dissolved in 30 mL of anhydrous tetrahydrofuran. At 0 °C, 1.5 mL (10.9 mmol, 1.2 equiv.) of triethylamine was added. 1.05 mL (10.7 mmol, 1.2 equiv.) of methacryloyl chloride was added dropwise via syringe and the reaction mixture was stirred at room temperature overnight. A brown suspension with a white precipitate was obtained. The suspension was diluted with dichloromethane and consecutively washed with saturated aqueous solutions of ammonium chloride, sodium carbonate and sodium chloride. The organic phase was dried over $MgSO_4$ and the solvent was removed in vacuo, yielding a colorless oil. The product was purified by column chromatography (20:1 pentane to ethyl

acetate) over silica gel. 1.550 g (5.4 mmol, 59%) of a colorless crystalline solid were obtained.

^{1}H-NMR (400 MHz, $CDCl_3$, 300 K) δ = 7.84 (m, 2H, H_7), 7.13 (m, 2H, H_6), 6.35 (dq, $^{2}J_{HH}$ = 1.5 Hz, $^{4}J_{HH}$ = 1.0 Hz, 1H, H_{3b}), 5.75 (p, $^{2}J_{HH}$ = 1.5 Hz, $^{4}J_{HH}$ = 1.5 Hz, 1H, H_{3a}), 2.06 (dd, $^{4}J_{HH}$ = 1.5 Hz, $^{4}J_{HH}$ = 1.0 Hz, 3H, H_1), 1.34 (s, 12H, H_{10}) ppm.

^{13}C{^{1}*H*}-NMR (151 MHz, $CDCl_3$, 300 K) δ = 165.77 (C_4), 153.64 (C_5), 136.31 (C_7), 136.04 (C_2), 127.40 (C_3), 121.11 (C_6), 120.76 (C_8), 84.04 (C_9), 25.02 (C_{10}), 18.54 (C_1) ppm.

HR ESI-MS: $[M+Na]^+$ theo.: 311.14 u found: 311.15 u

Synthesis of 4-(4,4,5,5-tetramethyl-1,3,2-dioxaborolan-2-yl)phenyl 2-bromo-2-methylpropanoate

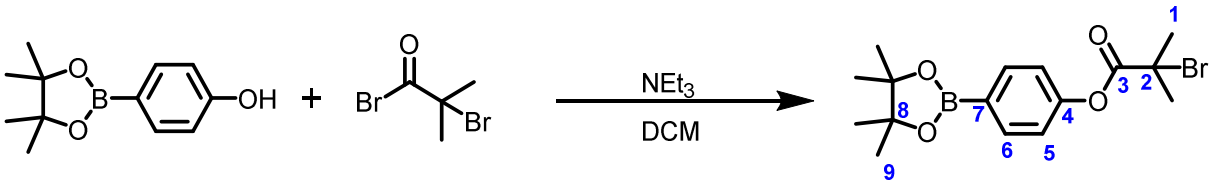

2 g (9.1 mmol, 1 equiv.) of 4-hydroxyphenylboronic acid pinacol ester was dissolved in 50 mL of dry dichloromethane and 1.5 mL (10.9 mmol, 1.2 equiv.) of dry triethylamine was added. The mixture was cooled to 0 °C and 1.34 mL (10.9 mmol, 1.2 equiv.) of 2-bromo-2-methylpropionyl bromide was added dropwise over a period of 15 min. The mixture was stirred at 0 °C for one hour and at room temperature overnight. The organic phase was successively washed with saturated aqueous solutions of ammonium chloride, sodium carbonate and sodium chloride. The organic phase was dried over sodium sulfate and the solvent was evaporated in *vacuo*. The resulting powder was recrystallized from ethanol, yielding 1.35 g (40%, 3.6 mmol) of a colorless powder.

^{1}H-NMR (400 MHz, $CDCl_3$, 300 K) δ = 8.16 – 7.63 (m, 1H, H_6), 7.39 – 6.65 (m, 1H, H_5), 2.07 (s, 6H, H_1), 1.35 (s, 12H, H_9) ppm.

^{1}H-NMR (400 MHz, CD_2Cl_2, 300 K) δ = 7.88 – 7.78 (m, 2H, $H_{6,}$), 7.20 – 7.06 (m, 2H, H_5), 2.06 (s, 6H, H_1), 1.34 (s, 12H, H_9) ppm.

^{13}C{^{1}*H*}-NMR (101 MHz, $CDCl_3$, 300 K) δ = 170.14 (C_3), 153.39 (C_4), 136.38 (C_6), 127.11 (C_7, broad), 120.53 (C_5), 84.08 (C_8), 55.48 (C_2), 30.78 (C_1), 25.00 (C_9) ppm.

^{13}C{^{1}*H*}-NMR (101 MHz, CD_2Cl_2, 300 K) δ = 170.68 (C_3), 153.85 (C_4), 136.65 (C_6), 127.43 (C_7, broad) 121.03 (C_5), 84.57 (C_8), 56.28 (C_2), 31.03 (C_1), 25.24 (C_9) ppm.

Synthesis of *p*-tolyl 2-bromo-2-methylpropanoate

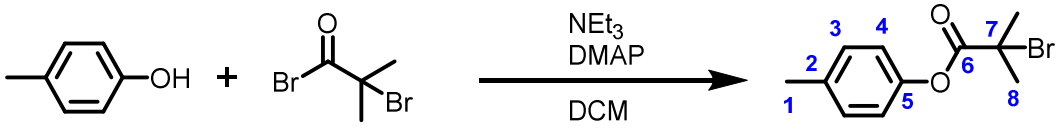

4 g (36.9 mmol, 1 equiv.) of 4-methylphenol, 15.4 mL (110.7 mmol, 3 equiv.) of dry triethylamine and 450 mg (3.67 mmol, 0.1 equiv.) of 4-dimethylaminopyridine were dissolved in 200 mL of dry dichloromethane and cooled to 0 °C. 9.2 mL (44.2 mmol, 1.2 equiv.) of 2-bromo-2-methylpropionyl bromide was added dropwise over a period of 15 min. The mixture was stirred at room temperature overnight, filtered, and the filtrate was washed with a saturated solution of sodium carbonate (3*100 mL) and water (2*100 mL). The organic phase was dried over $MgSO_4$ and the solvent was evaporated in *vacuo*. The product was purified by column chromatography using a mixture of 10 : 1 petrol ether and ethyl acetate. 8 g (84%, 30.9 mmol) of the product was isolated as a slightly yellow liquid.

^{1}H-NMR (400 MHz, CD_2Cl_2, 300 K) δ = 7.26 – 7.19 (m, 2H, H_3), 7.04 – 6.93 (m, 2H, H_4), 2.36 (s, 3H, H_1), 2.05 (s, 6H, H_8) ppm.

^{13}C{*^{1}H*}-NMR (101 MHz, CD_2Cl_2, 300 K) δ = 171.07 (C_6), 149.22 (C_5), 136.63 (C_2), 130.54 (C_3), 121.26 (C_4), 56.41 (C_7), 31.06 (C_8), 21.15 (C_1) ppm.

Synthesis of 4-(4,4,5,5-tetramethyl-1,3,2-dioxaborolan-2-yl)phenyl 4-cyano-4-((phenylcarbonothioyl)thio)pentanoate

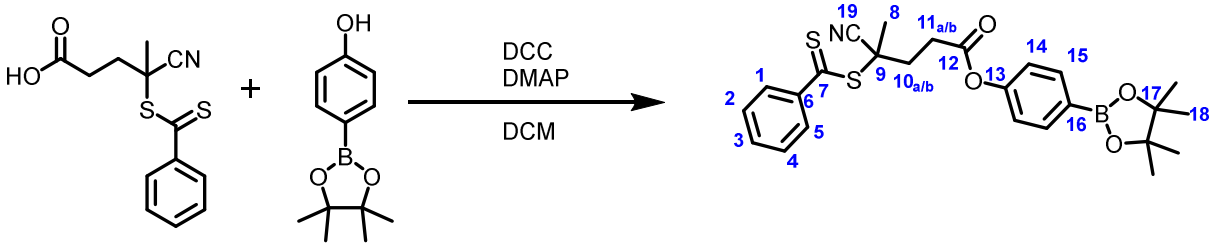

1 g (3.57 mmol, 1 equiv.) of 4-cyano-4-((phenylcarbonothioyl)thio)pentanoic acid and 795.5 mg (3.85 mmol, 1.08equiv.) of dicyclohexylcarbodiimide were dissolved in 25 mL of dry dichloromethane under a nitrogen atmosphere and cooled down to 0 °C. 945 mg (4.29 mmol, 1.2 equiv.) of (4-(4,4,5,5-tetramethyl-1,3,2-dioxaborolan-2-yl)phenol were dissolved in 5 mL of dichloromethane and slowly added. Then, 87 mg (0.714 mmol, 0.2 equiv.) of 4-dimethylaminopyridine dissolved in 5 mL of dichloromethane was added and the mixture was stirred at 0 °C for 2 hours and at room temperature for 20 hours. The turbid mixture was filtered, and the solvent of the filtrate evaporated under reduced

pressure. Purification was performed by column chromatography (dichloromethane : ethyl acetate 20 : 1) yielding 1.0 g (2.8 mmol, 70%) of a pink powder.
^{1}H-NMR (400 MHz, $CDCl_3$) δ = 7.99 – 7.92 (m, 2H, H_1), 7.90 – 7.83 (m, 2H, H_{15}), 7.63 – 7.56 (m, 1H, H_3), 7.43 (m, 2H, H_2), 7.17 – 7.08 (m, 2H. H_{14}), 3.04 – 2.90 (m, 2H, $H_{11a/b}$), 2.75 (ddd, $^2J_{HH}$ = 14.3, $^3J_{HH}$ = 9.3, $^3J_{HH}$ = 6.5, 1H, $H_{10a/b}$), 2.57 (ddd, $^2J_{HH}$ = 14.3, $^3J_{HH}$ = 9.3, $^3J_{HH}$ = 6.5, 1H, $H_{10a/b}$), 2.01 (s, 3H, H_8), 1.36 (s, 12H, H_{18}) ppm.
^{13}C{^{1}*H*}-NMR (101 MHz, $CDCl_3$) δ = 222.28 (C_7), 170.01 (C_{12}), 153.05 (C_{13}), 144.67 (C_6), 136.40 (C_{15}), 133.21 (C_3), 128.74 (C_2), 126.85 (C_1), 120.86 (C_{14}), 118.58 (C_{19}), 84.08 (C_{17}), 45.88 (C_9), 33.51 (C_{10}), 30.22 (C_{11}), 25.01 (C_{18}), 24.45 (C_8) ppm.

4.4.4 General Procedures for Controlled Suzuki-Miyaura Cross-Coupling Polymerizations

General Procedure for Poly(9,9′-dioctylfluorene) – Isolated Initiator

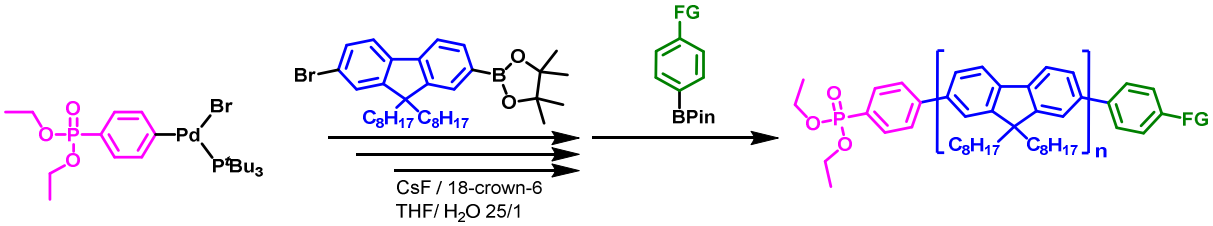

In a typical polymerization, 88 mg (0.149 mmol, 10 equiv.) of 2-(7-bromo-9,9'-dioctyl-9H-fluoren-2-yl)-4,4,5,5-tetramethyl-1,3,2-dioxaborolane, 89.9 mg (0.596 mmol, 40 equiv.) of CsF and 157 mg (0.596 mmol, 40 equiv.) of 18-crown-6 were dissolved in 23 mL of dry and degassed tetrahydrofuran and 1 mL of degassed water. The mixture was thoroughly degassed by three additional freeze-pump-thaw cycles and cooled to 0 °C in an ice bath. Inside a nitrogen glovebox, 9 mg (0.0149 mmol, 1 equiv.) of (bromo)(4-diethoxyphosphoryl-phenyl)(tri-*tert*-butylphosphine) palladium(II) was dissolved in 2 mL of tetrahydrofuran. The Pd initiator was quickly injected into the monomer solution. After one hour, 0.178 mmol (12 equiv.) of the respective end capping agent dissolved in 5 mL of tetrahydrofuran was injected at 0 °C. After stirring over night, 50 mL of dichloromethane and 20 mL of distilled water was added, and the organic phase was separated. The water phase was extracted with 20 mL of dichloromethane two more times. The combined organic phases were washed with brine and the solvent was removed in *vacuo*. The polymer was dissolved in 4 mL of toluene and precipitated from 6 mL of cold methanol. After centrifugation at 6000 g for 10 min, the supernatant was discarded. The polymer was dissolved in 2 mL of toluene and precipitated by addition of

6 mL of cold methanol. After centrifugation at 6000 g for 10 min, the supernatant was discarded again. Finally, the polymer was dissolved in 3 mL of benzene and freeze-dried. The yields were in the range of 60–85%.

General Procedure for Poly(9,9'-dioctylfluorene) – *In Situ* Initiator

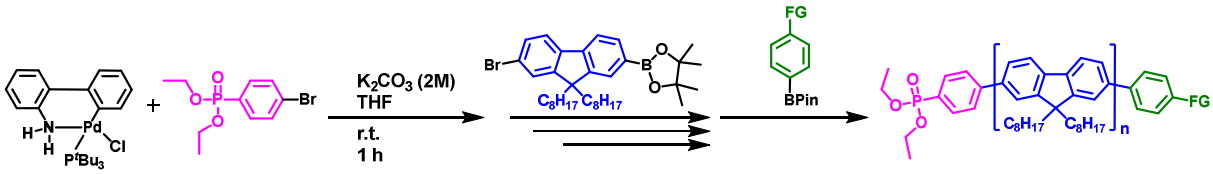

In a typical polymerization, 200 mg (0.336 mmol, 10 equiv.) of 2-(7-bromo-9,9'-dioctyl-9H-fluoren-2-yl)-4,4,5,5-tetramethyl-1,3,2-dioxaborolane was dissolved in 18.7 mL of dry and degassed tetrahydrofuran and afterwards cooled to 0 °C in an ice bath. The initiator solution was prepared by mixing 17 mg (0.0336 mmol, 1 equiv.) of chloro[(tri-*tert*-butylphosphine)-2-(2-aminobiphenyl)] palladium(II) and 15.7 mg (0.054 mmol, 1.6 equiv.) of diethyl (4-bromophenyl)phosphonate in 1.7 mL of tetrahydrofuran inside a nitrogen glovebox. 1.68 mL (3.34 mmol, 100 equiv.) of a thoroughly degassed 2 M aqueous solution of potassium carbonate was added and the mixture was stirred vigorously at room temperature for 1 h. Afterwards, the initiator solution was swiftly injected into the monomer solution. After one hour of polymerization at 0 °C, the polymerization was quenched by injecting the respective end capping agent.

Quenching of the polymerization as well as the work-up of the crude reaction mixture was performed in analogy to the polymerization using the isolated Pd(II) initiator.

The yields were in the range of 70–90%.

Polymerization conditions for different DP_n:

DP_n = 5: 20 min at 0 °C, n(monomer)/n(Pd) = 5, 50 equiv. of K_2CO_3, 6 equiv. of end capping agent.

DP_n = 15: 80 min at 0 °C, n(monomer)/n(Pd) = 15, 150 equiv. of K_2CO_3, 12 equiv. of end capping agent.

DP_n = 20: 120 min at 0 °C, n(monomer)n/(Pd) = 20, 200 equiv. of K_2CO_3, 12 equiv. of end capping agent.

General Procedure for Poly(3-hexylthiophenes) – Isolated Initiator

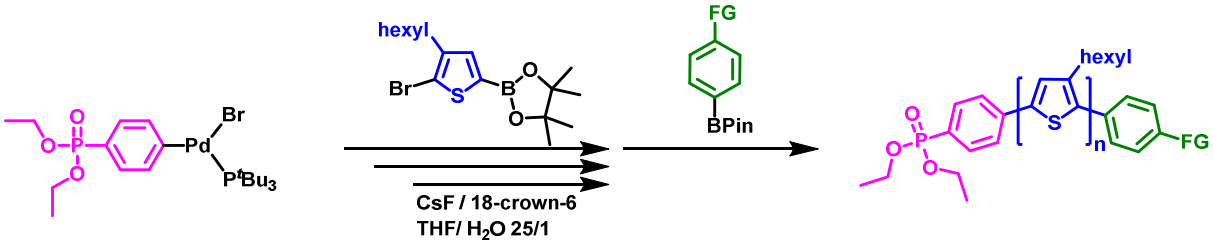

The polymerization of 2-(5-bromo-4-hexylthiophen-2-yl)-4,4,5,5-tetramethyl-1,3,2-dioxaborolane was performed under the same conditions as the polymerization of 2-(7-bromo-9,9'-dioctyl-9H-fluoren-2-yl)-4,4,5,5-tetramethyl-1,3,2-dioxaborolane using (bromo)(4-diethoxyphosphoryl-phenyl)(tri-*tert*-butylphosphine) palladium(II) as initiator. The polymerization time was reduced to 15 min to target a degree of polymerization of 15.

General Procedure for Poly(3-hexylthiophenes) – *In Situ* Initiator

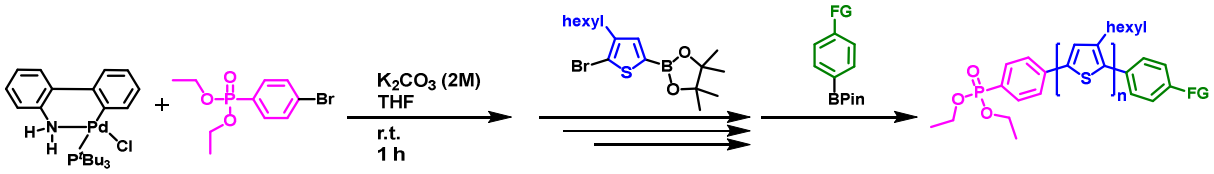

The polymerization of 2-(5-bromo-4-hexylthiophen-2-yl)-4,4,5,5-tetramethyl-1,3,2-dioxaborolane was conducted under the same conditions as the polymerization of 2-(7-bromo-9,9'-dioctyl-9H-fluoren-2-yl)-4,4,5,5-tetramethyl-1,3,2-dioxaborolane using chloro[(tri-*tert*-butylphosphine)-2-(2-aminobiphenyl)] palladium(II) and diethyl (4-bromophenyl)phosphonate as *in situ* initiator system. The polymerization time was reduced to 15 min for a targeted degree of polymerization of 15.

4.4.5 Synthesis of Conjugated Nonconjugated Block Copolymers by ATRP

Exemplary Procedure for the Synthesis of Phos-PF8-*b*-PMMA

A stock solution of the copper catalyst was prepared by mixing 10 mg (0.0447 mmol, 1 equiv.) of $CuBr_2$ and 38.9 mg (0.134 mmol, 3 equiv.) of tris(2-pyridylmethyl)amine (TPMA) in 10 mL of anisole.

Phos-PF8-AlkylBr macroinitiator was dissolved in anisole in a 10 mL Schlenk tube which was sealed by a rubber septum and the mixture was thoroughly degassed by three freeze-pump-thaw cycles. The amount of anisole was adjusted such that the total volume of anisole was twice the volume of methyl methacrylate.

A monomer solution was prepared by mixing methyl methacrylate (e.g. 200 equiv. vs. amount of Phos-PF8-AlkylBr macroinitiator), 200 ppm of copper catalyst (amount vs. monomer) and tin(II) 2-ethylhexanoate (12 equiv. vs. amount of copper). This solution was degassed by three freeze-pump-thaw cycles.

The solution of the Phos-PF8-AlkylBr macroinitiator was placed in a heating block at 90 °C and the monomer mixture was quickly injected via a degassed syringe. Samples were taken at timed intervals and analyzed by GPC and ^{1}H NMR spectroscopy to follow the progress of the reaction.

After the desired conversion had been reached, the Schlenk tube was taken out of the heating block and opened to air. 3 mL of tetrahydrofuran was added. The mixture was filtered over basic alumina and precipitated from petrol ether. The polymer was collected by centrifugation and dissolved in a minimal amount of tetrahydrofuran and precipitated by the addition of methanol and collected by centrifugation. Finally, the polymer was dried under reduced pressure.

Phos-PF8-*b*-PS

The synthesis of Phos-PF8-*b*-PS followed the same procedure as the synthesis of Phos-PF8-*b*-PMMA. The polymerization temperature was raised to 110 °C and the polymer was precipitated from methanol. The conversion of styrene was determined by ^{1}H NMR spectroscopy.

Phos-PF8-*b*-PEHMA

The synthesis of Phos-PF8-Sty-*b*-PEHMA followed the same procedure as the synthesis of Phos-PF8-Sty-*b*-PMMA. The polymerization temperature was set to 90 °C and the polymer was precipitated from methanol. The conversion of 2-ethylhexylmethacrylate was determined by ^{1}H NMR spectroscopy.

4.4.6 Synthesis of Conjugated Nonconjugated Comb Polymers by ATRP

Exemplary Procedure for the Synthesis of Phos-PF8-Sty-*co*-PMMA

All following steps were performed inside a nitrogen-filled glovebox. A stock solution of $CuCl_2$/$(TPMA)_3$ in anisole (0.60 mg $CuCl_2$/mL), a stock solution of $Sn(octoate)_2$ in anisole (32 mg $Sn(octoate)_2$/mL) and a stock solution of *p*-tolyl 2-bromo-2-methylpropanoate in anisole (61 mg/mL) were prepared. In all polymerizations, 200 ppm of copper catalyst relative to the amount of monomer and 200 equiv. of monomer vs. initiator were used.

The Phos-PF8-Sty macromonomer was dissolved in an 8 mL vial in a mixture of anisole (the monomer to anisole ratio was adjusted by the addition of the required amount of anisole), MMA, a stock solution of $CuCl_2/(TPMA)_3$ in anisole and a stock solution of $Sn(octoate)_2$ in anisole (12 equiv. Sn vs. Cu). This mixture was stirred for 10 min at room temperature and a stock solution of *p*-tolyl 2-bromo-2-methylpropanoate in anisole was added. The 8 mL vial was placed in a preheated aluminum block at 90 °C. Conversion of MMA was determined by ^{1}H NMR spectroscopy by comparison of the integral of the olefinic protons of MMA and the integral of the methoxy group of PMMA.

The polymerization was stopped by opening the vial outside the glovebox and the addition of 4 mL of tetrahydrofuran. The polymer mixture was filtered over neutral alumina to remove the cooper catalyst and precipitated from petrol ether. The polymer was dried in vacuum at 60 °C for 24 h.

Phos-PF8-Sty-*co*-PS

The synthesis of Phos-PF8-Sty-*co*-PS followed the same procedure as the synthesis of Phos-PF8-Sty-*co*-PMMA. The polymerization temperature was raised to 110 °C and the polymer was precipitated from methanol. The conversion of styrene was determined by ^{1}H NMR spectroscopy.

Phos-PF8-Sty-*co*-PEHMA

The synthesis of Phos-PF8-Sty-*co*-PEHMA followed the same procedure as the synthesis of Phos-PF8-Sty-*co*-PMMA. The polymerization temperature was set to 90 °C and the polymer was precipitated from methanol. The conversion of 2-ethylhexylmethacrylate was determined by ^{1}H NMR spectroscopy.

4.4.7 Deprotection of Polymers

General procedure for the deprotection of diethyl arylphosphonate-functionalized polymers

Note: It is important to use Teflon grease instead of silicone grease and glass stoppers instead of silicone rubber septa, as silicone grease and silicone rubber septa are destroyed/ dissolved by trimethylsilyl bromide.

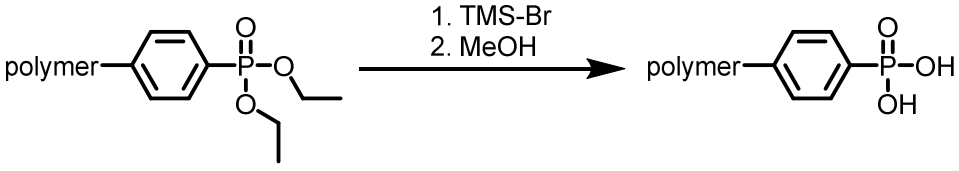

The diethyl phenylphosphonate- or diethyl benzylphosphonate-functionalized polymer was dried under reduced pressure and then dissolved in dry dichloromethane. The mixture was cooled to 0 °C in an ice bath and trimethylsilyl bromide (10 equiv. per phosphonate group) was slowly added. The mixture was allowed to warm to room temperature and stirred for 4 hours. Solvent and unreacted trimethylsilyl bromide were removed in vacuo. The polymer was dissolved in dichloromethane which was again removed under reduced pressure. The polymer was dissolved in tetrahydrofuran and methanol was added until a slight turbidity could be observed. The mixture was stirred for 24 hours. The polymer was precipitated from cold methanol and collected by centrifugation. The polymer was dissolved in a minimal amount of tetrahydrofuran and precipitated from a 6 : 1 v/v mixture of methanol and 2M HCl, collected by centrifugation and finally freeze-dried from benzene. The average yield was about 85%.

General procedure for the deprotection of carboxylic acid ester-functionalized polymers

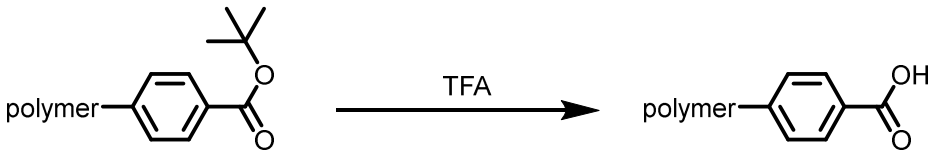

The *tert*-butyl benzoate-functionalized polymer was dissolved in a 4 : 1 v/v mixture of dichloromethane and trifluoroacetic acid. The mixture was stirred overnight at room temperature. Distilled water was added, and the pH value was adjusted to around 6 by addition of a saturated solution of potassium carbonate. After phase separation, the organic phase was washed with water, and the volume of the liquid of the organic phase was reduced to around 5 mL. The polymer was precipitated from cold methanol, collected by centrifugation and freeze-dried from benzene. The average yield was around 90%.

5 Hybrid Particles Consisting of Semiconductor Nanocrystals and Conjugated Polymers

5.1 Introduction

Semiconductor nanocrystals as well as conjugated polymers are relevant material classes because of their opto-electronic properties. The materials can be utilized in solar cells[12,95], light-emitting diodes[14,49,93] and in state-of-the-art high-end displays.[49,50,93] Also, the combination of both materials is of interest because of the possible charge and/or energy transfer (ET) between the organic and inorganic components.[101,250] The aim of the combination of two materials is not only to yield a compound which combines the properties of its constituents but ideally to unlock new properties. One example is the possible charge separation between two semiconductor materials upon optical excitation which allows to use these compounds as solar cells.[12]

Nanocrystals after their synthesis are covered with long-chain aliphatic ligands which limits their miscibility with a conjugated polymer matrix. Moreover, these ligands insulate the nanoparticles from the surrounding matrix. [8,10,109,116,122] For this reason, it is beneficial to employ nanocrystals with conjugated polymer chains directly tethered to their surface to enable a strong coupling between the two materials which allows for an efficient energy and/or charge transfer between the two materials.[8,251] The direct binding of the polymer to the nanoparticle's surface is additionally crucial to enable an optimal integration into opto-electronic devices. A detailed review on the challenging synthesis of hybrid particles consisting of conjugated polymers and semiconductor nanocrystals is given in the general introduction (**Chapter 1.2**).

As outlined before, the hybrid system of polyfluorene (PF8) and CdSe/CdS nanocrystals is of particular interest as a potential single-photon source. A sketch of the energy levels of such a hybrid system is shown in **Scheme 5.1**. Upon excitation of the PF8 an electron

transfer from the LUMO (conduction band) of the PF8 to the LUMO of the CdSe core should occur in principle. The CdS shell layer should block the transfer of a hole from the valence band of a photoexcited nanocrystal to the polymer. However, this process might occur by a tunneling process through the relatively thin shell.

The possible charge transfer between PF8 and CdSe/CdS nanocrystals might lead to a negatively charged nanocrystal which would have a tremendous impact on the optical properties of the nano-sized emitter (**Chapter 6.2.5**).

Scheme 5.1. Schematic energy level diagram of a PF8-functionalized CdSe/CdS core-shell nanocrystal. Upon excitation of the polymer an electron transfer to the inorganic core and/or an ET to the inorganic core can occur. Energy levels are based on literature values.[23,24,25]

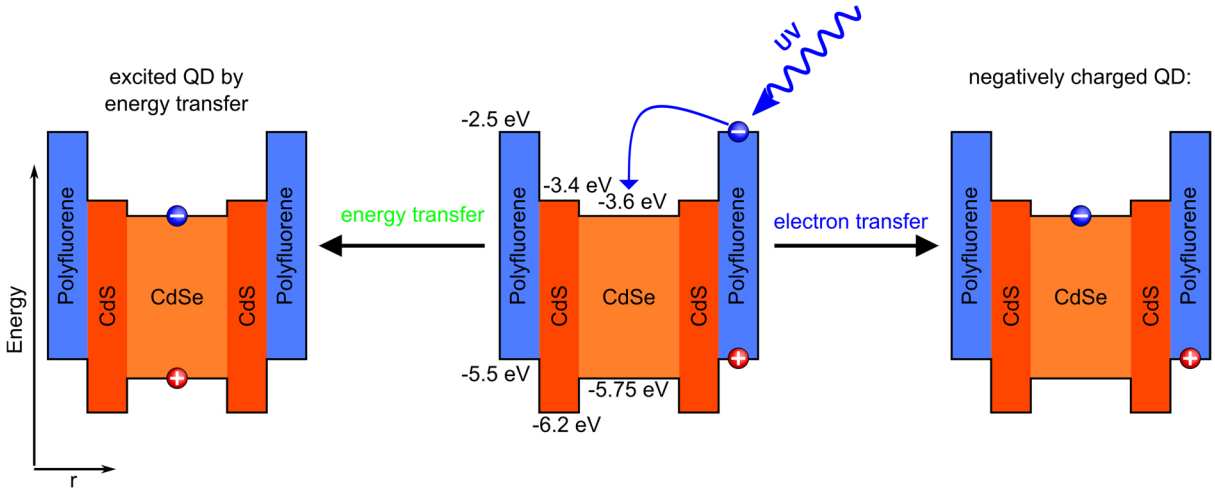

Besides these charge transfer processes, also an ET from excited PF8 (band gap ~3 eV) to the CdSe core (band gap ~2.15 eV) is possible in principle which would result in the generation of an excited nanocrystal. The same processes should be feasible in a hybrid particle consisting of graded-shell CdSe/$Cd_xZn_{1-x}S$ QDs and PF8 (**Scheme 8.1**).

Here, the functionalization of high-quality CdSe-based core-shell QDs with various PF8s (different binding moieties, homo vs. block copolymers, multi-valent comb polymers) was investigated by a ligand exchange procedure as well as by direct approaches. The successful direct approach could be extended to the synthesis of PF8 CdSe/CdS and CdSe/CdS/CdS hybrid NRs. This approach allowed in the case of CdSe/CdS/CdS NRs for a controllable functionalization of the NRs with PF8. For all studied systems, particles with PF8 tethered to their surface showed a strong interaction between the two materials and a strong and efficient ET from the polymer to nanocrystal, contributing to its emission, was observed at room temperature.

5.2 Results and Discussion

5.2.1 Hybrid Particle Synthesis by a Direct Ligand Exchange

For the synthesis of hybrid particles, the direct ligand exchange approach is a widely used method and also considered the most straightforward method (**Chapter 1.2.1**). Previously synthesized nanoparticles are mixed with previously synthesized polymers bearing a functional group capable of binding to the nanoparticle's surface. By a ligand exchange reaction (**Chapter 1.1.2**) with the native ligands of the nanoparticles, the polymer can bind to the surface of the nanoparticles. Phosphonic acids are strongly binding X-type ligands and are able to quantitatively replace carboxylic acids from the surface of CdSe nanocrystals.[76]

Here, CdSe/CdS QDs (QY = 50%; d = 7.6 nm; σ = 0.8 nm), synthesized by a SILAR process (**Chapter 3.2.2**) were functionalized by a direct ligand exchange reaction with the polyfluorene PA-PF8-MA (**Scheme 5.2**).

The QDs are stabilized by the X-type ligands dodecylphosphonic acid (DOPA) and oleic acid and the L-type ligand oleylamine. The polymer bearing a phenylphosphonic acid end group should be able to partially replace the oleic acid from the surface. However, the binding strength of polymers is generally considered weaker as compared to small molecules because of the polymer's steric demand.

Scheme 5.2. Schematic illustration of the functionalization of CdSe/CdS QDs with the polyfluorene PA-PF8-MA. For clarity only the first 3 repeat units of the polymer are shown.

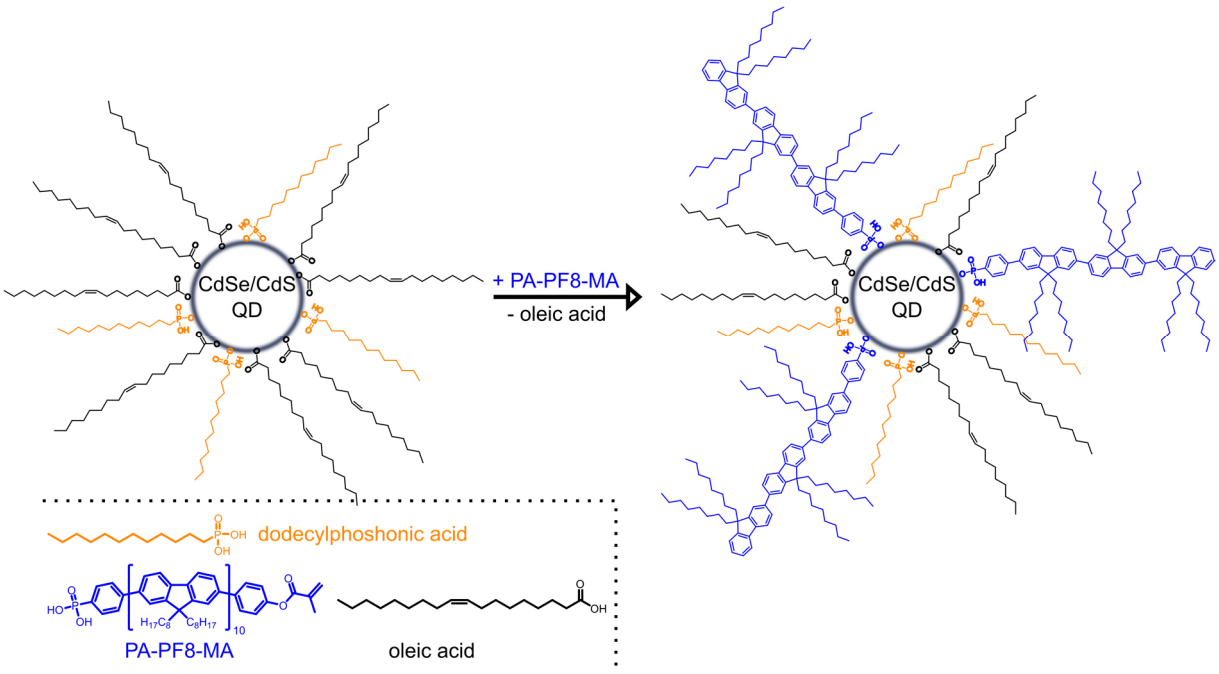

The functionalization of the QDs with the polyfluorene PA-Ph-PF8-MA was studied under various conditions (**Table 5.1**) concerning solvent and temperature. Besides the phenylphosphonic acid functionality, the PF8 bears a phenyl methacrylate moiety as second terminus which might be beneficial for the intended encapsulation of the particles into a larger polymer particle consisting of PMMA by a miniemulsion polymerization approach (**Chapter 6.2.1**). Moreover, the separation of unbound PF8 from hybrid particles was investigated.

All ligand exchange reactions were performed using a PF8 to QD ratio of 175 : 1 and 140 : 1 respectively. For the functionalization, the QDs were precipitated once in methanol and redispersed in the respective solvent. Afterwards, the polymer solution was added, and the mixture was stirred for 24 hours.

Table 5.1. Functionalization of CdSe/CdS QDs with the polyfluorene PA-PF8-MA by a direct ligand exchange reaction.

#	PF8/QD	solvent	temp. [°C]	QY[b] [%]	bound[c]	chains/QD[d]
1	175	DCM	25	49	70%	~120
2[a]	175	DCM	25	36	61%	~105
3	175	toluene	50	50	71%	~120
4	175	toluene	100	48	70%	~120
5	140	toluene	50	49	73%	~100

In all experiments 16 nmol of CdSe/CdS QDs were used. The exchange reactions were performed under a nitrogen atmosphere using dry and degassed solvents. a: Previous ligand exchange with pyridine. b: $\lambda_{exc.}$ = 450 nm, only the QDs are excited. c: Determined from the PF8 concentration before and after centrifugation at 20 000 g in combination with MW-AUC results. d: PF8 chains bound to one QD. Calculated with the number of added chains and the percentage of bound PF8.

The absorption spectrum of a hybrid dispersion is a superposition of the spectra of the polymer and the QDs (**Figure 5.1**, left). As it is unlikely that all PF8 binds to the nanocrystals, the separation of unbound PF8 from nanoparticles was studied by a precipitation and a centrifugation approach, respectively.

In the precipitation approach, a precipitating agent was added carefully to the dispersion until a slight turbidity was observed and subsequently, the formed precipitate was collected by centrifugation at a relative centrifugal force (RCF) of 2000 g. Without a precipitating agent no sedimentation arose at such a centrifugal force. As precipitating agents, solvents such as methanol, ethanol, acetone and acetonitrile which are commonly used in the cleaning process during the synthesis of QDs, were tested. However, the dispersibility of QDs and the solubility of the conjugated polymer are quite similar as for

both compounds the solubility/dispersibility is mostly ensured by long aliphatic carbon chains.

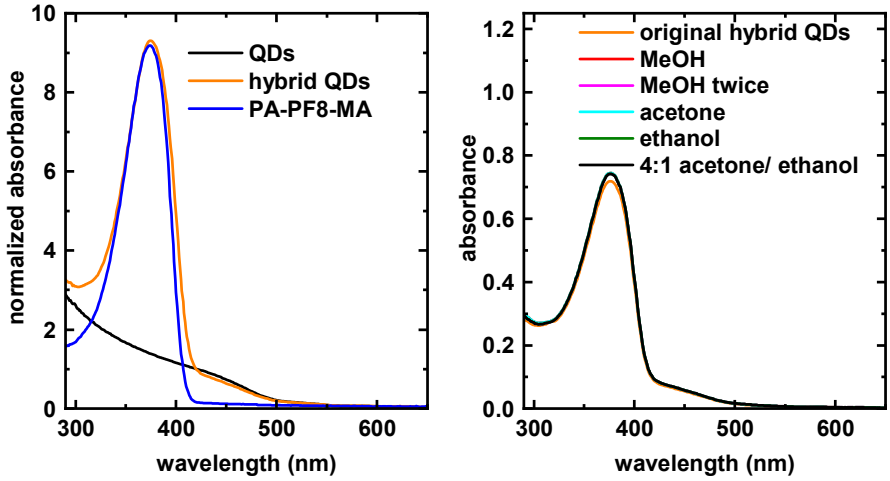

Figure 5.1. Left: Absorption spectra of CdSe/CdS QDs, hybrid particles (entry 1) and the polymer PA-PF8-MA. Right: Absorption spectra of a hybrid particle dispersion (entry 4) and the same dispersion after precipitation in various solvents followed by redispersion in toluene.

The ratio of QDs to PF8 in the dispersion can be analyzed by absorption spectroscopy (**Figure 5.1**, right). A quantitative precipitation could not be achieved by using acetonitrile, as a significant ratio of the solid components maintained dispersed. The other solvents used led to a complete precipitation after centrifugation and a colorless and non-fluorescent supernatant was obtained, which hints at a precipitation of both polymer and QDs. The separated pellet was redispersed in toluene. The ratio of QDs and PF8 in the redispersed dispersions was identical to the ratio in the original dispersion according to the absorption spectra (**Figure 5.1**, right). Therefore, no separation between unbound polymer and QDs was obtained. Nevertheless, these results are important for the interpretation of the direct functionalization approaches (see **Chapter 5.2.2** and **5.2.3**). In these experiments, the polymer was added during the synthesis of nanocrystals. Afterwards, the nanocrystals were purified by the repetitive precipitation in methanol, acetone or ethanol which will – given these results – not change the ratio between nanocrystals and polymer.

Another attempt to separate the two species was based on centrifugation as the hybrid particles and unbound PF8 show a huge difference in their density and molar mass and thus a significant difference in their sedimentation coefficient. By centrifugation (20.000 g, 2 hours) without a precipitating agent, it was possible to partially sediment the hybrid QDs while the unbound polymer stayed in solution (**Figure 5.2**, left), as apparent

from the reduced PF8 absorbance in the redispersed sediment as compared to the crude original dispersion. However, the sedimentation of the nanocrystals was not complete, and a significant amount of the hybrid nanocrystals stayed in the supernatant as reflected by its deep-red color (**Figure 8.33**).

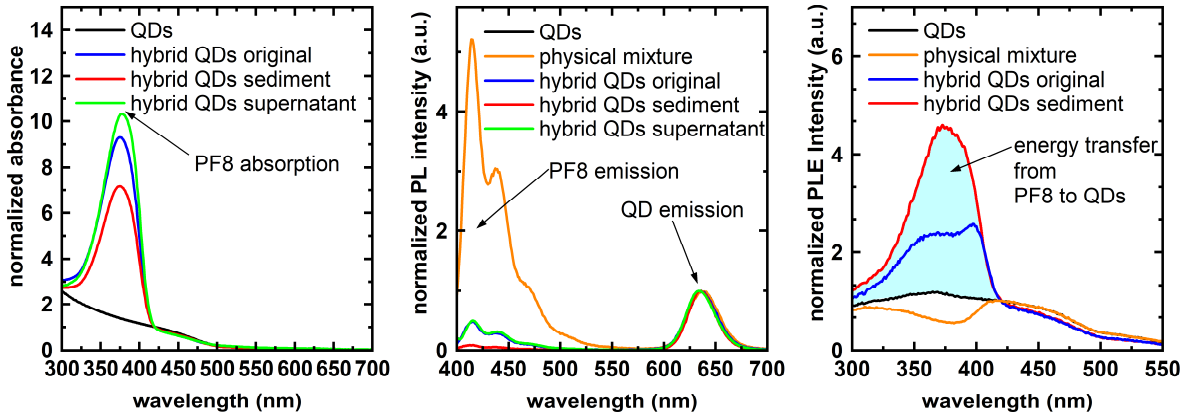

Figure 5.2. Absorption (left), photoluminescence (PL, center, $\lambda_{exc.}$ = 380nm) and photoluminescence excitation (PLE, right, $\lambda_{det.}$ = 630 nm) spectra of the QD dispersion, the respective original hybrid QD dispersion (entry 1) and the hybrid QD dispersion after preparative centrifugation (redispersed sediment and supernatant). The absorption and PLE spectra are normalized at λ = 420 nm to the QD concentration. The PL spectra are normalized at the maximal QD emission. The physical mixture consists of QDs and unfunctionalized PF8 in the same ratio as the original hybrid QD dispersion.

The sedimented pellet, obtained after centrifugation at 20.000 g for 2 hours, was redispersed in toluene and the binding of the PF8 to the QDs was analyzed by multi-wavelength analytical ultracentrifugation (MW-AUC). The procedure how to determine the percentage of PF8 bound to nanocrystals is explained in detail in the analytical methods section (**Chapter 5.4.2**). The MW-AUC measurement data for CdSe/CdS QDs functionalized with PA-PF8-MA (entry 1, **Table 5.1**) after preceding separation of unbound PF8 by preparative centrifugation are shown in **Figure 5.3**. At a wavelength of 300 nm, the absorption of PF8 is negligible and the absorbance is only caused by the inorganic nanocrystals. Therefore, their sedimentation can be tracked at this wavelength without interference of the PF8 absorption. A complete sedimentation of the QDs was observed. At 380 nm, the sedimentation of the hybrid particles is tracked. At a centrifugation velocity of 15000 rpm PF8 dissolved in toluene does not sediment. Therefore, remaining absorbance at 380 nm would be an indication for unbound PF8. But as a simultaneous and quantitative sedimentation at both wavelengths was recorded, it can be concluded that all PF8 in the dispersion is bound to CdSe/CdS nanocrystals. By

preparative centrifugation after the ligand exchange reaction, it was possible to separate unbound PF8 from a part of the hybrid particles and to collect hybrid QDs free of unbound polymer.

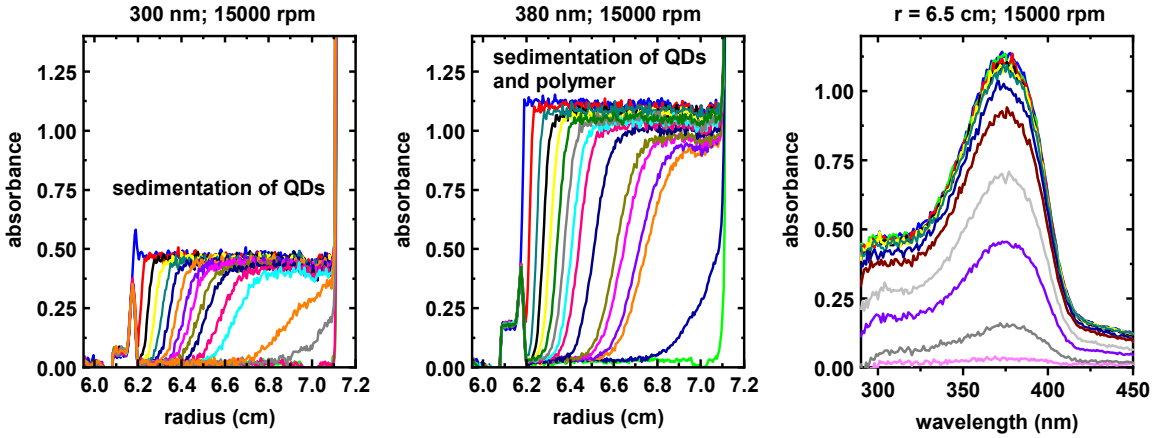

Figure 5.3. MW-AUC measurement data for CdSe/CdS QDs functionalized with PA-PF8-MA after preliminary separation of hybrid particles and unbound PF8 by preparative centrifugation. Left: Sedimentation tracked at λ = 300 nm. Center: Sedimentation tracked at λ = 380 nm. Right: Sedimentation profile at a fixed radius.

The binding of the PF8 to the nanocrystals had a tremendous impact on the optical properties (**Figure 5.2**). The absorption spectra prove that a separation of hybrid particles and unbound PF8 by preparative centrifugation was partially successful, as the concentration of PF8 in the sediment is decreased (-30%) compared to the original dispersion and increased in the supernatant. However, the supernatant contains a mixture of hybrid particles and unbound PF8. The influence of binding PF8 to the nanocrystals can be seen in the photoluminescence (PL) and photoluminescence excitation (PLE) (detection at the emission wavelength of the QDs) spectra. PL spectra of the original hybrid QD dispersion, the redispersed sediment and the supernatant dispersion are compared with a mixture of unfunctionalized PF8 and QDs having the same concentration as the original dispersion. The spectrum of the physical mixture is dominated by the emission of the polymer, whereas the polymer emission is nearly completely quenched in the other hybrid dispersions. The redispersed sediment, in which all PF8 is bound to the nanocrystals, shows basically no PF8 emission (2% integrated intensity as compared to the physical mixture). PLE spectroscopy (detection at a wavelength at which the QDs fluoresce) can reveal which absorption processes result in emission of the QDs. The PLE spectrum of the redispersed sediment (**Figure 5.2**) resembles the corresponding absorption spectrum and features a maximum at a

wavelength of maximal PF8 absorption. Thus, the emission of PF8 is not just quenched, but an ET takes place from the PF8 chains to the QDs, resulting in fluorescence of the QDs. This ET is only observable for the hybrid dispersions and not for the physical mixture of unfunctionalized PF8 and QDs. The physical mixture even shows a reduced PLE intensity in the absorption range of PF8 as compared to the pure QDs. The QY measured at an excitation wavelength outside of the absorption range of PF8 ($\lambda_{exc.}$ = 450 nm) is the same for the pure QDs as well as for the hybrid particles (49%). Additionally, the QY ($\lambda_{exc.}$ = 380 nm, PF8 and QDs are excited) of the QDs (detection from 520–700 nm) in the hybrid particle dispersion (redispersed sediment) is basically the same (48%), which means that the ET to the QDs is quantitative. From these results, it can be concluded that indeed a binding of the PF8 to the nanocrystal is necessary to impact the optical properties. Only bound PF8 is strongly quenched by the QDs. Moreover, an ET from excited PF8 to QDs occurs at room temperature. With the AUC results and absorption spectra of the redispersed sediment and original hybrid QD dispersion, it can be calculated that roughly 120 polymer chains are tethered to one QD. Assuming a spherical particle with a surface area of roughly 180 nm^2, this corresponds to 0.6 PF8 chains/nm^2. The literature values for completely covered surfaces of semiconductor nanocrystals are in the range of 3.5 molecules/nm^2 up to 4.6 molecules/nm^2 depending on the system and analytical method used.[69,70,119,252]

In literature, it is reported that the functionalization of QDs with conjugated polymers can be increased if the native QD ligands are first displaced by an excess of pyridine.[108,109,253] Afterwards, the weakly binding pyridine can be replaced by the polymer ligand. However, none of these reports provides convincing evidence for their claim. In order to clarify this point, the functionalization of QDs with 175 equiv. of PA-Ph-PF8-MA in DCM at 25 °C (entry 1, **Table 5.1**) was repeated with previously exchanging the native QD ligands with pyridine (entry 2, **Table 5.1,** see **Chapter 5.4.3** for preparative details). The amount of PF8 bound to the CdSe/CdS nanocrystals was nearly identical for the two approaches — the amount in the sample without exchange by pyridine was even slightly higher (nominally 120 vs. 105 chains/QD) — and no improved binding due to the previous displacement by pyridine was observed (**Figure 8.34**). However, the nanocrystals suffered due to the treatment with pyridine. The QY of the QDs measured outside the absorption range of PF8 ($\lambda_{exc.}$ = 450 nm) before the direct functionalization with PF8 was 50%. After the functionalization with PF8, the QY of the QDs was still at 49%, however, for the pyridine approach the QY dropped to 36%. Pyridine is a L-type ligand and L-type

ligands can, added in excess, displace Z-type ligands such as Cd(oleate)$_2$ (**Chapter 1.1.2**) which is detrimental for the optical properties of the QDs. Therefore, the claim of improved functionalization of nanocrystals by a previous ligand exchange with pyridine appears doubtful.

In experiments 3–4, toluene was used as solvent instead of dichloromethane and the ligand exchange was conducted at 50 °C and 100 °C. However, increasing the temperature did not increase the amount of bound polymer. The number of PF8 chains bound to one nanocrystal is basically the same for experiments 1, 3 and 4. In experiment 5, the amount of added PF8 was decreased to 140 equivalents. However, no complete binding of the polymer was observed and only around 100 chains were bound per nanocrystals.

In conclusion, CdSe/CdS QDs could be functionalized with PA-PF8-Ph-MA in a direct ligand exchange reaction and about 70% of the added polymer bound to the nanocrystals. The reaction temperature (25 °C vs. 100 °C) and choice of solvent (toluene vs. dichloromethane) did not significantly influence the functionalization.

P3HT has a lower band gap (~1.9–2.2 eV) than PF8 (~3eV) and is often used as hole transport layer and/or as electron donor (HOMO level ~-5.2 eV and LUMO level ~-3.2 eV) component in opto-electronic devices.[254,255,256] Therefore, excited P3HT could also act as electron donor for CdSe-based QDs, but due to the similar band gap as compared to the CdSe core, ET processes should be disfavored. Following the procedure for the functionalization of CdSe/CdS QDs with PF8, also hybrid particles consisting of CdSe/CdS QDs and phosphonic acid-functionalized polythiophene (PA-Ph-P3HT-MA) were synthesized (**Figure 8.35**). However, for this system a weak ET from the polymer to the QDs was still observed. Moreover, the fluorescence of the P3HT and the QDs overlap in this system due to the similar band gap, which impedes the use of these particles in high-resolution single-particle PL studies. Therefore, only PF8-based polymers were used for the functionalization of nanocrystals in the following.

Using Conjugated Nonconjugated Copolymers

In **Chapters 4.2.3** and **4.2.4**, the synthesis of novel conjugated nonconjugated diblock and multi-valent comb copolymers was reported. Especially the multi-valent comb polymers promise a higher degree of functionalization. These polymers were also employed as functional ligands for the functionalization of high-quality (QY = 86%; d = 6.1 nm) CdSe/$Cd_xZn_{1-x}S$ QDs (**Table 5.2**). In all experiments, 100 equivalents of phosphonic acid vs. QDs were used. The ratio of phosphonic acid groups to QDs was decreased compared

to the previous experiments as the graded-shell QDs are smaller and as in the previous experiments no quantitative binding was observed. In the reference experiment (entry 1), the 'standard' polyfluorene PA-Ph-PF8 was used as benchmark. In experiments 2–4, PF8 diblock copolymers were employed and in experiments 5–7 the respective multi-valent comb polymers.

In case of the reference polymer PA-Ph-PF8, only 50% of the chains were bound to the nanocrystals according to MW-AUC measurements. An ET from the polymer to the nanocrystals was observed by PLE measurements (**Figure 5.4**). Measuring the QY of the system at $\lambda_{exc.}$ = 380 nm, the polymer as well the nanocrystals are excited. The ratio of the overall QY (detection from 400-700 nm) and the QY of the nanocrystals (500-700nm) in this system is a good indication of the quenching of the PF8 emission. For this system, the overall QY is 80% but only 33% originating from the QD. Thus, only a minor number of the PF8 chains are quenched by the QDs in accordance with a binding of 50%.

Table 5.2. Functionalization of $CdSe/Cd_xZn_{1-x}S$ QDs with conjugated nonconjugated polymers by a ligand exchange reaction.

#	polymer	M_n [kg mol^{-1}]	PA/ chain[c]	PA/ QD	solvent	QY [%][d]	PF8 bound[e] [%]
1	PA-Ph-PF8	5	1	100	toluene	80/33	50
2	PA-PF8-*b*-PEHMA[a]	24	1	100	toluene	81/48	60
3	PA-PF8-*b*-PMMA[a]	19	1	100	THF	80/30	40
4	PA-PF8-*b*-PS[a]	19	1	100	THF	75/42	65
5	PA-PF8-Sty-*co*-PEHMA[a,b]	100	15	100	toluene	68/44	90
6	PA-PF8-Sty-*co*-PMMA[a,b]	95	15	100	THF	67/52	90
7	PA-PF8-Sty-*co*-PS[a,b]	68	12	100	THF	67/46	75

5 nmol of $CdSe/Cd_xZn_{1-x}S$ QDs and 1.5 mL of solvent were used in all experiments. a: See **Table 4.2** and **Table 4.3** for details on polymers. b: 0.1 mL of oleic acid was added to dissolve the comb polymers. c: Phosphonic acid (PA) groups per polymer chain. d: $\lambda_{exc.}$ = 380 nm (excitation of QDs and PF8), the first value is the total QY of the system, the second value only the QY of the QDs in this system. The QY ($\lambda_{exc.}$ = 450 nm; only absorption by the QDs) is in the range of 86–90% for all systems. e: Percentage of PF8 bound to the QDs according to MW-AUC measurements.

In **Figure 5.4**, the optical properties of the dispersions consisting of conjugated nonconjugated block copolymers and QDs (entries 2–4) and the reference experiment (entry 1) are compared. The amount of PA-Ph-PF8 in the dispersion was higher (15%) compared to the block copolymers PA-PF8-*b*-PEHMA and PA-PF8-*b*-PMMA. This might result from the fact, that the molecular weight of PA-Ph-PF8 is known with a higher

precision than the molecular weight of the copolymers. After the ligand exchange reaction, the particles were filtered through a syringe filter to remove any formed agglomerates. Roughly 30% of the PA-PF8-*b*-PS was filtered off at this step, whereas for the other dispersions the ratio between QDs and polymer did not change. The amount of polymer bound to the nanocrystals was analyzed by MW-AUC measurements (cf. **Figure 8.36** for exemplary MW-AUC data). The binding strengths of PA-Ph-PF8 and the block copolymer PA-PF8-*b*-PEHMA were similar (50–60% bound) whereas the PA-PF8-*b*-PMMA was more weakly binding (40% bound). The percentage of bound PA-PF8-*b*-PS was slightly higher (65%); however, the concentration of this polymer was also significantly lower. The impact of binding was illustrated in the PL properties of the dispersions. The concentration of PA-PF8-*b*-PEHMA and PA-PF8-*b*-PMMA in the dispersions were identical; however, the emission of the PF8 part was more strongly quenched in the case of PA-PF8-*b*-PEHMA as more chains were bound to the nanocrystals. For all dispersions, an ET from the PF8 to QD was observed, with intensities correlating with the amount of bound chains. From the series of block copolymers, PA-PF8-*b*-PEHMA is the most suited ligand as its solubility in a lipophilic environment is higher compared to the other block copolymers.

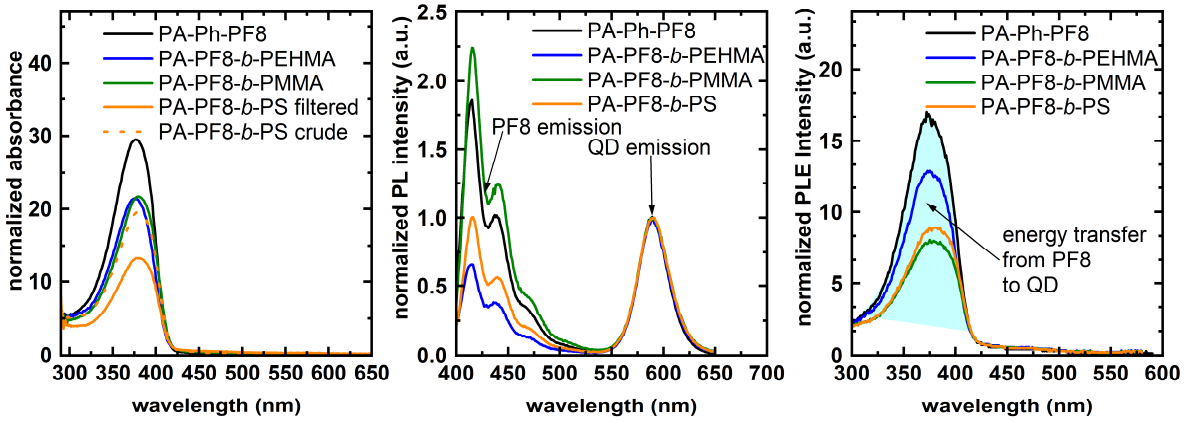

Figure 5.4. Absorption, PL ($\lambda_{exc.}$ = 380 nm) and PLE spectra ($\lambda_{det.}$ = 590 nm) of the hybrid particle dispersions consisting of CdSe/$Cd_xZn_{1-x}S$ QDs and conjugated nonconjugated diblock copolymers. The absorption and PLE spectra are normalized at λ = 420 nm, the PL spectra are normalized at the maximum of the QD emission.

In experiments 4–7, the binding behavior of the corresponding multi-valent comb polymers (PA-PF8-Sty-*co*-PEHMA, PA-PF8-Sty-*co*-PMMA, PA-PF8-Sty-*co*-PS) was investigated. These polymers consist of a nonconjugated backbone with 12–15 phenylphosphonic acid-terminated PF8 side chains (**Chapter 4.2.4**). PA-PF8-Sty-*co*-

PEHMA was dissolved in toluene and PA-PF8-Sty-*co*-PS and PA-PF8-Sty-*co*-PMMA were dissolved in tetrahydrofuran. In order to increase the solubility of the polymers a small amount of oleic acid (~6 vol%) was added. In all three experiments, a precipitate formed in the course of the ligand exchange reaction which was separated by centrifugation (cf. **Figure 8.37** for photos). This precipitate could not be redispersed and given its color, it consists of QDs and mostly polymer. This explains why the concentration of PF8 (**Figure 5.5**) in these dispersions was significantly lower (50–60%) in comparison to the reference sample synthesized with PA-Ph-PF8. However, according to MW-AUC measurements (cf. **Figure 8.38** for exemplary AUC data) the remaining comb polymer was mostly (70% for PA-PF8-Sty-*co*-PS and 90% for PA-PF8-Sty-*co*-PEHMA and PA-PF8-Sty-*co*-PMMA) bound to the nanocrystals. This was reflected in a strong quenching of the PF8 emission and a strong ET to the nanocrystals. Due to the stronger binding of the comb polymers, the total ET from the PF8 moiety to the QD was equally strong for the comb polymers and the reference polymer PA-Ph-PF8, although the concentration of the comb polymer was much lower (only 40–50%).

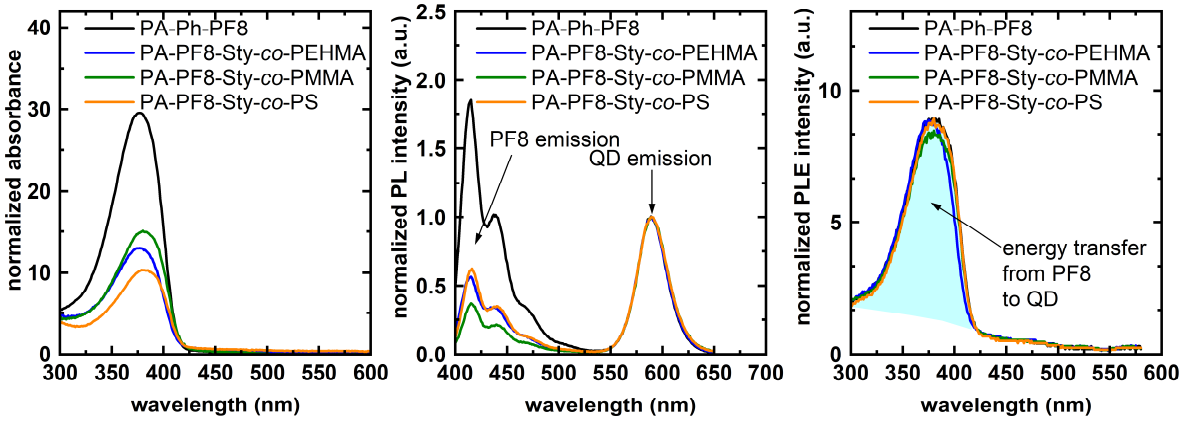

Figure 5.5. Absorption, PL ($\lambda_{exc.}$ = 380 nm), and PLE spectra ($\lambda_{det.}$ = 590 nm) of the hybrid particle dispersions consisting of CdSe/$Cd_xZn_{1-x}S$ QDs and conjugated nonconjugated comb copolymers. The absorption and PLE spectra are normalized at λ = 420 nm, the PL spectra are normalized at the maximum of the QD emission.

The sedimentation profile of these hybrid particles does not show a single hybrid QD species, but several sedimenting species (**Figure 8.38**). These are most likely QDs covered with a different amount of high molecular weight comb polymer chains.

In conclusion, the functionalization of QDs in a direct ligand exchange reaction was possible, and a high amount of the added phenylphosphonic acid-functionalized PF8 was bound to the nanocrystals. The emission of PF8 bound to nanocrystals was quenched and an ET from photoexcited PF8 to the nanocrystals was observed, which is not the case for

physical mixtures of unfunctionalized PF8 and QDs. The binding behavior of the polyfluorene PA-Ph-PF8 and the block copolymer PA-PF8-*b*-PEHMA is quite similar. The multi-valent comb polymers are indeed more strongly binding; however, also a partial precipitation of polymer and QDs was observed.

5.2.2 Functionalization of CdSe/$Cd_xZn_{1-x}S$ Quantum Dots by a Direct Approach

The ligand exchange reaction yielded hybrid particles; however, in the case of the high-quality CdSe/$Cd_xZn_{1-x}S$ QDs only around 50% of the added polymer was bound to the nanocrystals. A direct functionalization approach offers the benefit to omit a second ligand exchange reaction. Moreover, the direct approach provides the possibility to add the polymer ligand at high temperatures and a stage of the particle formation where the final particle surface has not been formed yet. This might allow for higher and more controllable functionalization.[257] As the literature-reported synthesis of CdSe/$(CdS)_x(ZnS)_y$ QDs could be well reproduced and as these QDs show superior optical properties compared to the CdSe/CdS QDs synthesized by a SILAR process, the direct functionalization approach was conducted with these graded-shell QDs. The system consisting of a shell composed of 2 ML of CdS and 2 ML of ZnS was chosen, as a thin shell might facilitate energy and charge transfer processes.[123] Regarding the synthesis of hybrid particles, two possibilities to introduce the various phosphonic acid-functionalized PF8s were investigated (**Scheme 5.3**). In method A, the PF8 was added after the deposition of the CdS shell along with oleic acid. Afterwards, the mixture was annealed for 1 hour and degassed by applying vacuum for 30 min, before continuing with the addition of the ZnS precursors.

Scheme 5.3. Synthetic procedure for the functionalization of CdSe/$(CdS)_2(ZnS)_2$ QDs with PF8 by a direct approach.

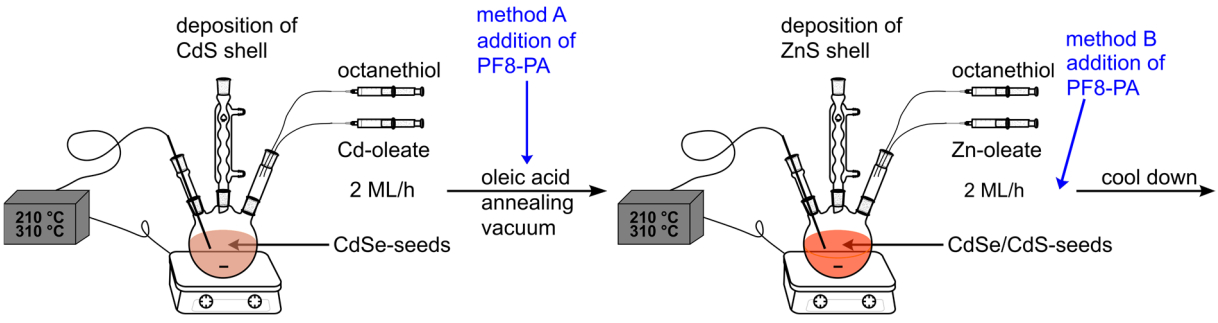

In method B, the PF8 was added after the addition of the ZnS shell had been completed. Thereby, the influence on the particle formation is minimalized and the possibility to introduce the polymer at the high reaction temperature might be beneficial in comparison to the direct ligand exchange reaction as presented before. Moreover, as no additional ligand exchange procedure has to be conducted, this process is also time saving.

Method A: Polymer Addition Before Deposition of the ZnS Shell

In the established synthesis of CdSe/$Cd_xZn_{1-x}S$ QDs, the CdS shell is deposited on the CdSe core in the first step. After the deposition, 0.5 mL of oleic acid (50 nmol CdSe seeds used) is added at 200 °C, and the mixture is annealed at 150 °C for 1 hour. This step is important for the optical properties of the QDs and offers the possibility to add phosphonic acid-functionalized PF8 as an additional ligand along with the oleic acid.

Table 5.3. Synthesis of CdSe/$(CdS)_2(ZnS)_2$ PF8 hybrid QDs by the addition of phosphonic acid-functionalized PF8 after the deposition of the CdS shell.

#	polymer	M_n [kg mol^{-1}]	PA/ chain[b]	solvent [mL]	PA/QD	observation
1	PA-PF8-Sty-*co*-PEHMA[a]	100	15	ODE/HOAc 1/1	100	partial precipitation
2	PA-PF8-Sty-*co*-PMMA[a]	95	15	ODE/HOAc 1.5/1	100	complete precipitation
3	PA-PF8-Sty-*co*-PS[a]	68	12	ODE/HOAc 1.5/1	100	complete precipitation
4	PA-Ph-PF8	5	1	ODE/HOAc 1/0.5	100	bimodal size distribution

The polymer solution heated to 80 °C was added slowly to the QD dispersion at 200 °C. Afterwards, the dispersion was annealed at 150 °C for 1 hour. a: See **Table 4.3** for details on polymers. b: Phosphonic acid (PA) groups per polymer chain. ODE = octadecene; HOAc = oleic acid.

As polymer ligands, the newly synthesized multi-valent PF8 comb polymers were tested (**Table 5.3**, entry 1–3) and the standard phenylphosphonic acid-functionalized polyfluorene (PA-Ph-PF8) was employed as reference material. The polymers were sought to be dissolved in only 0.5 mL of oleic acid. Only PA-Ph-PF8 dissolved completely, however, a highly viscous solution formed, which was diluted by the addition of 1 mL of ODE. The comb polymers could only be dissolved by using 1 mL of oleic acid in combination with 1 mL or 1.5 mL of ODE.

Upon addition of the PA-PF8-Sty-*co*-PEHMA oleic acid mixture to the CdSe/$(CdS)_2$ particles, the reaction mixture became turbid and a partial QD precipitation was observed. After the addition of the PA-PF8-Sty-*co*-PMMA or PA-PF8-Sty-*co*-PS comb copolymer an instantaneous precipitation of all QDs occurred (**Figure 5.6**, left). Only the addition of the reference polymer PA-Ph-PF8 did not cause any precipitation and it was possible to deposit the ZnS shell afterwards.

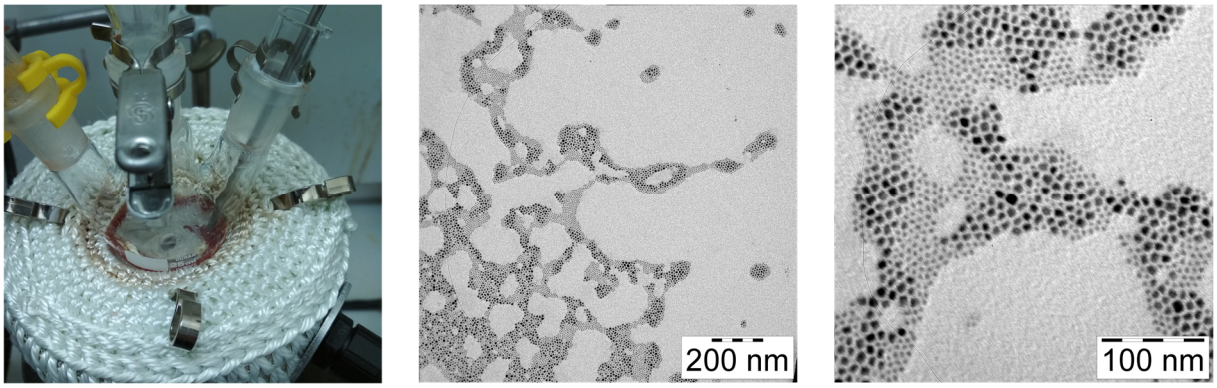

Figure 5.6. Left: Exemplary photograph of the precipitated QDs after the addition of a comb polymer (clear, colorless solution, red QD agglomerates stick to flask's surface). Center and Right: TEM images displaying the bimodal size distribution of the QDs after addition of PA-Ph-PF8 (entry 4). Small particles have a diameter around 4.0–6 nm as determined from the TEM images. The larger particles are in the range of 7–10 nm. The CdSe seed particles had an average diameter of 3.6 nm.

However, a bimodal particle size distribution was obtained (**Figure 5.6**, center and right) consisting of particles in the size range of 4–6 nm and the larger particles being in the range of 7–10 nm. The presence of the PA-Ph-PF8 during the deposition of the ZnS seems to partially disturb the deposition of the ZnS shell.

As already seen for the functionalization of preformed QDs by a ligand exchange reaction, the addition of the multivalent comb polymers led to a precipitation of the QDs. This could have several reasons: one possibility is the bridging of several particles by the multivalent polymer, causing agglomeration. Additionally, the solubility of the comb polymers themselves is limited. Moreover, a high amount of bound comb polymers could also lead to precipitation as the comb architecture might not be well suited to stabilize a nanocrystal.

Method B: Polymer Addition After Deposition of the ZnS Shell

As the addition of phosphonic acid-functionalized PF8s before deposition of the ZnS shell led to a precipitation of the particles or disturbed the deposition of the ZnS shell, the addition of polymer directly after the growth of the ZnS shell (method B) was investigated.

Thereby, the influence on the particle formation is minimalized. As polymeric components three different phosphonic acid-functionalized PF8s were employed and compared (**Scheme 5.4**). The binding affinity of an aromatic phenylphosphonic acid moiety (PA-Ph-PF8) was compared to a benzylphosphonic acid moiety (PA-Bn-PF8). The more flexible benzylphosphonic acid group might bind more strongly, whereas the phenylphosphonic group might enable a stronger electronic coupling between the two materials. The second terminus of the polymer PA-Ph-PF8-MA additionally bears a phenyl methacrylate group which might facilitate the intended subsequent encapsulation of the hybrid particles. All polymers had a similar degree of polymerization of 9–10 and were well soluble in octadecene, or in a mixture of oleic acid/octadecene/oleylamine as present in the reaction mixture. However, probing the stability of the polymer PA-Ph-PF8-MA in a solvent mixture under reaction comparable conditions at 150 °C revealed that the carboxylic acid phenylester is cleaved under these harsh conditions.

Scheme 5.4. Polyfluorenes used for the functionalization of CdSe/$(CdS)_2(ZnS)_2$ QDs.

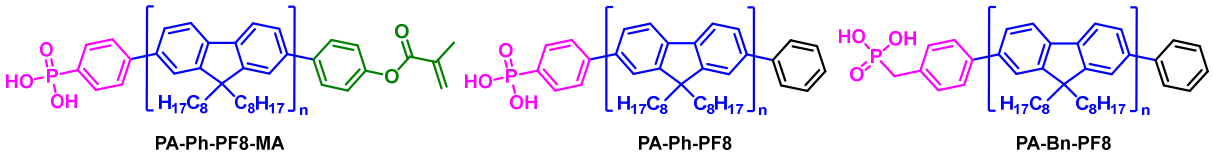

The polymer of interest (**Table 5.4**) was dissolved in 1 mL of octadecene and added to the reaction at the respective temperature (150 °C or 310 °C) after the addition of the ZnS precursors had been completed. Afterwards, the reaction mixture was allowed to cool down to 150 °C and was annealed for 1 hour.

In all experiments, highly fluorescent dispersions were obtained. The QY of the QDs ($\lambda_{exc.}$ = 450 nm) ranges from 78–84% in all experiments and is only slightly lower than the QY of the reference CdSe/$(CdS)_2(ZnS)_2$ QDs (87%). The addition of the PF8 had no negative impact on the particle formation and crystalline and uniform (particle size distributions ~8–10%) particles were formed (**Figure 5.7**, cf. **Figure 8.39** for additional TEM images). The particles align in superstructures on the TEM grid, although they do not pack as closely as the bare CdSe/$(CdS)_2(ZnS)_2$ QDs (cf. **Figure 3.7**). This hints at a stronger repulsion between the QDs which might be caused by potentially bound long polymer chains.

Table 5.4. Conditions for the synthesis of PF8 CdSe/$(CdS)_2(ZnS)_2$ hybrid QDs by a direct approach.

#	polymer	PF8/QD	addition temp. [°C]	QY[a] (450 nm) [%]	QY[b] (380 nm) [%]	% PF8 bound (AUC)[c]	PF8 chains bound/ QD[d]
1	PA-Ph-PF8	75	150	78	78 (40)	60	45
2	PA-Ph-PF8	75	310	82	80 (45)	65	49
3	PA-Bn-PF8	75	150	81	85 (22)	40	30
4	PA-Bn-PF8	75	310	79	87 (30)	50	37
5	PA-Ph-PF8	160	310	84	80 (22)	35	56
6	PA-Ph-PF8	54	310	81	76 (50)	80	44
7	PA-Ph-PF8	27	310	80	82 (30)	70	19

As seed particles, two batches of CdSe QDs with a size of 3.3 nm respect. 3.4 nm and a FWHM of the PL peak of 25–26 nm were used. The polymers were dissolved in 1 mL of ODE and heated to 80 °C. After polymer addition, all samples were cooled to 150 °C and annealed for 1 hour. a: At $\lambda_{exc.}$ = 450 nm only the QD is excited. b: At $\lambda_{exc.}$ = 380 nm both the QDs and the PF8 are excited, the first value is the total QY of the system ($\lambda_{det.}$ = 400–700 nm), the second value is the QY of the QDs in this system ($\lambda_{det.}$ = 550–700 nm).c: Determined by MW-AUC measurements (see **Chapter 5.4.2** for details). D: Calculated by the added number of PF8 chains per QD and the percentage of PF8 chains bound according to MW-AUC measurements.

In order to elucidate whether indeed hybrid particles had been formed, MW-AUC measurements were performed to determine the percentage of PF8 bound to the nanocrystals (cf. **Figure 8.40** for an exemplary AUC evaluation). In all experiments, a significant amount of PF8 was bound to the nanocrystals, however, the values range from only 35% to 80%. In experiments 1–4, the influence of the addition temperature (310 °C vs. 150 °C) and the influence of the binding group (phenyl vs. benzylphosphonic acid) was analyzed. For both binding groups, the higher addition temperature led to a slightly higher amount of bound PF8 (60% vs. 65% and 40% vs 50%).

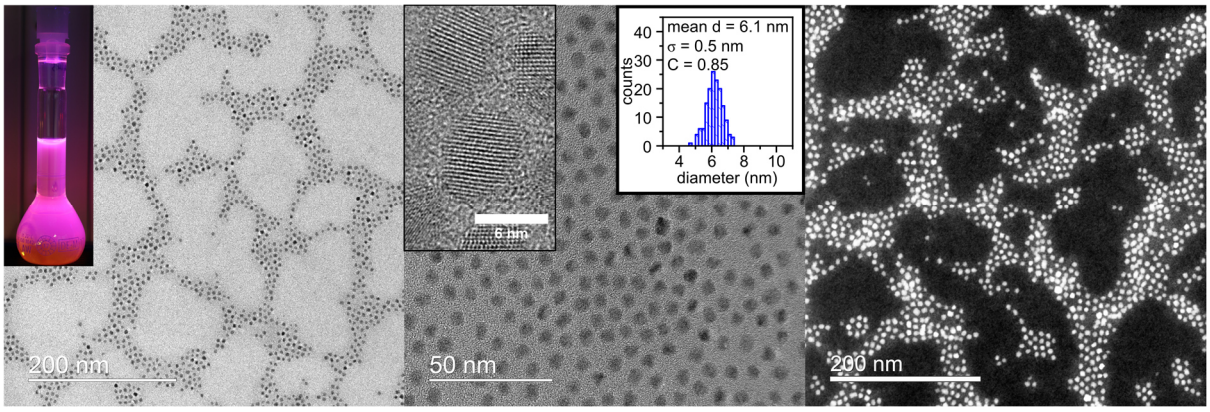

Figure 5.7. Photograph (UV light illumination) and TEM images of the hybrid particles obtained in entry 2, **Table 5.4**. The right image was recorded in dark field scanning TEM mode.

Comparing the binding strength of the functional group, the phenylphosphonic acid-functionalized PF8 binds slightly more strongly than the benzylphosphonic acid-functionalized PF8 (60% vs. 40% and 65% vs. 50%). Therefore, in the experiments 5–7, in which the amount of added polymer was varied, the polymer addition was conducted at 310 °C and PA-Ph-PF8 was used as polymer.

The absorption spectra of the hybrid nanoparticles (**Figure 5.8**) are a superposition of the spectra of the QDs and the polymer. The amount of the PF8 in the dispersions scaled linearly with the added amount of PF8. The ratio between QDs and PF8 should not have been changed by the repeated precipitation in methanol and/or acetone and redispersion in toluene during the clean-up process of the hybrid particles (cf. **Chapter 5.2.1**). Therefore, the number of PF8 chains bound to one QDs can be estimated from the percentage of bound PF8 chains (AUC results) and the number of PF8 chains added per QD (right column **Table 5.4**). Adding 160 chains per QD did not increase the amount of bound PF8 chains significantly compared to the experiments with addition of 54 or 75 chains per QDs. It seems that the maximal number of chains bound to one QDs is in the range of 45–56.

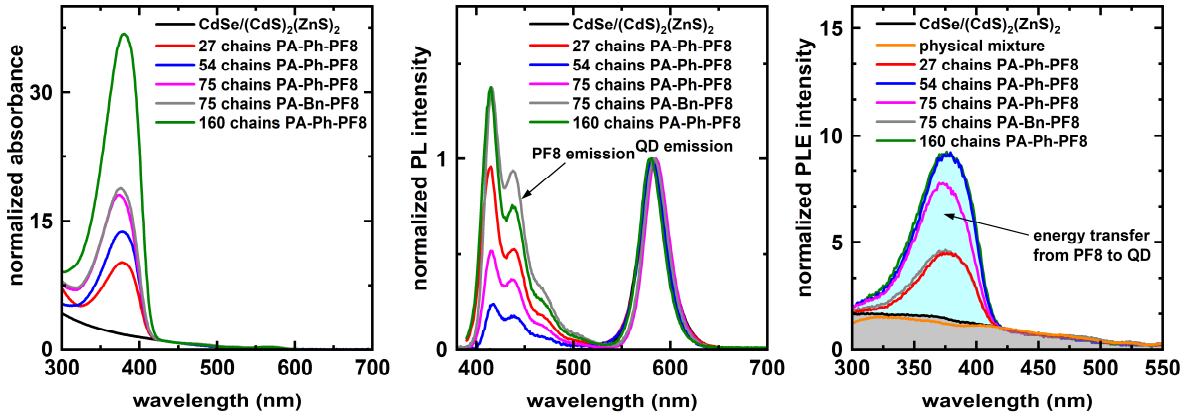

Figure 5.8. Absorption (left), PL ($\lambda_{exc.}$ = 380 nm; center) and PLE ($\lambda_{det.}$ = 580 nm; right) spectra of PF8 CdSe/$(CdS)_2(ZnS)_2$ hybrid particles. For clarity only the samples synthesized at 310 °C are displayed. The absorption and PLE spectra are normalized at λ = 420 nm outside the absorption range of PF8 to the QD concentration and the PL spectra at maximal QD emission.

With these values, the surface density of the PF8 molecules on the surface of the QDs can be calculated from the size of the nanoparticles (d = ~6.1 nm, A = ~116 nm^2) as determined by TEM measurement assuming the particles to be spherical. The density ranges between ~0.2 molecules/nm^2 up to ~0.5 molecules/nm^2. As outlined earlier, the literature values for completely covered surfaces of semiconductor nanocrystals are in the range of 3.5 molecules/nm^2 up to 4.6 molecules/nm^2 depending on the system and

analytical method used.[69,70,119,252] Regarding the steric bulk of a polymer chain, it seems reasonable that a maximum of roughly 10% of the ligands on the surface are PF8 chains.
The binding of the PF8 to the QD enabled an energetic coupling between the two systems. The PLE spectra (maxima at λ = ~378 nm, in accordance with the PF8 absorption maximum) show a strong ET from the excited polymer to the QDs (**Figure 5.8**). This ET was only observed for hybrid particles and not for a dispersion of unfunctionalized PF8 and QDs. The intensity of the ET correlates reasonably well with the number of PF8 chains bound to one QD. However, in the case of QDs functionalized with PA-Bn-PF8 (75 chains/QD added, entry 4) this ET is significantly weaker (~50%) than for QDs functionalized with PA-Ph-PF8 (75 chains/QD added, entry 2). In both dispersion the ratio between PF8 and QDs is identical (cf. absorption spectra **Figure 5.8**), but the amount of bound PF8 chains is only slightly higher for the sample synthesized with PA-Ph-PF8 (~25%). Thus, it can be concluded that the ET efficiency is already significantly (~25%) reduced by the single insulating aliphatic CH_2 group between the conjugated π-system and the binding group in the polymer PA-Bn-PF8.
This ET is also reflected in the PL spectra (**Figure 5.8**, center) of the dispersions. For all samples, the PF8 emission is strongly quenched, especially for samples with a high percentage of bound PF8. Moreover, the PL peak of the QDs is narrow (FWHM 29–34 nm), indicating the reproducible high quality of the obtained QDs.
The influence of the binding of the PF8 chains to the QDs on the photoluminescence dynamics was analyzed by measuring the time-resolved photoluminescence decay of the nanocrystals (**Figure 5.9**). The decay dynamics of unfunctionalized reference QDs and a physical mixture of these with unfunctionalized PF8 are identical. However, both batches of analyzed hybrid QDs (dispersions obtained in entries 2 and 5, **Table 5.4**) show a slightly faster PL decay than the unfunctionalized QDs. The PL decay can be simplistically fitted with a biexponential fit resulting in an intensity-weighted average fluorescence lifetime of 15 ns for the hybrid QDs and 18 ns for the reference QDs. A similar observation was made by Cotlet et al. for the functionalization of CdSe/ZnS QDs with conjugated polymer chains which they attributed to a charge transfer between the two materials.[123] The fluorescence lifetime τ can be defined in a simple model as $\tau = \frac{1}{\sum k_r + \sum k_{nr}}$, with the radiative and nonradiative decay constants k_r and k_{nr}.[123] For the hybrid nanocrystals consisting of PF8 chains tethered to CdSe/$Cd_xZn_{1-x}S$ QDs an ET from photoexcited polymer to the QD was observed, however, also an electron transfer from excited PF8 to

the QD or a hole transfer from an excited QD to the polymer could potentially take place which would both result in the formation a charged QD. By excitation of charged QDs, trion states can be formed, which open additional radiative and nonradiative recombination pathways.[258,259] Charged QDs might show a faster PL decay because of the following two effects: Excited charged QDs (trions) feature a shorter (factor ~1.5–5)[2,258,260,261] radiative lifetime than neutral excitons. However, charging of QDs, which can also randomly happen photophysically driven in non-functionalized QDs, is also considered as one main pathway for exhibiting intermittency in their emission, which is termed PL 'blinking' (cf. ref.[262] for a detailed review on the not-completely understood topic of QD blinking).[262] Excited charged QDs are prone to non-radiative Auger recombination, whereby the recombination energy is transferred to the extra charge carrier and no phonon is emitted. At room temperature, the Auger recombination process is normally orders of magnitude faster than or for special systems in the range of the radiative decay of the trion which can decrease the QY of the emitter.[260,262] This relationship would also explain that the synthesized hybrid QDs exhibit a slightly lower QY than the reference QDs (78–84% vs. 87%). However, at cryogenic temperatures (the temperature at which single-particle PL measurements are conducted), Auger recombination is often strongly suppressed and the radiative trion decay can be dominant.[260,262] Therefore, the observed shortened PL decay of the hybrid QDs as compared to the reference QDs at room temperature could be a hint at an additional charging of the QDs due to an interaction with the bound PF8 chains

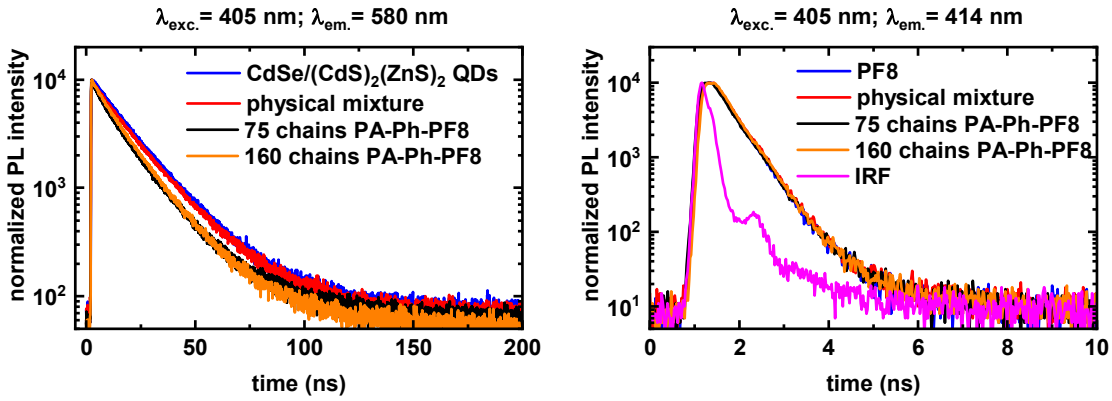

Figure 5.9. Time-resolved photoluminescence decay traces of $CdSe/(CdS)_2(Zns)_2$ PF8 hybrid particles. Left: The PL decays of the QD fluorescence in two hybrid QD dispersions, a reference QD dispersion and a physical mixture of unfunctionalized PF8 and QDs are shown. At $\lambda_{exc.}$ = 405 nm, the QDs and the PF8 are excited. Right: The PL decays of the polymer fluorescence in these hybrid dispersions and the polymer dissolved in toluene are shown. IRF = instrument response function.

The PL decays of the reference polymer and polymer in the hybrid dispersions (**Figure 5.9**, right) are identical (single exponential decay, τ = 0.4 ns). As the bound polymer is efficiently quenched by the QDs, probably only emission of unbound polymer is detected, which of course shows the same PL dynamics as the reference polymer.

Method B: Addition of Conjugated Nonconjugated Copolymers After Deposition of the ZnS Shell

The addition of phosphonic acid-functionalized polyfluorene (PA-Ph-PF8) directly after the deposition of the ZnS shell yielded high-quality hybrid particles. However, still no complete binding of the added PF8 to the QDs was observed. Therefore, this approach was also conducted with conjugated nonconjugated diblock and comb copolymers (**Table 5.5**). As the comb polymers have proven to be strongly binding, they might enable a complete binding of the added polymer. However, for the diblock copolymers only PA-PF8-*b*-PEHMA was soluble in the reaction mixture, whereas PA-PF8-*b*-PMMA and PA-PF8-*b*-PS were not.

The block copolymer PA-PF8-*b*-PEHMA was dissolved in 2 mL of octadecene and added to the reaction mixture at 310 °C, as the higher addition temperature has proven to beneficial for the binding of the polymer. However, a very viscous and oily dispersion was formed, no quantitative precipitation of the QDs was possible, and the optical properties of the final dispersion were dominated by the polymer.

In experiments 2–4, multi-valent comb polymers were employed for the functionalization. In all experiments, the amount of polymer in the final dispersion was very limited, as observed from the absorption spectra (**Figure 5.10**). During the work-up of the QDs by precipitation in acetone/ethanol, the supernatant showed a strong blue fluorescence indicating the presence of non-bound polymer. However, the polymer, which was left in the final dispersion, was completely bound to the nanocrystals. The addition of PA-PF8-Sty-*co*-PS (experiment 5) led to a complete precipitation of the QDs.

Table 5.5. Functionalization of CdSe/$(CdS)_2(ZnS)_2$ QDs using conjugated nonconjugated polymers by a direct approach.

#	polymer	M_n [kg mol^{-1}]	PA groups/ chain	PF8-PA/ QD	QY[d] [%]	% PF8 bound (AUC)[e]
1	PA-PF8-*b*-PEHMA[a]	24	1	100	86/6	n.d.
2	PA-PF8-Sty-*co*-PEHMA[b]	52	4	100	71/53	100
3	PA-PF8-Sty-*co*-PEHMA[b]	100	15	100	75/16	100
4	PA-PF8-Sty-*co*-PMMA[c]	95	15	100	71/65	100
5	PA-PF8-Sty-*co*-PS[c]	68	12	100	n.p.	n.p

As seed particles, CdSe QDs with a size 3.4 nm and a FWHM of the PL peak of 25 nm were used. a: Solvent 2 mL of octadecene. b: Solvent 2 mL of octadecene and 0.5 mL of oleic acid. c: Solvent 2 mL of octadecene and 1 mL of oleic acid. The dissolved polymers were heated to 80 °C. After polymer addition, all samples were cooled to 150 °C and annealed for 1 hour. d: At $\lambda_{exc.}$ = 380 nm both the QDs and the PF8 are excited, the first value is the total QY of the system ($\lambda_{det.}$ = 400–700 nm), the second value is the QY of the QDs in this system ($\lambda_{det.}$ = 500-700 nm). e: Percentage of bound PF8 determined by MW-AUC measurements.

For the functionalization of CdSe/$(CdS)_2(ZnS)_2$ QDs in a direct approach the conjugated PF8 functionalized with a phenyl phosphonic acid moiety has proven to be much better suited than the conjugated nonconjugated copolymers. As the direct functionalization approach using the polyfluorene PA-Ph-PF8 was successful in terms of delivering monodisperse QDs of high-optical quality which are functionalized with polyfluorene chains, the functionalization with these conjugated nonconjugated copolymers was not further studied.

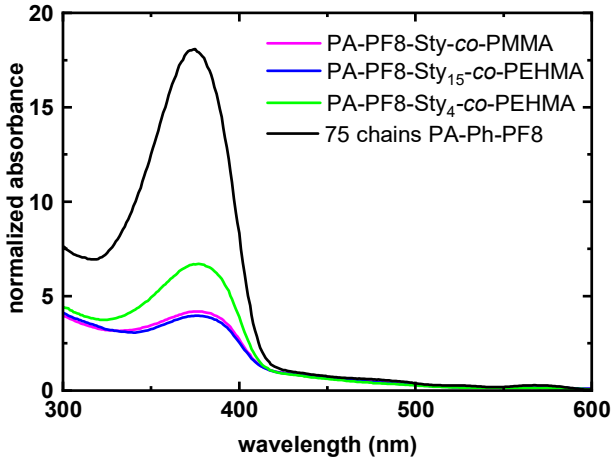

Figure 5.10. Absorption spectra of the hybrid particle dispersions obtained in experiments 2–4, **Table 5.5**. For comparison, the spectra of CdSe/$(CdS)_2(ZnS)_2$ hybrid particles synthesized with addition of 75 chains of PA-Ph-PF8 (entry 2, **Table 5.4**) is shown. The spectra are normalized at λ = 420 nm to the QD concentration.

5.2.3 Polyfluorene CdSe/CdS and CdSe/CdS/CdS Hybrid Nanorods

Functionalization of CdSe/CdS Nanorods by a Direct Approach

As pointed out in **Chapter 3.2.4**, CdSe/CdS NRs are interesting for single-particle PL studies and especially for charging experiments. However, these NRs are synthesized in a mixture of strongly binding X-type phosphonic acids. Moreover, only a precise ligand mixture ensures the anisotropic growth of the particles. Therefore, the functionalization of these NRs will even be more challenging than the functionalization of quasi-spherical QDs. So far, the conjugated polymer PA-Ph-PF8 has proven to be the most suited polymer ligand.

Here, three different direct approaches were pursued to functionalize CdSe/CdS NRs with PF8-Ph-PA (**Scheme 5.5**). In all experiments, 100 equiv. of PF8-Ph-PA vs. the CdSe-seed particles were used. In method A, the end-functionalized PF8 was added as additional phosphonic acid to the Cd-precursor mixture consisting of CdO, *n*-octadecylphosphonic acid, hexylphosphonic acid, tri-*n*-octylphosphine oxide and tri-*n*-octylphosphine. The addition of PF8-Ph-PA did not disturb the complexation of CdO. As in the synthesis of unfunctionalized CdSe/CdS NRs, a mixture of CdSe seed particles and sulfur dissolved in TOP was swiftly added to this mixture at a temperature of 350 °C. In method B, the PF8-Ph-PA was added to the dispersion containing sulfur and the CdSe seed particles. Afterwards, this mixture was swiftly injected into the standard Cd-precursor solution at 350 °C. In method C, the synthesis of CdSe/CdS NRs was conducted according to the standard protocol developed by Carbone et al.[4], but after a growth time of 8 min, PF8-Ph-PA dissolved in TOP was added at 350 °C and the mixture was cooled down to room temperature.

Scheme 5.5. Schematic illustration of the methods used for the functionalization of CdSe/CdS NRs with phenylphosphonic acid-functionalized PF8.

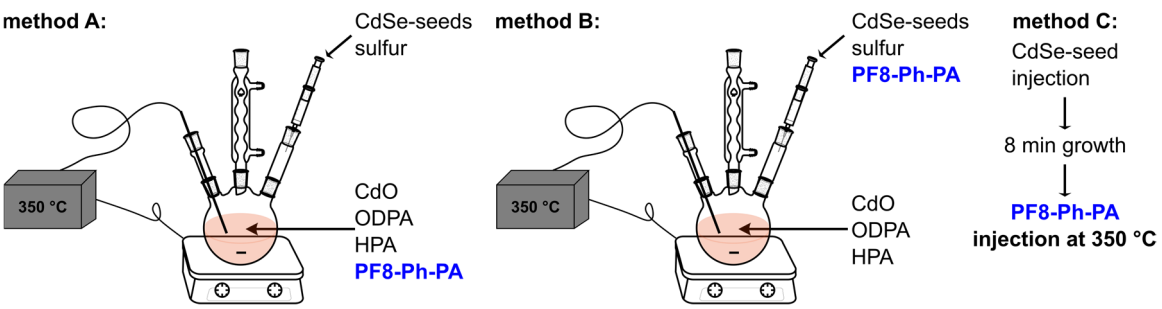

In **Figure 5.11**, the absorption, PL and PLE spectra of the obtained dispersions in toluene are depicted. The absorption spectra are superpositions of the spectra of NRs and PF8. In all spectra, a strong absorption band of PF8 centered at 378 nm is visible, indicating that PF8 is still present in the dispersion. The PL spectra are dominated by the fluorescence of PF8. The PL maximum of the CdSe seeds was red shifted from 565 nm to 590–592 nm. Photoluminescence excitation spectra were recorded at a detection wavelength of 595 nm to probe a possible ET from the polymer to the NRs. For all three samples, the maximum of the PLE is at 378 nm in coincident with the absorption maximum of PF8 indicating an ET from the conjugated polymer to the NRs. The physical mixture of unfunctionalized PF8 and CdSe/CdS NRs shows the same PLE spectrum as pure CdSe/CdS NRs. However, the contribution of the polymer to the NRs' emission is relatively weak in all three samples indicating a poor interaction between the two species and probably a low amount of bound PF8. Therefore, the PL spectra are dominated by the emission of the polymer as only a minor amount of polymer is quenched by the NRs.

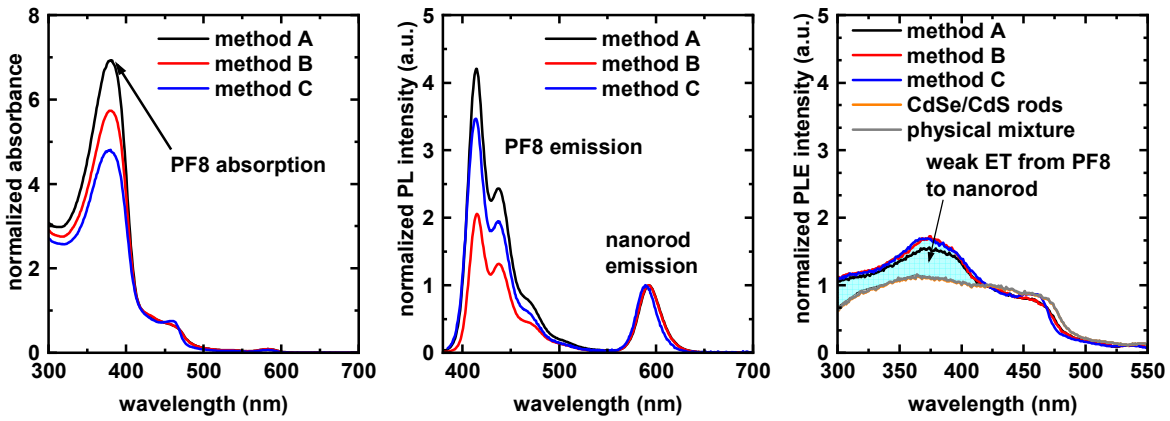

Figure 5.11. Absorption, PL ($\lambda_{exc.}$ = 380 nm) and PLE ($\lambda_{det.}$ = 595 nm) spectra of PF8 CdSe/CdS hybrid NRs. Absorption and PLE spectra are normalized at λ = 420 nm.

In order to elucidate whether the polymer was indeed bound to the NRs or not, MW-AUC measurements were performed (**Figure 5.12**). The percentage of PF8 bound to the NRs can be derived in the same way as for the hybrid QDs. As CdSe/CdS NRs feature a stronger absorption at 420 nm in comparison to QDs, the sedimentation was tracked at a wavelength of 420 nm and 380 nm. At λ = 420 nm, the absorption of PF8 is negligible, and therefore the sedimentation of the NRs can be tracked at this wavelength without any interference of PF8 absorption. **Figure 5.12** shows the sedimentation profile for the hybrid dispersion obtained according to method A. At 14000 rpm, a complete

sedimentation of the NRs was observed (**Figure 5.12**, left). Simultaneously, a small decrease of absorption at a wavelength of 380 nm was monitored. This decrease was caused by the sedimentation of hybrid NRs. From this decrease, it can be calculated that only 20% of the PF8 in the dispersion is indeed bound to the NRs.

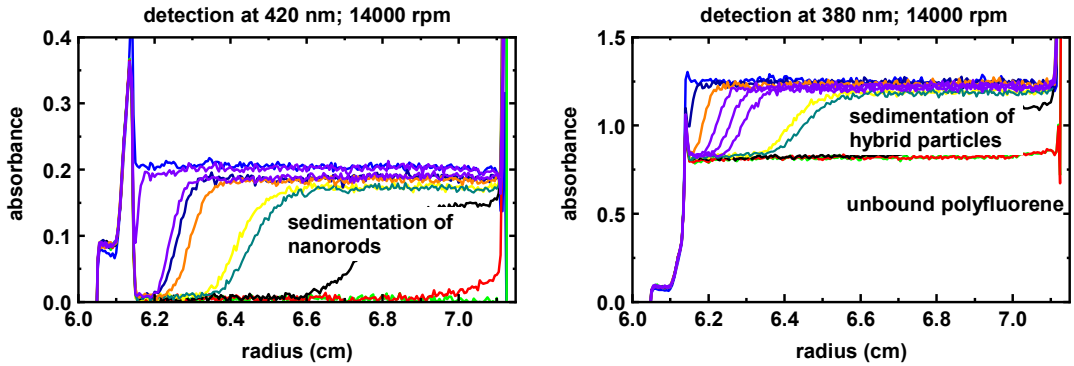

Figure 5.12. MW-AUC measurement data of the PF8-Ph-PA CdSe/CdS hybrid NRs obtained according to method A. The sedimentation of the NRs was tracked at λ = 420 nm outside the absorption range of PF8 and at λ = 380 nm where both NRs and PF8 absorb.

Also, for the dispersions obtained according to method B and method C only 20–25% of the PF8 was bound to the nanocrystals. These MW-AUC results agree with the optical spectra of the dispersions in which only a weak ET from the PF8 to the NRs was observed. In **Figure 5.13**, TEM images of dried films of the three dispersion are shown. Employing method A, polydisperse NRs were obtained. Moreover, spherical particles which do not consist of Cd were obtained which are most probably PF8 particles. Using method B, uniform NRs with the expected length of 20 nm were obtained. The rods aligned into fiber-like structures and many rods also stood upright in a hexagonal pattern on the TEM grid.

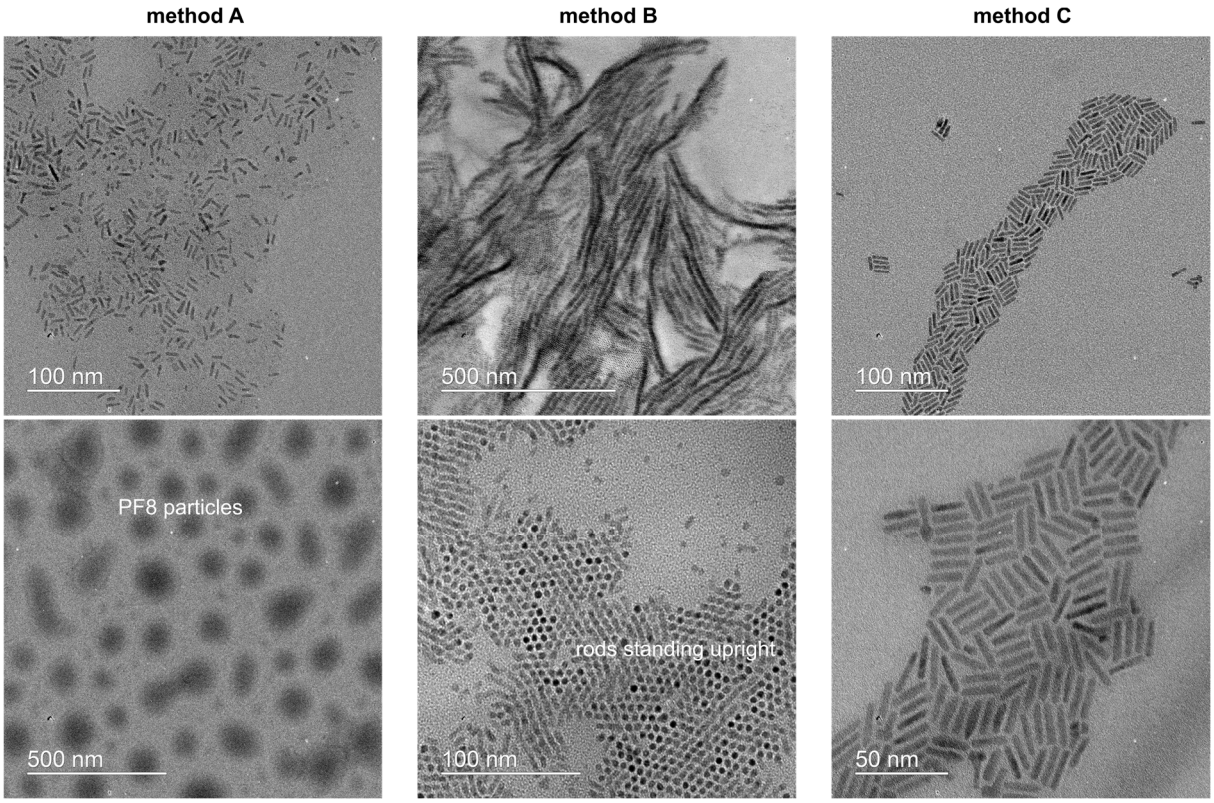

Figure 5.13. TEM images of the PF8-Ph-PA CdSe/CdS hybrid NRs obtained by the three different methods.

As only a small amount of the polymer is indeed tethered to the NRs, the assembly was probably not triggered by the polymer. Additionally, the formation of such 2D superstructures has also been rarely observed for CdSe/CdS NRs which were synthesized without addition of PF8-Ph-PA. The TEM samples were prepared by drop-casting a dilute NR dispersion onto a TEM grid followed by evaporation. In literature, drop-casting and evaporation conditions were reported, which can induce a drying-mediated self-assembly of monodisperse nanorods.[263] Such conditions can coincidentally be fulfilled during the preparation of the TEM samples. By synthesizing hybrid NRs according to method C, uniformly shaped NRs with the expected length and width were obtained, comparable to NRs synthesized without the addition of PF8-Ph-PA. This behavior was expected as the polymer was added after the growth time of the rods had been finished.

During the synthesis of CdSe/CdS a precise mixture of hexylphosphonic acid and octadecylphosphonic acid is used, which enables the anisotropic growth of the NRs and ensures colloidal stability. These alkylphosphonic acids are strongly binding X-type ligands. As they are present in excess compared to the added PF8-Ph-PA, it is comprehensible that only a relatively small portion of the polymer binds to the NRs. None of the three methods explored is suited for a controlled functionalization of NRs with PF8.

In order to ensure a complete and controllable binding, different strategies are possible. The binding strength of the PF8 could be increased by employing a multi-dentate ligand or by increasing the binding strength of the functional group. However, only thiols are known to bind more strongly than phosphonic acids.[76] The synthesis of a thiol-functionalized PF8 is difficult, and thiol-stabilized nanocrystal suffer from poor long-term stability and often poor optical properties as result of hole trap states introduced by the thiol ligands.[264,265] So far, the multidentate PF8 comb copolymers, synthesized in **Chapter 4.2.4**, have not been well suited for the functionalization of nanocrystals (cf. **Chapters 5.2.1–5.2.2**). An alternative method could be to functionalize NRs with surfaces covered by more weakly binding X-type ligands such as oleate which can be replaced by more strongly binding X-type ligands such as phosphonic acids or even by other carboxylic acids. The second strategy was pursued in the following chapter.

Synthesis of Polyfluorene CdSe/CdS/CdS Hybrid Nanorods

The functionalization of CdSe/CdS nanorods yielded only particles with a low amount (<~ 25%) of bound PF8, as the nanorods' surface is covered by strongly binding phosphonic acids which are difficult to replace. In **Chapter 3.2.4**, it was shown that the optical properties of CdSe/CdS NRs can be improved by the deposition of an additional CdS shell, using Cd-oleate as Cd-precursor. Moreover, it was reported that after the deposition of the CdS shell also oleate is bound to the surface of the NRs which is considered a more weakly binding X-type ligand as compared to phosphonic acids.

For the functionalization of CdSe/CdS/CdS NRs with PF8 two different approaches and the attachment of two different polymers were pursued and compared (**Scheme 5.6**). In the first approach, PF8-COOH and accordingly PF8-PA were reacted with CdO and oleic acid to form a Cd-PF8-oleate complex which was mixed with Cd-oleate and used in combination with octanethiol as precursors for the growth of a theoretical 2 monolayers thick CdS shell (cf. **Chapters 5.4.5** and **5.4.7** for experimental details). The second approach is based on the successful functionalization of CdSe/$Cd_xZn_{1-x}S$ QDs (**Chapter 5.2.2**). In this procedure, the CdS shell was deposited using Cd-oleate and octanethiol as precursors. Directly after the end of precursor addition, the respective functionalized PF8 dissolved in octadecene was added to the nanocrystal dispersion at 310 °C which was then annealed at 150 °C for 1 hour.

Scheme 5.6. Schematic illustration of the methods used to functionalize CdSe/CdS/CdS NRs with the polyfluorenes PF8-PA and PF8-COOH.

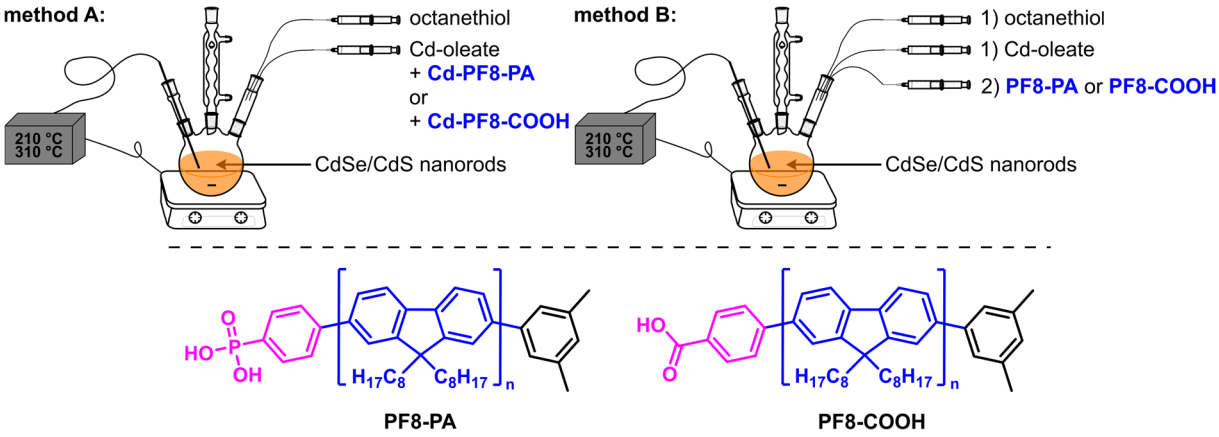

As seed rods, CdSe/CdS rods (different batches, all synthesized from the same batch of CdSe seeds) with a length of 19–20 nm, a width of 3.7–4.7 nm and an emission maximum between 593–595 nm were used (**Table 5.6**). In the first experiments (entries 2–7) following method A, 50, 100 or 200 equiv. of the respective Cd-PF8-oleate was used as precursor in combination with Cd-oleate for the growth of the second CdS shell. In all experiments highly fluorescent dispersions with QYs ($\lambda_{exc.}$ = 450 nm) of 71–80% were obtained (**Table 5.6**). The width of the NRs increased to 5-6 nm which is reflected in the red shift of the emission maximum by 15–16 nm while the emission stayed narrow with a FWHM of 25–27 nm as observed for the used seed rods. The length of the NRs stayed almost unchanged or a slight decrease in length occurred. This phenomenon was also observed in the synthesis of unfunctionalized CdSe/CdS/CdS NRs, described in the previous **Chapter 3.2.4** and was also observed by Bawendi and co-workers.[181] Shim et al.[182] showed that metal-carboxylates can induce etching preferentially along the axial direction of CdSe/CdS NRs which probably (over) balances the growth along this direction. The UV-VIS spectra (**Figure 5.14** a and b) of the hybrid particle dispersions are a superposition of the absorption spectra of NRs and PF8. The concentration of PF8 (band at 378 nm) increased with the amount of Cd-PF8-oleate precursor added. However, the amount of PF8 in the dispersion did not always increase linearly with the added amount of PF8. From experiment 2 to 4 the concentration of PF8 increased by a factor of 4.8 in accordance with the theoretical factor of 4. However, from experiment 5 to 7 the concentration increased only by a factor of 2.2 (theoretical factor = 4).

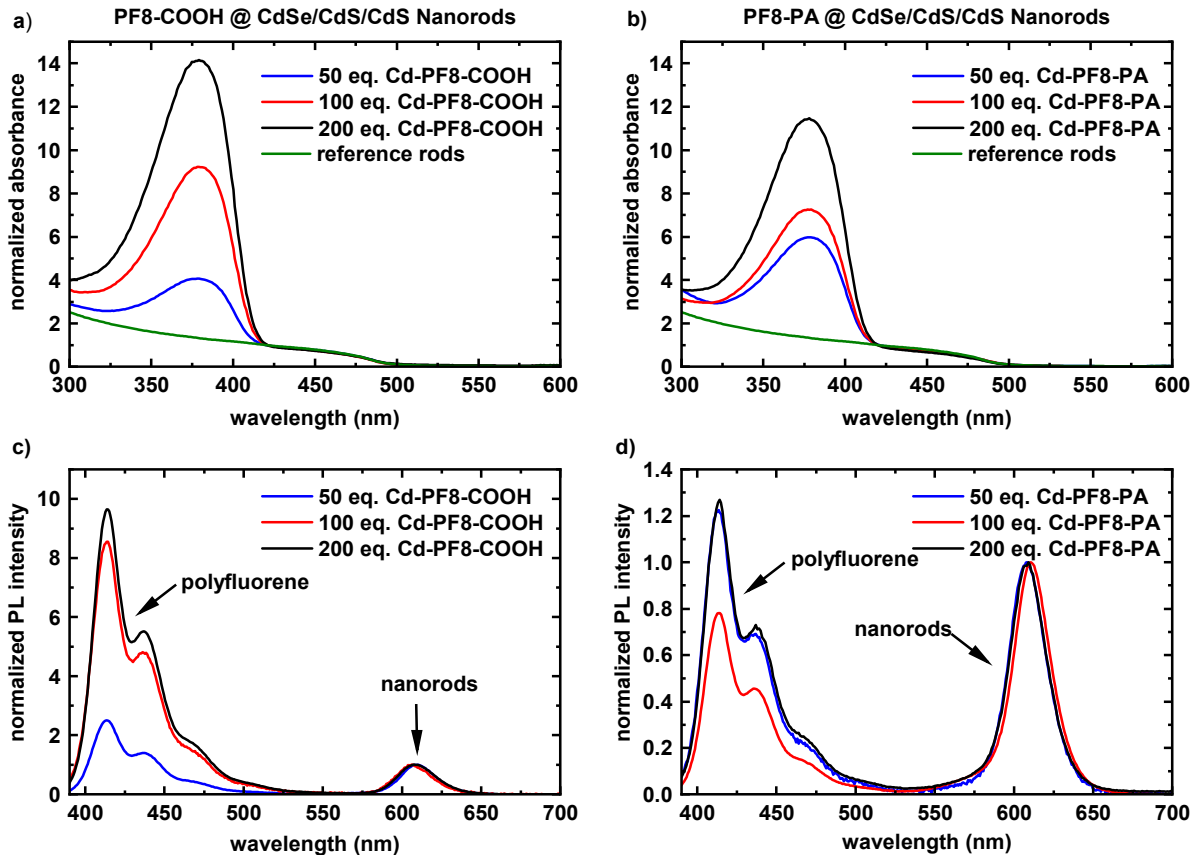

Figure 5.14. Absorption and PL ($\lambda_{exc.}$ = 380 nm) spectra of CdSe/CdS/CdS PF8 hybrid NRs. In the synthesis of the outer CdS shell Cd-oleate and Cd-PF8-oleate were used as precursors. The absorption spectra are normalized at λ = 420 nm outside the absorption range of PF8. The PL spectra are normalized to the maximum of the NRs' emission.

Regarding the PL spectra, a significant difference between the samples synthesized with Cd-PF8-COOH (**Figure 5.14**, c) and Cd-PF8-PA (**Figure 5.14**, d) is visible. The emission spectra for the "hybrid" particle dispersions synthesized with Cd-PF8-COOH are dominated by the PF8 emission. The emission of PF8 in the hybrid particle dispersions synthesized using Cd-PF8-PA is much weaker (factor ~10) hinting to a different binding behavior. However, the PF8 emission is still strong and comparable to the NRs' emission. The percentage of bound PF8 was determined by MW-AUC measurement. In case of Cd-PF8-COOH, only a minor amount (< 10%) of the PF8 was indeed bound to the nanocrystals. For the Cd-PF8-PA a significantly higher amount (45–65%) of the PF8 bound and indeed hybrid NRs were formed which also explains the observed partial quenching of the PF8 fluorescence in these samples (cf. **Figure 8.41** for exemplary MW-AUC data).

Table 5.6. Synthesis and properties of short PF8 CdSe/CdS/CdS hybrid NRs. As seed rods, short (L = 20 nm) CdSe/CdS NRs were used.

#	PF8 source	amount of PF8 (equiv. vs. CdSe/CdS rods)	length width [nm]	$\lambda_{emi.;\ rods}$ [nm]	FWHM [nm]	QY[d] (380 nm) [%]	QY (450 nm) [%]	PF8 bound[e] [%]
1[a]	no	0	18 ± 2. 5.1 ± 0.7	605	27	78	80	-
2[a]	Cd-PF8-COOH	50	17 ± 4 5.4 ± 1.0	609	26	84 (33)	80	< 5
3[a]	Cd-PF8-COOH	100	17 ± 3 5.1 ± 0.7	605	26	88 (12)	76	10
4[a]	Cd-PF8-COOH	200	18 ± 3 5.6 ± 1.1	607	27	80 (15)	80	10
5[b]	Cd-PF8-PA	50	20 ± 5 5.9 ± 0.9	609	27	73 (35)	71	45
6[b]	Cd-PF8-PA	100	18 ± 5 5.9 ±1.0	610	27	70 (40)	70	65
7[b]	Cd-PF8-PA	200	21 ± 6 6.1 ± 0.9	609	27	78 (40)	71	55
8[a]	PF8-COOH	100	18 ± 4 5.2 ± 0.9	605	27	78 (24)	75	20
9[b]	PF8-COOH	200	17 ± 2 5.3 ± 0.7	607	27	88(12)	75	20
10[b]	PF8-COOH	300	18 ± 2 5.1 ± 0.7	607	27	95(11)	73	15
11[c]	PF8-PA	100	19 ± 3 6.3 ± 0.9	607	27	70 (66)	69	> 95
12[c]	PF8-PA	200	18 ± 3 6.3 ± 0.8	609	27	73 (58)	76	95
13[c]	PF8-PA	300	18 ± 3 5.9 ± 0.7	609	27	75 (57)	75	90

a: CdSe/CdS rods, QY = 42%; $\lambda_{emi.}$ = 593 nm; FWHM = 27 nm; L = 20 nm ± 3 nm; W = 3.7 nm ± 0.6 nm b: CdSe/CdS rods, QY = 43%; $\lambda_{emi.}$ = 594 nm; FWHM = 27 nm; L = 20 nm ± 2 nm; W = 3.9 nm ± 0.5 nm c: CdSe/CdS rods, QY = 40%; $\lambda_{emi.}$ = 595 nm; FWHM = 27 nm; L = 19 nm ± 2 nm; W = 4.7 nm ± 0.6 nm d: First value accounts for the emission from 400–700 nm, value in brackets is the QY ($\lambda_{det.}$ = 550–700 nm) of the NRs in this system. e) Percentage of PF8 bound to NRs according to MW-AUC measurements.

The experiments 8–13 were conducted according to method B (**Scheme 5.6**). The functionalized PF8-PA or PF8-COOH was dissolved in octadecene and added to the reaction mixture at 310 °C after the deposition of the CdS shell had been finished.

High-quality NRs were yielded (**Table 5.6**) and the QY ($\lambda_{exc.}$ = 450 nm) ranges from 69-76%. The addition of the polymer had no negative impact on the quality of the nanocrystals and the obtained nanocrystal sizes were comparable to the syntheses without polymer addition (see **Figure 8.42** for exemplary TEM images). The amount of PF8 in the final dispersions scales with the amount of PF8 added (**Figure 5.15**, a and b). However, it does not scale linearly (factor 3.6 from 100 equiv. of PF8-COOH to 300 equiv. and factor 1.9 from 100 equiv. of PF8-PA to 300 equiv.). A major difference between the samples synthesized with PF8-PA and PF8-COOH is visible in the PL spectra (**Figure 5.15**, c and d) but also between the samples synthesized with Cd-PF8-PA and PF8-PA (**Figure 5.14** d and **Figure 5.15** d). In the case of PF8-PA, the PL caused by PF8 is nearly completely quenched whereas in the case of PF8-COOH the PL spectra is dominated by the PF8 emission. For the samples synthesized with Cd-PF8-PA, the emission intensity of PF8 and the NRs is comparably strong, whereas for the samples synthesized with PF8-PA, the PF8 emission is negligible in comparison to the NRs' emission. These findings indicate a higher percentage of bound PF8 in case of utilizing PF8-PA. According to MW-AUC measurements, basically all PF8-PA in the dispersion is indeed bound to the nanocrystals (cf. **Figure 8.43** for exemplary MW-AUC measurement data), which explains the nearly complete quenched PF8 fluorescence in these samples (cf. **Figure 8.44** for an additional experiment demonstrating the quenching). Using 100 equiv. of PF8-PA, all polymer in the dispersion is bound to the nanocrystals and using 300 equiv. of PF8-PA, still around 90% of the polymer binds to the nanocrystals. Regarding the binding density, this would result in a roughly calculated density in the range of 0.2–0.8 PF8 chains/nm^2 which is comparable to the binding density observed for the functionalization of CdSe/$Cd_xZn_{1-x}S$ QDs with polyfluorene.

The approach using Cd-PF8-COOH as precursor during the CdS shell growth was not successful in the functionalization of the NRs. Only around less than 10% (entries 2–4) of the PF8 in the dispersion was bound to the NRs and more of physical mixtures than hybrid particles were formed. The addition of the PF8-COOH directly after the precursor addition increased the amount of bound PF8 to around 15–20% (entries 8–10) according to MW-AUC measurements. Using Cd-PF8-PA as precursor (entries 5–7), a significant amount (45–65%) of the PF8 was bound to the nanocrystals. The addition of PF8-PA after the deposition of the second CdS shell yielded dispersions in which basically all (> 90%) PF8 was bound to nanocrystals.

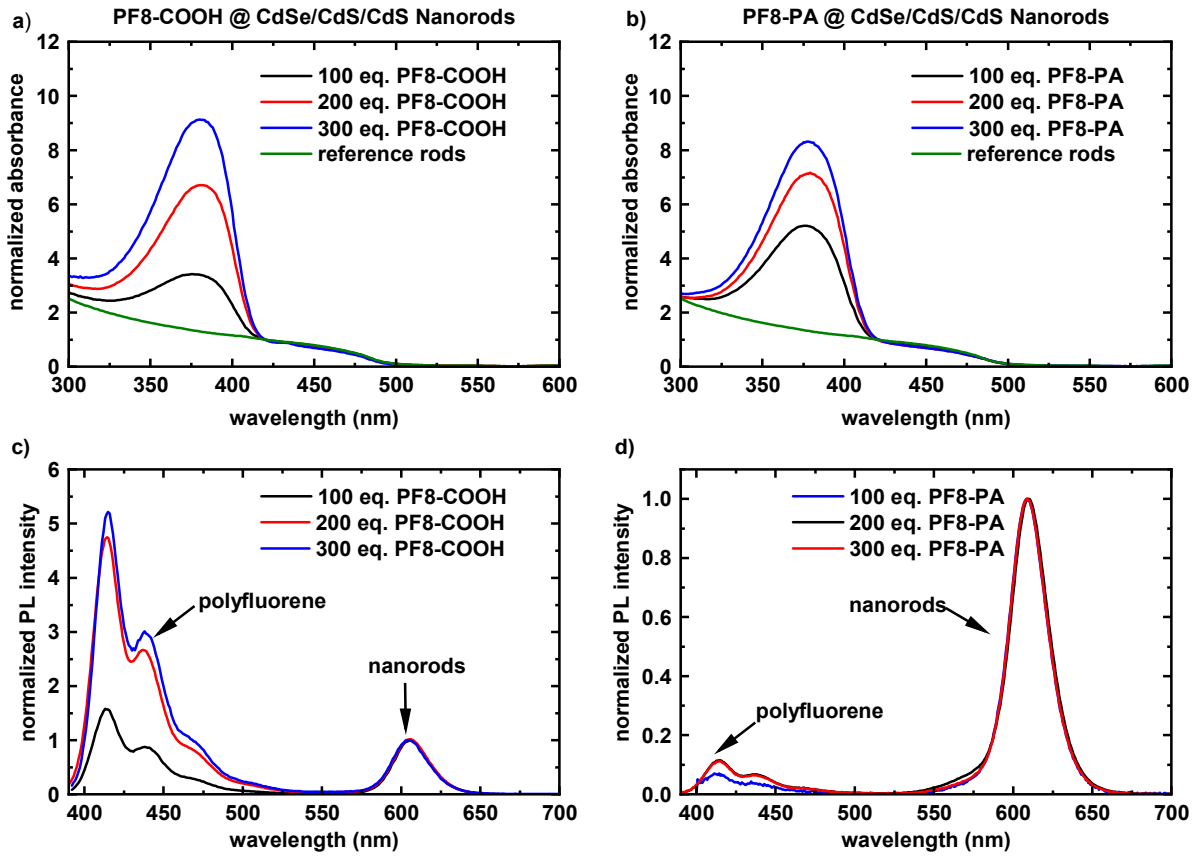

Figure 5.15. Absorption and PL ($\lambda_{exc.}$ = 380 nm) spectra of CdSe/CdS/CdS PF8 hybrid NRs. The PF8 was directly added after the end of the precursor solutions addition. The absorption spectra are normalized at λ = 420 nm outside the absorption range of PF8. The PL spectra are normalized to the maximum of the NRs' emission.

Evaluating the AUC results, it has to be considered that the measurements are performed in highly diluted dispersions which leads to an underestimation of the percentage of bound polymer. The observed lower functionalization by using Cd-PF8 precursors instead of the free-acid-functionalized PF8 might be explained by the general reaction mechanism. Cd-carboxylate or Cd-phosphonate precursors are decomposed to Cd^{2+} and the respective anhydride during the formation of CdS. Carboxylic acid anhydrides are not known to bind to nanoparticles, but phosphonic acid anhydrides are.[68] However, given the reaction composition, the formation of a phosphonic acid anhydride is unlikely. The major X-type ligand used in this synthesis of the CdSe/CdS/CdS NRs is oleic acid. Oleic acid probably has a similar or slightly stronger binding affinity towards the CdS surface than PF8-COOH but is present in excess compared to the polymer (~300-1900 equiv.), therefore only a small amount of the PF8-COOH binds to the surface. In general, phosphonic acids are known to be stronger ligands for CdSe surfaces than carboxylic acids and as shown by Dempsey et al. phosphonic acids can irreversibly displace carboxylic

acids.[76,70,72] The same trend was observed here for the CdS surface of the NRs. Although only a small amount of PF8-PA in comparison to oleic acid and Cd-oleate (total oleic acid excess ~300–1900) was added, all PF8-PA chains in the dispersion bound to the nanocrystals.

To elucidate whether the strong binding of the PF8 and quenching of the PF8 emission in some of the samples leads to an ET from the PF8 to the nanocrystals resulting in fluorescence of the NRs, photoluminescence excitation measurements (**Figure 5.16**) were performed in which the contribution to the NR fluorescence at 605 nm was recorded.

The left side of **Figure 5.16** displays the PLE spectra for the functionalization of the NRs with Cd-PF8-COOH or with PF8-POOH compared to the PLE spectra of a physical mixture of unfunctionalized PF8 and NRs and pure NRs. Above 400 nm, all spectra are identical, below 400 nm there are small deviations between the spectra, but no sample shows a significant contribution of the PF8 absorption to the NRs emission. This observation is logical as the samples synthesized with Cd-PF8-COOH are basically nothing else than a physical mixture of PF8 and NRs. Surprisingly, also for the samples synthesized with PF8-COOH, no significant ET transfer was observed, although up to 20% of the polymer is bound to the NRs according to MW-AUC measurements. The reason could be that the carboxylate anchor group might be more 'insulating' than the phosphonate group. The PLE spectra (**Figure 5.16**, right side) of the NRs functionalized with PF8-PA or Cd-PF8-PA feature a strong band in coincidence with the absorption maximum of PF8 around 378 nm which strongly contributes to the NRs emission. A strong ET from excited PF8 to the NRs is observed which becomes more intense with increasing amount of PF8 bound to the nanocrystals. This finding also explains the almost complete quenching of the PF8 emission in these samples as observable in the PL spectra (**Figure 5.14** and **Figure 5.15**). Combined with the binding behavior elucidated from the AUC measurements, it becomes apparent that for a strong interaction between the two semiconductor materials a strong binding of the PF8 to the NRs is necessary and a simple physical mixture of the two components is not sufficient which is in accordance with the results for the functionalization of quasi-spherical QDs.

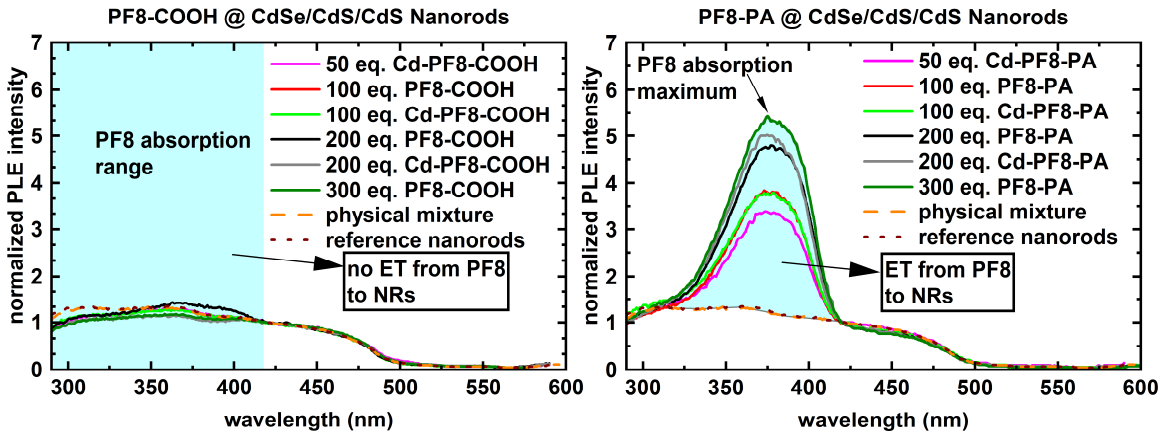

Figure 5.16. PLE spectra ($\lambda_{det.}$ = 605 nm) of CdSe/CdS/CdS PF8 hybrid NRs. Left: NRs functionalized with PF8-COOH. Right: NRs functionalized with PF8-PA. The PLE spectra are normalized at λ = 420 nm outside the absorption range of PF8. The physical mixture of CdSe/CdS/CdS NRs and unfunctionalized PF8 was adjusted to have the same absorption spectra as the sample synthesized with the addition of 100 equiv. of Cd-PF8-COOH.

In **Figure 5.17**, the intensity of the ET from the PF8 polymer to the nanocrystals is plotted as a function of the amount of bound PF8 chains. In this region of functionalization (50–300 equiv. of PF8 per nanocrystal added), the ET scales linearly with the amount of bound PF8 chains. In the samples synthesized with PF8-PA, the percentage of bound PF8 is higher than in samples synthesized with Cd-PF8-PA. However, the concentration of PF8 in the final dispersions is higher in the samples synthesized with Cd-PF8-PA than is the case for PF8-PA (nominal addition of same equiv. of PF8) which results in roughly the same absolute number of bound chains and in an equally strong ET.

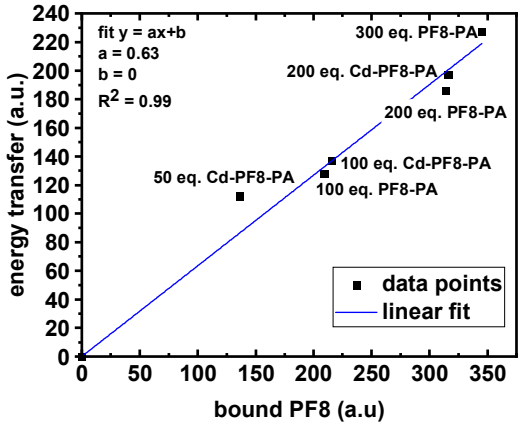

Figure 5.17. Energy transfer from PF8 to nanocrystals vs. amount of bound PF8. ET = $\int_{300\,nm}^{550\,nm}$ PLE(Hybrid) − $\int_{300\,nm}^{550\,nm}$ PLE (Rods) and bound PF8 = $\left(\int_{300\,nm}^{550\,nm} \text{Abs(Hybrid)} - \int_{300\,nm}^{550\,nm} \text{Abs (Rods)}\right) \cdot$ %bound(AUC).

The influence of the functionalization of the NRs with the conjugated polymer chains was analyzed by comparing the PL decay of the hybrid NRs to the parent unfunctionalized

CdSe/CdS and CdSe/CdS/CdS NRs (**Figure 5.18**). The PL decay of the NRs became slower by the deposition of the second CdS shell (**Figure 5.18** left and center) onto the CdSe/CdS seed NRs (see **Table 8.1** for lifetimes and fitting parameter). This behavior was expected, as the optical quality of the seed NRs was improved upon shell deposition. The functionalization of the CdSe/CdS/CdS NRs with the conjugated polymer PF8-PA caused a slight increase in the PL decay rate of the NRs. This difference in the decay dynamics of functionalized and unfunctionalized NRs could be observed for an excitation at λ = 405 nm (both polymer and nanocrystals are excited) and at λ = 485 nm (only the nanocrystals are excited) However, no difference in the PL dynamics between the two excitation wavelengths was observed.

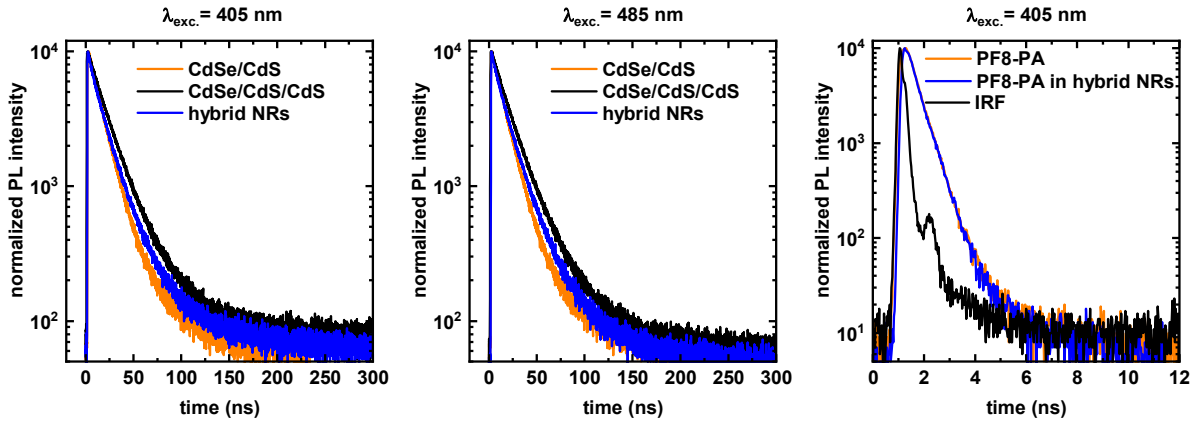

Figure 5.18. In the left and center graph the PL decay spectra of CdSe/CdS, CdSe/CdS/CdS NRs and the same CdSe/CdS/CdS NRs functionalized with PF8-PA (hybrid NRs) are shown for two different excitation wavelengths. At 405 nm the PF8 and the NRs are excited, whereas at 485 nm only the NRs are excited. The PL is recorded at the wavelength of the NRs maximal PL intensity. The right graph shows the PL decay spectra of dissolved PF8-PA and the respective PF8-PA in the hybrid particle dispersion ($\lambda_{det.}$ = 414 nm).

At both excitation wavelengths charge transfer processes between the two materials, which would lead to a charging of the inorganic emitter, should be possible in principle (cf. **Scheme 5.1** for energy level diagram). At both wavelengths, a hole transfer from an excited NR to the PF8 should be possible but requires a tunneling process. Exciting the system at λ = 405 nm, also an electron transfer from excited PF8 to the CdSe core should be feasible (this process competes with an ET from excited PF8 to the CdSe core). As in the case for quasi-spherical CdSe/$Cd_xZn_{1-x}S$ hybrid QDs, the shortened PL lifetime of the hybrid NRs as compared to the unfunctionalized NRs could be an indication for an additional charging of the inorganic emitter due to charge transfer processes with the PF8.

Additionally, the hybrid NRs possessed a slightly lower QY than the unfunctionalized NRs (69-75% vs. 75-80%) which might also hint at an additional charging of the emitter.
The fluorescence lifetime of PF8 in the hybrid particle dispersion was once again identical to the fluorescence lifetime of PF8 in solution (**Figure 5.18** right). Polymer bound to the NRs seems to be completely quenched by them in its fluorescence and the PF8-PA PL intensity originates from unbound PF8-PA chains which show the same PL decay dynamics as PF8-PA in solution.

Synthesis of Longer Polyfluorene-Functionalized CdSe/CdS/CdS Hybrid Nanorods

As method B (**Scheme 5.6**) has proven to be the best functionalization method for the functionalization of short CdSe/CdS/CdS NRs (L = 20 nm) with PF8, method B using PF8-PA as polymer was also applied to functionalize longer (L = 30 nm) CdSe/CdS NRs (**Table 5.7**). Also for the longer CdSe/CdS seed rods, high-quality CdSe/CdS/CdS hybrid NRs were obtained (cf. **Figure 8.45** for TEM images) showing a QY in the range of 70–80%. As for the syntheses of unfunctionalized CdSe/CdS/CdS NRs, a small decrease in length and an increase in width of the NRs occurred.

Table 5.7. Synthesis and properties of PF8-PA-functionalized CdSe/CdS/CdS hybrid NRs using long (30 nm) CdSe/CdS NRs as seed rods.

#	PF8 source	amount of PF8 (equiv. vs. CdSe/CdS rods)	length width [nm]	$\lambda_{emi.;\ rods}$ [nm]	FWHM [nm]	QY[c] (380 nm) [%]	QY (450 nm) [%]	PF8 bound[d] [%]
1[a]	no	0	28 ± 3 5.5 ± 0.8	605	25	75	78	-
2[a]	PF8-PA	75	27 ± 3 5.8 ± 0.7	607	26	70 (54)	70	> 95
3[b]	PF8-PA	100	27 ± 2 5.7 ± 0.7	605	25	70 (57)	80	95
4[b]	PF8-PA	200	27 ± 3 5.8 ± 0.7	609	26	72 (54)	77	90
5[b]	PF8-PA	400	27 ± 3 6.1 ± 0.7	609	26	75 (40)	75	80

a: Seed rods: QY = 36%; $\lambda_{emi.}$ = 592 nm; FWHM = 25 nm, L = 30 nm ± 2 nm; W = 4.0 nm ± 0.4 b: Seed rods QY = 40%; $\lambda_{emi.}$ = 598 nm; FWHM = 26 nm, L = 30 nm ± 2 nm; W = 4.2 nm ± 0.6 c: First value accounts for the emission from 400–700 nm, value in brackets is the QY ($\lambda_{det.}$ = 550–700 nm) of the NRs in this system. d: Percentage of bound PF8 as determined by MW-AUC measurements.

Here, also a complete binding of the PF8-PA to the NRs took place (experiments 2–4), the PL of the polymer was quenched and a strong ET from the polymer to the NRs was observed (**Figure 5.19**). However, the sample synthesized with 400 equiv. of PF8-PA showed a stronger PF8 emission (factor 3) compared to the other samples which indicates that this high amount of polymer was not completely bound to the nanocrystals. This is in accordance with the lower percentage of 80% bound PF8 as determined by MW-AUC measurements. As reported for the functionalization of QDs, a maximum number of chains could be tethered to one NR following this approach.

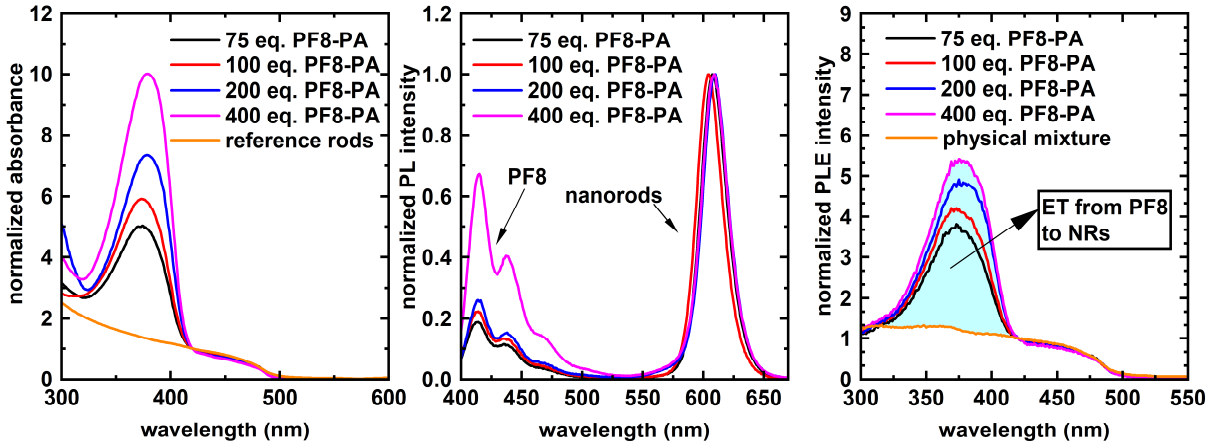

Figure 5.19. Absorption (left) and PL ($\lambda_{exc.}$ = 380 nm; center) spectra of long CdSe/CdS/CdS NRs functionalized with PF8-PA which was added directly after the deposition of the outer CdS shell (method B). The PLE spectra (right, $\lambda_{det.}$ = 605 nm) and absorption spectra are normalized at λ = 420 nm outside the absorption range of PF8. The physical mixture of CdSe/CdS/CdS NRs and unfunctionalized PF8 was adjusted to have the same absorption spectra as the sample synthesized with 100 equiv. of PF8-PA.

In conclusion, a novel way for the direct functionalization of semiconductor CdSe/CdS NRs with PF8 was presented elucidating the binding behavior of the polymer by multi-wavelength analytical ultracentrifugation measurements. The functionalization of CdSe/CdS NRs was basically unsuccessful; however, the functionalization of CdSe/CdS/CdS resulted in hybrid NRs with a high and partially controllable amount of bound PF8. Additionally, these NRs featured improved optical properties as compared to the single-shell CdSe/CdS NRs. Using Cd-PF8-PA as additional precursor in the synthesis of the outer CdS shell, around 45–65% of the PF8 was bound to the NRs. Basically, no binding was observed for utilizing Cd-PF8-COOH. Remarkably, the use of the additional precursor did not deteriorate the formation of the CdSe/CdS/CdS NRs. Addition of the free-acid-functionalized polymers PF8-PA or PF8-COOH directly after the deposition of the second CdS shell also yielded hybrid NRs. Only up to 20% of the polymer PF8-COOH

was bound to the nanocrystals whereas for PF8-PA a complete binding of the polymer was observed. For the samples synthesized with Cd-PF8-PA or PF8-PA a strong ET from photoexcited polymer to the NRs was observed, which depends linearly (in the analyzed range) on the amount of bound PF8 chains. The method presented here allows to tune the amount of conjugated polymer chains bound to semiconductor NRs. Due to the strong ET from the polymer to the NRs, these hybrid nanoparticles are interesting for the use in colloidal semiconductor lasers and for single-particle PL studies.

5.3 Summary and Conclusion

Hybrid particles consisting of semiconductor nanocrystals and conjugated polymers are a promising material class for the use in opto-electronic devices and on a fundamental level as single-photon source. However, their synthesis is challenging, and most reported methods lack a proof of binding (**Chapter 1.2**).

In this chapter, the synthesis of PF8 CdSe/CdS hybrid nanocrystals (QDs and NRs) was investigated employing different methods and using various functionalized PF8s. The binding of PF8 to the nanocrystals was proven and analyzed by multi-wavelength analytical ultracentrifugation measurements.

CdSe/CdS QD hybrid particles were successfully synthesized by a direct ligand exchange reaction with phenylphosphonic acid end-functionalized PF8 (PF8-Ph-$PO(OH)_2$). Around 70% of the added polymer chains (175 equiv.) was bound to the nanocrystals and unbound PF8 could be separated by preparative centrifugation. The fluorescence of PF8 bound to nanocrystals was completely quenched and a quantitative ET to the nanocrystal was observable, resulting in the emission of the nanocrystal (**Figure 5.20**). Such an ET was only observed when the polymer was bound to the QDs and not for a simple physical mixture.

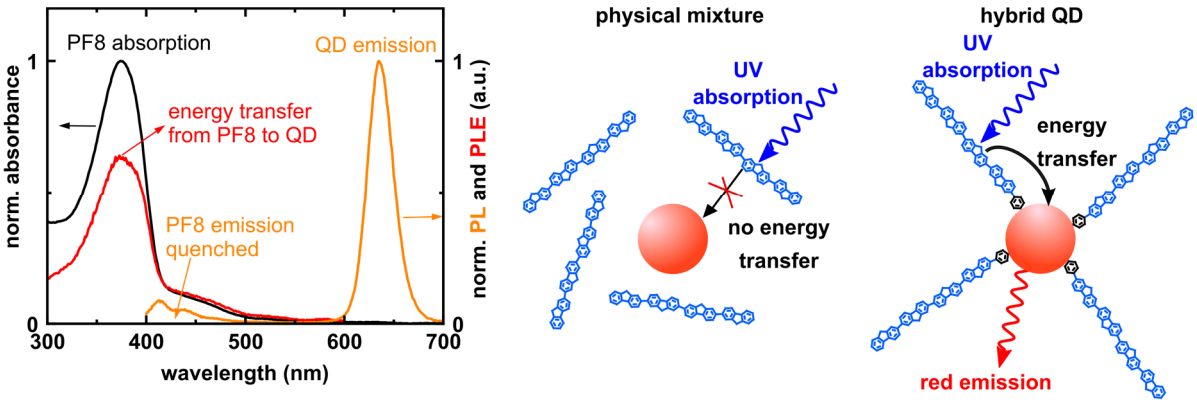

Figure 5.20. Left: Optical properties of a CdSe/CdS PF8 hybrid QDs synthesized by a ligand exchange reaction, followed by separation of unbound PF8 by centrifugation. The PLE is recorded at $\lambda_{det.}$ = 630 nm. Right: Schematic illustration of the ET process from excited PF8 to a QD which can only be observed for hybrid particles and not for a physical mixture of unfunctionalized PF8 and QDs.

In **Chapters 4.2.3–4.2.4**, the synthesis of novel diblock (PA-PF8-*b*-PEHMA, PA-PF8-*b*-PMMA and PA-PF8-*b*-PS) and multi-valent comb polymers (PA-PF8-Sty-*co*-PEHMA, PA-PF8-Sty-*co*-PMMA, PA-PF8-Sty-*co*-PS) was reported. These polymers were used in direct ligand exchange reactions to functionalize high-quality CdSe/$Cd_xZn_{1-x}S$ QDs. The binding

affinity of the diblock copolymer PA-PF8-*b*-PEHMA was comparable to the linear homotype polyfluorene PF8-Ph-$PO(OH)_2$ and around 50–60% (100 equiv. added) of the added polymer chains bound to the nanocrystals. The addition of the multi-valent comb polymers led to a partial precipitation of QDs and especially polymer. However, the remaining polymer bound strongly to the QDs and basically all polymer in the dispersion was bound to the nanocrystals.

The functionalization of QDs during their synthesis allows to add the polymer at high temperatures, at a stage where the particle formation is not completed, and a separate ligand exchange reaction is not necessary. To this end, the functionalization of high-quality $CdSe/(CdS)_2(ZnS)_2$ QDs was assessed in a direct approach, adding the phosphonic acid-functionalized PF8 during the synthesis of the nanocrystals. Addition of PF8-Ph-$PO(OH)_2$ before the deposition of the ZnS shell disturbed the further particle formation, and in the case of adding the multi-valent comb polymers, a (complete) precipitation of the QDs was observed. Thus, the addition of the polymer after the deposition of the ZnS shell was investigated. Conducting this approach with phosphonic acid-functionalized PF8s, high-quality hybrid QDs (QY = 78–84%) were obtained. Adding the polymer at 310 °C slightly increased the amount of bound polymer as compared to the addition at 150 °C. Moreover, benzylphosphonic acid-terminated PF8 was found to bind slightly less than PF8-Ph-$PO(OH)_2$. However, the amount of bound PF8 did not increase linearly with the added amount of polymer and it seems that roughly a maximum of around ~55 polymer chains can bind to one QD (d = 6.1 nm) using this method. For these hybrid QDs, an ET from excited PF8 to the QDs was revealed whose intensity depended on the amount of bound PF8. The ET from benzylphosphonic acid-functionalized PF8 to the QD was significantly weaker (~25%) in comparison to the phenylphosphonic acid-terminated PF8, which can be related to the 'insulating' -CH_2- group between the conjugated system and the binding group. Hybrid QDs showed a slightly faster PL decay than unfunctionalized QDs, which hints at an additional charging of the QDs due to the functionalization with PF8.

Employing the multi-valent comb and diblock copolymers in this approach resulted in a significantly lower functionalization due to solubility issues. These multi-valent comb polymers are indeed strongly binding; however, they seem to destabilize the nanoparticles.

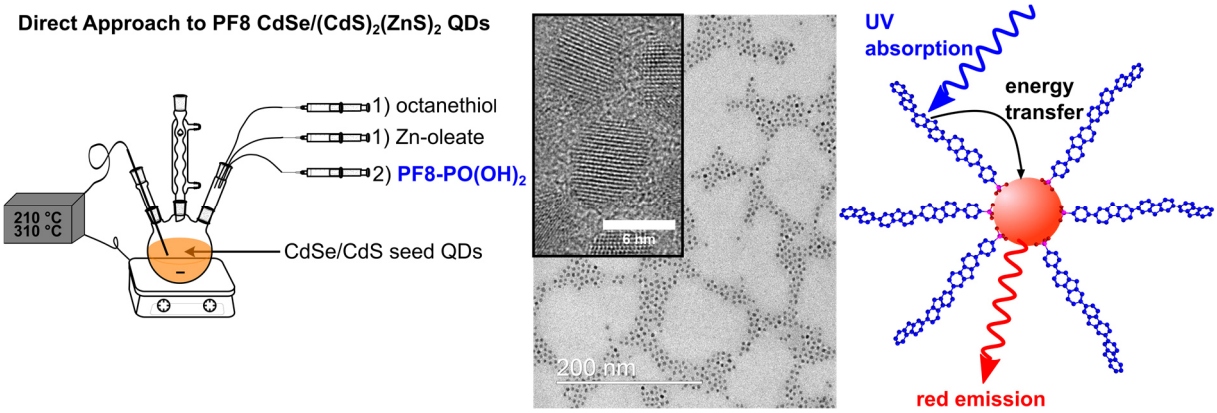

Figure 5.21. Functionalization of graded-shell CdSe/$(CdS)_2(ZnS)_2$ QDs with PF8-$PO(OH)_2$ in a direct approach.

As high-quality CdSe/$(CdS)_2(ZnS)_2$ hybrid QDs were obtained by the described direct approach, the functionalization of CdSe/CdS NRs was investigated by different direct methods using PF8-Ph-$PO(OH)_2$. However, the functionalization of standard CdSe/CdS NRs was basically unsuccessful. The surface of these NRs was saturated by a mixture of strongly binding phosphonic acids which could not be displaced by the functionalized polymers to a significant amount. Therefore, the functionalization of CdSe/CdS/CdS NRs with surfaces partially occupied by more weakly binding oleate ligands and with superior optical properties as compared to the standard CdSe/CdS NRs (cf. **Chapter 3.2.4**) was explored. In the first approach, Cd-PF8-X (X=Ph-COOH or Ph-$PO(OH)_2$) was used as additional precursor besides Cd-oleate in the deposition of the outer shell. The formation of the CdS shell was not disturbed and high-quality NRs (QY = 71–80%) were obtained. Only by using Cd-PF8-Ph-$PO(OH)_2$ hybrid NRs (45–65% of bound PF8) were formed whereas PF8-Ph-COOH did not bind. In the second approach, the free-acid-functionalized polymers PF8-Ph-$PO(OH)_2$ and accordingly PF8-Ph-COOH were directly added at 310 °C after the deposition of the second CdS shell. For PF8-Ph-COOH, no significant binding was observed; however, basically all PF8-Ph-$PO(OH)_2$ in the dispersion was bound to the nanocrystals. This method allows to partially control the amount of PF8 bound to the NRs — a complete binding was detected for adding up to 300 equiv. of polymer to the nanocrystals. The PL decay of hybrid NRs was slightly shortened compared to unfunctionalized NRs which could be a hint at an additional charging of the NRs due to a charge transfer process with the polymer. Additionally, the fluorescence of bound PF8 was quenched and an ET from the PF8 to the NRs was observed (**Figure 5.22**). The intensity of this ET scaled linearly – in the investigated range - with the amount of bound

PF8. Therefore, these novel hybrid NRs are of interest for the use in semiconductor NRs based lasers and for charging experiments in single-particle PL studies.

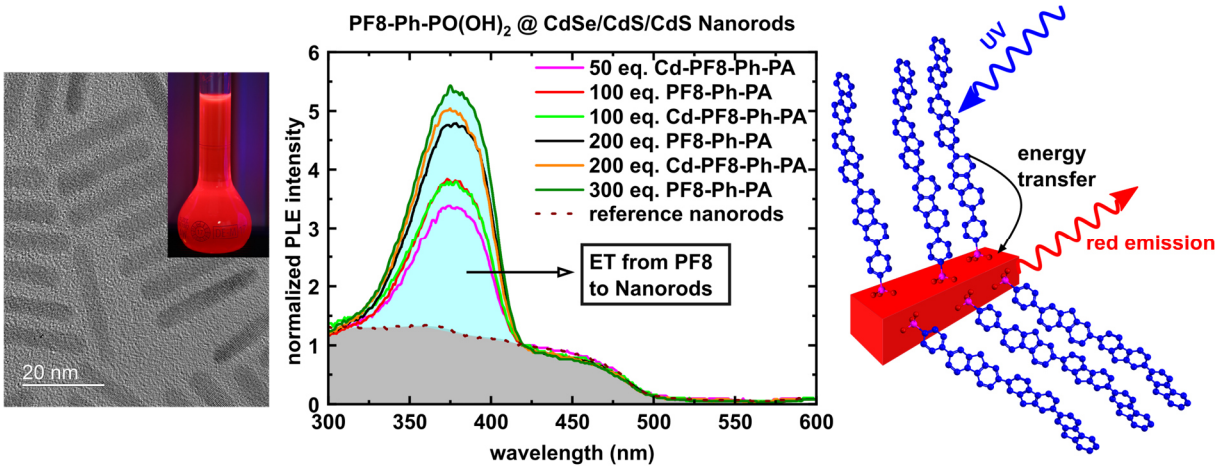

Figure 5.22. Left: Exemplary TEM image of PF8 CdSe/CdS/CdS hybrid NRs and a photograph of such a dispersion under UV light illumination. Center: PLE spectra ($\lambda_{det.}$ = 605 nm) of these hybrid NRs, showing an increasing ET from the PF8 to the NRs with an increasing number of bound PF8 chains. Right: Schematic illustration of the ET process.

5.4 Experimental Section

5.4.1 Materials and General Considerations

All manipulations of air- and/or water sensitive compounds were carried out under inert atmosphere using standard glove box and Schlenk techniques. Glassware were dried at 80 °C for at least 24 h.

Cadmium oxide (> 99.99%-Cd, lot MKBT7524V), hexylphosphonic acid (HPA; 95%, lot MKBX1133V), oleylamine (70%), oleic acid (90%), octanethiol (> 98.5%), tri-*n*-octylphosphine (TOP; 99%), tri-*n*-octylphosphine oxide (TOPO; 99%), zinc acetate (99.99%, lot MKCC8484), and octadecene (90%) were purchased from Sigma-Aldrich. *n*-Octadecylphosphonic (ODPA, 98%, lot 807601N16) acid was obtained from PCI and trimethylsilyl chloride (98%) from Acros Organics. 1-Dodecylphosphonic acid (95%, lot 1343062) was purchased from ABCR.

Octadecene, oleic acid and oleylamine were degassed by sparging with nitrogen for two hours and by applying vacuum at 80 °C for 20 h.

CdSe seed particles (from Cd-ODPA precursor), CdSe/CdS QDs, CdSe/$(CdS)_x(ZnS)_y$ QDs, CdSe/CdS NRs and functionalized PF8s were synthesized as described in **Chapter 3.4** and **Chapter 4.4** respectively.

5.4.2 Analytical Methods

Absorption spectroscopy (UV-VIS spectroscopy):

Absorption spectra were recorded on a Varian Cary 100 scan spectrometer with the neat respective solvent as reference.

Photoluminescence measurements and Quantum Yield Determination:

Ensemble emission spectra and quantum yields were measured using a Hamamatsu Absolute PL Quantum Yield Measurement System C9920-02 equipped with an integrating sphere.

Photoluminescence Excitation Measurements and PL Lifetimes:

Photoluminescence spectra, photoluminescence excitation spectra and fluorescence lifetimes were measured in dispersions of the particles on a PicoQuant FluoTime 300 spectrometer (excitation sources: 300 W Xenon arc lamp or Picosecond Laser Diode Heads (LDH series from PicoQuant)). PL lifetimes were fitted with the FluoFit software package.

Analytical Ultracentrifugation:

The AUC measurements were carried out on a custom built UV/Vis multiwavelength detecting analytical ultracentrifuge equipped with an AN 60 Ti Rotor.[266] For all measurements Titanium 2 channel cells with an optical path length of 12 mm were used. Experiments were carried out at 25 °C. Toluene served as an optical reference. The sample volume was 330 µL and the toluene volume 350 µL. The functionalized QDs were diluted in toluene until the maximum of the absorbance had a value of 0.8–1.2.

Transmission Electron Microscopy (TEM):

TEM micrographs were aquired using a Jeol JEM-2200FS transmission electron microscope using a FEG with 200 kV acceleration voltage or using a Zeiss Libra120 employing a LaB6 emitter with 120 kV acceleration voltage. Samples were prepared by drop casting 2 µL of a diluted particle dispersion on a TEM grid (Quantifoil S 7/2 + 2 nm C, Cu 400).

Determination of the Percentage of Bound Polyfluorene by Analytical Ultracentrifugation:

Inorganic nanocrystals and polymer chains show a huge different in molar mass (QD > 150000 g/mol; PF8 ~5000 g/mol, density (QD ~5 g/mL; PF8 ~1 g/mL) and thus in their sedimentation coefficient.

Therefore, unbound PF8 and PF8 bound to nanoparticles show different sedimentation coefficients and can be separated in a centrifugal field.[113] By multi-wavelength analytical ultracentrifugation (MW-AUC), it possible to measure UV-VIS spectra of different species during their sedimentation in the centrifugal field.[266,267] Hence, it is possible to distinguish between bound and unbound PF8 in a hybrid particle dispersion. In the following, the procedure is exemplarily explained for CdSe/CdS/CdS NR hybrid particles but can also be used for the analysis of QD hybrids. **Figure 5.23** depicts the absorption spectra of a hybrid particle dispersion of PF8 @ CdSe/CdS/CdS NRs (black line), unfunctionalized CdSe/CdS/CdS NRs (red line) and PF8 (green line) dissolved in toluene. The sedimentation of the NRs can be monitored at a wavelength of 300 nm and 420 nm at which the absorption by PF8 is negligible. The sedimentation of PF8 (hybrid particles) is monitored at a wavelength of 380 nm.

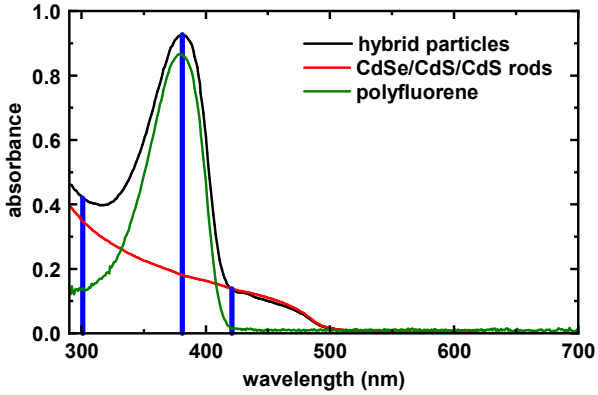

Figure 5.23. UV-VIS spectra of hybrid NRs (black line), non-functionalized CdSe/CdS/CdS rods (red line) and PF8 (green). The blue lines indicate wavelength values suitable to track the individual species during sedimentation.

At this wavelength, the absorption is caused by the NRs and the PF8. The contribution of the NRs at this wavelength can be subtracted by using Lambert-Beer's law. The ratio of NR absorption at 380 nm and 300 nm or 420 nm is equal to the ratio of the absorption coefficients at the different wavelengths. This ratio can be obtained from the UV-VIS spectra of an unfunctionalized reference NR or QD dispersion. With this ratio, it is possible to subtract the contribution of NRs from the absorption at 380 nm of a hybrid dispersion. The percentage of PF8 bound to the NRs can be calculated using equations (1) and (2):

$$\mathrm{Abs(nanorods;\,380\ nm)} = \Delta\mathrm{Abs(420\ nm)} \cdot \frac{\mathrm{Abs(nanorods_{ref};\,380\ nm)}}{\mathrm{Abs(nanorods_{ref};\,420\ nm)}}. \qquad (1)$$

$$\%\mathrm{(PF8\ bound)} = \frac{\Delta\mathrm{Abs(380\ nm)} - \mathrm{Abs(nanorods;\,380\ nm)}}{\mathrm{Abs(380\ nm)} - \mathrm{Abs(nanorods;\,380\ nm)}}. \qquad (2)$$

Here, Abs(nanorods;380 nm) is the contribution of the nanorods to the absorbance of the hybrid particle dispersion at 380 nm, ΔAbs stands for the change in absorbance at a certain wavelength during the sedimentation process and other absorbance values are values measured before sedimentation.

Instead of using equation (1) for the calculation of the absorption of the NRs at 380 nm, also equation (3),

$$\mathrm{Abs(nanorods;\,380\ nm)} = \Delta\mathrm{Abs(300\ nm)} \cdot \frac{\mathrm{Abs(nanorods_{ref};\,380\ nm)}}{\mathrm{Abs(nanorods_{ref};\,300\ nm)}}, \qquad (3)$$

can be employed. Here, the sedimentation of the NRs is tracked at 300 nm. For the final calculation of the percentage of bound PF8 no significantly different results (±1%) were obtained by using equation 1 or 3.

The same procedure can be used to calculate the percentage of PF8 bound to spherical QDs. QDs do not show a strong absorption band at 420 nm. Therefore, their sedimentation can only be tracked at a wavelength of 300 nm and the percentage of bound PF8 is calculated using equations (5) and (6):

$$\mathrm{Abs}(\mathrm{QDs};\,380\ \mathrm{nm}) = \Delta\mathrm{Abs}(300\ \mathrm{nm}) \cdot \frac{\mathrm{Abs}(\mathrm{QDs_{ref}};\,380\ \mathrm{nm})}{\mathrm{Abs}(\mathrm{QDs_{ref}};\,300\ \mathrm{nm})}. \quad (5)$$

$$\%(\mathrm{PF8\ bound}) = \frac{\Delta\mathrm{Abs}(380\ \mathrm{nm}) - \mathrm{Abs}(\mathrm{QDs};\,380\ \mathrm{nm})}{\mathrm{Abs}(380\ \mathrm{nm}) - \mathrm{Abs}(\mathrm{QDs};\,380\ \mathrm{nm})}. \quad (6)$$

5.4.3 Direct Ligand Exchange

Ligand Exchange with Functionalized Polymers

The required amount of QDs was precipitated by the addition of methanol, collected by centrifugation and the QD pellet dried in a stream of nitrogen. Afterwards, the QDs were dispersed in the respective degassed and dried solvent (toluene, tetrahydrofuran or dichloromethane) and the functionalized PF8 of interest was added. The mixture was stirred at a certain temperature for 24 hours.

Prior Ligand Exchange by Pyridine

The required amount of QDs was precipitated by the addition of methanol, collected by centrifugation and the QD pellet was dried in a stream of nitrogen. The residual solid was dispersed in 1 mL of dry and degassed pyridine. The dispersion was stirred overnight and precipitated from *n*-hexane and the precipitate was collected by centrifugation. The QDs were redispersed in 1 mL of dry and degassed DCM. 175 equivalents of PA-Ph-PF8-MA were dissolved in 1.0 mL of dry and degassed DCM, and the solution was added to the QD dispersion and stirred for 24 hours.

Separation of Hybrid Particles from Unbound Polymer

Precipitation:

The hybrid QDs (in toluene or dichloromethane) were precipitated by the addition of a precipitation agent (methanol, acetone, ethanol, acetonitrile, or mixtures of those). Only as much precipitation agent as necessary to cause a slight turbidity of the dispersion was added. Afterwards, the QDs were collected by centrifugation (2000 g for 5 min). For optical measurements, the sedimented QDs were redispersed in the same volume of solvent as originally used for the exchange reaction.

Centrifugation:

The hybrid QD dispersion was diluted with the respective solvent to a total volume of 8 mL. The dilution is necessary as the centrifuge tube has to be filled to a certain level for centrifugation at high-rotational speed. The dispersion was centrifuged at 20.000 g (maximum speed of the centrifuge) for 2 hours. Afterwards, the sedimented pellet and supernatant were carefully separated. The pellet was redispersed in the same amount of toluene as original hybrid dispersion used.

5.4.4 Functionalization of CdSe/$Cd_xZn_{1-x}S$ Quantum Dots by a Direct Approach

The synthesis of CdSe/$(CdS)_x(ZnS)_y$ PF8 hybrid QDs followed the procedure for the synthesis of CdSe/$(CdS)_x(ZnS)_y$ QDs as described in **Chapter 3.4.5**, but phosphonic acid-functionalized PF8 and PF8 copolymers (block or comb polymer) were added at certain step of the synthesis.

Polyfluorene Addition After Deposition of the CdS Shell

Phosphonic acid-functionalized PF8 was degassed by applying vacuum for 30 min and dissolved in 0.5 mL of degassed oleic acid and 1 mL of degassed octadecene. To ensure a complete solvation of the PF8, the mixture was heated to 80 °C under a nitrogen atmosphere.

The synthesis of CdSe/$(CdS)_2(ZnS)_2$ QDs was performed as described in **Chapter 3.4.5**. After the addition of the CdS shell had been completed, the mixture was cooled down to 200 °C and the PF8 solution in octadecene and oleic acid was added dropwise. Attention, strong bumping often occurs at this step. The reaction mixture was annealed at 150 °C for one hour. Afterwards, the synthesis followed the same procedure as described for the non-functionalized QDs.

Polyfluorene Addition After Deposition of the ZnS Shell

The CdSe/$(CdS)_2(ZnS)_2$ QDs were synthesized as described in **Chapter 3.4.5**. After the addition of the ZnS precursor solutions had been finished, 1 mL of a degassed solution of phosphonic acid-functionalized polyfluorene in octadecene (80 °C) was added to the reaction mixture at a certain temperature (310 °C or 150 °C). The mixture was cooled down to a temperature of 150 °C and annealed for 1 hour. The mixture was worked-up as describe for the synthesis of non-functionalized CdSe/$Cd_xZn_{1-x}S$ QDs.

5.4.5 Synthesis of Cd-Polyfluorene Precursors

Synthesis of Cd-PF8-PA

In a 25 mL three neck flask, equipped with a septum, thermo couple and reflux condenser (set-up as shown in **Figure 3.13**), CdO (5.0 mg, 0.038 mmol, 1 equiv.), phenylphosphonic acid end-functionalized PF8 (1 equiv.) and oleic acid (25 µL, 2 eq.) were mixed in 7.6 mL of octadecene. The mixture was degassed by applying vacuum at room temperature for 40 min, at 120 °C for 45 min and heated under nitrogen until the solution became clear (200 °C). The mixture was cooled to 100 °C, degassed for 1 hour by applying vacuum, placed under nitrogen and oleylamine (2 equiv.) was added. The mixture was stored in a nitrogen-filled glovebox.

Final concentration: c(Cd) = 0.005 mol/L; c(PF8-PA) = 0.005 mol/L

Note: In a reference experiment, complexating CdO with 2 equiv. of oleic acid under the conditions as described above was attempted. The red CdO powder was not dissolved and remained at the bottom of the flask. Complexation of CdO by oleic results in the formation of colourless and clear solution. Therefore, it can be concluded that the CdO was not or only to a minor amount complexated.

Synthesis of Cd-PF8-COOH

In a 25 mL three neck flask, equipped with a septum, thermo couple and reflux condenser (set-up as shown in **Figure 3.13**), CdO (5.0 mg, 0.038 mmol, 1 equiv.), phenylcarboxylic acid functionalized PF8 (1 equiv.) and oleic acid (25 µL, 2 eq.) were mixed in 7.6 mL of octadecene. The mixture was degassed by applying vacuum at room temperature for 40 min, at 120 °C for 45 min and heated under nitrogen until the solution became clear (200 °C). The mixture was cooled to 100 °C, degassed for 1 hour by applying vacuum, placed under nitrogen and oleylamine (2 equiv.) was added. The mixture was stored in a nitrogen-filled glovebox.

Final concentration: c(Cd) = 0.005 mol/L; c(PF8-COOH) = 0.005 mol/L

5.4.6 Synthesis of CdSe/CdS Polyfluorene Hybrid Nanorods

The synthesis of CdSe/CdS NRs functionalized with PF8 followed the procedure described in **Chapter 3.4.5** which is based on the procedure reported by Carbone et al.[4], but phenylphosphonic acid-functionalized PF8 was added to the CdSe seed particles dispersion, to the Cd-precursor solution or directly after the growth of the NRs.

Method A: Addition to Cd-Precursor Solution:

TOPO (3.0 g), ODPA (290 mg, 0.87 mmol), HPA (80 mg, 0.48 mmol) and CdO (for a rod length of 20 nm: 57 mg, 0.44 mmol) and 28 mg of phenylphosphonic acid end-functionalized PF8 (8 µmol, 100 equiv. vs. CdSe seed particles) were degassed in a 25 mL three neck flask, equipped with a septum, thermo couple and reflux condenser (set-up as shown in **Figure 3.13**), for 1 hour at 150 °C and then heated to 330 °C under a nitrogen atmosphere. The mixture was kept at this temperature until it turned clear, indicating the complexation of Cd. At this step, 2 mL of TOP is slowly added, and the temperature is increased to the injection temperature of 350 °C. Simultaneously, a mixture consisting of 120 mg (3.7 mmol) of sulfur, 1.8 mL of TOP and 80 nmol of CdSe seed cores in hexane was prepared and the hexane was removed in vacuum at 80 °C over a period of 1 hour. When the temperature of the CdO reaction mixture had reached 350 °C, the core precursor solution was rapidly injected. After stirring the mixture for 8 min at 350 °C, it was cooled down by removing the heating mantle and cooling with compressed air. The NRs were purified by three rounds of precipitation by the addition of a 3 : 1 v/v acetone/methanol mixture, centrifugation and discarding the supernatant and redispersion in toluene. Finally, the NRs were precipitated from acetone/methanol, collected by centrifugation, dried in a stream of nitrogen gas and redispersed in 4 mL of toluene, filtered through a syringe filter and stored under exclusion of light.

Method B: Addition to the CdSe Seed Particle Dispersion

The Cd precursor solution was prepared as described in method A but without addition of PF8. The seed particle dispersion was prepared by mixing 120 mg (3.7 mmol) of sulfur and 28 mg (8 µmol, 100 equiv. vs. CdSe seed particles) of PF8-Ph-PA. This mixture was degassed by applying vacuum for 30 min and purging with nitrogen. 1.8 mL of TOP and 80 nmol of CdSe seed particles in hexane were added. The hexane was removed in vacuo at 80 °C over a period of one hour. The PF8 dissolved well in the reaction mixture. The following steps were identical to the procedure described in Method A.

Method C: Addition directly after the Growth of the Nanorods

The CdSe/CdS NRs were synthesized as described in **Chapter 3.4.5**. After the growth time of 8 min had been over, the PF8-Ph-PA (100 equiv. vs. CdSe seeds) dissolved in 1 mL of TOP was added at 350 °C. Afterwards, the work-up was performed as described for the unfunctionalized standard CdSe/CdS NRs.

5.4.7 Synthesis of Polyfluorene CdSe/CdS/CdS Hybrid Nanorods

Using Cd-Polyfluorene Precursors

The synthesis of hybrid particles followed the same protocol as the synthesis of CdSe/CdS/CdS NRs described in **Chapter 3.4.5**. But in this case, the Cd-precursor solution was prepared by diluting a mixture of a solution of Cd-oleate in octadecene and a solution of Cd-PF8-oleate in octadecene with additional amounts of octadecene to yield a total injection volume of 3 mL. In comparison to the synthesis of unfunctionalized CdSe/CdS/CdS NRs, an additional annealing step (1 h at 150 °C) after the precursor addition was introduced.

Addition of Functionalized Polyfluorene Directly After Shell Growth

The synthesis of CdSe/CdS/CdS NRs was performed as described in **Chapter 3.4.5**, but after the addition of Cd-oleate and octanethiol had been completed, a 80 °C hot solution of phenylphosphonic acid (PF8-Ph-PA) or phenylcarboxylic acid (PF8-Ph-COOH) functionalized polyfluorene dissolved in 2 mL of octadecene was added at 310 °C. The mixture was cooled down to 150 °C, annealed for 1 h, and then worked up according to the synthesis of pure CdSe/CdS/CdS NRs.

6 Encapsulation of (Hybrid) Inorganic Nanocrystals in Polymer Nanoparticles and Single-Particle Photoluminescence Experiments

6.1 Introduction

Single semiconductor nanocrystals are an interesting material for photoluminescence studies on the single-particle level. These systems can serve as model system to study the interplay between charge carriers, photons and phonons in a fully quantized system.[168] Moreover, these materials are relevant for their potential use as single-photon sources.[162] For these experiments, single particles are required. For this purpose, a very dilute dispersion of the nanoparticles can be spin coated onto a substrate. However, the stability of bare semiconductor nanocrystals against environmental influences, mechanical manipulation and strong optical excitation is limited.[141,143] Thus, the nanocrystals are often embedded in a continuous polymer matrix. Thereby, the nanocrystals obviously lose their single-particle character, and mechanical manipulation of individual nanocrystals becomes impossible. As shown by Leitenstorfer and co-workers, the placement of a single nanocrystal embedded in a PMMA shell into a plasmonic bullseye resonator with the tip of an AFM can lead to an efficient enhancement of the nanocrystal's emission.[34] For this procedure, individual particles which are large and mechanically stable enough to be moved around with an AFM tip are needed. The encapsulation of spherical CdSe/CdS QDs into cross-linked PMMA particles by a miniemulsion polymerization is a proven solution to ensure a high mechanical as well as optical stability of the nanocrystals.[150] Moreover, the nanocrystals are efficiently mechanically decoupled from the substrate which allows to study the interplay between photons, charge carriers and phonons in a fully quantized

system.[168] The chemical background of the embedding techniques is explained in detail in the general introduction (**Chapter 1.3**).

CdSe/CdS dot-in-rod nanorods (NRs) feature a strongly polarized emission, a permanent dipole moment, and both high absorption coefficients and high QYs.[4,169,172,173] Moreover, they have recently been identified as promising single-photon emitters, which might exhibit efficient trion (quasiparticle consisting of two electrons and one hole or two holes and one electron) emission due to reduced Auger recombination.[2,170,171] These facts render NRs and especially hybrid NRs interesting for single-particle PL studies. However, to the best of our knowledge, no procedure for the encapsulation of single CdSe/CdS NRs into polymer particles has been reported so far. NRs show a strong tendency to align due to the strong attractive interactions between individual particles.[263,268,269] Moreover, NRs are even more hydrophobic than spherical QDs which further impedes their embedment in rather hydrophilic polymer particles, such as PMMA particles. Therefore, the development of an encapsulation process to embed CdSe/CdS NRs and PF8 CdSe/CdS hybrid NRs into larger polymer particles was one objective of this chapter.

One main aim of this research was the generation of charged inorganic CdSe-based emitters by a charge transfer between the nanocrystal and bound conjugated polymer chains (polyfluorene). As part of her dissertation, Carla Negele encapsulated CdSe/CdS nanocrystals into polyfluorene particles by a miniemulsion polymerization.[270] However, the conjugated polymer was not chemically bound to the nanocrystals. Due to the high amount of conjugated polymer in the close proximity of the nanocrystals, the optical properties of these hybrid particles were mainly dominated by the polymer. Nevertheless, a partial quenching of the polymer fluorescence around the QDs was reported. During his dissertation, Tjaard de Roo synthesized CdSe/CdS PF8 hybrid particles by a direct approach and by a grafting-from approach, which were successfully encapsulated into cross-linked PMMA particles.[150] However, especially the particles obtained by the grafting-from approach showed a low colloidal and optical stability. For both particle systems, no charging of the inorganic nanocrystals has been observed in single-particle PL experiments yet.

In **Chapters 5.2.2** and **5.2.3**, the synthesis of PF8 CdSe/$(CdS)_2(ZnS)_2$ hybrid QDs and PF8 CdSe/CdS/CdS hybrid NRs was reported. The nanocrystals in these systems revealed excellent optical properties (high QYs, narrow emission line widths). Moreover, an efficient energy transfer (ET) from the polyfluorene to the nanocrystal resulting in fluorescence of the latter was detected indicating the strong coupling between the two

semiconductor materials. Therefore, these new promising hybrid particles were embedded into polymer particles to make them suitable for single-particle PL studies. So far, both the nanocrystals and the hybrid particles in the single-particle PL studies have only been excited by a laser at a wavelength of ~530–570 nm outside the absorption range of PF8. In doing so, only a hole transfer from the valence band (VB) of an excited nanocrystal to the VB of the polymer — requiring a tunneling process — was possible (**Scheme 6.1**, b). The new hybrid particles were simultaneously excited by a LED at λ = 370 nm, a wavelength of strong PF8 absorption. Given the energy levels of the polymer and the nanocrystals, the excitation of the polymer should allow additional two processes:

Scheme 6.1. Possible formation of charged CdSe/CdS nanocrystals by charge transfer processes with PF8 ligands upon optical excitation. Processes b and c require a tunneling of the hole through the CdS shell layer.

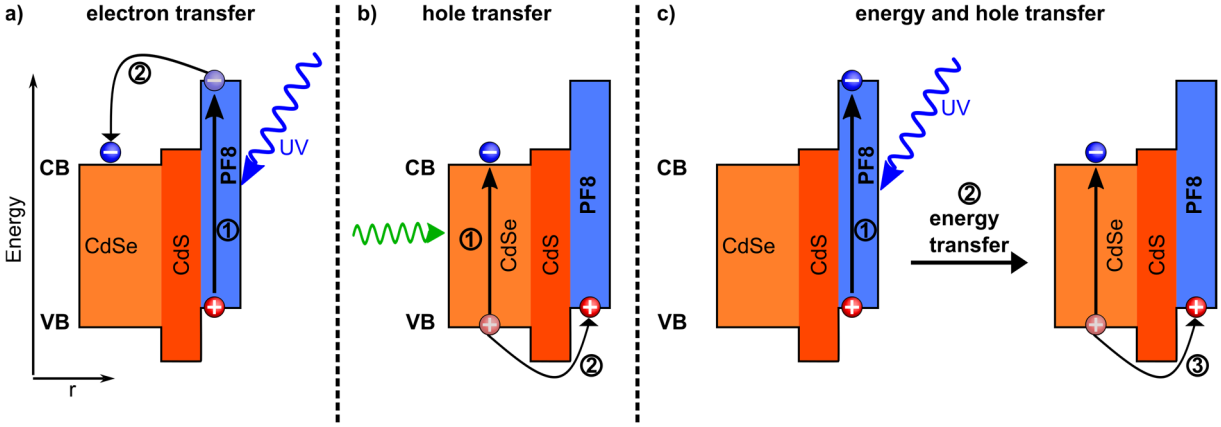

Firstly, an electron transfer from the conduction band (CB) (LUMO) of photoexcited PF8 to the CB of the nanocrystal should become possible, which would lead to a charging of the CdSe core. Secondly, an ET from the photoexcited polymer to the nanocrystal is possible and was also detected for ensemble PLE measurements at room temperature. A subsequent hole transfer from the VB of the excited nanocrystal to the VB of the polymer could additionally lead to a charged nanocrystal. The charging of the CdSe core and the formation of a trion was indeed observed for PF8 hybrid CdSe/$Cd_xZn_{1-x}S$ QDs and PF8 CdSe/CdS/CdS hybrid nanorods. The charged nanocrystals are presumably formed by an electron transfer between the two semiconductor materials. The formed charged inorganic emitters indeed show a PL fine structure consisting of a single emission line, a significantly shortened fluorescence lifetime and an increased PL intensity as compared to their uncharged counterparts.

6.2 Results and Discussion

6.2.1 Encapsulation of Graded-Shell Quantum Dots by a Miniemulsion Polymerization Approach

The synthesis of CdSe/$(CdS)_x(ZnS)_y$ graded-shell QDs of high optical quality was described in **Chapter 3.2.3**. These QDs have the potential to replace the comparatively lower quality CdSe/CdS QDs synthesized by a SILAR process which have been used for single-particle PL studies so far. Moreover, these QDs serve as a reference material for the charging experiments with CdSe/$(CdS)_2(ZnS)_2$ PF8 hybrid QDs.

The QDs were encapsulated into cross-linked PMMA particles by a miniemulsion polymerization approach (**Scheme 1.6**) based on a procedure developed by Carla Negele and Tjaard de Roo in course of their dissertations.[150,178] The oil phase in these encapsulations consisted of MMA, hexadecane, cross-linking reagent, AIBN and the QDs dispersed in toluene. The aqueous phase consisted of water and sodium dodecyl sulfate (SDS) as surfactant. A miniemulsion was generated by ultrasonication with a sonotrode, and afterwards the polymerization was conducted at 75 °C. The results for the embedding of the four different CdSe/$(CdS)_x(ZnS)_y$ (x,y = 1–2) samples are shown in **Table 6.1**. In order to yield a reference sample, the QD sample CdSe/$(CdS)_2(ZnS)_2$ was also embedded with a mixture of 7 : 3 vol% of MMA/EHMA as this has proven to be beneficial for the encapsulation of hybrid particles (**Table 6.2**). In all experiments, particles with a size around 60 nm (number average hydrodynamic diameter obtained from dynamic light scattering (DLS)) and a narrow size distribution ($PDI_{DLS} \leq 0.1$) were obtained. Also, the embedding in the mixture of MMA/EHMA (experiment 2) yielded particles with an average size in this range. In experiments 1–2 and 4–5, the QYs of the dispersions were decreased from 85–87% for the non-embedded QDs to 49–56% upon encapsulation. In former studies, a decrease in QY was observed for the embedding of CdSe/CdS QDs. Tjaard de Roo, for instance, reported a decrease from ~40% to 20–30%.[150] The embedded graded-shell CdSe/$(CdS)_x(ZnS)_y$ QDs show superior properties (in terms of QY) in comparison to the CdSe/CdS QDs in the encapsulated state. The decreased QY of encapsulated QDs compared to non-embedded QDs is probably caused by the change of the chemical environment. Moreover, QDs can be deteriorated by contact with radicals and water during the heterophase radical polymerization.[143,271] In experiment 3, the QY was even lowered down to 25% but from a starting value of only 67%. However, in this

experiment the CdSe QDs covered with 2 monolayers (ML) of CdS and 4 ML of ZnS were used, which in general possess inferior optical properties due to the relatively thick and strain inducing layer of ZnS. Regarding the QY measurements, it has to be emphasized that the reported QYs of non-embedded nanocrystals and of the embedded nanocrystals are ensemble averages. For single-particle PL measurements, the optical properties of the single particles are essential and not the ensemble average. However, experimental experience has shown that the probability to randomly pick or find a single particle which is 'bright' and optically stable in single-particle PL measurements is higher for dispersions with a higher ensemble QY. As single-particle measurements are very time-consuming, it is not feasible to screen many encapsulated QD dispersions. Therefore, dispersions showing a high ensemble QY are preferentially selected for these measurements.

Table 6.1. Encapsulation of $CdSe/(CdS)_x(ZnS)_y$ QDs into polymer particles by a miniemulsion polymerization approach.

#	QD	monomer [mL]	d_z[a] [nm]	d_n[a] [nm]	PDI	QY_{QD}[b] [%]	$QY_{emb.}$[c] [%]
1	$CdSe/(CdS)_2(ZnS)_2$	MMA	92	66	0.08	87	52
2	$CdSe/(CdS)_2(ZnS)_2$	MMA/EHMA 0.7 : 0.3	82	58	0.08	87	49
3	$CdSe/(CdS)_2(ZnS)_4$	MMA	85	56	0.10	67	25
4	$CdSe/(CdS)_4(ZnS)_2$	MMA	90	65	0.08	85	64
5	$CdSe/(CdS)_4(ZnS)_4$	MMA	90	56	0.10	86	56

Encapsulation conditions: Aqueous phase: 80 mL of degassed H_2O and 100 mg of SDS; oil phase: 100 µL of *n*-hexadecane, 1 mL of monomer, 10 µL of ethylene glycol dimethacrylate, 10 nmol (0.6 ml) of QDs in toluene, 10 mg of AIBN; 2 min ultrasonication with a sonotrode at 60% intensity; polymerization for 5 hours at 75 °C. a: Z-average, number average diameter and PDI obtained by DLS. b: Ensemble QY of the non-embedded QDs measured in toluene. c: Ensemble QY of the embedded QDs measured in H_2O.

The size and QY of the $CdSe/(CdS)_x(ZnS)_y$ PMMA multi-shell particles renders them highly usable for single-particle spectroscopy studies. However, also the adjustment of embedding statistics is required, as only polymer particles containing exactly one QD per particle can be used. In **Figure 6.1**, TEM images of $CdSe/(CdS)_2(ZnS)_2$ QDs embedded in PMMA are displayed. Most of the particles are empty (~60%; in total 175 particles counted), many contain exactly one QD (~35%) and only a few particles are occupied by several QDs (~5%). Due to the interaction of the polymer particles with the TEM beam, resulting in melting and fusion of the polymer particles, it remains challenging in some cases to tell whether a particle contains several QDs or was formed from several particles

containing individual QDs. Within experimental error, the relative portion of empty polymer particles, single QD polymer particles, and polymer particles with multiple QDs corresponds to a statistical distribution of the QDs over the polymer particles.[151] This finding suggests, that there is no tendency for QD aggregating in the original miniemulsion polymerization mixture.

In single-particle PL studies, only a limited number of particles can be analyzed due to the time-consuming nature of the measurement. Therefore, promising particles containing QDs are often pre-selected based on their PL emission intensity. Thereby, unfortunately preferentially particles containing several nanocrystals, which cannot be used as single-photon source, are selected. However, this process is not disturbed by empty polymer particles. A high proportion of empty polymer particles is not directly detrimental for single-particle PL studies, however, can be prejudicial to the placement of individual particles into optical resonator systems without a prior PL-based preselection. Thus, the percentage of particles containing several QDs in the dispersion should be low and lower than the proportion of single QD particles. Therefore, the obtained distribution is well suited for the intended measurements.

The encapsulation of the other CdSe/$Cd_xZn_{1-x}S$ QDs yielded similar desirable results concerning the incorporation (cf. **Figure 8.46** for exemplary TEM images) of the QDs.

In summary, CdSe/$Cd_xZn_{1-x}S$ QDs were successfully encapsulated in PMMA-based polymer particles, and given their superior optical properties as compared to the CdSe/CdS particles, they are a promising reference material for single-particle PL studies.

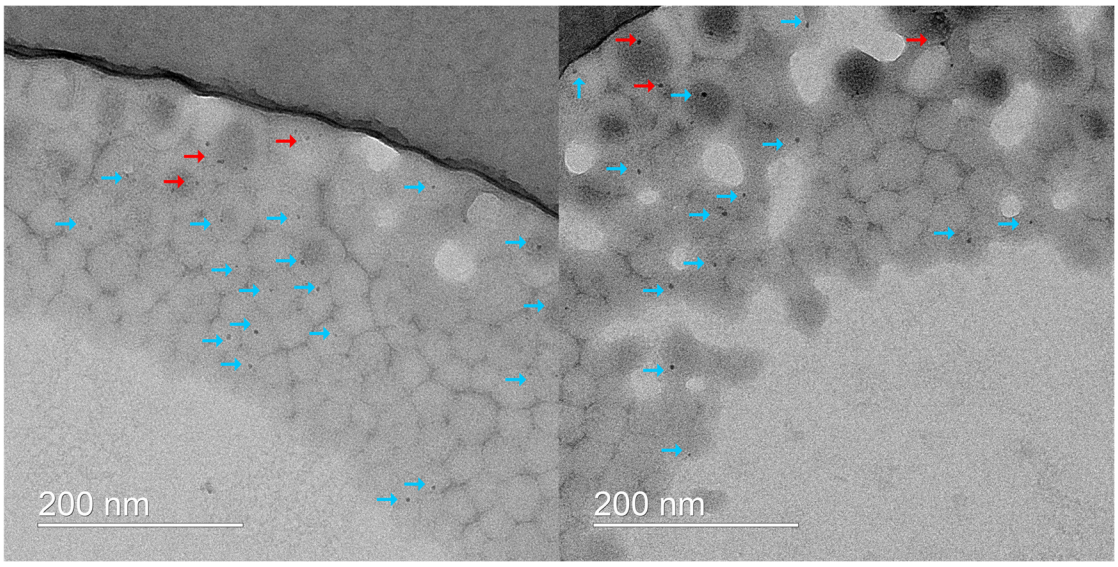

Figure 6.1. TEM images of CdSe/$(CdS)_2(ZnS)_2$ QDs encapsulated in cross-linked PMMA particles. The blue arrows indicate polymer particles with one QD and the red arrows particles with several QDs per particle.

6.2.2 Encapsulation of Polyfluorene-Functionalized Quantum Dots by a Miniemulsion Polymerization Approach

The synthesis of high-quality hybrid particles consisting of PF8 and CdSe-based QDs by various methods was reported in **Chapter 5**. In order to evaluate the optical properties on the single-particle level and to perform charging experiments on these hybrid nanocrystals, they were encapsulated into larger polymer particles. By the miniemulsion polymerization approach CdSe/$Cd_xZn_{1-x}S$ graded-shell QDs were successfully encapsulated in PMMA particles with a size around 60 nm (**Chapter 6.2.1**). Therefore, the same approach was investigated for the encapsulation of different hybrid particles. In experiments 1,2 and 7–9, hybrid particles obtained by a ligand exchange reaction between functionalized PF8 and QDs were encapsulated, whereas in experiments 3–6 hybrid particles obtained by a direct approach were encapsulated (**Table 6.2**). In experiments 1 and 2, hybrid particles consisting of CdSe/CdS QDs and PA-Ph-PF8-MA were encapsulated into cross-linked PMMA particles following the same protocol as for the embedding of the unfunctionalized graded-shell QDs (**Chapter 6.2.1**). The polymer was end-functionalized with a polymerizable end group which might facilitate encapsulation. The two hybrid particles differ in the amount of bound PF8 chains (~120 vs. ~100, cf. **Table 5.1**). In both experiments, uniform polymer particles (PDI ~0.1) with a hydrodynamic diameter of 60 nm and 66 nm, respectively, were obtained. The QY decreased from 49% for non-embedded QDs dispersed in toluene to only 30% for the QDs encapsulated in PMMA particles dispersed in water. This decrease was accompanied by an increase of the PF8 emission (factor ~1.5) compared to the QDs' emission (**Figure 6.2**) due to the embedding process. Moreover, the emission maximum of the nanocrystals was blue shifted by 1-2 nm during the embedding process due to a change in the permittivity of the surrounding medium.

Besides the optical properties, also the embedding statistic is important for the use as single-photon source. In **Figure 6.3**, TEM images of the dispersion are shown. Apparently, the functionalization of PF8 with a polymerizable end group did not significantly improve or deteriorate the embedding process. For both samples the embedding statistics are comparable: most particles are empty (~60%, 200 particles were analyzed for each sample) many particles contain exactly one QD (~25%) but also a significant number of particles contain several QDs (~15%). However, for many larger particles containing

several QDs, it is not clear if they were formed by fusion of several particles during the TEM analysis.

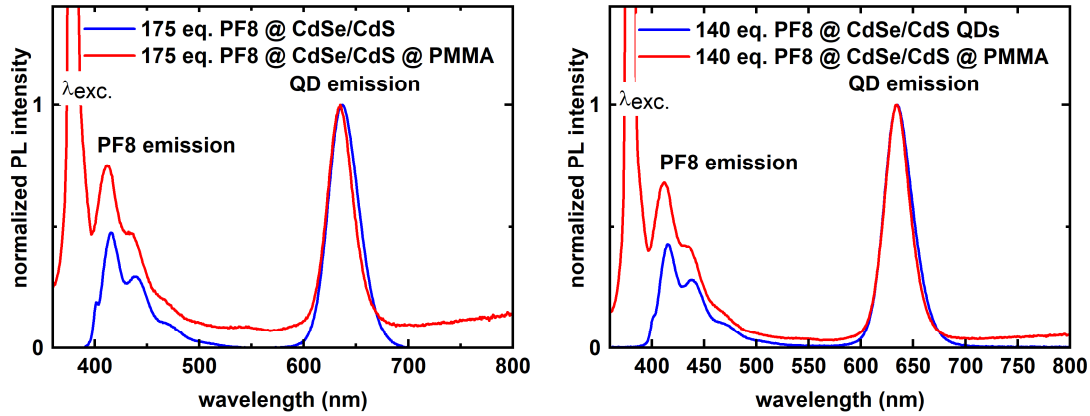

Figure 6.2. PL spectra ($\lambda_{exc.}$ = 380 nm) of PF8 CdSe/CdS hybrid QDs embedded in PMMA particles dispersed in water and the corresponding non-embedded hybrid particles dispersed in toluene. $\lambda_{exc.}$ = 380 nm is visible due to scattering on the relatively large polymer particles. The PL spectra are normalized at the maximal emission wavelength of the QDs.

These particles were investigated in single-particle PL studies (**Chapter 6.2.4**). However, they turned out be relatively 'dark' and optically unstable, thus unsuitable for the intended use as single-photon source. Therefore, in the experiments 3-6 selected hybrid particles consisting of high-quality graded-shell QDs and PF8-Ph-PA, which had been synthesized by a direct approach (**Chapter 5.2.2**), were encapsulated into cross-linked PMMA-based polymer particles.

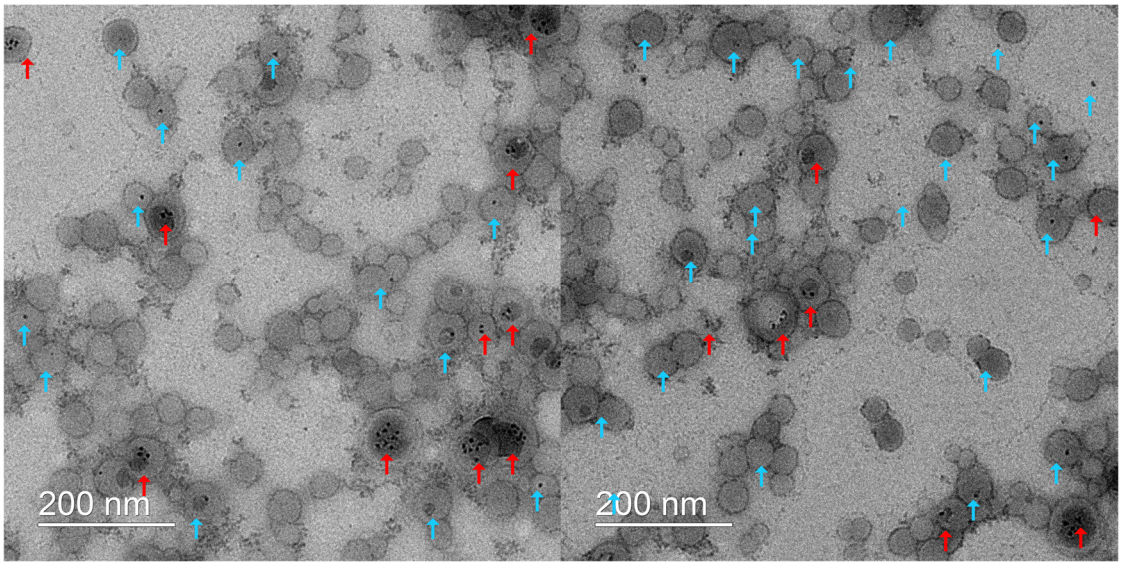

Figure 6.3. TEM images of CdSe/CdS PA-Ph-PF8-MA hybrid particles encapsulated in PMMA. Left: CdSe/CdS particles mixed with 175 equiv. of PA-Ph-PF8-MA and right QDs mixed with 140 equiv. PA-Ph-PF8-MA. Red arrows mark particles with several QDs per particles. Blue arrows mark particles with one QD per particle.

Table 6.2. Encapsulation of PF8 QD hybrid particles into polymer nanoparticles by a miniemulsion polymerization approach.

#	QD	monomer [mL]	d_z[a] [nm]	d_n[a] [nm]	PDI	QY_{QD}[b] [%]	$QY_{emb.}$[c] [%]
1	CdSe/CdS 175 equiv. MA-PF8-Ph-PA	MMA 1	98	66	0.11	49	30
2	CdSe/CdS 140 equiv. MA-PF8-Ph-PA	MMA 1	88	60	0.10	49	30
3	CdSe/$Cd_xZn_{1-x}S$ 75 equiv. PF8-Ph-PA	MMA 1	77	44	0.17	81	45
4	CdSe/$Cd_xZn_{1-x}S$ 75 equiv. PF8-Ph-PA	MMA/EHMA 0.7/0.3	86	50	0.10	81	50
5	CdSe/$Cd_xZn_{1-x}S$ 160 equiv.PF8-Ph-PA	MMA 1	76	47	0.12	84	30
6	CdSe/$Cd_xZn_{1-x}S$ 160 equiv. PF8-Ph-PA	MMA/EHMA 0.7/0.3	92	63	0.09	84	50
7[d]	CdSe/$Cd_xZn_{1-x}S$ 100 equiv. PA-PF8-*b*-PMMA	MMA/EHMA 0.35/0.15	77	54	0.09	87	55
8[d]	CdSe/$Cd_xZn_{1-x}S$ 100 equiv. PA-PF8-*b*-PEHMA	MMA/EHMA 0.25/0.25	105	81	0.05	90	60
9[d]	CdSe/$Cd_xZn_{1-x}S$ 100 equiv. PA-PF8-*b*-PS	styrene 0.5	89	74	0.01	86	40

Particles used in experiments 1,2 and 7–9 were synthesized by a ligand exchange (Chapter 5.2.1), hybrid QDs in experiments 3–6 were synthesized by a direct approach (Chapter 5.2.2). Encapsulation conditions: Aqueous phase: 80 mL of degassed H_2O and 100 mg of SDS; Oil phase: 100 µL of *n*-hexadecane, 1 mL of monomer, 10 µL of ethylene glycol dimethacrylate, 10 nmol (0.6 ml) of QDs in toluene, 10 mg of AIBN; 2 min ultrasonication with a sonotrode at 60% intensity; polymerization for 5 hours at 75 °C. a: Z-average, number average hydrodynamic diameter and PDI obtained by DLS. b: Ensemble QY of the non-embedded hybrid QDs dispersed in toluene. c: Ensemble QY of embedded hybrid QDs dispersed in H_2O d: Only 5 nmol of QDs and 50% of all other reagents used.

For the encapsulation, QDs which had been synthesized with the addition of 75 equiv. and 160 equiv. of PA-Ph-PF8 respectively, were chosen. In experiments 3 and 5, the QDs were encapsulated into cross-linked PMMA particles. The organic phase turned slightly turbid when the hybrid QDs were added to the mixture of monomer, hexadecane and cross-linker indicating a destabilization and partial agglomeration of the QDs. Therefore, in experiments 4 and 6 a mixture of 0.7 mL of MMA and 0.3 mL of EHMA was used as monomer as the colloidal stability of the hybrid QDs should be improved due to the more hydrophobic monomer EHMA. The mixture of MMA/EHMA, hydrophobe and cross-linker did not turn turbid upon QD addition which confirms the improved colloidal stability of the hybrid QDs in this monomer mixture. The polymer particles consisting of

PMMA-*co*-PEHMA were slightly larger than the homo-PMMA particles (44 nm and 47 nm vs. 50 nm and 63 nm). The QY of the QDs in the polymer dispersion was lower than the QY of the QDs dispersed in toluene. In experiment 3–4 (QDs with 75 equiv. of PF8), the QY of the QDs in the PMMA and PMMA-*co*-PEHMA dispersion is quite similar (45% vs. 50%). However, for experiments 5–6 (QDs with 160 equiv. of PF8) the QY of the PMMA-*co*-PEHMA dispersion is significantly higher (50% vs. 30%) which is probably caused by the better dispersibility of PF8 and QDs in the EHMA-copolymer than in the homo-PMMA.

In **Figure 6.4**, the PL spectra of the encapsulated hybrid QDs are compared to the PL spectra of the toluene dispersions of the non-embedded hybrid QDs. The PF8 emission (relative to the QD emission) in the polymer dispersion is weaker than the PF8 emission in the toluene dispersions which can have several reasons: In the toluene dispersions of the hybrid QDs not all PF8 is bound to the QDs and thereby not quenched by the QDs. After the miniemulsion polymerization, unbound PF8-Ph-PA is most likely located inside the nonconjugated polymer particles due to its low solubility in water. Embedded in the nonconjugated polymer particles, also the 'free' conjugated polymer is now more likely to be in close proximity to the QDs and a part might be quenched by the QDs. Also, not all polymer particles contain QDs, but probably contain PF8 chains which were not bound to QDs. The QY of PF8 dissolved in toluene is ~95% but the QY of PF8 embedded in particles or of stabilized PF8 particles dispersed in water is only in the range of 45%.[200,270]

The embedded hybrid QDs still possess a strong ET from excited PF8 to the QDs (**Figure 6.4**, right). The encapsulation of the hybrid QDs in PMMA-*co*-PEHMA impacted the morphology of the PF8 polymer. Encapsulated in PMMA, the PF8 is present in a glassy phase; however, embedded in PMMA-*co*-PEHMA the PF8 is partially present in the more ordered mesomorphic β-phase. This difference is indicated by a red shift of the PL spectra (maximum shifted from 417 nm to 438 nm) which is caused by an increased conjugation length of the polymer chains.[272] The portion of PF8 in the β-phase is relatively small which is reflected in only a small peak at 432 nm in the UV-VIS spectra of the dispersion which is attributed to the β-phase (**Figure 8.47**). PF8 present in the β-phase strongly contributes to the ET from the PF8 to the QD which is evidenced by the pronounced peak at 432 nm in the PLE spectrum. The formation of the β-phase is probably triggered by interactions between the long octyl side chains of PF8 and the 2-ethylhexyl side chains of incorporated EHMA.

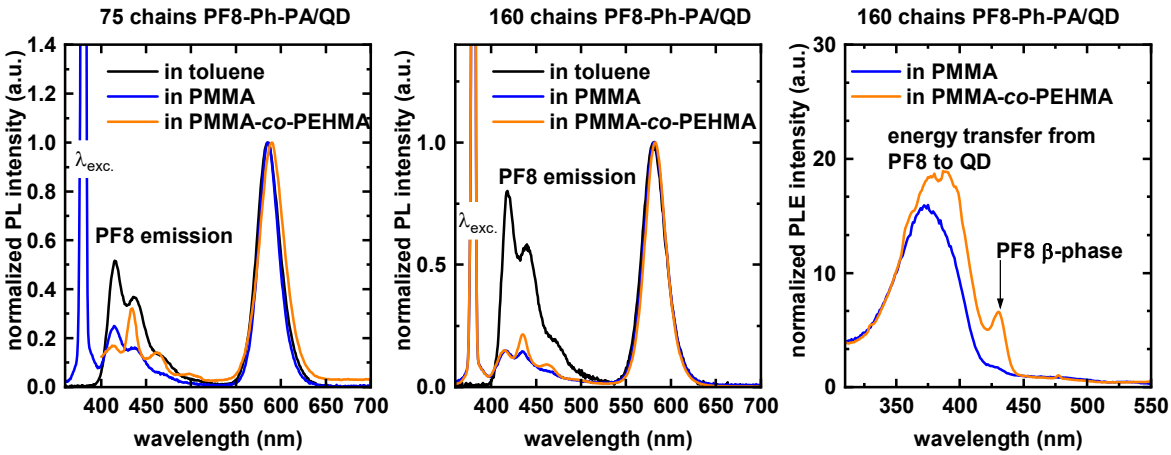

Figure 6.4. PL ($\lambda_{exc.}$ = 380 nm) and PLE ($\lambda_{det.}$ = 590 nm) spectra of PF8 CdSe/$(CdS)_2(ZnS)_2$ hybrid QDs dispersed in toluene (black line), encapsulated in PMMA particles (blue lines) and in PMMA-*co*-PEHMA particles (orange lines). The PL spectra are normalized at the maximal emission of the QDs. The PLE spectra are normalized at 300 nm.

TEM images of the dispersions obtained in experiment 5–6 are shown in **Figure 6.5**. In both experiments, most particles are empty (75% and 75%; 150 particles were analyzed in both experiments). However, within experimental error the number of particles with 2 or more QDs per particles is higher for the embedding in PMMA (10% vs. 5%). Thus, the number of particles containing a single QD is higher for the encapsulation in PMMA-*co*-PEHMA (20% vs. 15%) particles than for the encapsulation in pure PMMA.

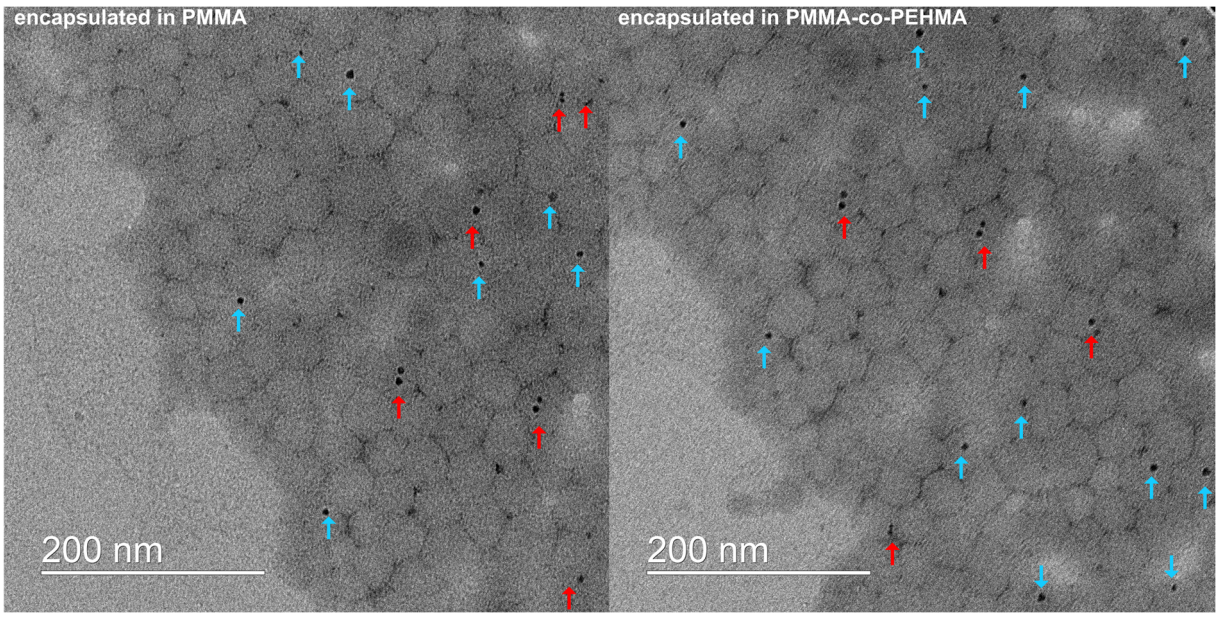

Figure 6.5. TEM images of the dispersions obtained in experiment 5 (left) and 6 (right). Polymer particles containing one QD are marked with blue arrows, particles containing several QDs are marked with red arrows.

The slightly more favorable encapsulation in the PMMA-*co*-PEHMA copolymer is probably caused by the better dispersibility of the hybrid QDs in the monomer mixture of MMA and EHMA than in pure MMA.

In experiments 7–9, the encapsulation of graded-shell QDs which had been functionalized with the conjugated nonconjugated block copolymers PA-PF8-*b*-PEHMA, PA-PF8-*b*-PMMA and PA-PF8-*b*-PS was investigated. The aim of the functionalization with these block copolymers was a potentially better incorporation in the respective polymer particles due to a favorable interaction between the nonconjugated block of the polymer and the monomer (mixture) and formed polymer. The QDs functionalized with the PA-PF8-*b*-PMMA and PA-PF8-*b*-PEHMA block copolymer, respectively, were encapsulated in a mixture of MMA and EHMA (70/30 vol% and 50/50 vol%, respectively). The QYs of the resulting polymer dispersions of 55–60% were, as expected, lower than the QY of the non-embedded QDs dispersed in toluene (86-90%).

In experiment 7, the use of PA-PF8-*b*-PMMA-functionalized QDs led to an agglomeration of the QDs during the embedding process (**Figure 6.6**). The PA-PF8-*b*-PEHMA-functionalized particles were embedded in a 1 : 1 mixture of MMA and EHMA (entry 8). The resulting polymer interacted strongly with the electron beam during TEM measurements resulting in melting and fusion of the particles, which hampers conclusion on the encapsulation statistics. However, the TEM images show many spots with clusters of nanoparticles and it seems that many particles formally contained several QDs. In experiment 9, PA-PF8-*b*-PS-functionalized QDs were encapsulated in styrene. The QY of the QDs decreased significantly from 86% for the non-embedded QDs to only 38% due to the miniemulsion polymerization. One reason for this significant decrease in QY might be that many QDs are located at the interface to the aqueous phase which has been shown to be potentially detrimental for the optical properties.[31,149] Very uniform particles (PDI 0.01) with a hydrodynamic diameter around 75 nm were formed. However, most particles are empty (78%, 175 particles were analyzed in total), many particles contain several QDs (15%) and fewer particles contain exactly one QD (7%). This distribution indicates a partial agglomeration of QDs during the formation of the miniemulsion which deems this dispersion less suited for single-particle PL measurements compared to the dispersions obtained in experiments 3-6.

None of the particle dispersions containing the conjugated nonconjugated block copolymers is particularly suitable for single-particle spectroscopy studies, as they do not contain a high proportion of particles with exactly one QD per particle compared to

particles with several QDs. The functionalization with the block copolymers led to an increased agglomeration of the QDs during the miniemulsion procedure, which is presumably caused by favorable interactions between the rather long polymer chains. However, the encapsulation of graded-shell CdSe/$(CdS)_2(ZnS)_2$ QDs functionalized with PA-Ph-PF8 was successful in terms of optical properties (high QY, ET from PF8 to QD) and embedding statistics. Therefore, these particles were considered more suitable for single-particle PL and charging studies and preferentially further analyzed (**Chapter 6.2.5**).

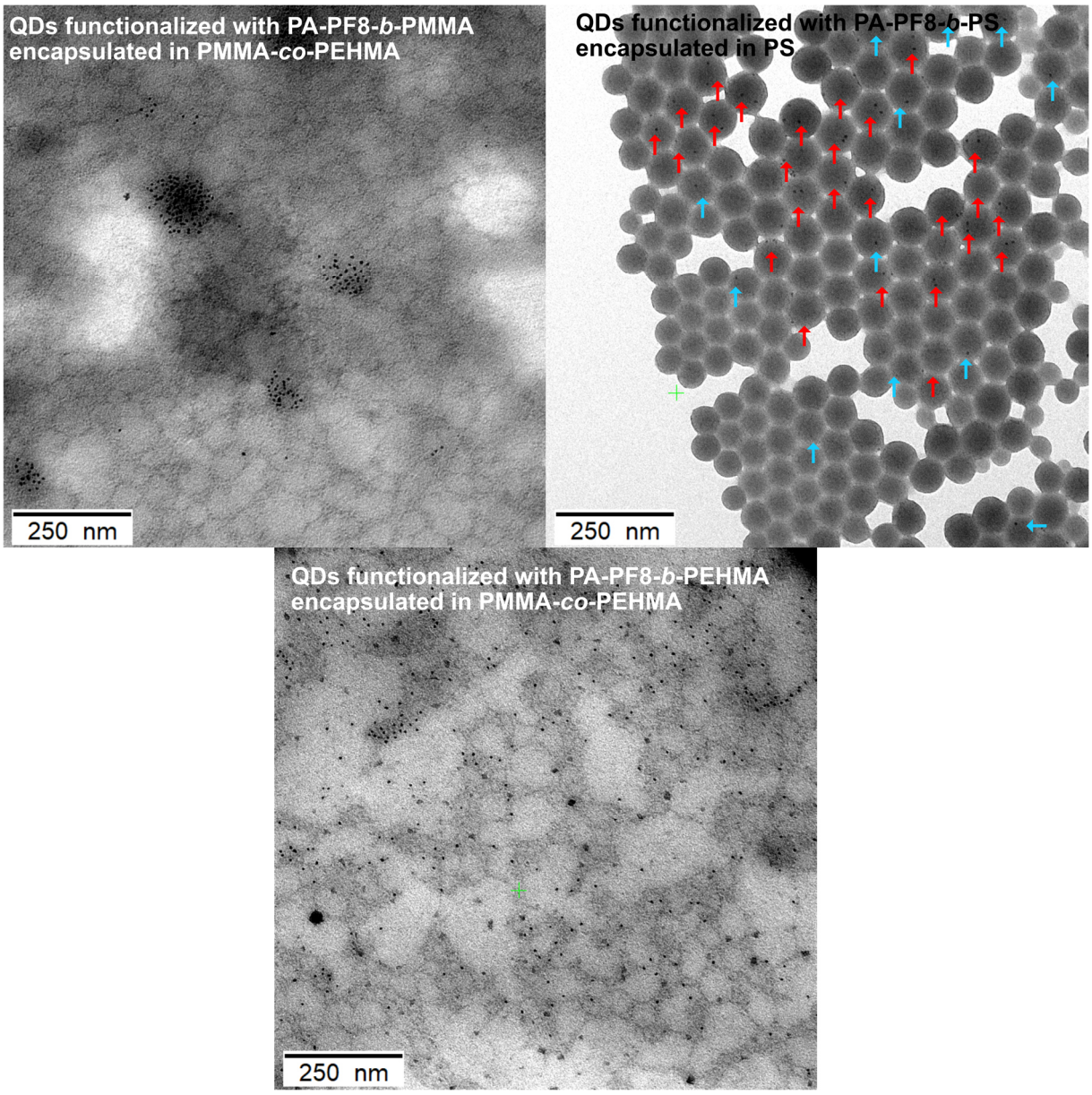

Figure 6.6. TEM images of dried dispersions obtained in the encapsulation experiments (entries 7–9) employing conjugated nonconjugated block copolymer-functionalized QDs. The blue arrows mark particles with one QD, the red arrows mark particles with several QDs.

6.2.3 Encapsulation of CdSe/CdS Nanorods and CdSe/CdS/CdS Polyfluorene Hybrid Nanorods by a Miniemulsion Polymerization Approach

As pointed out previously, CdSe/CdS NRs and PF8-functionalized hybrid NRs are an interesting material for single-particle PL measurements and especially charging experiments. For this purpose, they were encapsulated into polymer nanoparticles. Compared to the embedding of spherical hybrid particles, the encapsulation of NRs was more difficult due to the strong attractive forces between individual NRs, their tendency to align into superstructures and their larger size. The nonconjugated polymer shell has to fulfill certain prerequisites: it has to be of adequate size in the range of roughly 60–150 nm. It must not be too sticky which would prevent the placement of the particles into resonator structures via an AFM tip. This fact requires the use of polymers with a sufficiently high T_g. Moreover, the polymer has to be transparent for light in the range of 300–700 nm. Therefore, the dispersibility of CdSe/CdS NRs in various monomers was investigated (**Table 6.3**).

Table 6.3. Dispersibility of CdSe/CdS NRs in various monomers.

monomer	appearance	after centrifugation[a]
Sty	clear	no precipitation
DOMA	clear	no precipitation
MMA	precipitation	complete precipitation
MMA/EHMA 70/30	turbid	partial precipitation
MeMBL	turbid	partial precipitation
MeMBL/DOMA 50/50	slightly turbid	partial precipitation
MeMBL/DOMA 20/80	clear	no precipitation

Sty: styrene (T_g(PS) 100 °C); DOMA: dodecyl methacrylate (T_g(PDOMA) -56 °C); MMA: methyl methacrylate (T_g(PMMA) 105 °C); EHMA: 2-ethylhexyl methacrylate (T_g(PEHMA) -10 °C); MeMBL: α-methylene-γ-valerolactone (T_g(PMeMBL) 220 °C). In all experiments 5 nmol of NRs and 1 mL of monomer were used. a: Centrifugation at 4000 g for 2 min.

CdSe/CdS NRs are dispersible in styrene (Sty) but precipitate in pure MMA. α-Methylene-γ-valerolactone (MeMBL) shows a similar reactivity to MMA, is less hydrophilic than MMA and the resulting polymer PMeMBL has a very high T_g of 220 °C.[273,274] The mixing of CdSe/CdS NRs with MeMBL did not cause an instantaneous precipitation of the NRs, but a slight turbidity was noted. CdSe/CdS NRs are dispersible in dodecyl methacrylate

(DOMA). However, homo-PDOMA has a T_g of -56 °C and is very sticky at room temperature. The NRs are well dispersible in a mixture of 80/20 DOMA/MeMBL and only a slight turbidity is observed in a 50/50 mixture.

Therefore, the embedding in these mixtures of MeMBL and DOMA was investigated. **Table 6.4** summarizes the encapsulation conditions and results for the embedding of CdSe/CdS NRs in various monomers and monomer mixtures.

Table 6.4. Encapsulation of semiconductor CdSe/CdS or CdSe/CdS/CdS NRs into polymer nanoparticles by a miniemulsion polymerization approach.

#	n (NR) [nmol]	monomer	L (NR) [nm]	d_n[b] [nm]	PDI[b]	QY[c] [%]	1 NR/ particle[d] [%]	≥2 NRs/ particle[d] [%]
1	7	MMA	30	63	0.17	34(50)	a.g.	a.g.
2	7	MMA/EHMA 70/30	30	65	0.13	48(50)	a.g.	a.g.
3	0	Sty	-	74	0.02	-	-	-
4	7	Sty	30	70	0.03	20(32)	15	15
5	7	Sty	20	88	0.2	36(52)	20	35
6	0	Sty/DOMA 85/15	-	120	0.13	-	-	-
7	7	Sty/DOMA 85/15	30	126	0.16	35(40)	n.p.	n.p.
8	0	DOMA/MeMBL 80/20	-	95	0.06	-	-	-
9	0	DOMA/MeMBL 50/50	-	90	0.09	-	-	-
10	7	DOMA/MeMBL 80/20	30	84	0.05	25(32)	n.p.	n.p.
11	7	DOMA/MeMBL 50/50	30	91	0.04	30(32)	30	5
12	7	DOMA/MeMBL 50/50	20	84	0.07	35(52)	30	5
13[a]	5	DOMA/MeMBL 50/50	20	110	0.07	53(78)	20	5
14[a]	5	DOMA/MeMBL 50/50	30	82	0.1	40(70)	25	5

General conditions: Oil phase: 1 mL of monomer, 10 µL of 1,4-divinylbenzene, 100 µL of *n*-hexadecane, 10 mg of AIBN, 0.3 mL of NRs in toluene, aqueous phase: 80 mL of H_2O, 100 mg of SDS; 3 min ultrasonication (sonotrode at 60% intensity); polymerization at 75 °C for 5 h. a: CdSe/CdS/CdS NRs used. b: Determined by DLS. c: First value is the QY of the NRs embedded in polymer particles dispersed in water, value in brackets is the QY of non-embedded NRs dispersed in toluene. d: Determined by analyzing at least 150 particles in TEM images. a.g. = agglomerated; n.p. = not possible.

In experiments 1–2, the encapsulation of CdSe/CdS NRs in PMMA and PMMA-*co*-PEHMA was investigated. The same conditions as for the encapsulation of graded-shell hybrid QDs were used (**Table 6.2**). However, in both experiments a pronounced clustering of several NRs in a single polymer particle was observed (**Figure 8.48**). This finding might be explained by the limited colloidal stability of the NRs in MMA.

The NRs are well dispersible in styrene, thus the encapsulation in polystyrene and styrene copolymers was analyzed (entries 3–7). The same miniemulsion polymerization conditions as used for the polymerization of MMA can be used for the polymerization of styrene (entry 3) yielding uniform particles with a diameter of 74 nm. Using these conditions, the encapsulation of NRs with a length of 20 nm and 30 nm, respectively, was investigated (entries 4–5). Embedding 30 nm long NRs did not change the size of the obtained nanoparticles significantly (70 nm vs. 74 nm). As expected, the QY of the NRs decreased during the embedding process (32% vs. 20%). Most particles (70%) are not filled with NRs. However, the number of particles containing one NR (15%) is equal to the number of particles containing 2 or more NRs (**Figure 6.7**). The embedding statistic was less favorable for the encapsulation of short (L = 20 nm) NRs yielding more particles containing several NRs (35%) than particles containing exactly one NR (20%).

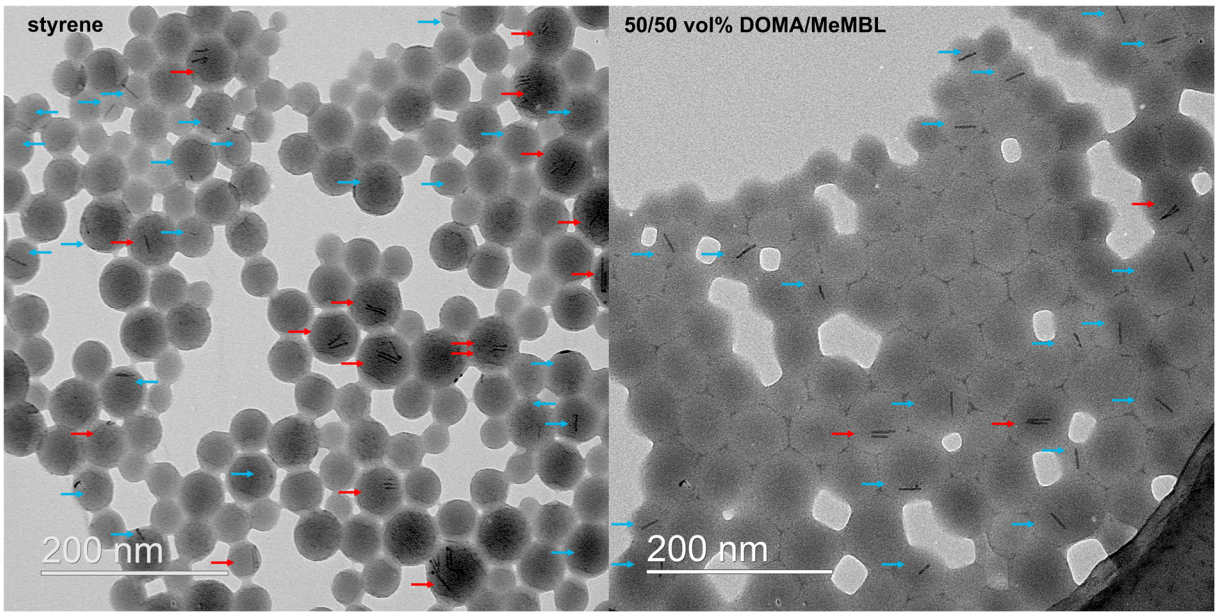

Figure 6.7. TEM images of the encapsulation of CdSe/CdS NRs in PS nanoparticles (left, entry 4) and in PDOMA-*co*-PMeMBL nanoparticles (right, entry 11). Particles containing one NR are marked with blue arrows, particles containing several NRs are marked with red arrows.

As the encapsulation of NRs in PS particles delivered dispersions which are not particularly suitable for single-particle measurements as they contain an unfavorable high proportion of particles enclosing several NRs, the encapsulation into further

monomer mixtures was studied. The NRs are well dispersible in DOMA; however, PDOMA is very sticky and has a low T_g of -56 °C. Therefore, a mixture of Sty and DOMA of 85/15 vol% was used. Miniemulsion polymerization of this mixture yielded larger particles (120 nm) as compared to the polymerization of styrene (74 nm). Only a slight decrease in QY from 40% for non-embedded NRs to 35% for embedded NRs occurred. However, it was not possible to determine the encapsulation statistics. No individual particles but a polymer film was observed in TEM images. This film formation could be caused by interaction of the polymer with the electron beam or the dispersion could show a low minimum film-forming temperature. This finding is an indication for the formation of soft and sticky particles which would also render them unsuited for mechanical manipulations with the AFM. Therefore, the combination of DOMA with the monomer MeMBL was studied for the encapsulation of NRs as PMeMBL has a very high T_g of 220 °C. First, mixtures of DOMA and MeMBL (80/20 vol% and 50/50 vol%) were polymerized without addition of NRs (entries 8–9). These mixtures could be copolymerized under the previously established miniemulsion polymerization conditions, and uniform particles with sizes around 90 nm were formed. Using the 80/20 mixture for the encapsulation of NRs (entry 10), again particles were formed which tend to melt and fuse under the TEM beam or even during the drying process. However, using a 50/50 vol% mixture of the two monomers for the encapsulation of CdSe/CdS NRs, uniform polymer nanoparticles were formed, and individual particles can be clearly identified in the TEM images of the dried dispersion (**Figure 6.7**). Additionally, the QY decreased only marginally from 32% to 30% during the embedding process. As 30% of the particles contain exactly one NR and only 5% contain 2 or more NRs, also the embedding statistic is favorable for single-particle PL measurements. Additionally, short CdSe/CdS NRs (L = 20 nm) could be successfully encapsulated (same favorable embedding distribution as experiment 11) using this monomer mixture (entry 12). This approach was also used for the encapsulation of the CdSe/CdS/CdS NRs of higher optical quality (entries 13–14). Although these NRs feature a slightly different ligand shell compared to the standard CdSe/CdS NRs, the encapsulation was successful and dispersions with high QYs of 53% and 40%, respectively, were obtained. Additionally, the ratio between empty particles (65–70%), particles with exactly one NR (20–25%) and particles containing several NRs (5%) is favorable. The combination of a monomer in which the NRs are well dispersible with a monomer whose corresponding polymer has a very high T_g seems to be ideally suited for

the encapsulation of semiconductor NRs. However, it was not yet clear if this copolymer also performs well in terms of optical and mechanical stability and isolation properties in single-particle PL measurements.

Therefore, a second encapsulation approach into styrene nanoparticles was also pursued. Leiza and co-workers reported the encapsulation of CdSe/ZnS QDs into large (D = 100–200 nm) PS and PS/PMMA nanoparticles, thereby minimizing the fluorescence loss over time.[31] Employing their approach for the synthesis of PS particles, significantly larger polymer particles with a diameter of 130 nm compared to the previously synthesized PMMA or PS particles with a diameter of 65–90 nm, were formed (entry 1, **Table 6.5**). This increase in size was expected as the ratio of monomer to surfactant was drastically increased (here: 26 mg of SDS per mL of monomer; previously 100 mg/mL). Using this approach, the encapsulation of short (L = 20 nm) and long (L = 30 nm) CdSe/CdS as well as CdSe/CdS/CdS NRs was successful (**Table 6.5** and **Figure 8.49** for exemplary TEM images) as dispersions with high QYs and favorable encapsulation statistics (20–25% of single NR particles and only around 5% of particles containing several NRs) were obtained.

Table 6.5. Encapsulation of semiconductor CdSe/CdS and CdSe/CdS/CdS NRs into larger polystyrene nanoparticles by a miniemulsion polymerization approach.

#	n (NR) [nmol]	monomer	L (NR) [nm]	d_n[b] [nm]	PDI[b]	QY[c] [%]	1 NR/ particle[c] [%]	≥2 NRs/ particle[d] [%]
1	0	Sty	-	133	0.01	-	-	-
2	7	Sty	30	128	0.01	30(32)	25	5
3	7	Sty	20	110	0.18	38(55)	20	5
4[a]	5	Sty	30	104	0.02	46(70)	20	5
5[a]	5	Sty	20	103	0.02	64(78)	20	5

General conditions: Oil phase: 2.3 mL of Sty, 84 µL of *n*-hexadecane, 21 µL of *p*-divinylbenzene, 0.6 mL of NRs in toluene; aqueous phase: 25 mL of H_2O, 42 mg of SDS, 21 mg of $NaHCO_3$, sonication with a sonotrode at 80% intensity for 4 min, addition of 10 mL of H_2O and 21 mg of SDS after sonication; addition of 4 mL of H_2O and 11 mg of potassium peroxydisulfate at 75 °; polymerization at 75 °C for 6 h. a: CdSe/CdS/CdS NRs encapsulated. b: Determined by DLS. c: The first value is the QY of the NRs embedded in polymer particles dispersed in water, the value in brackets is the QY of the non-embedded NRs dispersed in toluene. d: Determined by analyzing at least 150 particles in TEM images.

The final dispersions have a solid content in the range of 4.5–5.3 wt% which fits well to the theoretical value of 5.2 wt% and indicates a high monomer conversion (>86%) during the polymerization. Many NRs are located at the periphery of the particles which might

lead to a deterioration of the optical properties over time as the NRs might come into contact with the aqueous phase or even migrate into the aqueous phase. Therefore, the particles were overcoated with a second shell of cross-linked PMMA as Leiza and co-workers showed that this can preserve the optical properties of the nanocrystals.[31] A theoretically 15 nm thick shell of cross-linked PMMA was deposited onto the PS seed particles (see **Chapter 6.4.3** for experimental details). The optical properties did not change due to the additional shell, no secondary nucleation was observed, and the size increase fits well to the theoretical value (**Figure 8.50**).

As two different approaches were successfully developed for the encapsulation of semiconductor NRs, also PF8 CdSe/CdS/CdS hybrid NRs were encapsulated into PS and PDOMA-*co*-PMeMBL nanoparticles (**Table 6.6**). Short (L = 18 nm) and long (L = 27 nm) CdSe/CdS/CdS hybrid NRs which had been functionalized with 200 equiv. of PF8-PA in a direct approach (**Chapter 5.2.3**) were successfully encapsulated. Therein, the QY decreased only slightly from 76–77% to 45–55%. The obtained dispersions possess embedding distributions (see **Figure 6.8** for exemplary TEM images) which are favorable for single-particle PL measurements as many particles (15–30%) contain exactly one hybrid NR while only a few particles contain 2 or more particles (2–5%).

Table 6.6. Encapsulation of PF8-functionalized CdSe/CdS/CdS hybrid NRs into polymer nanoparticles.

#	PF8-PA/NR	monomer	L (NR) [nm]	d_n[c] [nm]	PDI[c]	QY[d] [%]	1 NR/ particle[e] [%]	≥2 NRs/ particle[e] [%]
1[a]	200	DOMA/MeMBL 50/50	18	120	0.05	45(76)	25	5
2[b]	200	Sty	18	109	0.01	50(76)	20	5
3[a]	200	DOMA/MeMBL 50/50	27	109	0.07	55(77)	30	5
4[b]	200	Sty	27	105	0.2	50(77)	15	2

a: Encapsulated according to conditions in **Table 6.4**. b: Encapsulated according to conditions in **Table 6.5**. Half of the PS particles were coated with an additional layer of cross-linked PMMA. c: Determined by DLS measurements. d: The first value is the QY of NRs embedded in polymer particles dispersed in water, the value in brackets is the QY of the non-embedded NRs dispersed in toluene. e: Determined by analyzing at least 150 particles in TEM images.

The PS particles were furthermore coated with an additional shell of cross-linked PMMA (theoretical thickness 15 nm) which did not change the optical properties in terms of QY

but a size increase fitting to the theoretical value was observed (**Figure 8.51**). The optical properties of the NRs encapsulated in PS/PMMA or in PDOMA-*co*-PMeMBL are comparable in terms of QY.

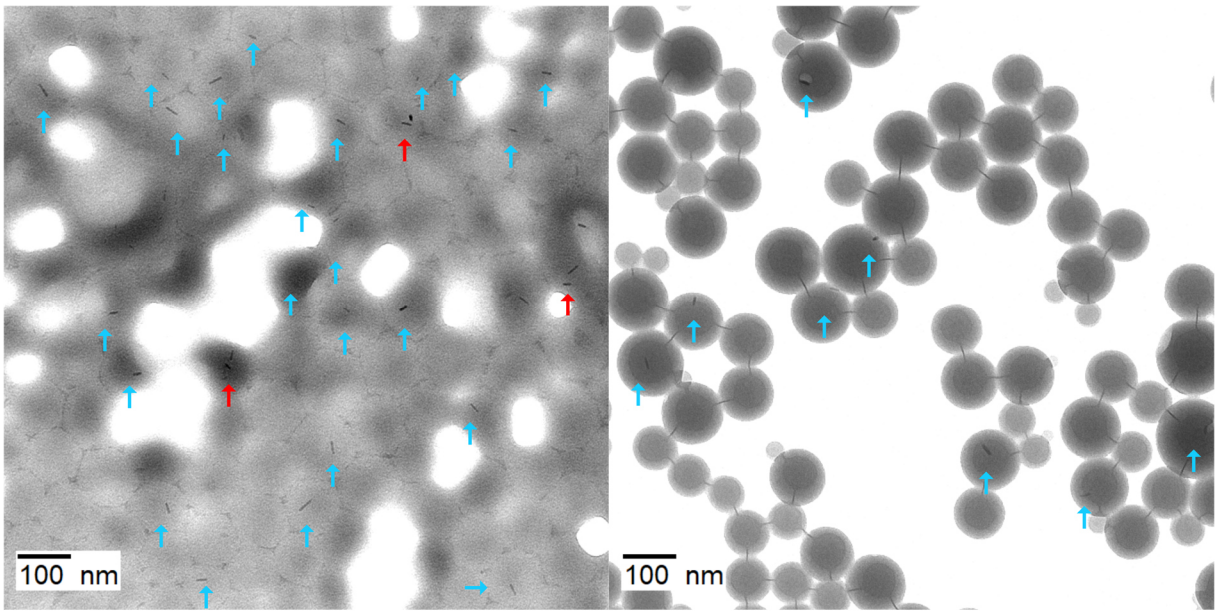

Figure 6.8. TEM images of the dried dispersions obtained in experiments 3 (left) and 4 (right), **Table 6.6**. Particles containing one NR are marked with blue arrows and particles containing several NRs are marked with red arrows.

In **Figure 6.9**, the PL and PLE spectra of the dispersions obtained in experiments 1–2 (**Table 6.6**) are compared to the spectra of the same non-embedded hybrid NRs dispersed in toluene. In the PL spectra, no significant change in the PF8 emission intensity (relative to the NRs emission intensity) is evident due to the embedding process. In contrast, during the embedding of PF8 CdSe/$Cd_xZn_{1-x}S$ hybrid QDs (entries 3–6, **Table 6.2**), the PF8 emission intensity (relative to the QDs' PL intensity) decreased significantly (**Figure 6.4**). This divergence is most likely caused by the difference in the percentage of PF8 bound to the nanocrystals before the embedding, as only bound PF8 is quenched by the semiconductor nanocrystals. In case of the QDs, only 35–65% of the PF8 was bound whereas basically all PF8 (>95%) was bound to the NRs before the miniemulsion process. After the encapsulation, the PL of the PF8 is still nearly completely quenched by the NRs indicating that the PF8 is still completely bound to the NRs. Additionally, the PLE spectra of the hybrid NRs dispersed in toluene and encapsulated in PS/PMMA particles dispersed in water are basically identical and a strong ET from excited PF8 to the NRs occurs indicating the strong interaction between the two materials. The encapsulation in the PDOMA-*co*-PMeMBL copolymer partially changed the conformation of the PF8 from the glassy phase to the β-phase which is evidenced by a strong red shift of the PL and PLE

spectra. Moreover, the PLE spectra features a pronounced peak at 432 nm which is typical for PF8 in the β-phase.

These aqueous dispersions consisting of PF8-functionalized CdSe/CdS/CdS hybrid NRs (PF8 completely bound to the NRs before the miniemulsion process) encapsulated in PS/PMMA or PDOMA-*co*-PMeMBL polymer nanoparticles show a favorable embedding distribution and a strong ET from the PF8 to the nanocrystals and are therefore interesting for further single-particle PL experiments.

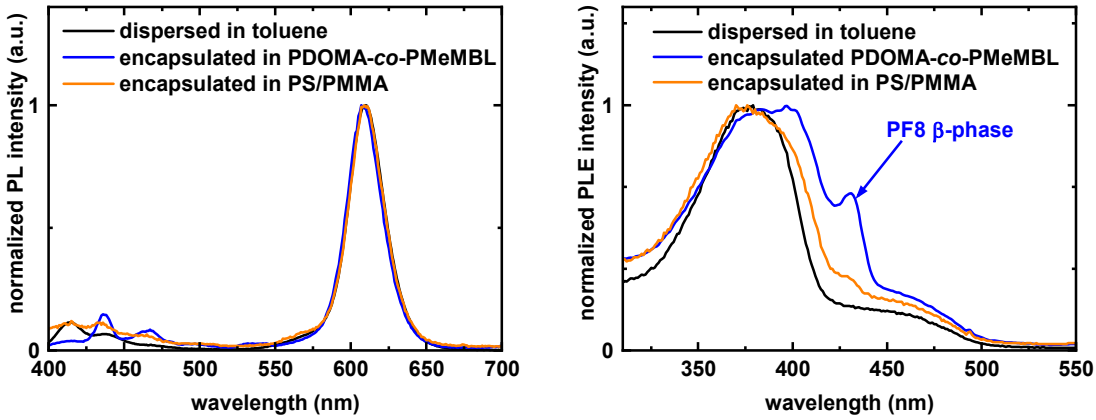

Figure 6.9. PL ($\lambda_{exc.}$ = 380 nm, left) and PLE ($\lambda_{det.}$ = 605 nm, right,) spectra of PF8-PA CdSe/CdS/CdS hybrid NRs dispersed in toluene (black line) and the same hybrid NRs encapsulated in PS/PMMA core-shell polymer nanoparticles (orange line, experiment 2, **Table 6.6**) and encapsulated in a PDOMA-*co*-PMeMBL copolymer nanoparticles (blue line, experiment 2, **Table 6.6**) both dispersed in water.

6.2.4 Single-Particle Micro-Photoluminescence Measurements on Encapsulated Semiconductor Nanoparticles

The single particle PL experiments were performed by Pascal Gumbsheimer and Frieder Conradt in the experimental physics group of Prof. Dr. Alfred Leitenstorfer at University of Konstanz. The presence of single QD emitters can be confirmed by a second-order photon correlation as a function of time delay measurements ($g^{(2)}$) recorded with a Hanbury-Brown and Twiss setup.[275]

In this chapter, encapsulated CdSe/$Cd_xZn_{1-x}S$ QDs and CdSe/CdS/CdS NRs, which had not been functionalized with PF8, were analyzed by single particle micro-photoluminescence experiments at cryogenic temperatures of T = 4–6 K.

The graded-shell CdSe/$Cd_xZn_{1-x}S$ QDs turned out to be exceptionally well suited for single-particle measurements. Already CdSe particles covered with a shell consisting of 2 ML of CdS and 2 ML of ZnS were bright and stable. As the fluorescent active core of these

QDs also consists of CdSe, the CdSe/$(CdS)_2(ZnS)_2$ QDs show the typical PL fine structure of a neutral, non-perfectly spherical wurtzite-type CdSe QD (**Figure 6.10**) consisting of three emission lines (F, A1, A2).[26,276] They are caused by the transition from the exciton ground states (X^0-GS) to QD-GS. The energetically lowest X^0-GS to QD-GS transition (F) is nominally dipole-forbidden which explains why its intensity is only slightly higher compared to the dipole-allowed transition A1 at higher energy.[26]

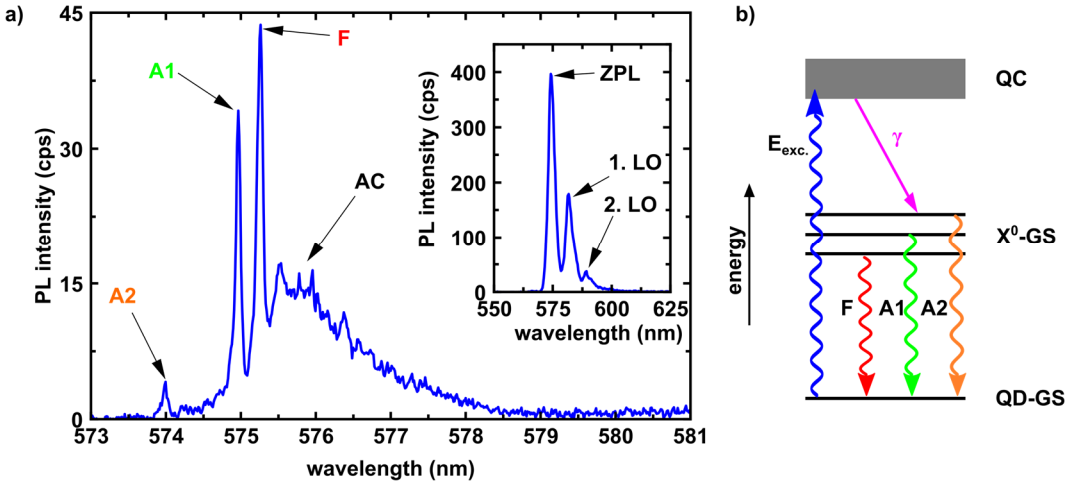

Figure 6.10. a: Highly resolved PL spectrum at cryogenic temperature (T = 6 K; $\lambda_{exc.}$ = 532 nm, $P_{exc.}$ = 240 nW) of a single CdSe/$(CdS)_2(ZnS)_2$ QD embedded in a PMMA-*co*-PEHMA particle. Inset: Lower resolution PL spectrum showing the zero-phonon line (ZPL) and the first and second longitudinal-optical (LO) phonon replica. b: Energy scheme: Excitation of the QD to the quasi-continuum (QC) is followed by rapid non-radiative relaxation γ to the exciton ground states (X^0-GS) and a radiative recombination to the QD ground state (QD-GS) resulting in three fine structure lines (A1, A2 and F) which are well resolved in the PL spectrum. In the PL spectrum, also the acoustic phonon (AC) replica are visible. The measurement data were provided by Frieder Conradt (Leitenstorfer group, University of Konstanz).

Moreover, the acoustic (AC) phonon replica are well visible and the first and second longitudinal-optical (LO) phonon replica are well resolved demonstrating the quality and stability of these embedded QDs. The QDs are brighter than the currently employed CdSe/CdS QDs which will be beneficial to reduce the measurement time in future quantum-optical studies. Thus, the better ensemble optical properties of the graded-shell CdSe/$Cd_xZn_{1-x}S$ QDs as compared to CdSe/CdS QDs are also reflected in single-particle measurements. Importantly, these CdSe/$(CdS)_2(ZnS)_2$ QDs (roughly 25 analyzed so far), which were not functionalized with PF8, did not exhibit any characteristics typical for a charged QD.[a] Even additional excitation with an UV LED ($\lambda_{exc.}$ = 370 nm, a wavelength of

[a] In the past, only two QDs (not functionalized with PF8) out of roughly 300 analyzed CdSe/CdS QDs showed PL properties typical for a charged QD in single particle PL studies.

strong PF8 absorption) did not change the PL properties of the QDs and they still showed the typical PL fine structure of a neutral CdSe/CdS QD. Therefore, these QDs are an excellent reference material to study the influence of functionalization with polyfluorene (**Chapter 6.2.5**).

As pointed out previously, CdSe/CdS NRs are also an auspicious material for single-particle PL measurements. Therefore, CdSe/CdS/CdS dot-in-rod NRs, which had been encapsulated in polymer particles (cf. **Chapter 6.2.3**), were analyzed in PL measurements at cryogenic temperatures. **Figure 6.11** (a) shows an exemplary highly resolved PL spectrum of an encapsulated (entry 5, **Table 6.5**) single NR (L ~ 20 nm, W ~5 nm). The single CdSe/CdS/CdS NRs were highly emissive and optically stable during the PL measurements. Moreover, a PL fine structure consisting of three distinct emission lines was revealed for the zero-phonon line and the related first LO phonon replica. For the syntheses of CdSe/CdS/CdS NRs and CdSe/$Cd_xZn_{1-x}S$ graded-shell QDs, the same type of non-perfectly spherical wurtzite-type CdSe seed QDs were used. As the fluorescence in both multi-shell nanocrystals occurs in the CdSe core, a similar PL fine structure for both types of nanocrystals was expected. Noteworthy, the observation of PL fine structure consisting of multiple emission lines indicates emission from an uncharged CdSe-based emitter. Fluctuations of the PL intensity occurred over time; however, a multi-line PL fine structure was observed continuously (**Figure 6.11** b). Therefore, these NRs are also suitable as reference material to study the influence of PF8 functionalization.

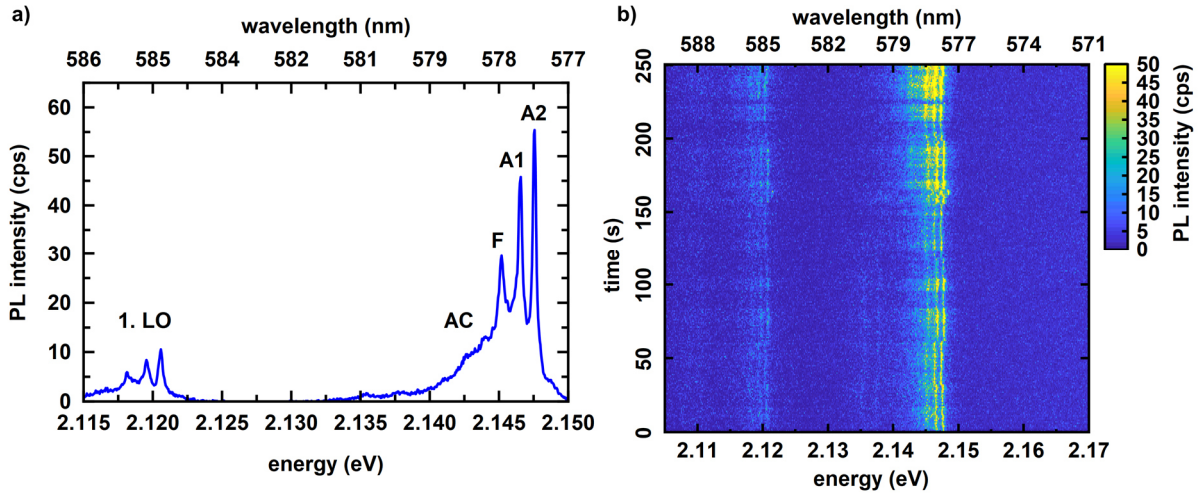

Figure 6.11. Exemplary highly resolved PL spectrum (a) and PL time trace (b) of an encapsulated CdSe/CdS/CdS NR (T = 4.3 K, $\lambda_{exc.}$ = 540 nm, $P_{exc.}$ = 150 nW). The measurement data were provided by Frieder Conradt (Leitenstorfer group, University of Konstanz).

6.2.5 Controlled Charging of Encapsulated Hybrid Semiconductor Nanocrystals in Single-Particle Micro-Photoluminescence Experiments

One major aim of this research was the generation of charged CdSe-based emitters, by charge transfer processes between tethered conjugated polymer chains and the inorganic emitter. A CdSe emitter in the trion (T) state should show a single dipole-allowed T-GS to QD-GS transition, a significantly shortened PL lifetime and a higher PL intensity compared to the neutral emitter.[258,277,278] These features render charged CdSe-based nanocrystals attractive for ultrafast quantum-optical studies and as potential single-photon source in ultrafast amplifiers or quantum computers. The formation of trion states has been randomly reported for individual CdSe/CdS or CdSe/ZnS QDs at cryogenic temperatures where a spurious photo charging of the QDs supposedly took place.[260,276,278] Moreover, charged colloidal QDs and trion states were observed for QDs which had been charged by applying a voltage to a thin film of QDs.[258] However, the controlled formation of charged CdSe-based nanocrystals on the single-particle level by the interaction with a conjugated polymer ligand is an unexplored field.

CdSe/$Cd_xZn_{1-x}S$ graded-shell QDs which had been functionalized with phenylphosphonic acid end-functionalized PF8 in a direct approach (**chapter 5.2.2**) and encapsulated in cross-linked PMMA-*co*-PEHMA particles (**chapter 6.2.2**) were employed in these studies. In **Figure 6.12** (a), the PL time trace of an individual hybrid QD is shown. The emitter was excited at λ = 532 nm outside the absorption range of the PF8 polymer (t_1). After 15 s, the emitter was additionally illuminated with a UV LED (λ = 370 nm) in the absorption range of PF8 (t_2). After 5 s of illumination with UV light (t_3), the PL maximum of the QD shifted by 18.8 meV to lower energies and the integrated emission intensity increased significantly (~3). The PL emission continued at this wavelength after the additional illumination with UV light had been stopped (t_4). A similar red shift (20 meV) of the PL maxima and an increase in the PL intensity was also occasionally observed for hybrid QDs — not for the corresponding unfunctionalized nanocrystals — which were not additionally illuminated by UV light (**Figure 6.12 b**), but still by the laser. The significant red shift of the emission maxima and the increased PL intensity are indications for a charging of the QDs and the formation of CdSe trions. The formation of these trion states should be additionally manifested in a change of the PL fine structure and fluorescence lifetime of the QDs.

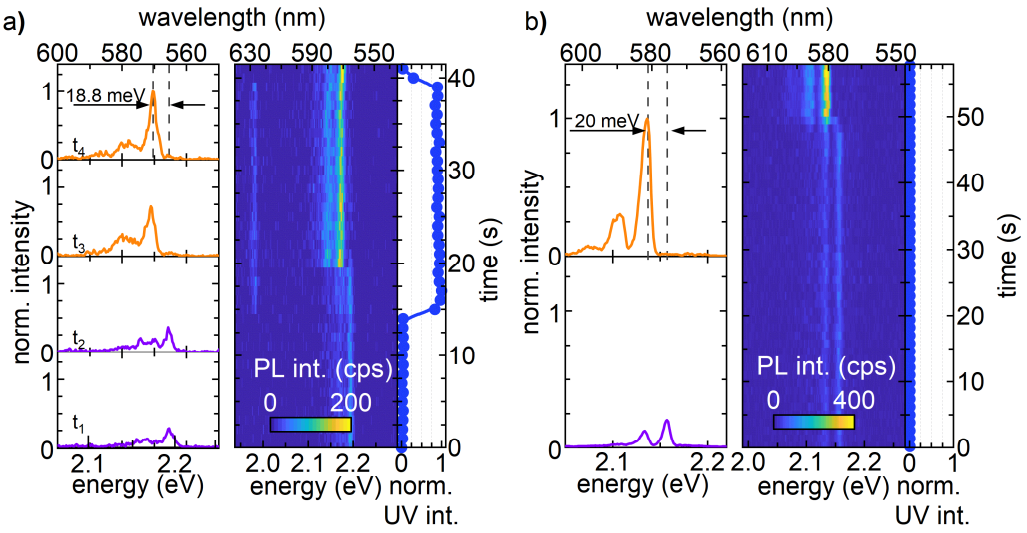

Figure 6.12. a) PL intensity of a single PF8 CdSe/$Cd_xZn_{1-x}S$ hybrid QD (T = 4.2 K, $\lambda_{exc.}$ = 532 nm, $P_{exc.}$ = 240 nW) as function of time and energy (center). On the left, single PL spectra (integration time 1 s) at certain time steps of the measurement are shown. The spectra display the fundamental and 1. LO phonon replica emission lines. From 15 to 40 s measurement time, the sample is additionally illuminated with UV light ($\lambda_{exc.}$ = 370 nm, right). b) Same measurement on another hybrid QD without additional UV light illumination. The figure was provided by Frieder Conradt (Leitenstorfer group, University of Konstanz).

In **Figure 6.13** (a), exemplary highly resolved PL spectra of a hybrid QD before illumination with UV light (left) and after illumination with UV light and red shift of the PL maxima (right) are displayed. Additionally, the PL decay curves of a hybrid QD before and after occurrence of the red shift of the PL maxima are displayed (**Figure 6.13** b). The QD before the red shift of the PL maxima, shows a PL fine structure typical for an uncharged emitter consisting of three distinct X^0-GS to QD-GS transitions.[27] After the red shift of the PL maxima occurred, the highly resolved PL spectrum of the hybrid QD displays a single optical transition (X^-) with the related AC phonon replica. Additionally, the PL intensity was increased (factor ~3), as expected for a charging of the emitter. The observed change in the PL properties indicate the presence of a CdSe emitter in the trion state which can be formed by charging and excitation of the inorganic emitter.[278] The changes in the PL dynamics corroborate this hypothesis. The uncharged QD (**Figure 6.13** b, left) exhibits a biexponential PL decay with lifetimes of τ_1 = 55 ns and τ_2 = 2 ns for the two contributions, respectively, which we relate to the dipole-forbidden F transition (τ_1, 88% contribution) and to the dipole-allowed A1 and A2 transitions (τ_2, 12% contribution). The PL decay of the presumably charged QD (**Figure 6.13** b, right) is dominated (92% contribution) by a fast radiative recombination (τ_1 = 2 ns), which we assign to the dipole-allowed fundamental trion (X^-) resonance.

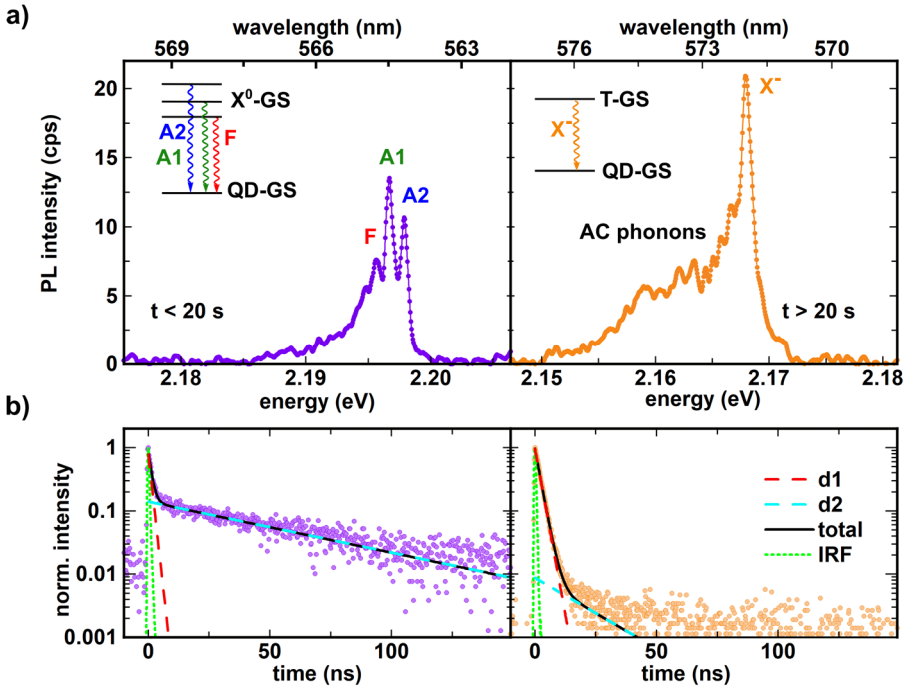

Figure 6.13. a) Highly resolved PL spectra (T = 4.2 K, $\lambda_{exc.}$ = 532 nm, $P_{exc.}$ = 240 nW) of a single PF8 CdSe/$Cd_xZn_{1-x}S$ hybrid QD before (left) and after (right) illumination with UV light. b) Radiative lifetime measurement (data points, T = 4.2 K, excitation 0.1 eV above QD emission energy) of a single hybrid QD in the presumably uncharged (left) and presumably charged (right) state. The black solid lines indicate least-square fits according to a biexponential decay model. The two contributions (d_1 and d_2) are depicted with dashed lines. Comparing the PL decay of a charged and uncharged QD reveals a tremendous lifetime shortening of the prominent contribution for the charged QD. The measurement data and curve fitting were provided by Frieder Conradt (Leitenstorfer group, University of Konstanz).

As such PL properties were not observed for unfunctionalized CdSe/$Cd_xZn_{1-x}S$ QDs, we attribute this behavior to an interaction between the inorganic emitter and the bound PF8 chains. The formation of CdSe trion states can be explained by a charge transfer between the conjugated polymer ligands and the inorganic emitter and subsequent excitation of the negatively charged QD. The charging can be explained by two different processes given the relative energy levels of the inorganic emitter and conjugated polymer (**Scheme 8.1**). In **Figure 6.12**, it was shown that additional excitation with light in the absorption range of PF8 led to a charging of the emitter. This charging can be accounted for by an electron transfer from the CB of photoexcited PF8 to the CB of the CdSe core (**Scheme 6.2**, left). The hole remains trapped on the conjugated polymer chain. A charging of the inorganic emitter also occasionally occurred without additional illumination in the absorption range of the PF8 polymer (**Figure 6.12**, right). This effect can be explained by a hole transfer from the VB of an excited QD to the VB of the polymer ligand (**Scheme 6.2**, right). This process requires a tunneling through the CdS/ZnS shell. Given the energy

levels of the graded shell, it should act as hole blocking layer, however, as the shell is relatively thin (2 monolayers of CdS and 2 monolayers of ZnS), the occurrence of a tunneling process is reasonable. As shown by ensemble PLE measurements, the QD can also be excited by an energy transfer from excited PF8 to the inorganic emitter. This process competes with the electron transfer, and probably decreases the efficiency of the stimulated charging by illumination with UV light. However, after the energy transfer, there is still the possibility of a hole transfer process leading to a negatively charged QD as illustrated on the right side in **Scheme 6.2**.

Scheme 6.2. Charging of a graded-shell CdSe/$Cd_xZn_{1-x}S$ QD by two mechanisms. Left: An electron is transferred from the CB of photoexcited PF8 to the CB of the CdSe core. Right: A hole is transferred from the VB of an excited QD to the VB of PF8 by a tunneling process through the CdS/ZnS shell.

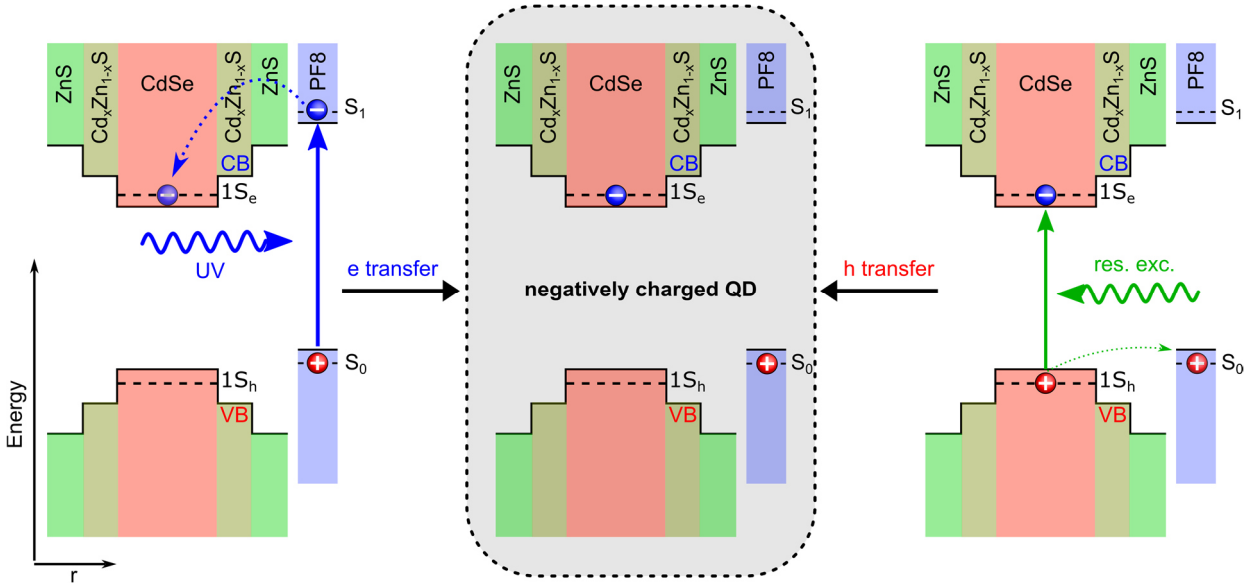

CdSe/CdS nanorods (NRs) are also an interesting material for the generation of charged nanocrystals as they feature a reduced Auger recombination.[2] Therefore, also the newly synthesized CdSe/CdS/CdS PF8 hybrid NRs (**Table 6.6**, entry 3, L = 28 nm, 200 equiv. of PF8), which had been encapsulated in PDOMA-*co*-PMeMBL particles were analyzed in single-particle PL studies. In **Figure 6.14**, an exemplary highly resolved PL spectrum (a) and a PL time trace (b) of such a hybrid nanocrystal are presented. The PL spectrum features a single fundamental emission line (X^-) with the related AC and first LO phonon replica, whereas unfunctionalized NRs show a PL fine structure consisting of three emission lines (**Figure 6.11**). This finding indicates the presence of a trion state and the formation of a charged CdSe-based emitter due to the functionalization with PF8. The PL time trace reveals a very stable emission (single emission line) over a long period of time

(100 s). Compared to quasi-spherical QDs, only minimal fluctuations and very discrete fluctuations of the emission wavelength due to the quantum-confined Stark effect were observed.[279,280] The extraordinary stability of NRs' emission is demonstrated by a PL time trace measurement on a cluster of several polymer particles where several NRs exhibit a very stable emission (single emission lines) over a period of at least 1000 s (**Figure 8.52**). As the NRs show a constantly strong PL intensity without 'dark' periods, Auger-recombination in the charged nanocrystals seems to be, as expected, strongly suppressed. Moreover, the emission intensity of these hybrid nanorods was higher compared to the charged hybrid QDs (maximal height of the X^- transition: ~90 cps for rods vs. 22 cps for QDs). Preliminary studies on these hybrid NRs revealed that all of these NRs were constantly charged even without additional illumination with UV light and no discharging has been detected, so far.

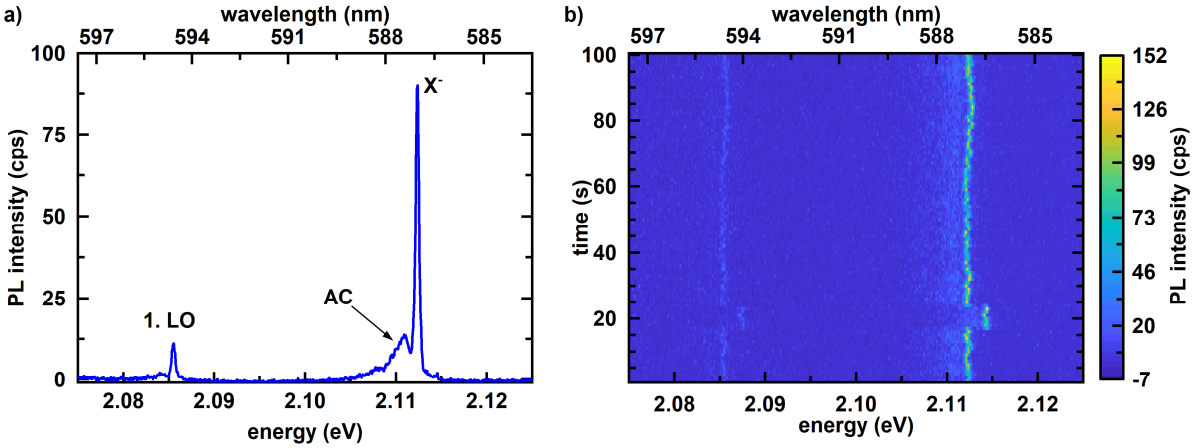

Figure 6.14. Highly resolved PL spectrum (a) and PL time trace (b) of a single PF8 CdSe/CdS/CdS hybrid nanorod encapsulated in PDOMA-*co*-PMeMBL ($\lambda_{exc.}$ = 532 nm, $P_{exc.}$ = 509 nW, T = 4 K). The single fundamental emission line indicates the presence of a charged CdSe-based emitter. The measurement data were provided by Frieder Conradt (Leitenstorfer group, University of Konstanz).

The functionalization of CdSe/$Cd_xZn_{1-x}S$ QDs and CdSe/CdS/CdS NRs with PF8 had the intended influence on the optical properties of the inorganic emitter and allows for a charging of the inorganic emitter by a charge transfer processes between the PF8 and the nanocrystals. Thereby, trion states are formed which show a single emission line, an increased PL intensity and a shorter PL lifetime compared to the neutral emitter. According to preliminary studies, the charging efficiency, emission stability and intensity of the hybrid polyfluorene CdSe/CdS/CdS NRs are superior as compared to the graded-shell hybrid QDs. Therefore, the PF8 hybrid QDs and PF8 hybrid NRs are auspicious for the use as single-photon sources in ultrafast quantum-optical studies. The detailed

analysis of these particles concerning the influence of the polymer shell, charging statistics, stability, PL lifetimes and use as single-photon source will be part of the PhD thesis of Frieder Conradt in the physics groups of Prof. Dr. Alfred Leitenstorfer.

6.3 Summary and Conclusion

In this chapter, the encapsulation of semiconductor (hybrid) nanocrystals into polymer nanoparticles by a miniemulsion polymerization approach was investigated. Graded-shell CdSe/$(CdS)_2(ZnS)_2$ were successfully encapsulated into cross-linked PMMA or PMMA-*co*-PEHMA particles with a size around 60 nm. The QY of the QDs decreased from 87% for non-embedded QDs to 49–52% for the embedded QDs but was still significantly higher than the QY of embedded CdSe/CdS QDs which only show a QY in the range of 20-30%. Mostly empty particles (~60%), a high percentage of single QD particles (~35%), and only a few particles occupied by several QDs (~5%) were obtained, thus an encapsulation distribution favorable to single-particle PL experiments.

The graded-shell QDs were functionalized with PA-PF8-*b*-PMMA, PA-PF8-*b*-PS and PA-PF8-*b*-PEHMA block copolymers in a ligand exchange reaction (**Chapter 5.2.1**). The nonconjugated blocks were introduced to facilitate the encapsulation in the respective methacrylate (or styrene) monomer and polymer, respectively. However, the functionalization with these block copolymers caused (partial) agglomeration of the QDs during the miniemulsion process and only an insignificant proportion of polymer particles containing single QDs were obtained. Thus, dispersions which are not particularly suitable for single-particle PL experiments.

Nonetheless, the encapsulation of graded-shell QDs which had been functionalized with the homo-type polyfluorene PF8-Ph-$PO(OH)_2$ resulted in an embedding distribution favorable to single-particle PL measurements. Mostly empty particles (~75%), many particles with exactly one QD per particle (~15%) and fewer particles containing several QDs (~10%) were obtained. The encapsulation in a mixture of MMA/EHMA of 70/30 vol% resulted in a slightly improved encapsulation in terms of QY and embedding statistics compared to the embedding in pure cross-linked PMMA. The hybrid QDs feature a strong ET from photoexcited PF8 to the nanocrystals which is also observable for the encapsulated hybrid QDs.

In the next step, an encapsulation for the embedding of semiconductor CdSe/CdS NRs and PF8 functionalized CdSe/CdS/CdS hybrid NRs by a miniemulsion polymerization approach was developed. The encapsulation in PMMA or PMMA-*co*-PEHMA led to an agglomeration of the NRs and an insufficient percentage of polymer particles containing a single NR were obtained. The solution for the successful encapsulation (retention of high QY and favorable embedding distribution) was the usage of a mixture of the monomers

dodecyl methacrylate (DOMA) and α-methylene-γ-valerolactone (MeMBL) in a ratio of 1:1 in combination with a cross-linking agent. DOMA ensures the dispersibility and colloidal stability of the NRs in the monomer mixture whereas MeMBL enables the formation of sufficiently hard and non-sticky particles. The particle size was around 90 nm, and a slight decrease in the QY of the NRs was observed (32% → 30% for long NRs and 52% → 35% for short NRs) during the embedding process. The QY of the optical higher-quality CdSe/CdS/CdS NRs decreased from 70–78% for non-embedded NRs down to 40–55%. Additionally, it was also possible to embed NRs in large (D = 130 nm) cross-linked PS particles which were overcoated by a PMMA shell (thickness ~ 15 nm) to ensure the optical stability of the NRs. Using these procedures, also PF8-functionalized CdSe/CdS/CdS NRs were successfully encapsulated into polymer nanoparticles (**Figure 6.15)**. Furthermore, for the embedded hybrid NRs a strong ET from the polymer to the NRs could still be observed.

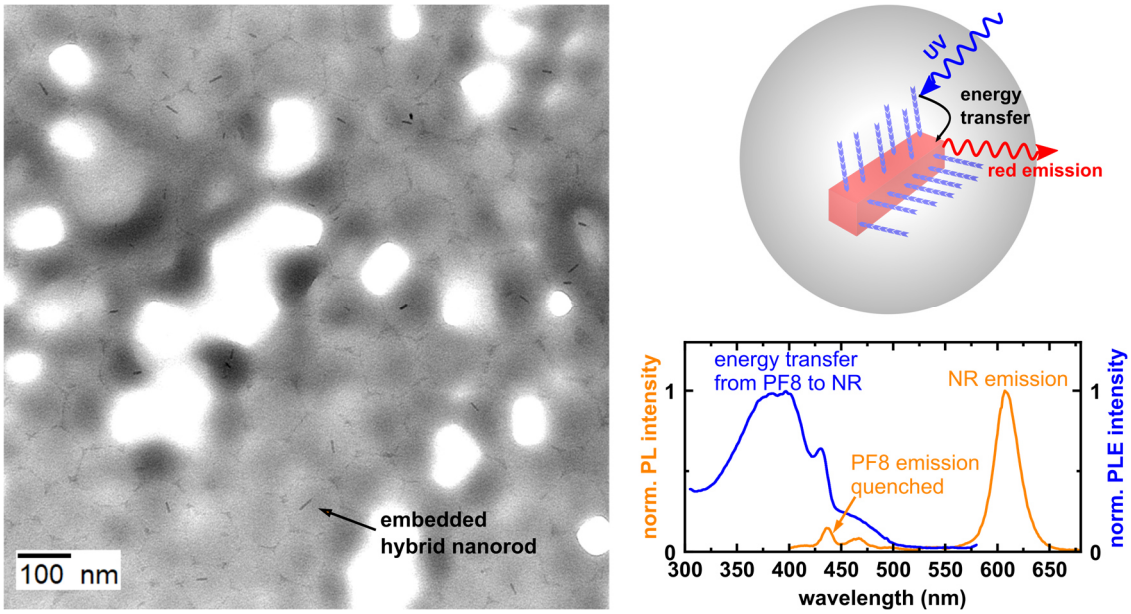

Figure 6.15. TEM image of PF8-Ph-PO(OH)$_2$ CdSe/CdS/CdS hybrid NRs embedded in PDOMA-*co*-PMeMBL nanoparticles (left). Sketch of such a hybrid particle (right top) and PL ($\lambda_{exc.}$ = 380 nm) and PLE ($\lambda_{det.}$ = 605 nm) spectra of the corresponding dispersion (right bottom).

The newly synthesized graded-shell CdSe/(CdS)$_2$(ZnS)$_2$ QDs encapsulated in PMMA-*co*-PEHMA polymer particles were analyzed in single-particle PL measurements at 4–6 K. These particles were exceptionally well suited for these experiments and brighter than the previously employed CdSe/CdS QDs. Importantly, for these particles no charging of the inorganic emitter was detected. Also, encapsulated CdSe/CdS/CdS NRs were analyzed in single-particle PL measurements. These NRs were highly emissive and featured a multi-

line PL fine structure similar to the fine structure observed for graded-shell QDs, indicating emission from uncharged nanocrystals.

The long-term objective of this research was the formation of charged semiconductor inorganic nanocrystals by a charge transfer between the conjugated polymer PF8 and the CdSe-based nanocrystals. PF8-functionalized CdSe/$(CdS)_2(ZnS)_2$ graded-shell QDs, which had been encapsulated into cross-linked PMMA-*co*-PEHMA particles, could be switched from a neutral to a charged state which was reflected in the PL fine structure of the single particles (**Figure 6.16**). Before the switching, the PL spectrum shows a PL fine structure consisting of three distinct emission lines (F, A1, A2), thus the typical excitonic band edge states of a neutral QD. After charging, the PL spectrum exhibits a single PL emission line, which is typical for a charged CdSe QD during optical excitation. Additionally, PL decay measurements of a charged and uncharged QD revealed a tremendous lifetime shortening upon charging. We attribute the charging process to an electron transfer from the conjugated polymer PF8 to the inorganic emitter. This process can be triggered by exciting the polymer with UV light (electron transfer from the PF8's CB to QD's CB) or by resonant excitation of the QD (hole transfer by tunneling from the QD's VB to the VB of the polymer).

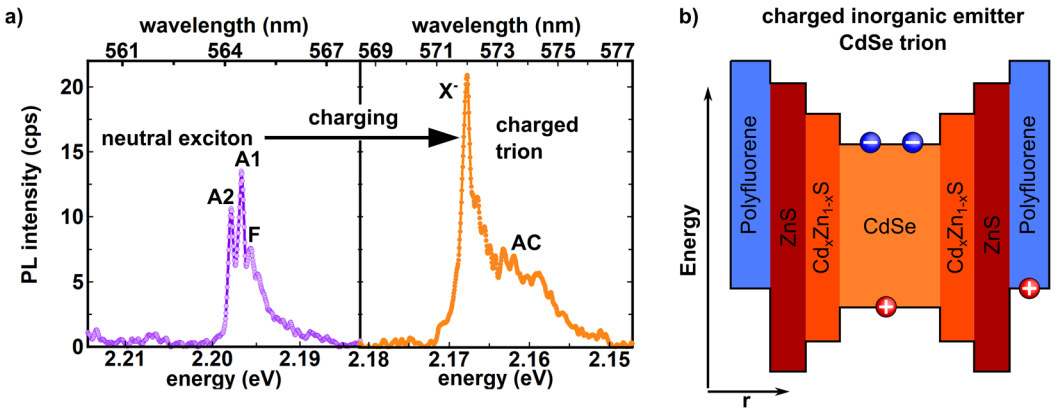

Figure 6.16. a) Highly resolved PL spectra of a single CdSe/$Cd_xZn_{1-x}S$ PF8 hybrid QD before (left) and after charging (right) by interaction with the bound PF8 ligands. b) Schematic illustration of the formed charged and excited QD (negative trion).

The charging of the CdSe-based emitter was also witnessed in single-particle PL measurements on polyfluorene CdSe/CdS/CdS hybrid nanorods. Preliminary studies revealed that all of the analyzed nanorods were charged even without additionally illumination with UV light. Moreover, the nanorods featured a very stable emission in the charged state and only minimal fluctuations in the emission wavelength were observed.

The functionalization of graded-shell CdSe/$Cd_xZn_{1-x}S$ QDs and CdSe/CdS/CdS nanorods with polyfluorene had the anticipated impact on the optical properties in single-particle PL studies: A charge transfer between the two semiconducting materials leads to a charging of the inorganic emitter and the formation of a trion state. The charged nanocrystals exhibit a single emission line with the related phonon replica, an increased PL intensity, and a shortened fluorescence lifetime compared to their uncharged counterparts. Therefore, these hybrid nanocrystals are an alluring material for the further use as single-photon sources in ultrafast quantum-optical studies and might potentially be used in ultrafast amplifiers.

6.4 Experimental Section

6.4.1 Materials and General Considerations

All chemicals were used as received unless stated otherwise. Standard organic solvents and chemicals were obtained from various commercial suppliers such as Sigma-Aldrich, ABCR, VWR and Roth. 2-Ethylhexyl methacrylate (EHMA) (> 99%, stabilized with MEHQ), α-methylene-γ-valerolactone (>97 %, stabilized with HQ) and dodecyl methacrylate (> 97%, stabilized with MEHQ) were acquired from TCI. Methyl methacrylate (MMA) (99%, contains < 30 ppm MEHQ as inhibitor), ethylene glycol dimethacrylate (98%, contains 90-110 ppm MEHQ as inhibitor), *p*-divinylbenzene (85%, stabilized with 4-*tert*-butylpyrocatechol), styrene (> 99%, contains 4-*tert*-butylcatechol as stabilizer), 2,2′-azobis(2-methylpropionitrile) (98%) and sodium dodecyl sulfate (> 99%, dust free pellets) were from Sigma-Aldrich.

Deionized water was distilled under a nitrogen atmosphere. Methacrylate and acrylate monomers were filtered over basic aluminum oxide, dried over 4 Å molecular sieves, degassed by three freeze-pump-thaw cycles and stored inside a glovebox at -30 °C. Styrene was vacuum transferred, degassed by three freeze-pump-thaw cycles and stored inside a glovebox at -30 °C.

6.4.2 Analytical Methods

Photoluminescence measurements and Quantum Yield Determination:

Ensemble emission spectra and quantum yields were measured using a Hamamatsu Absolute PL Quantum Yield Measurement System C9920-02 equipped with an integrating sphere. QY measurements were performed at $\lambda_{exc.}$ = 450 nm.

Absorption spectroscopy (UV-VIS spectroscopy):

Absorption spectra were recorded on a Varian Cary 100 scan spectrometer with the solvent as reference. If not otherwise stated, toluene was used as solvent.

Photoluminescence Excitation Measurements:

Photoluminescence spectra, photoluminescence excitation spectra and fluorescence lifetimes were measured on a PicoQuant FluoTime 300 spectrometer.

Transmission Electron Microscopy (TEM):

TEM micrographs were taken using a Jeol JEM-2200FS transmission electron microscope using a FEG with 200 kV acceleration voltage or using a Zeiss Libra 120 employing a LaB_6

emitter with 120 kV acceleration voltage. Samples were prepared by drop casting 2 µL of a diluted particle dispersion on a TEM grid (Quantifoil S 7/2 + 2 nm C, Cu 400).
Particle size and distributions were obtained by measuring the diameter of at least 150 particles in TEM images. Nanocrystal encapsulation efficiencies were determined by analysis of a minimum of 150 clearly distinguishable polymer particles in TEM images.

Dynamic Light Scattering:

Dynamic light scattering experiments were performed on a Malvern Nano-ZSEN 3600 particle sizer (173° back scattering, 633 nm LASER wavelength). The Malvern Zetasizer software 7.13 was used to analyze the autocorrelation function, yielding z-averages, intensity mean particle sizes, number mean particle sizes, size distributions and polydispersity indices (PDI; ≤ 0.1 narrow).

Determination of Solid Content by Gravimetry:

The solid content of the polymer dispersions was determined on a Sartorius Moisture Analyzer MA45. Around 2 g of the polymer dispersion was distributed on the heating pan and heated to 200 °C until a constant weight was obtained.

6.4.3 Procedures for the Encapsulation of Quantum Dots

The encapsulation of spherical QDs or hybrid QDs by a miniemulsion polymerization procedure is based on a method which was developed by Negele et al.[30] and improved by Tjaard deRoo[150].
Exemplary procedure:
0.1 mL of hexadecane, 10 mg of 2,2'-azobis(2-methylpropionitrile) (AIBN) and 10 nmol of QDs ($CdSe/Cd_xZn_{1-x}S$ or PF8 @ $CdSe/Cd_xZn_{1-x}S$) in 0.6 mL of toluene were dissolved in 0.01 mL of ethylenglycol dimethacrylate and in 1 mL of the respective monomer (e.g. methyl methacrylate) or monomer mixture. In a 100 mL Schlenk tube, 100 mg of SDS was degassed and dissolved in 80 mL of degassed and distilled water. The organic phase was added on top of the aqueous phase and emulsified by sonication with an ultrasonotrode (Bandelin GM3200 ultrasonotrode with KE76 tip, operated at 120 W) at 60% intensity for 2-3 min. During the emulsification process, the reaction mixture was cooled in an ice bath to prevent polymerization. Under vigorous stirring the generated miniemulsion was heated to 75 °C and polymerized for 5 hours under a nitrogen atmosphere followed by stirring in an open tube at 60 °C overnight.

6.4.4 Procedures for the Encapsulation of Nanorods

Encapsulation of Nanorods Similar to the Encapsulation of Quantum Dots

NRs (CdSe/CdS or CdSe/CdS/CdS) were embedded as described for the encapsulation of QDs. Here, 1,4-divinylbenzene was used as cross-linking agent and different monomers (e.g. dodecyl methacrylate, α-methylene-γ-valerolactone or styrene) or monomer mixture were used.

Encapsulation of Nanorods into Large Polystyrene Spheres by Miniemulsion Polymerization

This approach is based on a procedure developed by San Luis et al. for the encapsulation of spherical QDs.[31]

Exemplary Procedure:

The aqueous phase was prepared by degassing 42 mg of SDS and 21 mg of $NaHCO_3$ and dissolving them into 25 g of degassed and distilled water.

The organic phase was prepared by mixing 2.3 mL of styrene, 84 mg of hexadecane, 21 mg of 1,4-divinylbenzene and the NRs dispersed in toluene (0.6 mL). This mixture was stirred for ten minutes and then added on top of the aqueous phase. The miniemulsion was prepared by ultrasonication with an ultrasonotrode (Bandelin GM3200 ultrasonotrode with KE76 tip, operated at 120 W) at 80% intensity for 4 min. During the emulsification process, the reaction mixture was cooled in an ice bath to prevent polymerization. Afterwards, a mixture of 21 mg of SDS and 10 g of distilled water was added, and the mixture heated to 75 °C. In order to start the polymerization 11 mg of potassium peroxodisulfate dissolved in 4 g of distilled water was added. The polymerization was conducted for 6 hours at 75 °C.

Addition of an Additional Poly(methyl methacrylate) Shell onto Polystyrene Particles

Polystyrene particles were coated with an additional cross-linked PMMA shell. The amount of MMA needed was calculated by the solid content of the dispersion and size (DLS number average) of the initial particles and the desired shell thickness assuming the polystyrene particles to have a density of 1.05 g/mL.

Exemplary procedure: To 20 mL of a polystyrene dispersion, 2 mg of AIBN was added, the mixture heated to 75 °C, and a mixture of MMA and 1,4-divinylbenzene (1 w% with

respect to MMA) was added via a syringe pump with an injection rate of 0.25 mL/min. The mixture was stirred under a nitrogen atmosphere at 75 °C for 3 hours.

6.4.5 Single-Particle Micro-Photoluminescence Experiments

The single-particle micro-photoluminescence experiments were conducted by Frieder Conradt and Pascal Gumbsheimer in the physics group of Prof. Dr. Alfred Leitenstorfer at the University of Konstanz.

The measurements were performed on a home-built PL measurement set-up. Details on the set-up and measurement procedure can be found in ref.[280]

7 Conclusive Summary

Tethering semiconductor conjugated polymers to semiconductor nanocrystals yields hybrid particles which are of particular interest for opto-electronic devices such as solar cells, light-emitting diodes and flexible electronics. Moreover, these particles are an ideal system to perform fundamental quantum-optical studies concerning the interplay between charges, photons and phonons in a quantized system. Additionally, these particles are promising as potential single-photon sources for research in the field of ultrafast control of single electrons and photons. However, the controlled and reproducible synthesis of hybrid particles of high optical quality with the conjugated polymer directly tethered to the nanocrystals' surface was an unresolved challenge.

The synthesis of high-performance hybrid particles required nanocrystals with excellent optical properties. Based on a reported procedure[1], graded-shell CdSe/$Cd_xZn_{1-x}S$ quantum dots (QDs) were successfully synthesized. These QDs showed high QYs around 87% and a narrow size distribution (~10%). Already CdSe seed particles overcoated with 2 monolayers of CdS and 2 monolayers of ZnS exhibited a high QY of 87% (**Figure 7.1**). Upon deposition of the CdS shell, as expected, a red shift of the optical properties occurred due to the formation of a quasi-type-2 heterostructure. The deposition of ZnS led to an alloying of the CdS and ZnS layer which caused a blue shift of the optical properties and a type-1 heterostructure was formed.[1] Especially thin-shelled CdSe/$(CdS)_2(ZnS)_2$ QDs are promising for the functionalization with conjugated polymers, as the thin shell should facilitate energy and charge transfer processes. Anisotropic hybrid CdSe/CdS nanorods (NRs) are another interesting material for single-particle PL studies and charging experiments, as they have been shown to feature a reduced Auger recombination and to exhibit efficient trion emission.[2] High-quality CdSe/CdS NRs (length 20–40 nm, width ~5 nm) were successfully synthesized based on a literature-known procedure (**Figure 7.1**).[4] Similar to a procedure developed by Bawendi and co-workers[181] an additional CdS shell (2 monolayers) was deposited on these NRs in order to improve their optical quality. This deposition resulted in a significant increase in the QY of the NRs

(35–42% → 75–78%). Moreover, it was revealed that the surface of these CdSe/CdS/CdS NRs is partially covered by oleic acid, which should be beneficial for the functionalization with conjugated polymer chains.

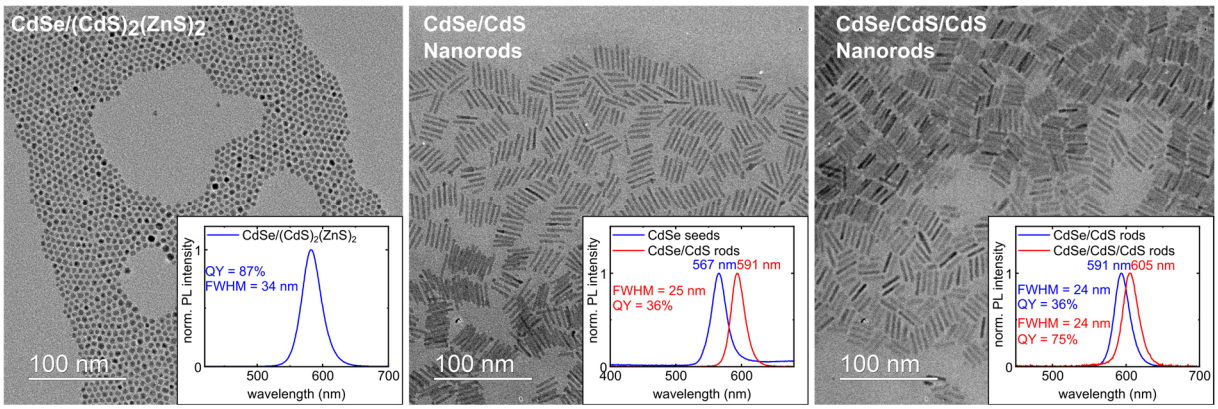

Figure 7.1. Overview over the synthesized high-quality semiconductor nanocrystals. Left: $CdSe/(CdS)_2(ZnS)_2$ QDs. Center: CdSe/CdS NRs. Right: CdSe/CdS/CdS NRs.

For the functionalization of nanocrystals with conjugated polymers, precisely functionalized polymers, bearing a functional group capable of binding to the nanocrystals' surface, were required. Multi-valent polymer ligands might facilitate the functionalization of the nanocrystals and enable a higher degree of functionalization. Additionally, conjugated nonconjugated block copolymers were targeted, as the nanocrystals' functionalization could facilitate the subsequent encapsulation of the hybrid particles into polymer nanoparticles. The controlled Suzuki-Miyaura cross-coupling polymerization (cSMCCP) is a powerful tool for the synthesis of heterodifunctional polymers. A novel and straightforward approach to the synthesis of conjugated nonconjugated copolymers by sequential cSMCCP and controlled radical polymerization was developed. As a first step, well-defined heterodifunctional polyfluorenes (PF8) ($M_w/M_n \leq 1.2$; DP_n 5–20) featuring a phosphonate group (initiating chain end) and a radically polymerizable or ATRP-initiating group (terminating chain end) were generated by catalytic chain growth (**Figure 7.2**).

Three-coordinate Pd(II) initiators generated *in situ* from the respective arylbromide and chloro[(tri-*tert*-butylphosphine)-2-(2-aminobiphenyl)] palladium(II) were shown to perform equally well compared to the corresponding tediously isolated Pd(II) complexes. The resulting polymers were directly employed for the synthesis of conjugated nonconjugated copolymers without further intermediate conversion steps (**Scheme 7.1**). Controlled atom transfer radical polymerization (ATRP) of styrene (Sty), methyl methacrylate (MMA) or 2-ethylhexyl methacrylate (EHMA), respectively, from PF8

macroinitiators under appropriate conditions afforded narrowly distributed diblock copolymers free of homopolymers. The diethyl phenylphosphonate group of these polymers could be transformed selectively to the corresponding phosphonic acid — only phosphonic acids bind strongly to CdSe or CdS surfaces and not the corresponding alkyl phosphonates — without cleavage of any carboxylic acid esters present in the polymers.

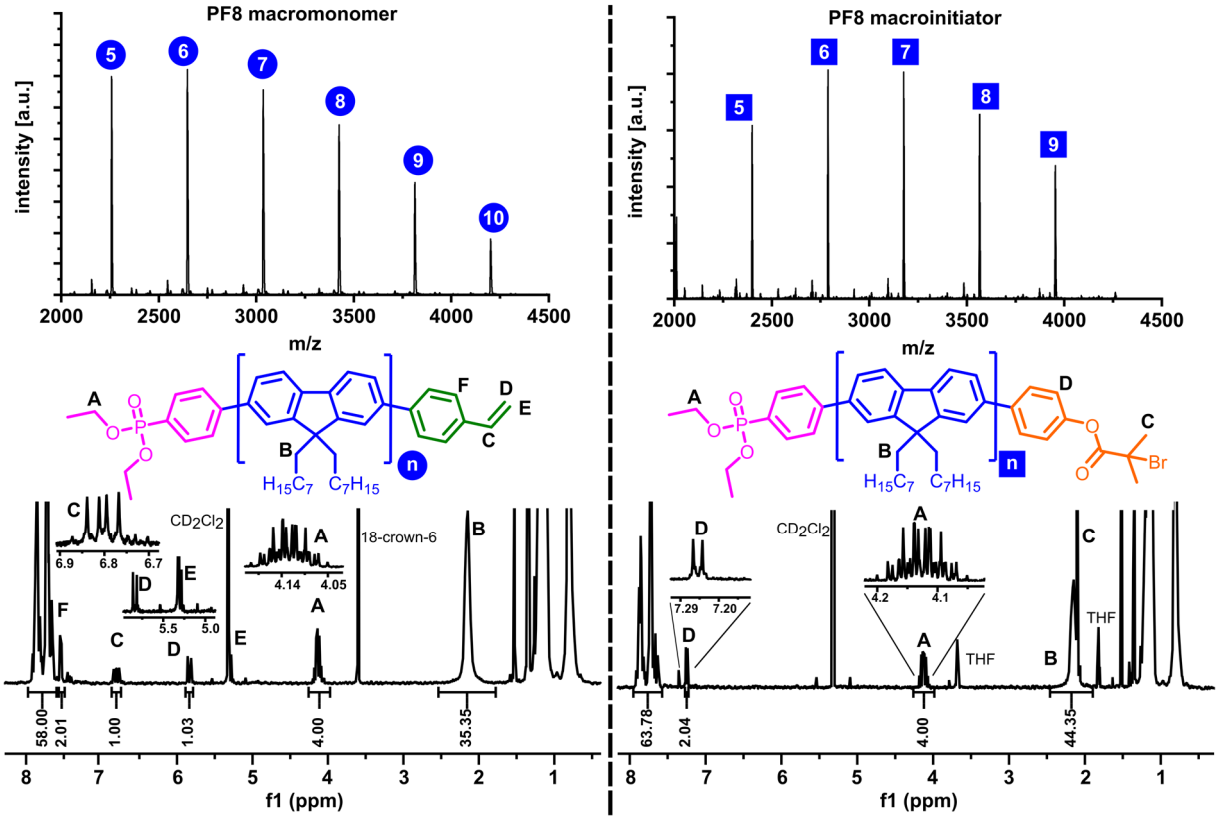

Figure 7.2. MALDI-TOF mass spectra (top) and ^{1}H NMR spectra (bottom) of the PF8 macromonomer Phos-PF8-Sty (left) and the PF8 macroinitiator Phos-PF8-AlkylBr (right) which were synthesized by cSMCCP. Reprinted with permission from ref.[5] Copyright **2019** American Chemical Society.

Controlled radical copolymerization of PF8 macromonomers bearing a styrene-type end group with styrene or methacrylates, respectively, gives access to novel conjugated nonconjugated comb polymers. The number of PF8 side chains per backbone chain can be tuned by the ratio of the two monomers employed (here: polymers chains with on average 2–14 side chains were synthesized). Notably, this approach allows the incorporation of functional end groups, as demonstrated here for phosphonates. The latter are relevant for binding to nanoparticle and macroscopic surfaces. The multivalent character of the comb polymers is of particular interest, as it may allow for an efficient and strong attachment to nanoparticles. For the intended functionalization of CdSe-based nanoparticles, the

phosphonate groups of these comb polymers were selectively transformed to the corresponding phosphonic acids. However, the deprotected comb polymers showed a reduced solubility in nonpolar solvents compared to their protected counterparts which limited their application as nanoparticle ligands.

Notwithstanding, two novel species of conjugated nonconjugated copolymers (block and comb) were synthesized in an unprecedented straightforward way.

Scheme 7.1. Straightforward synthesis of conjugated nonconjugated block copolymers by sequential cSMCCP and activators regenerated by electron transfer atom transfer radical polymerization (ARGET ATRP). Adapted from and with permission from ref.[5] Copyright **2019** American Chemical Society.

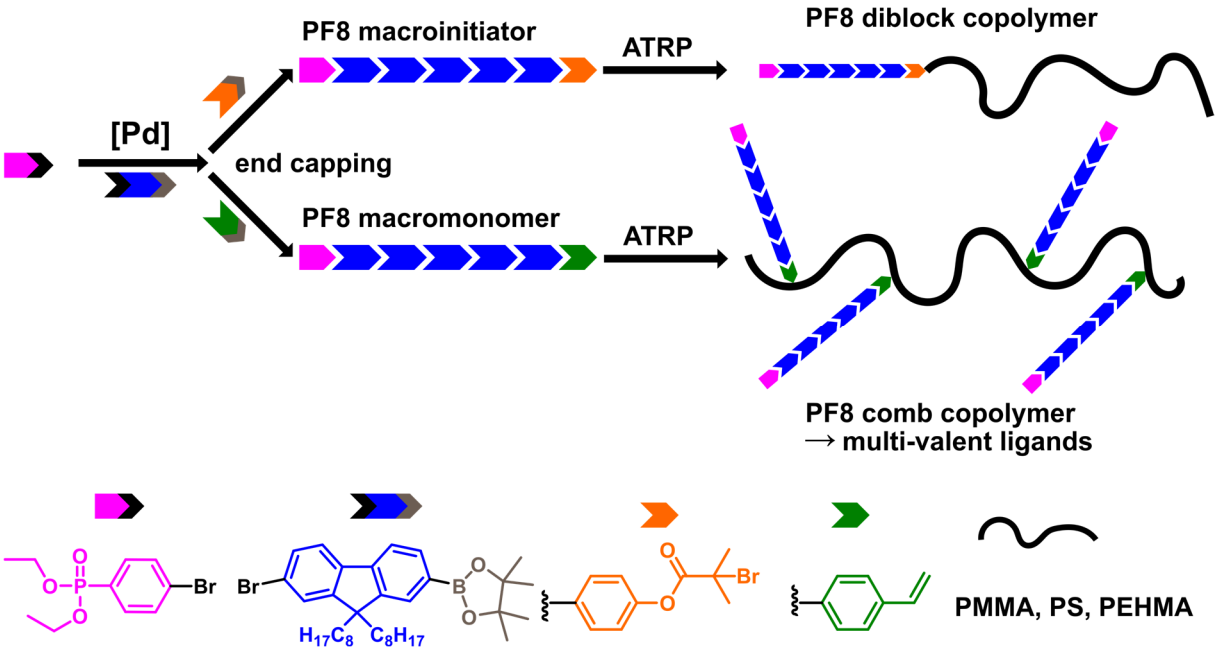

Hybrid particles of CdSe-based nanocrystals and PF8 were synthesized by direct ligand exchange reactions as well as by direct approaches employing various functionalized PF8s. The binding of the polymer was proven and quantified by multi-wavelength analytical ultracentrifugation measurements.

CdSe/CdS QD hybrid particles were successfully synthesized by a direct ligand exchange reaction with phenylphosphonic acid end-functionalized polyfluorene (PF8-Ph-$PO(OH)_2$, DP_n = 10) bearing a radically polymerizable group as second terminus. Around 70% of the added polymer chains (175 equiv. with respect to the QDs added) were bound to the nanocrystals and unbound PF8 could be separated by centrifugation. The fluorescence of PF8 bound to nanocrystals was completely quenched and a quantitative energy transfer (ET) to the nanocrystal was observed, resulting in emission of the nanocrystal exclusively.

Such an ET only took place when the polymer was bound to the QDs and not for a simple physical mixture.

The novel diblock ($PO(OH)_2$-PF8-*b*-PEHMA, $PO(OH)_2$-PF8-*b*-PMMA and $PO(OH)_2$-PF8-*b*-PS) and multi-valent comb copolymers ($PO(OH)_2$-PF8-Sty-*co*-PEHMA, $PO(OH)_2$-PF8-Sty-*co*-PMMA, $PO(OH)_2$-PF8-Sty-*co*-PS) were used in direct ligand exchange reactions to functionalize CdSe/$Cd_xZn_{1-x}S$ QDs of high optical quality. The binding affinity of the diblock copolymer $PO(OH)_2$-PF8-*b*-PEHMA was comparable to the polyfluorene PF8-Ph-$PO(OH)_2$ and around 50-60% (~100 equiv. added) of the polymer chains were tethered to the nanocrystals. The binding of the other two copolymers was less efficient due to their inappropriate solubility properties. The addition of the multi-valent comb polymers to QD dispersions led to a partial precipitation of QDs and polymer. However, the remaining polymer was strongly bound to the QDs and basically all remaining polymer in the dispersion was bound to the nanocrystals.

The functionalization of QDs during their synthesis, by adding the polymer at high temperatures and/or at an early stage of particle formation, might be beneficial for the functionalization. Thus, a subsequent separate ligand exchange reaction with isolated and purified QDs is not necessary. PF8 graded-shell CdSe/$(CdS)_2(ZnS)_2$ hybrid QDs were synthesized by a novel direct approach. The phosphonic acid (benzyl or phenyl) end-functionalized PF8 (DP_n = 10) was added directly during the nanoparticles' synthesis after the deposition of the CdS shell or the ZnS shell, respectively. Addition of the polymer after the deposition of the CdS shell disturbed the further particle formation. However, adding the polymer after the deposition of the ZnS shell, monodisperse QDs of high optical quality (QY = 78–84%, d = 6.1 nm, size distribution ~10%) were obtained and a high degree of the added polymer was bound to the nanocrystals (27–160 chains/QD were added, 35–80% bound). The binding was slightly improved by adding the polymer at a higher temperature (150 °C vs. 310 °C). However, it appears that a maximum of roughly 55 chains can bind to one QD (roughly 10% of surface ligands would be PF8 chains). A strong ET from excited PF8 to the QDs was observed which scales qualitatively with the amount of bound polymer chains. Phenylphosphonic acid-functionalized PF8 was found to bind slightly better than benzylphosphonic acid-functionalized PF8. Remarkably, the single 'insulating' CH_2 group between the conjugated π-system and the binding group in the benzylphosphonic acid-functionalized polymer already reduced the ET intensity significantly (roughly 25%) compared to the phenylphosphonic acid-functionalized

polymer. Hybrid QDs showed a slightly faster PL decay than unfunctionalized QDs which hints at an additional charging of the QDs due to the functionalization with PF8. Due to their solubility properties, the conjugated nonconjugated copolymers were found less suited for this functionalization approach.

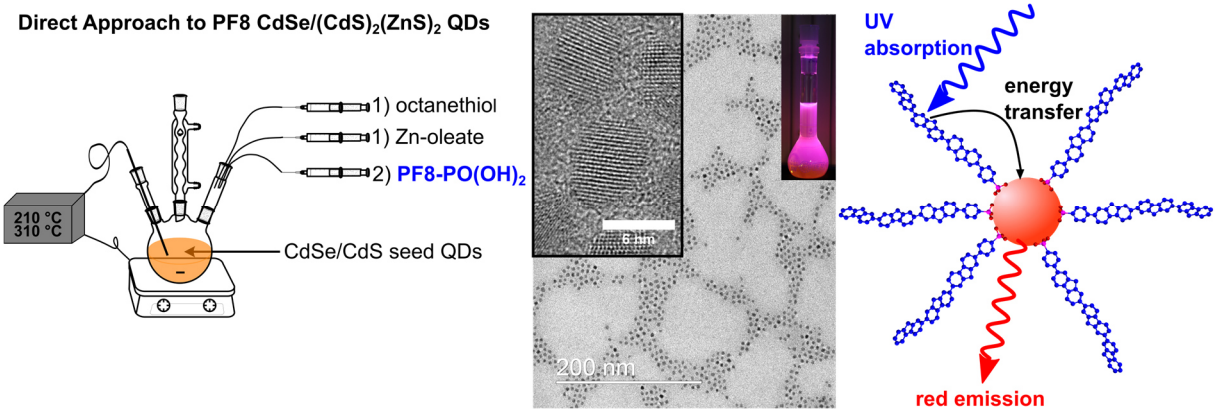

Figure 7.3. Functionalization of graded-shell CdSe/$(CdS)_2(ZnS)_2$ QDs with PF8 in a direct approach. Left: Illustration of the synthesis approach. Center: Exemplary TEM images and a photo of a hybrid QD dispersion under UV light illumination. Right: Illustration of the energy transfer process.

The functionalization of CdSe/CdS NRs by various approaches was basically unsuccessful as the NRs' surface is completely covered with strongly binding X-type phosphonic acids which could not be displaced by the functionalized polymers to a significant extend. However, two functionalization approaches (**Figure 7.4**) for CdSe/CdS/CdS NRs, with surfaces partially occupied by more weakly binding oleate ligands and with superior optical properties compared to the standard CdSe/CdS NRs, were successfully developed. In the first approach, Cd-PF8-Ph-X (X=-COOH or $PO(OH)_2$) was used as additional precursor besides Cd-oleate in the deposition of the outer CdS shell. The formation of the CdS shell was not disturbed and high-quality NRs (QY = 71–80%) were obtained. Only by using Cd-PF8-Ph-$PO(OH)_2$ hybrid NRs (45–65% of bound PF8) were formed, whereas PF8-Ph-COOH did not bind. In the second approach, the free-acid-functionalized polymers PF8-Ph-$PO(OH)_2$ or PF8-Ph-COOH, respectively, were directly added at 310 °C after the deposition of the second CdS shell had been completed. For PF8-Ph-COOH, no significant binding took place. In contrast, basically all PF8-Ph-$PO(OH)_2$ in the dispersion was bound to the nanocrystals. This method allowed to partially control the amount of PF8 bound to the NRs — a complete binding was observed for adding up to 300 equiv. of polymer to the nanocrystals. The PL decay of hybrid NRs was slightly shortened compared to unfunctionalized NRs which could be a hint at an additional charging of the NRs due to a

charge transfer process with the polymer. Additionally, the fluorescence of bound PF8 was completely quenched and an ET from excited PF8 to the NRs was observed (**Figure 7.4**). The intensity of this ET scales linearly – in the analyzed range – with the amount of bound PF8.

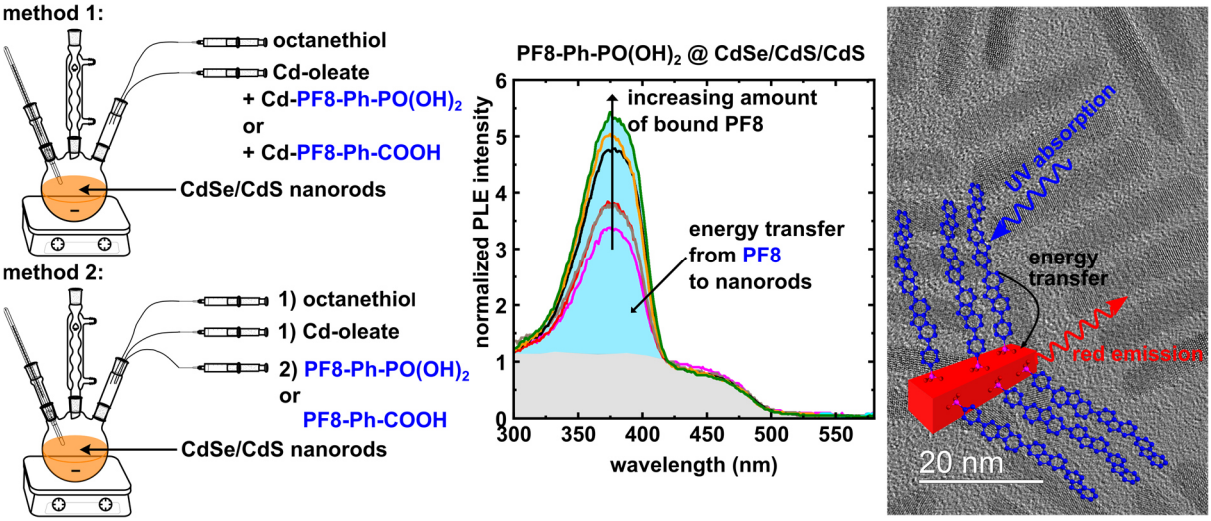

Figure 7.4. Functionalization of CdSe/CdS/CdS nanorods with functionalized PF8 by two methods (left). The photoluminescence excitation spectra ($\lambda_{det.}$ = 605 nm) show an increasing ET from PF8 to the NRs with an increasing amount of bound polymer (center). Exemplary TEM image of hybrid NRs and a schematic illustration of the ET process from the PF8 to the NR (right).

For all synthesized hybrid nanocrystals, the ET from the polyfluorene to the inorganic nanocrystal was only detected, if the polymer was directly tethered to the nanocrystals' surface. A simple physical mixing of unfunctionalized PF8 and nanocrystals did not yield hybrid particles and no ET processes could be observed in these systems.

In order to utilize these hybrid particles in single-particle micro-photoluminescence studies, in charging experiments, and potentially as single-photon source, they were encapsulated into larger polymer nanoparticles. Graded-shell CdSe/$(CdS)_2(ZnS)_2$ QDs were successfully encapsulated into cross-linked PMMA or PMMA-*co*-PEHMA (70/30 vol%) particles with sizes around 60 nm by a modified reported miniemulsion polymerization approach.[30,150] The QY of the QDs decreased from 87% for non-embedded QDs to 49–52% upon encapsulation which still excelled the QY of embedded CdSe/CdS QDs which only showed values in the range of 20–30%. Mostly empty particles (~60%), a high percentage of single QD particles (~35%), and only a few particles occupied by several QDs (~5%) were obtained. This result indicates that in the miniemulsion polymerization approach, the QDs did not aggregate unfavorable, and thus an encapsulation distribution favorable to single-particle PL experiments was gained.

Graded-shell QDs were functionalized with either $PO(OH)_2$-PF8-*b*-PMMA, $PO(OH)_2$-PF8-*b*-PS or $PO(OH)_2$-PF8-*b*-PEHMA block copolymers in a ligand exchange reaction. The nonconjugated blocks were used to facilitate the encapsulation in the respective methacrylate (or styrene) monomer and polymers, respectively. However, the functionalization with these block copolymers caused a (partial) clustering of the QDs and an unfavorable small fraction of particles containing a single QD were obtained, thus encapsulation distributions not particularly suited for single-particle PL studies.

Nevertheless, the encapsulation of graded-shell QDs, which had been functionalized with the polyfluorene PF8-Ph-$PO(OH)_2$, in cross-linked PMMA particles by a miniemulsion polymerization was successful. As anticipated, mostly empty particles (~75%), many particles with exactly one QD per particle (~15%) and only few particles containing several QDs (~10%) were obtained. The encapsulation in a mixture of MMA/EHMA of 70/30 vol% and a cross-linking agent resulted in a slightly improved encapsulation in terms of QY and embedding statistics compared to the embedding in pure cross-linked PMMA particles. The hybrid QDs featured a strong ET from photoexcited PF8 to the nanocrystals which was also observable for the encapsulated hybrid QDs.

In the next step, an encapsulation for the embedding of semiconductor CdSe/CdS NRs and PF8-functionalized hybrid NRs by a miniemulsion polymerization approach was developed. The encapsulation in PMMA or PMMA-*co*-PEHMA particles under the same conditions as employed for spherical QDs led to a clustering of the nanocrystals in single polymer particles. A successful encapsulation (retention of high QY, embedding distribution favorable to single-particle PL experiments) was achieved by using a mixture of the monomers dodecyl methacrylate (DOMA) and α-methylene-γ-valerolactone (MeMBL) in a ratio of 1 : 1 in combination with a cross-linking agent. In this approach, DOMA ensures the dispersibility and colloidal stability of the NRs in the monomer mixture, whereas MeMBL enables the formation of sufficiently hard and non-sticky particles. Additionally, it was also possible to embed NRs in large (D = 130 nm) cross-linked PS particles which were overcoated by a PMMA shell to ensure the optical stability of the NRs. Using these two procedures also PF8-functionalized CdSe/CdS/CdS NRs were successfully encapsulated into polymer nanoparticles (**Figure 7.5**). The embedded PF8-functionalized CdSe/CdS/CdS hybrid NRs still featured a strong ET from excited PF8 to the NRs.

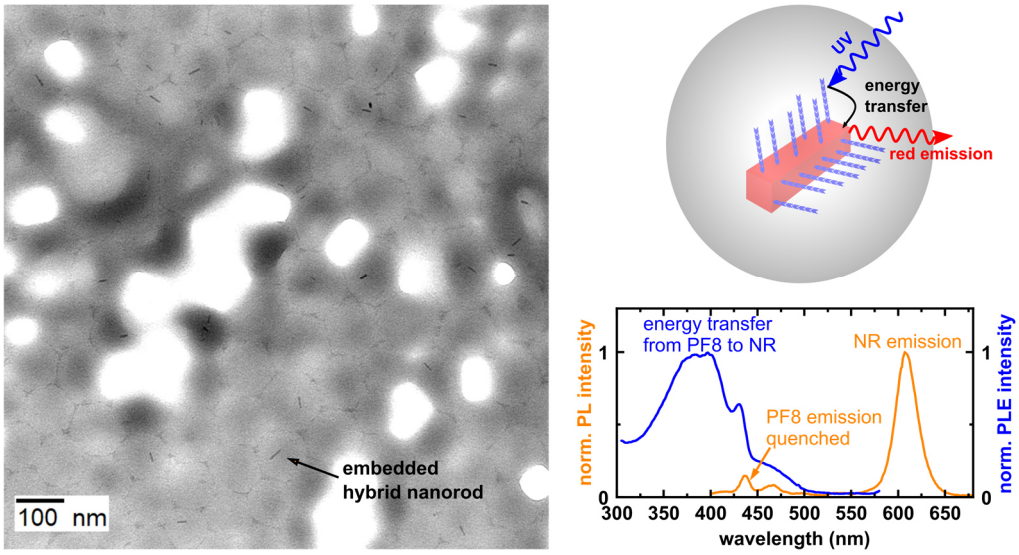

Figure 7.5. TEM image of PF8-Ph-PO(OH)$_2$ CdSe/CdS/CdS hybrid NRs embedded in PDOMA-*co*-PMeMBL nanoparticles (left). Sketch of an embedded hybrid particle (right top). Exemplary PL ($\lambda_{exc.}$ = 380 nm) and PLE ($\lambda_{det.}$ = 605 nm) spectra of a hybrid particle dispersion (right bottom).

One main goal of this research was the generation of charged CdSe-based nanocrystals for the use as single-photon source in ultrafast quantum-optical studies. CdSe/Cd$_x$Zn$_{1-x}$S graded-shell QDs encapsulated in PMMA-*co*-PEHMA particles were well suited for single-particle PL measurements and brighter than the previously employed CdSe/CdS QDs. The PL fine structure of these QDs features three distinct emissions lines (F, A1, A2), thus the typical excitonic band edge states of a neutral QD. The fundamental lowest energy transition is normally dipole-forbidden, resulting in a long fluorescence lifetime of the nanocrystal. Also, encapsulated CdSe/CdS/CdS NRs were analyzed in single-particle PL measurements. These NRs were highly emissive and showed a multi-line PL fine structure similar to the fine structure reported for graded-shell CdSe/Cd$_x$Zn$_{1-x}$S QDs. Importantly, none of the nanocrystals, which had not been functionalized with polyfluorene, featured PL characteristics associated with a charged nanocrystal.

Due to the functionalization with PF8, the PL properties of the graded-shell QDs changed fundamentally. The inorganic emitter of these hybrid QDs could be charged which was reflected in the PL fine structure of the single particles (**Figure 7.6 a**). The PL spectrum before the charging process shows three distinct emission lines (F, A1, A2), which are typical for a neutral emitter. After charging, the PL spectrum exhibits a single PL emission line (X^-) which indicates the formation of a CdSe trion. Moreover, an increase in the PL intensity and a tremendous fluorescence lifetime shortening were observed which additionally corroborate the formation of a CdSe emitter in the trion state.

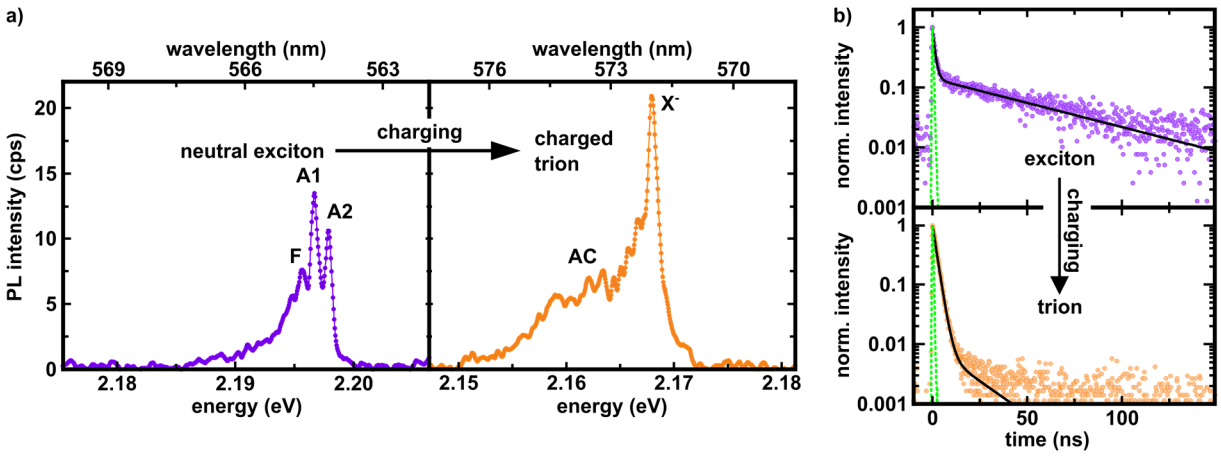

Figure 7.6. a) Highly resolved PL spectra (T = 4.2 K, $\lambda_{exc.}$ = 532 nm, $P_{exc.}$ = 240 nW) of a polyfluorene CdSe/$Cd_xZn_{1-x}S$ hybrid QD in the neutral (left) and charged state (right.) b) PL decay (data points, T = 4.2 K, excitation 0.1 eV above QD emission energy) of a neutral (top) and charged (bottom) PF8 CdSe/$Cd_xZn_{1-x}S$ hybrid QD. Comparing the PL decay of a charged and uncharged QD reveals a tremendous lifetime shortening of the prominent contribution to the PL decay upon charging. Black lines = biexponential fit; green dotted line = instrument response function.

We attribute the charging process to an electron transfer from the conjugated polymer PF8 to the inorganic emitter. This process can be triggered by additionally exciting the polymer with UV light (electron transfer from PF8 conduction band (CB) to QD CB) or by a resonant excitation of the QD (hole transfer by tunneling from the QD's valence band (VB) to the VB of the polymer). Due to the formation of a trion state, the fundamental optical recombination became dipole-allowed, which was reflected, as anticipated, in an increase in the PL intensity and a shortened fluorescence lifetime of the nanocrystals (**Figure 7.6**).

The charging of the inorganic emitter was not only be witnessed for quasi-spherical hybrid QDs, but also for anisotropic encapsulated CdSe/CdS/CdS polyfluorene hybrid NRs (**Figure 7.7**). The highly resolved PL spectra of these hybrid NRs feature a PL fine structure consisting of a single emission line (X^-), which indicates the presence of charged emitters. Preliminary studies revealed that all of the analyzed nanorods were charged even without additional illumination with UV light and no discharging processes have been observed, so far. Moreover, the charged nanorods showed a very stable emission (no 'dark' periods), only a minimal fluctuation in the emission wavelength and a higher PL intensity as compared to the quasi-spherical hybrid QDs.

In conclusion, it was proven that tethering conjugated polymer chains to inorganic semiconductor nanoparticles can indeed unlock new properties of the inorganic emitter (here: formation of trion states). These novel hybrid nanocrystals are an interesting

material for the use as single-photon sources in potential future ultrafast quantum-optical applications such as quantum computers or ultrafast single-photon amplifiers.

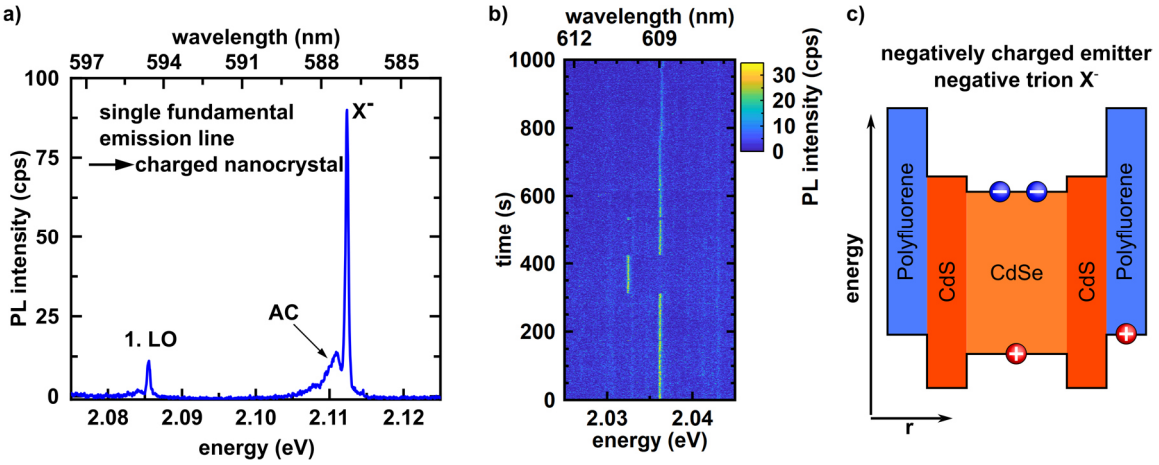

Figure 7.7. a) Highly resolved PL spectrum ($\lambda_{exc.}$ = 532 nm, $P_{exc.}$ = 509 nW, T = 4 K) of an encapsulated polyfluorene CdSe/CdS/CdS hybrid nanorod. The single emission line (X^-) with the related phonon replica indicates the presence of a charged emitter. b) PL time trace of a charged nanorod demonstrating the stability of the emission (single emission line) over time. c) Schematic illustration of the negatively charged and excited CdSe/CdS nanocrystal which was presumably formed by a charge transfer between the conjugated polymer and the inorganic emitter and excitation of the nanocrystal.

8 Appendix

8.1 Synthesis of Multi-Shell Semiconductor Nanocrystals

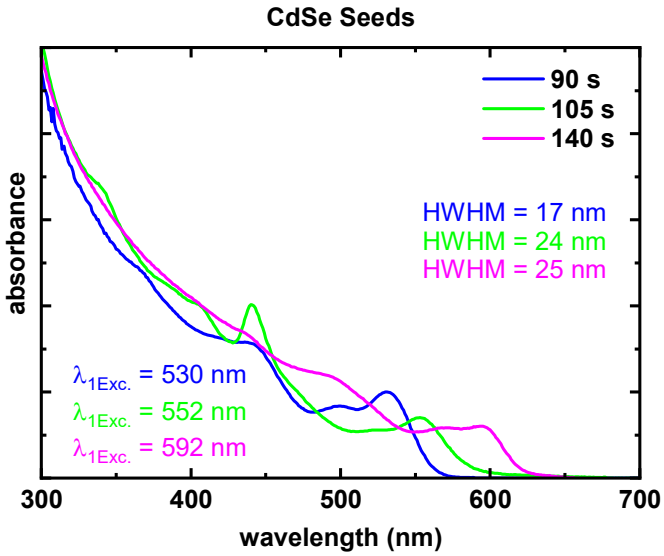

Figure 8.1. Absorption spectra of CdSe QDs synthesized according to the method by Manna and co-workers[4] with removal of water after the complexation of CdO. The removal of water led to a broadening of the particle size distribution and a slower growth of the particles. HWHM is the half width at half maximum on the low energy side of the first exciton transition peak.

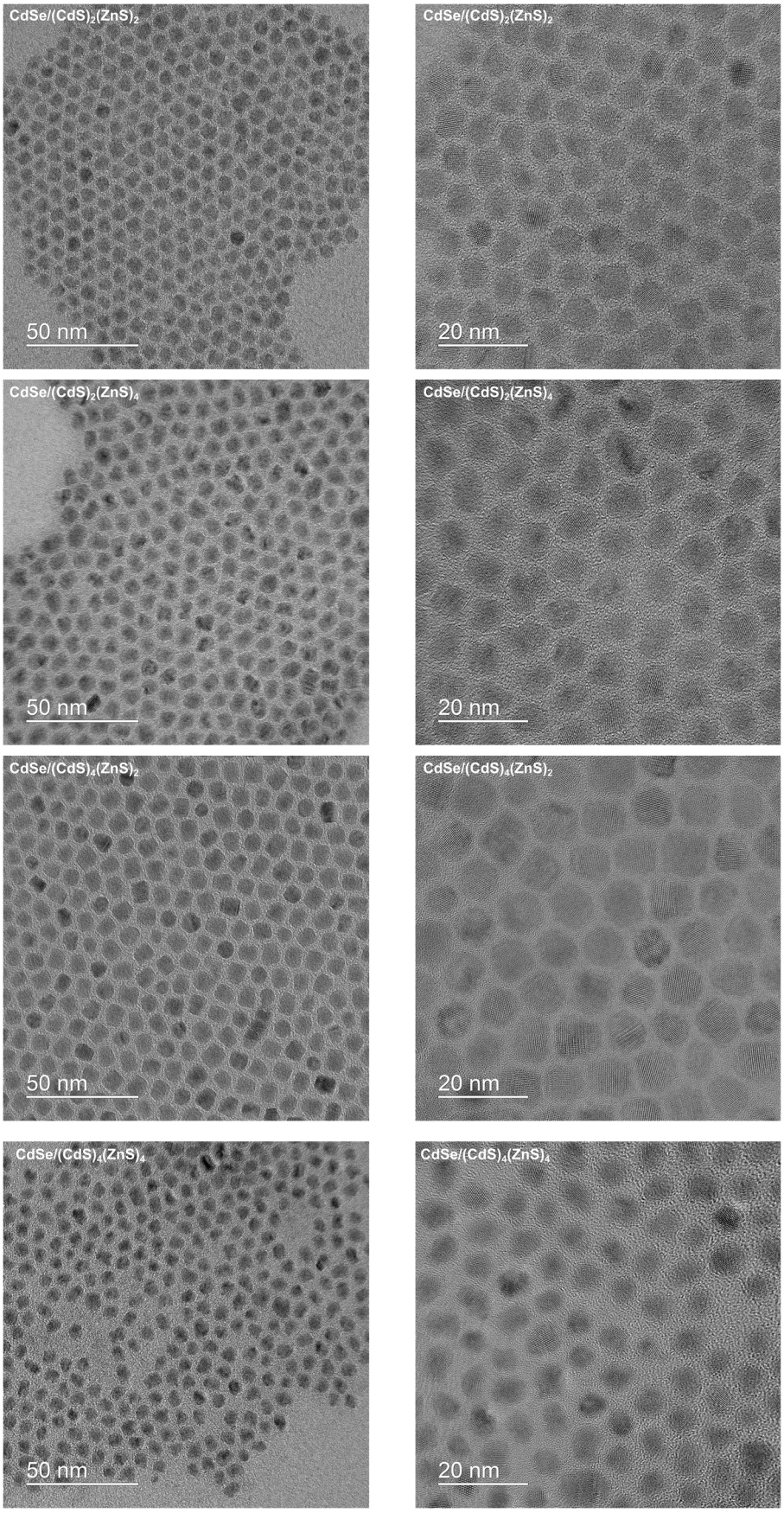

Figure 8.2. High-magnification (100000x left and 200000x right) TEM images of $CdSe/(CdS)_x(ZnS)_y$ QDs.

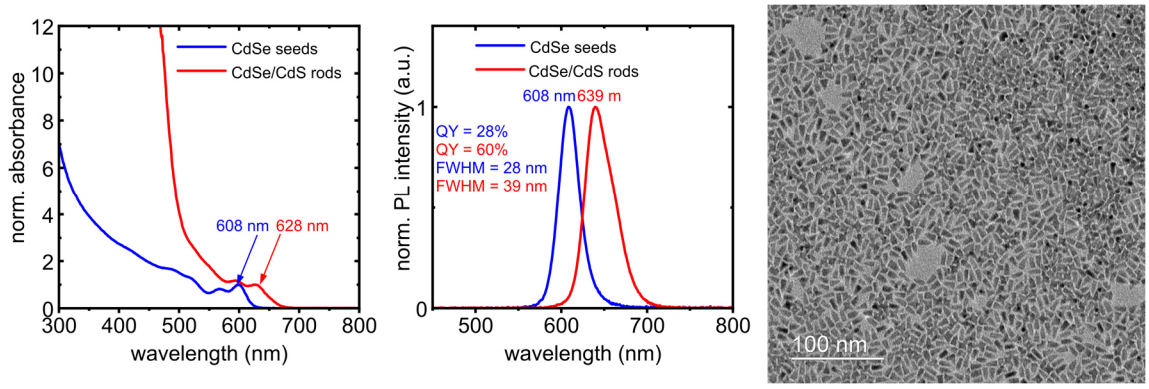

Figure 8.3. Absorption, photoluminescence ($\lambda_{exc.}$ = 380 nm) and TEM images of CdSe/CdS NRs which were synthesized by employing CdSe seeds which were prepared according to method A (**Scheme 3.1**).

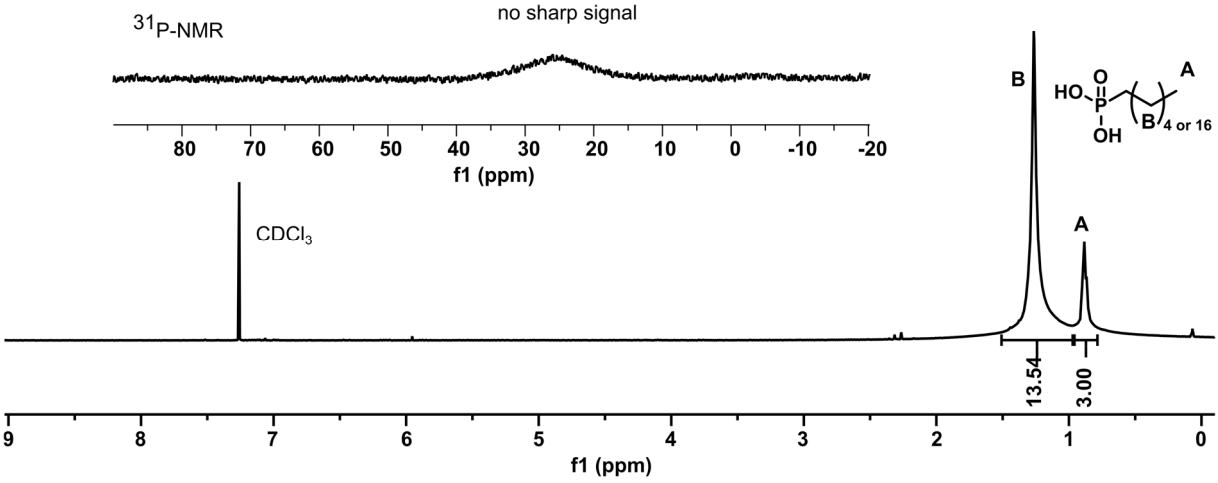

Figure 8.4. ^{1}H-NMR (400 MHz, 300 K, $CDCl_3$) (bottom) and $^{31}P\{^{1}H\}$-NMR (162 MHz, 300 K, $CDCl_3$) of CdSe/CdS NRs. Unbound phosphonic acids would show a sharp signal in the phosphorus NMR spectrum; therefore, it can be concluded that the phosphonic acids are completely bound to the nanorods.

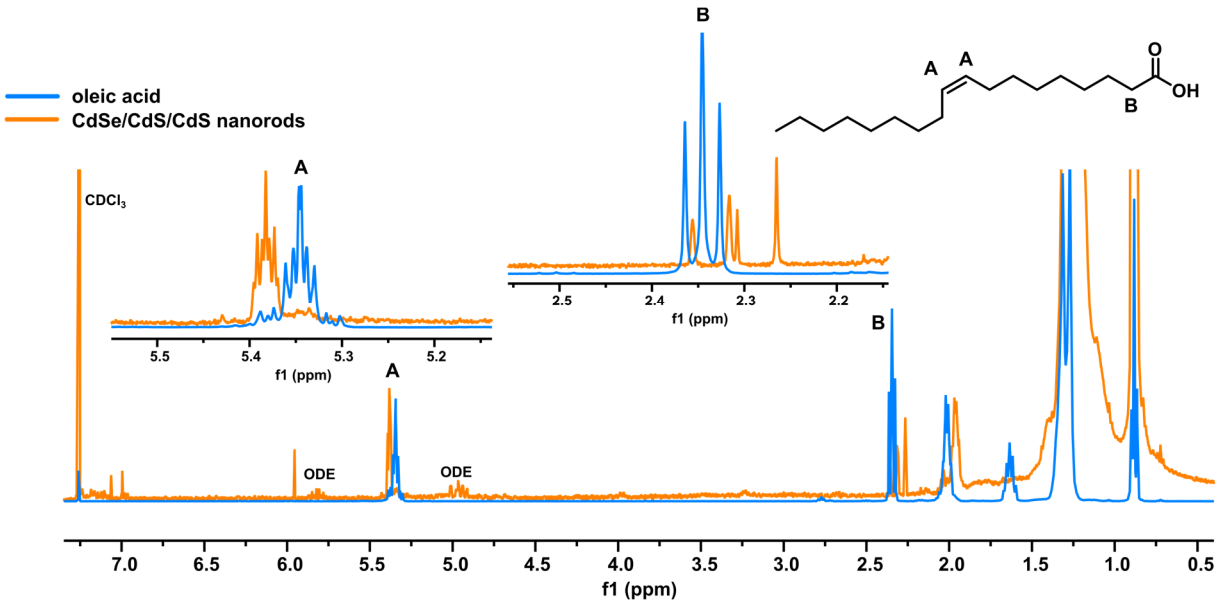

Figure 8.5. ^{1}H-NMR (400 MHz, 300 K, $CDCl_3$) spectra of CdSe/CdS/CdS NRs, and oleic acid for comparison. The increased chemical shift of the olefinic protons (marked with A) and the disappearance of the triplet signal of the α-protons next to the carboxylic acid group (marked with B) indicate that the oleic acid is bound to the nanocrystals.

8.2 Heterodifunctional Conjugated Polymers: Additional NMR, MALDI-ToF MS Spectra and GPC Traces

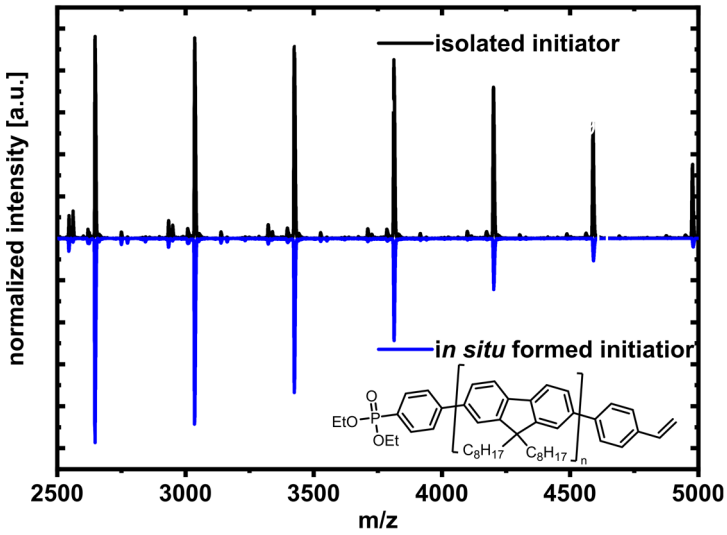

Figure 8.6. MALDI-TOF MS spectra of polyfluorene Phos-PF8-Sty synthesized by an isolated initiator (top, experiment 1, **Table 4.1**) and by an *in situ* formed initiator (bottom, experiment 2, **Table 4.1**). The main signals arise from the polymer shown. Both polymers are quantitatively double functionalized with the expected groups. Reprinted with permission from ref.[5] Copyright **2019** American Chemical Society.

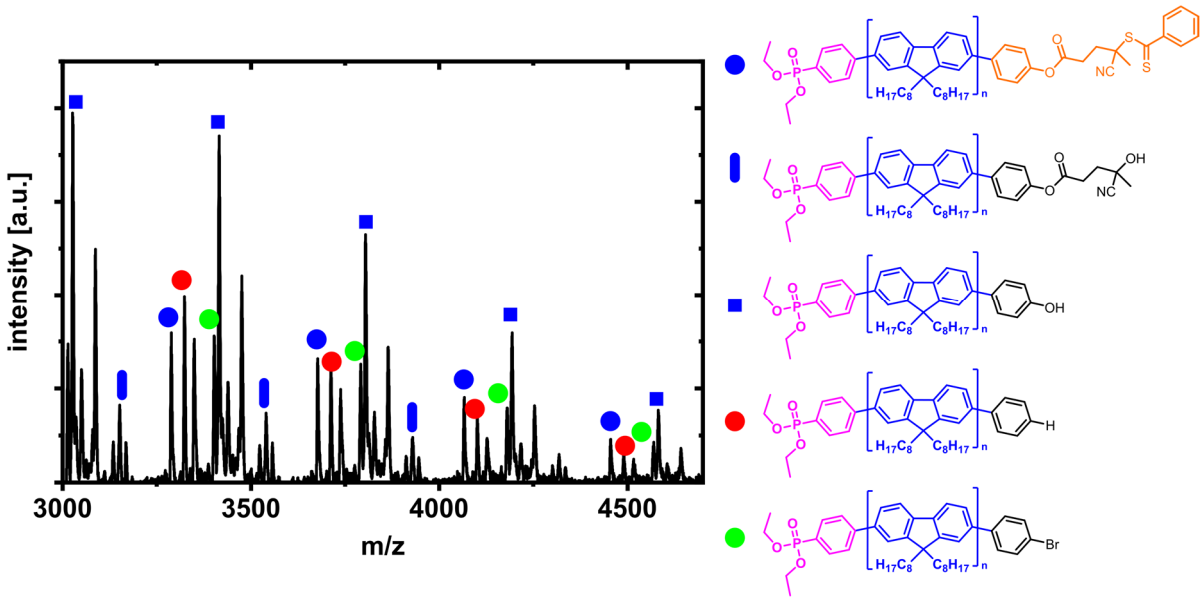

Figure 8.7. MALDI-TOF MS spectrum of Phos-PF8-Dithioester obtained in experiment 4, **Table 4.1**. Assigned peaks are labelled.

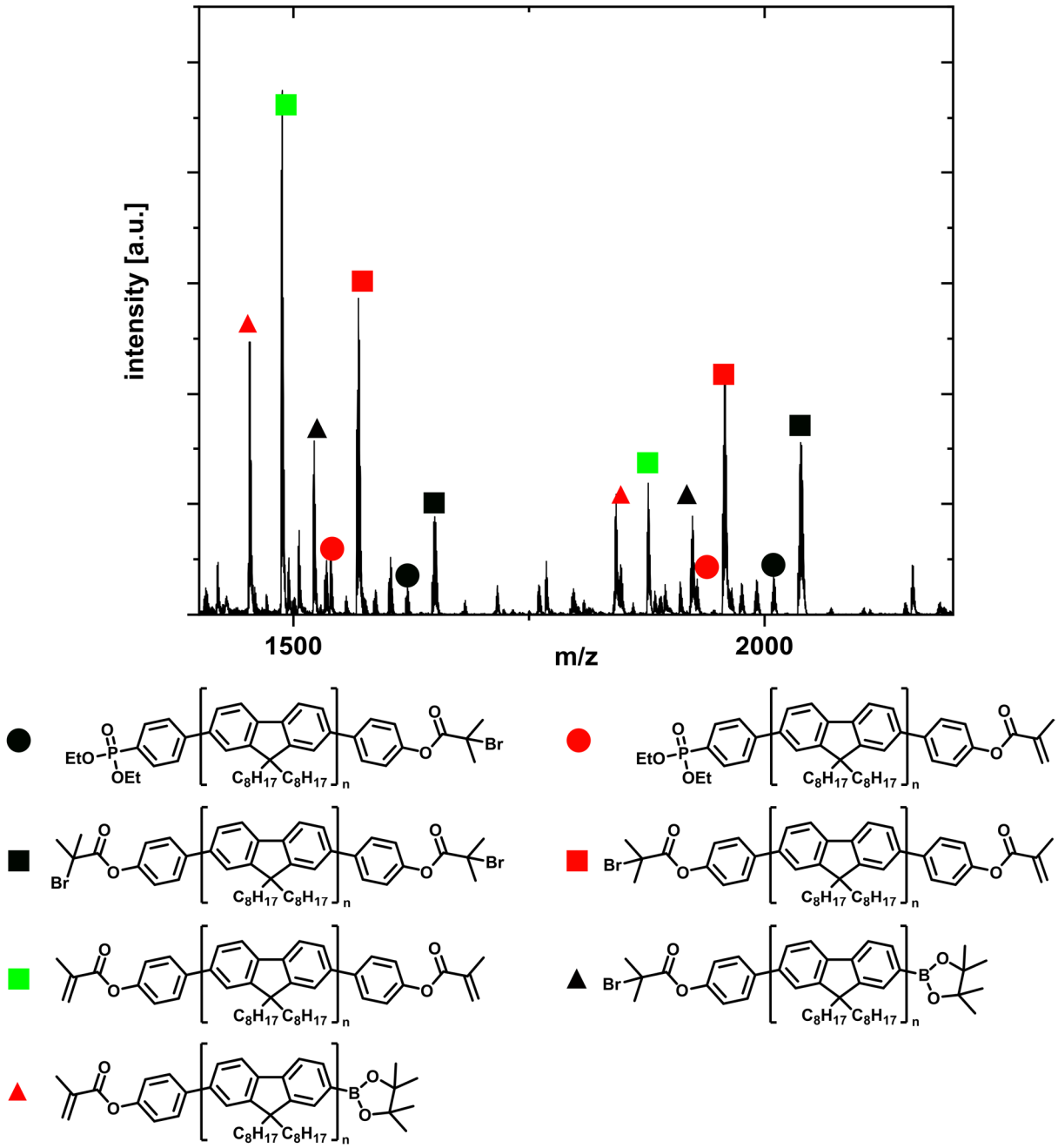

Figure 8.8. MALDI-TOF mass spectrum of Phos-PF8-AlkylBr obtained in experiment 7 (**Table 4.1**). The polymer was synthesized using the *in situ* Pd initiator system (**Ini2**) and CsF as base for activation and polymerization. Most chains lack a phosphonate terminus which evidences that bromo(4-diethoxyphosphoryl-phenyl)(tri-*tert*-butylphosphine)palladium (II) was only formed in a low yield and most chains were initiated from monomer-derived initiators. Also, the yield of the polymerization was low (~ 20%). Reprinted with permission from ref.[5] Copyright **2019** American Chemical Society.

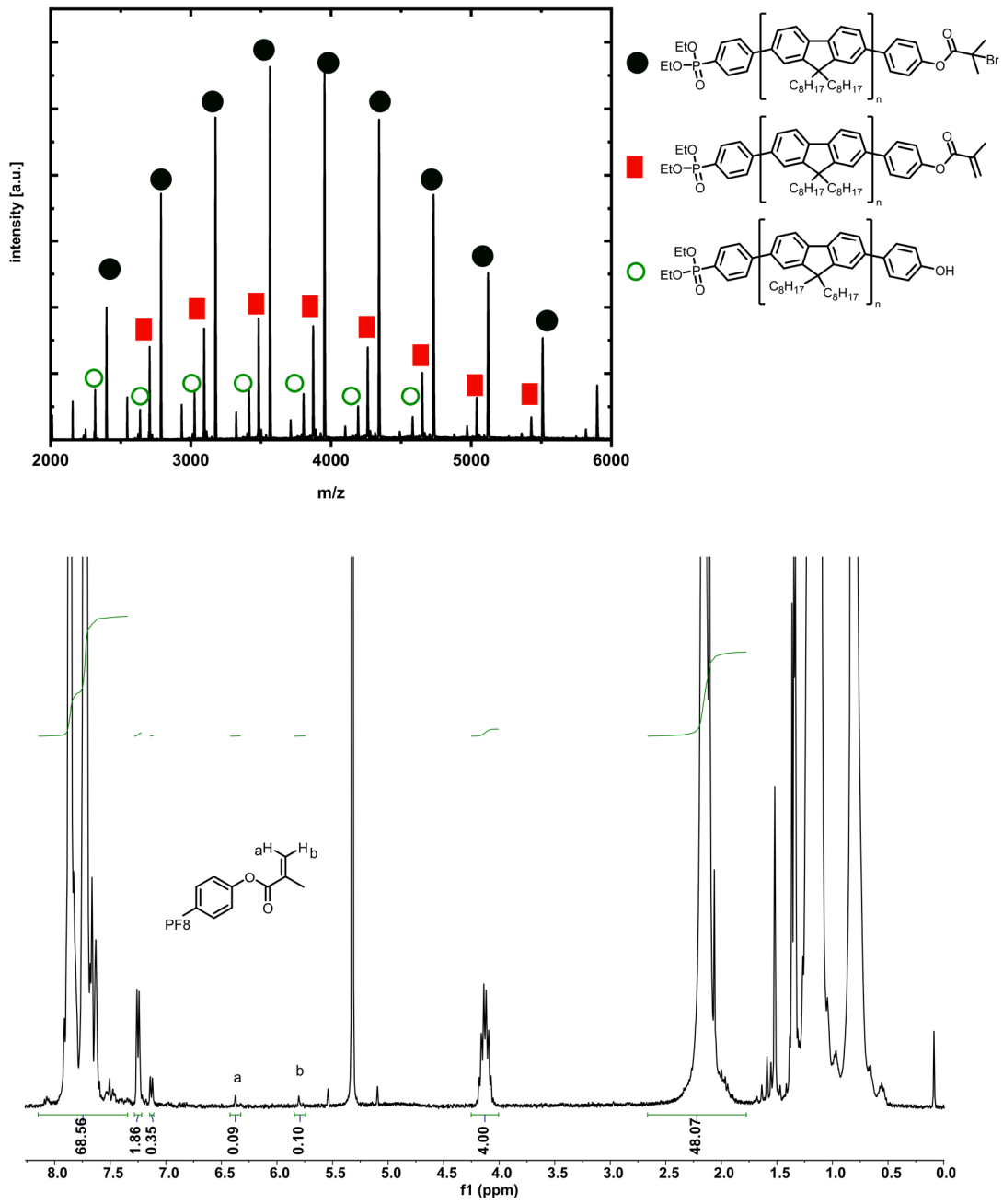

Figure 8.9. MALDI-TOF mass spectrum (top) and ^{1}H NMR (400 MHz, CD_2Cl_2, 300 K) spectrum (bottom) of the polyfluorene Phos-PF8-AlkylBr obtained from experiment 8 (**Table 4.1**) which was end-capped overnight using K_2CO_3 as base. All chains bear a phosphonate moiety, but the alkylbromide moiety was partially degraded by elimination and ester hydrolysis. Reprinted with permission from ref.[5] Copyright **2019** American Chemical Society.

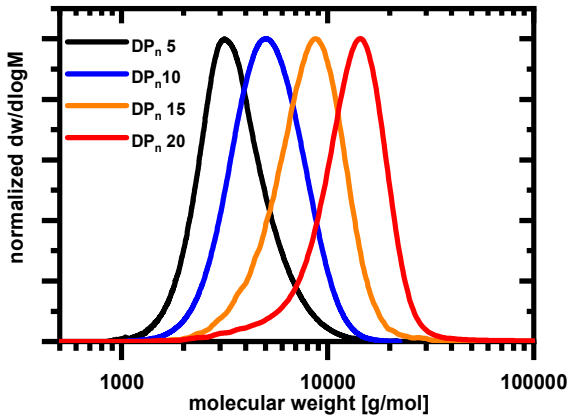

Figure 8.10. Molecular weight distributions (determined by GPC) for Phos-PF8-AlkylBr macroinitiators with different chain lengths (experiments 9–12, **Table 4.1**). The poly dispersity index is below 1.2 for all polymers shown. Reprinted with permission from ref.[5] Copyright **2019** American Chemical Society.

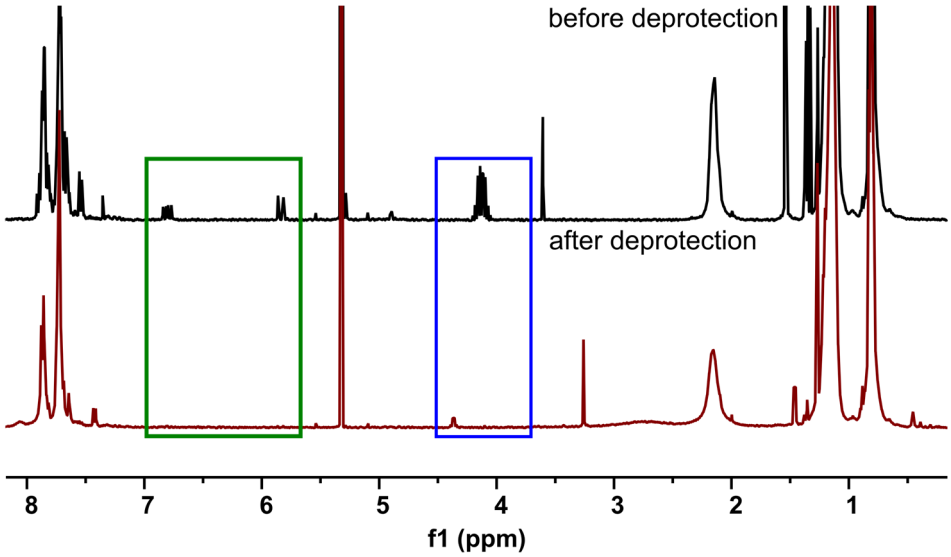

Figure 8.11. ^{1}H NMR (400 MHz, CD_2Cl_2, 300 K) spectra of the polymer Phos-PF8-Sty before and after deprotection with TMS-Br. During the deprotection not only the signals of the P-O-**CH_2**-CH_3 group (blue rectangle) have vanished but also the olefinic signals (green rectangle) have disappeared.

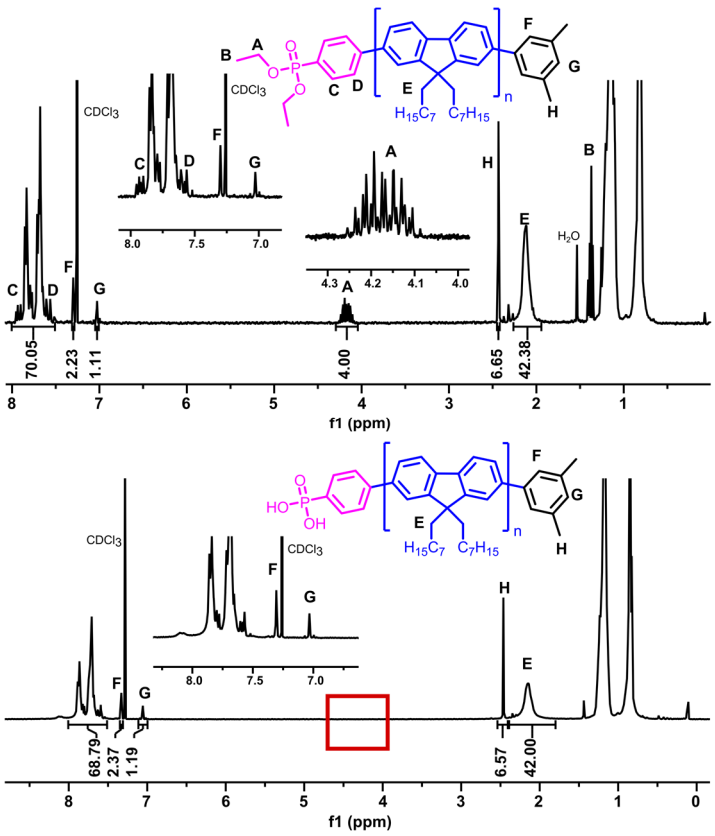

Figure 8.12. ^{1}H NMR (400 MHz, $CDCl_3$, 300 K) spectra of the polyfluorene Phos-Ph-PF8 (top) and the deprotected polymer PF8-Ph-PA (bottom). A complete deprotection of the diethyl phenylphosphonate moiety is proven by the disappearance of the signals of the P-O-**CH_2**-CH_3 group (red rectangle).

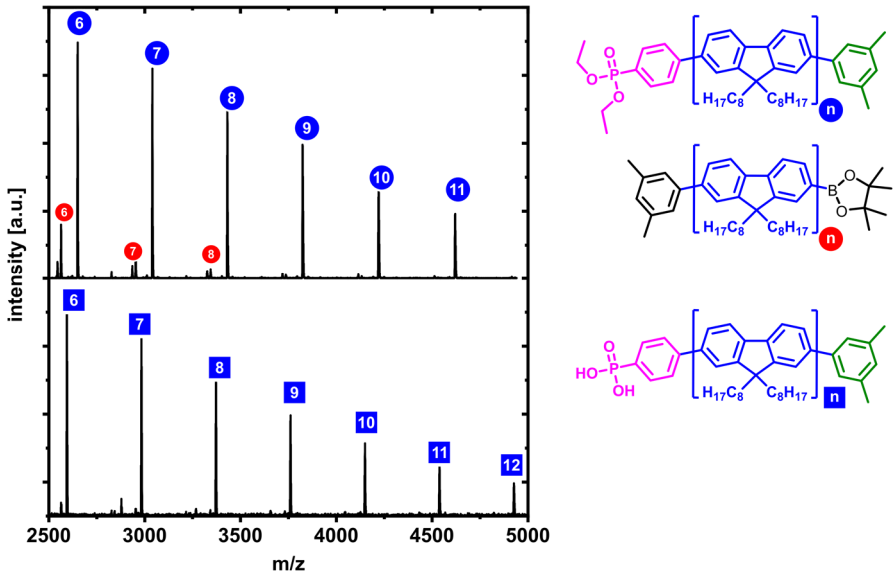

Figure 8.13. MALDI-TOF mass spectra of the polyfluorene Phos-Ph-PF8 (top) and the deprotected polymer PF8-Ph-PA (bottom).

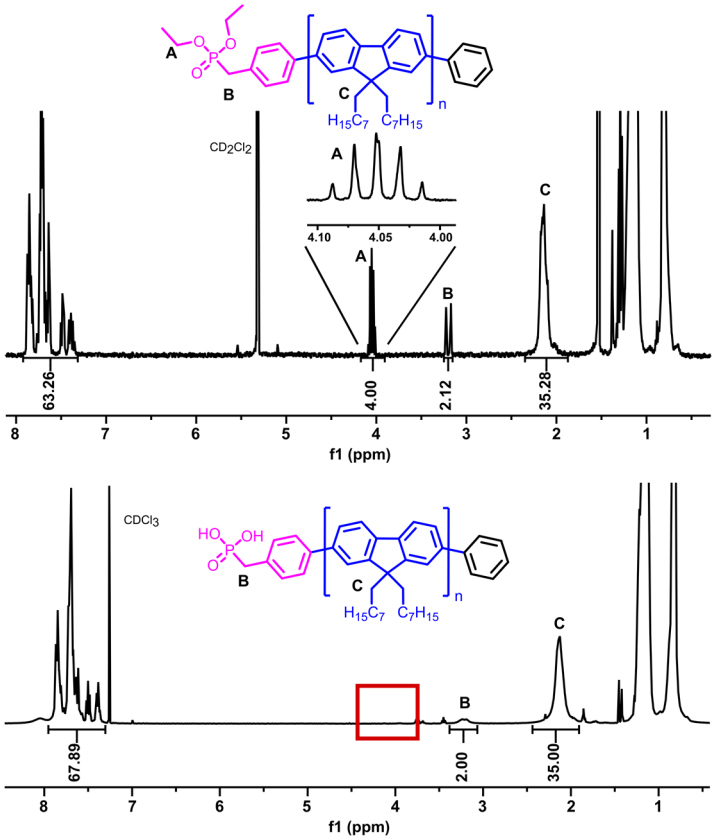

Figure 8.14. ^{1}H NMR (400 MHz, CD_2Cl_2 resp. $CDCl_3$, 300 K) spectra of the polyfluorene Phos-Bn-PF8 (top) and the deprotected polymer PA-Bn-PF8 (bottom). A complete deprotection of the diethyl benzylphosphonate moiety is proven by the disappearance of the signals of the P-O-**CH_2**-CH_3 group (red rectangle).

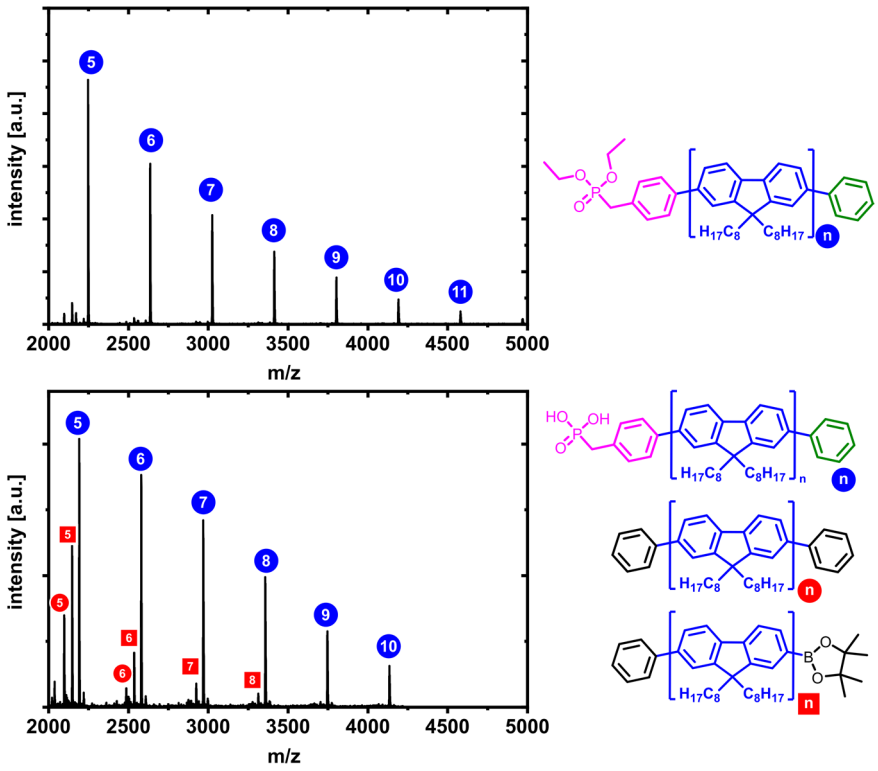

Figure 8.15. MALDI-TOF mass spectra of the polyfluorene Phos-Bn-PF8 (top) and the deprotected polymer PA-Bn-PF8 (bottom). Note, that the intensity of phosphonic acid-functionalized polymers is often underrepresented in MALDI-TOF mass spectra.

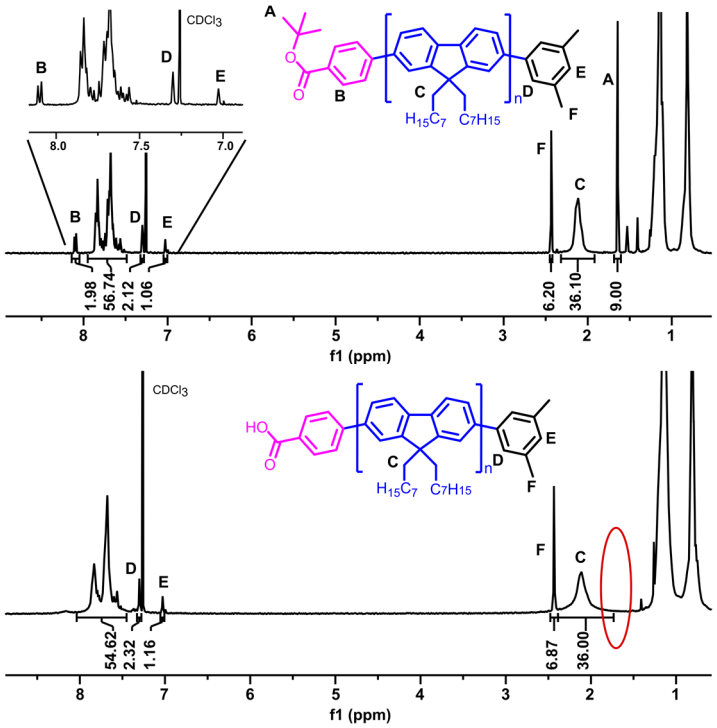

Figure 8.16. ^{1}H NMR (400 MHz, $CDCl_3$, 300 K) spectra of the polyfluorene COO^{t}Bu-Ph-PF8 (top) and the deprotected polymer COOH-Ph-PF8 (bottom). A complete deprotection of the carboxylic ester moiety is proven by the disappearance of the signals of the C-O-C(**CH**$_3$)$_3$ group (red oval).

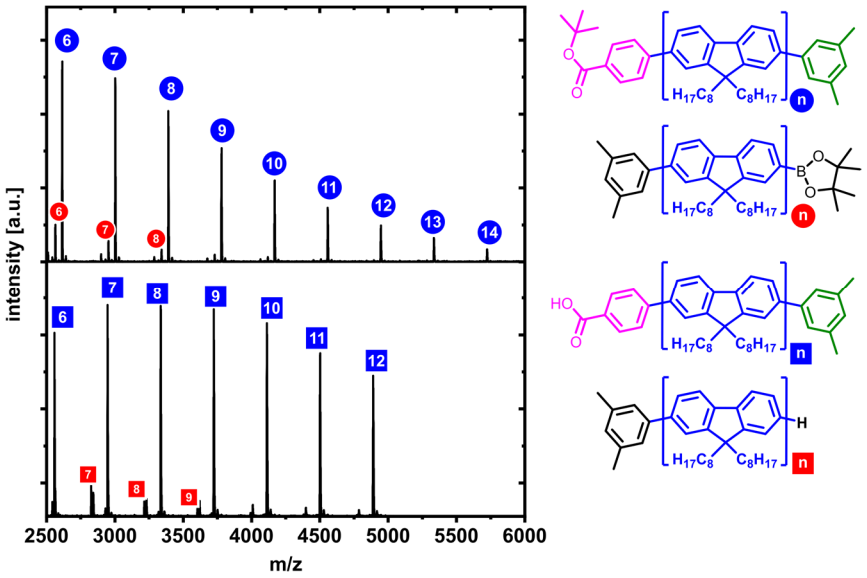

Figure 8.17. MALDI-TOF mass spectra of the polyfluorene COO^{t}Bu-Ph-PF8 (top) and the deprotected polymer COOH-Ph-PF8 (bottom).

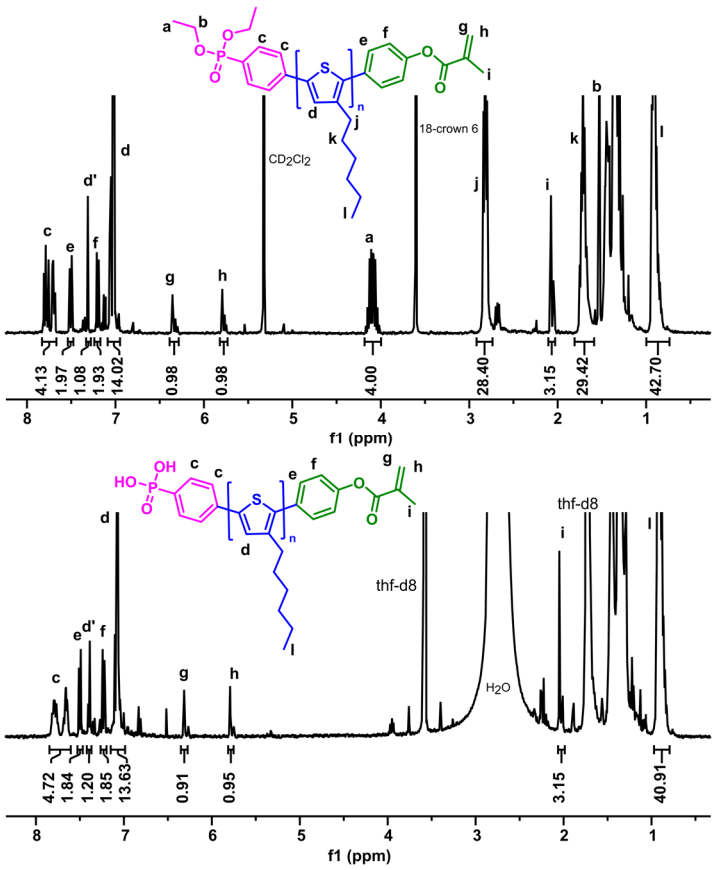

Figure 8.18. ^{1}H-NMR (400 MHz, 300 K, CD_2Cl_2 or thf-d8) spectra of the polythiophene Phos-P3HT-MA (top) and the deprotected polymer PA-P3HT-MA (bottom).

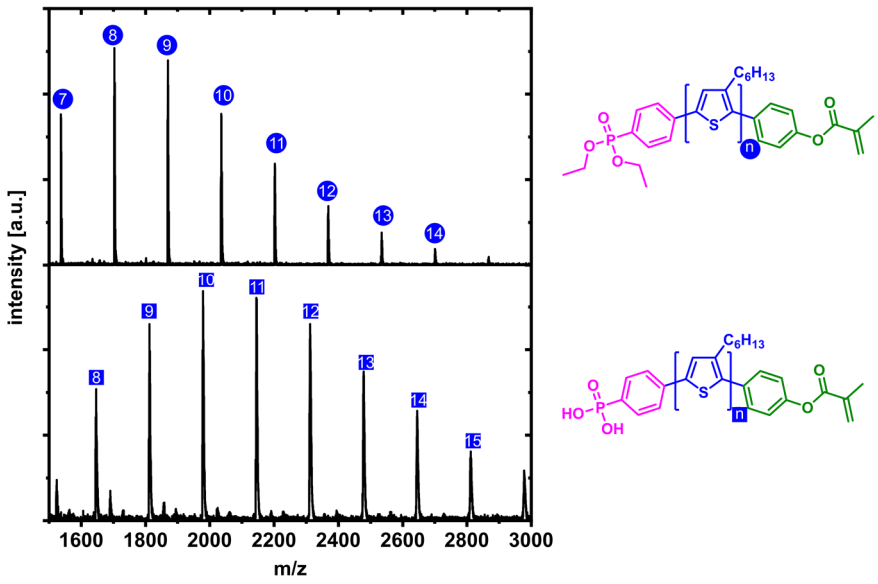

Figure 8.19. MALDI-TOF mass spectra of the polythiophene Phos-P3HT-MA (top) and the deprotected polymer PA-P3HT-MA (bottom).

8.3 Synthesis of Conjugated Nonconjugated Diblock Copolymers: Selected NMR Spectra

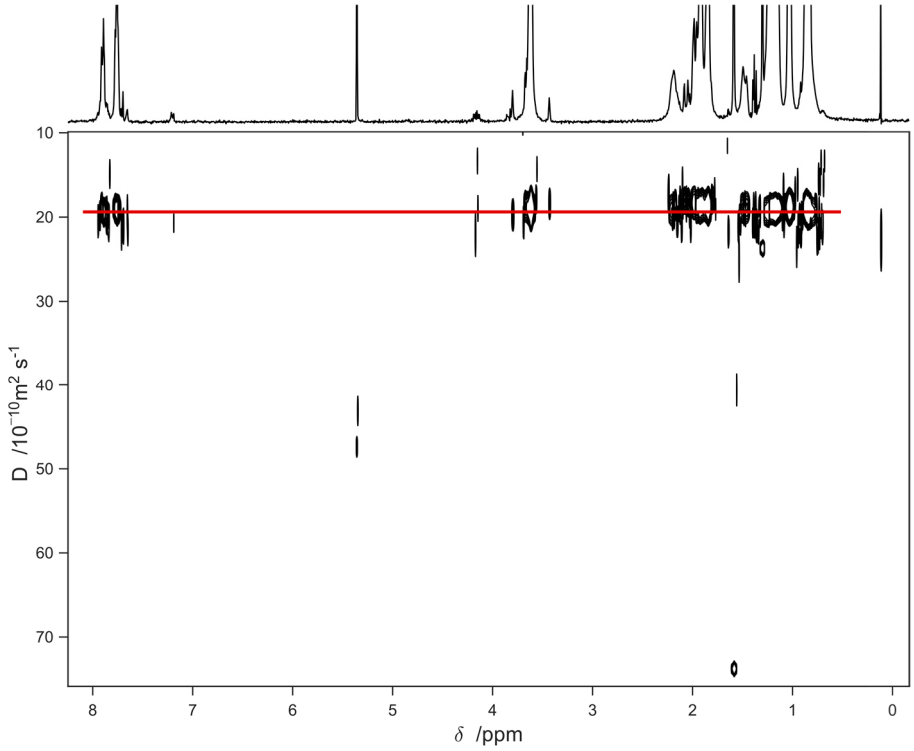

Figure 8.20. Exemplary DOSY NMR spectrum (400 MHz, CD_2Cl_2, 300 K) of Phos-PF8-*b*-PMMA. The red line serves as a guide to the eye to show that all signals arising from the polymer have the same diffusion coefficient. Reprinted with permission from ref.[5] Copyright **2019** American Chemical Society.

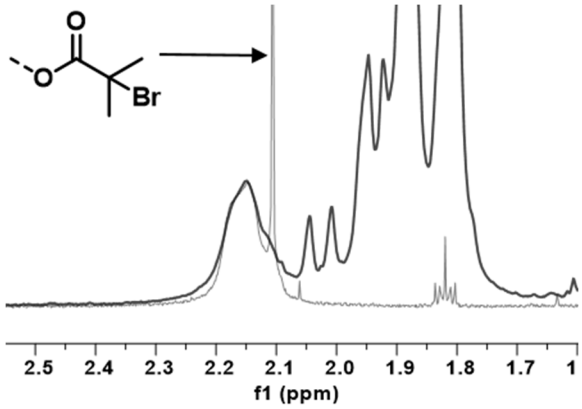

Figure 8.21. Comparison between the ^{1}H NMR spectra (400 MHz, $CDCl_3$, 300 K) of the Phos-PF8-AlkylBr macroinitiator (gray) and the Phos-PF8-*b*-PMMA diblock copolymer (black). The singlet at 2.11 ppm corresponding to the methyl groups of the ATRP initiator moiety is absent in the spectrum of the block copolymer, which evidences the complete consumption of the macroinitiator. Reprinted with permission from ref.[5] Copyright **2019** American Chemical Society.

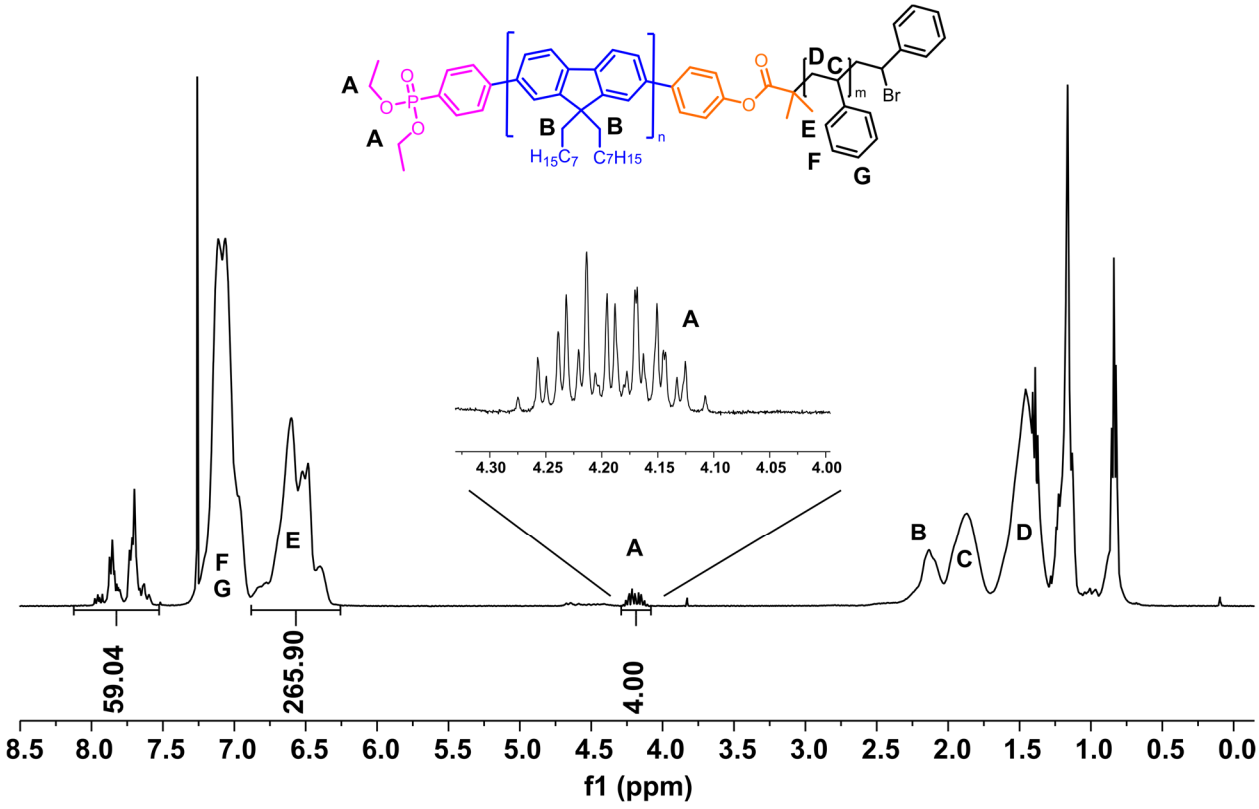

Figure 8.22. Exemplary ^{1}H NMR spectra (400 MHz, $CDCl_3$, 300 K) of the Phos-PF8-*b*-PS block copolymer obtained in experiment 7, **Table 4.2**. Reprinted with permission from ref.[5] Copyright **2019** American Chemical Society.

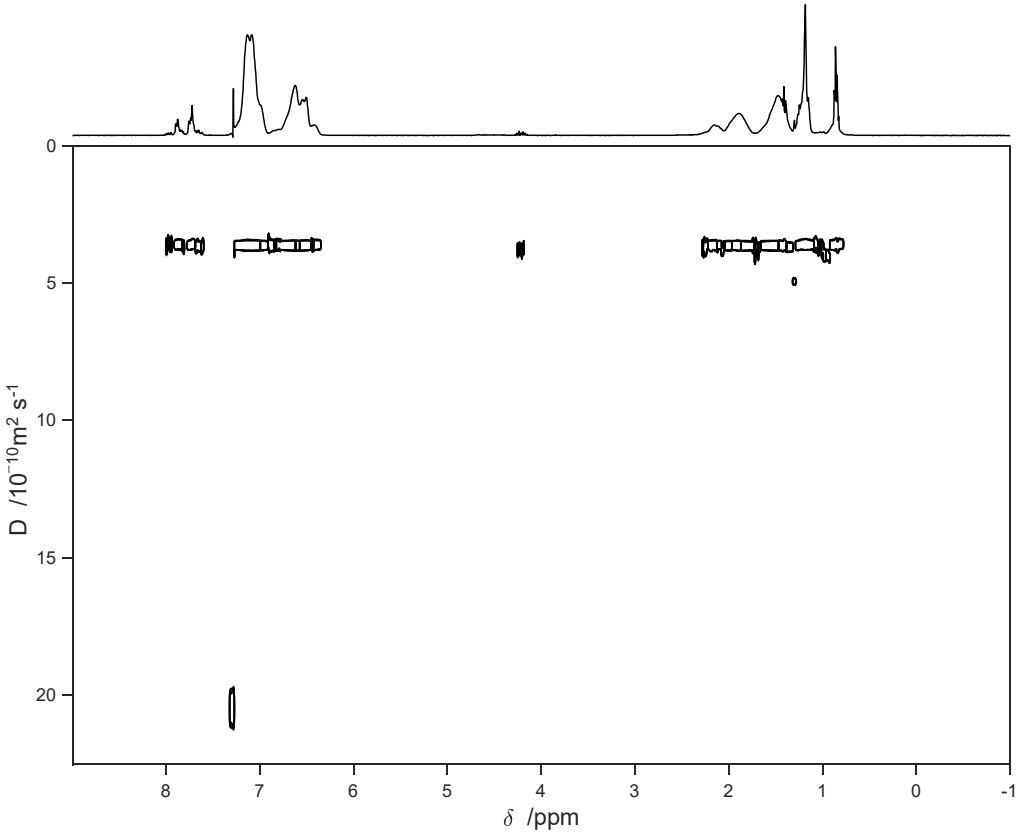

Figure 8.23. Exemplary DOSY NMR spectrum (400 MHz, $CDCl_3$, 300 K) of a Phos-PF8-*b*-PS diblock copolymer. Reprinted with permission from ref.[5] Copyright **2019** American Chemical Society.

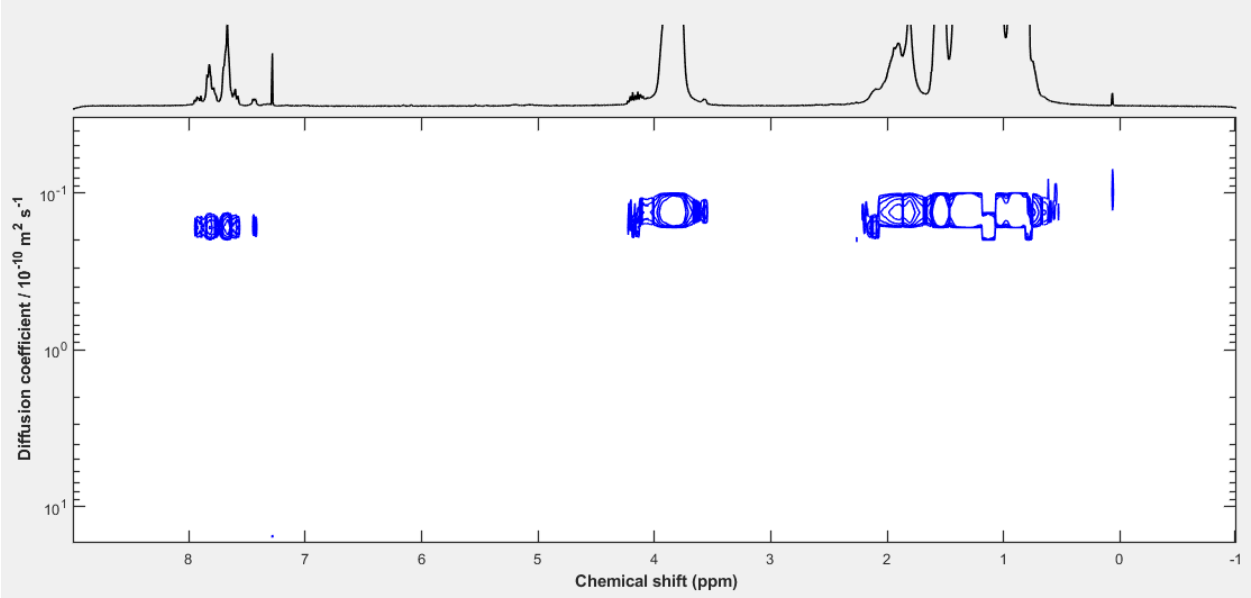

Figure 8.24. Exemplary DOSY NMR spectrum (400 MHz, $CDCl_3$, 300 K) of a Phos-PF8-*b*-PEHMA diblock copolymer. Reprinted with permission from ref.[5] Copyright **2019** American Chemical Society.

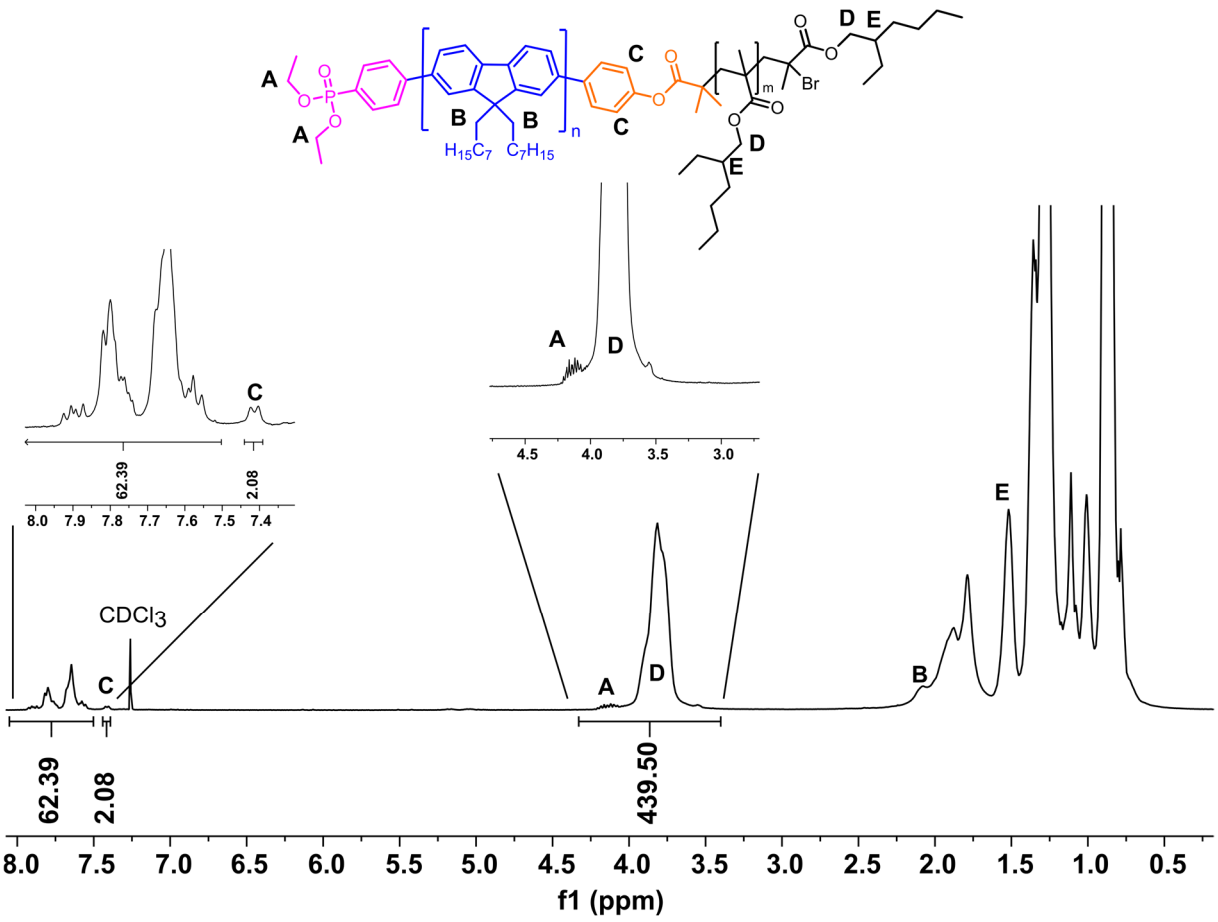

Figure 8.25. ^{1}H NMR spectrum (400 MHz, $CDCl_3$, 300 K) of the diblock copolymer Phos-PF8-*b*-PEHMA obtained in entry 11, **Table 4.2**. The number of EHMA-derived units per chains was calculated by setting the integral of the aromatic backbone to the same value as in the macroinitiator. The integral of protons D was obtained by subtraction of 4 from the combined integral of A and D and divided by 2 to yield the number of EHMA units per PF8 chain. Reprinted with permission from ref.[5] Copyright **2019** American Chemical Society.

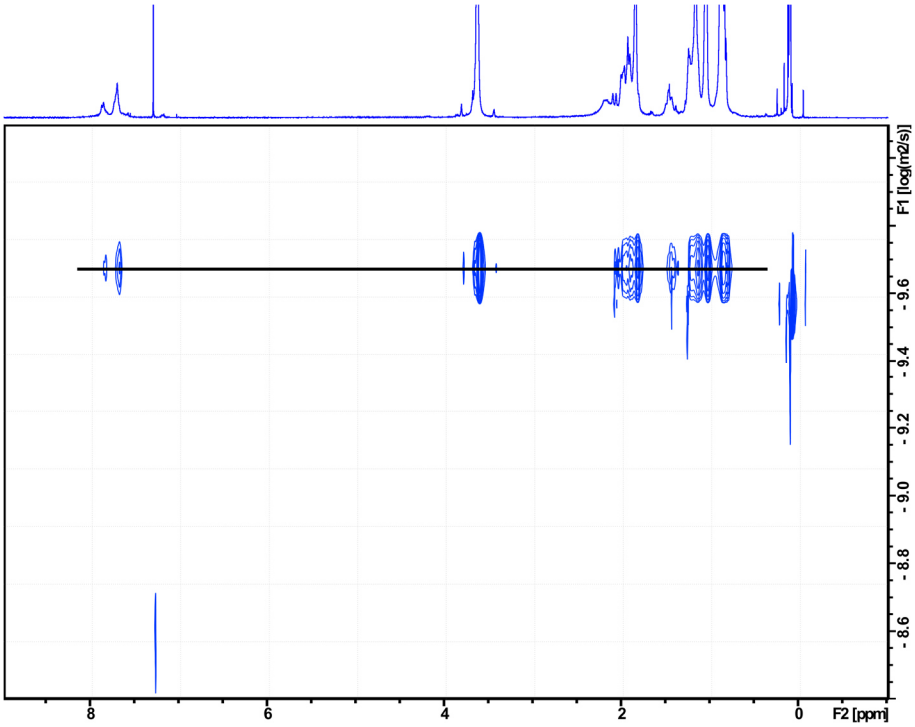

Figure 8.26. Exemplary DOSY NMR spectrum (400 MHz, $CDCl_3$, 300 K) of a deprotected PA-PF8-*b*-PMMA block copolymer. The black line serves as a guide to the eye to show that all signals belonging to the polymer have the same diffusion coefficient.

8.4 Conjugated Nonconjugated Comb Polymers: Additional NMR spectra and GPC traces

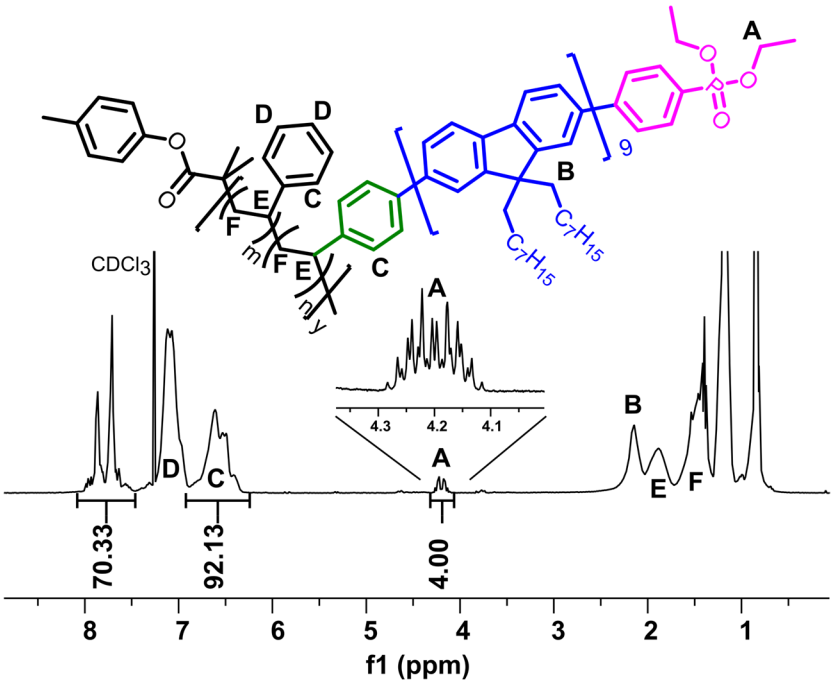

Figure 8.27. ^{1}H NMR spectrum of the comb polymer Phos-PF8-Sty-*co*-PS obtained in experiment 3, **Table 4.3.** Reprinted with permission from ref.[5] Copyright **2019** American Chemical Society.

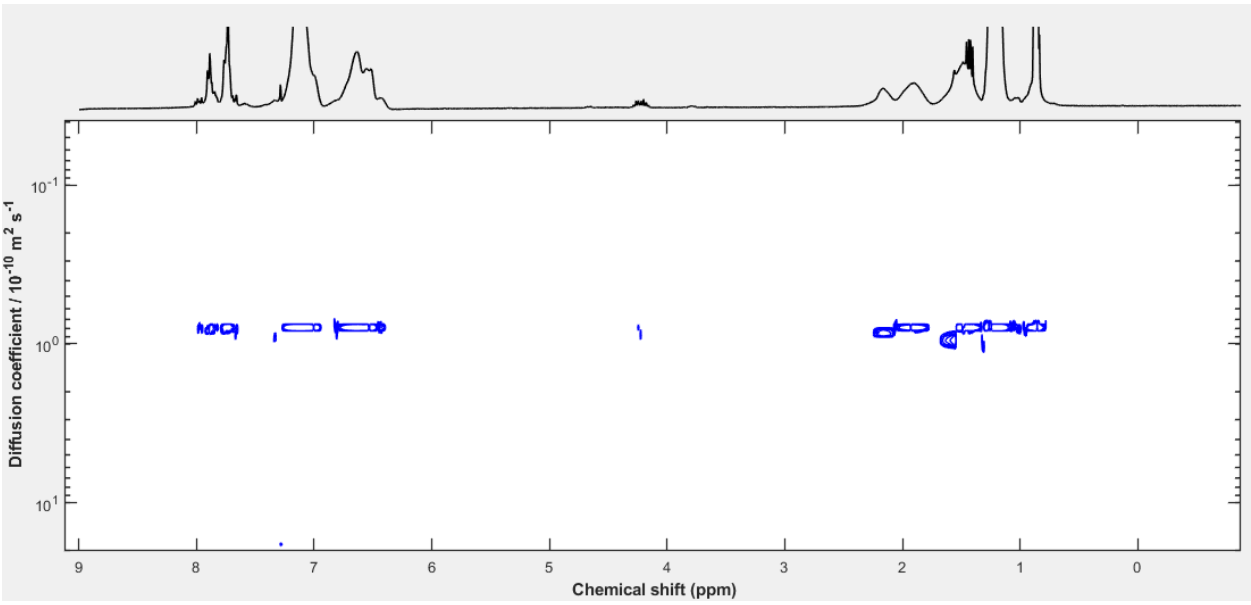

Figure 8.28. Exemplary DOSY NMR spectrum (400 MHz, $CDCl_3$, 300 K) of a Phos-PF8-Sty-*co*-PS comb polymer. Reprinted with permission from ref.[5] Copyright **2019** American Chemical Society.

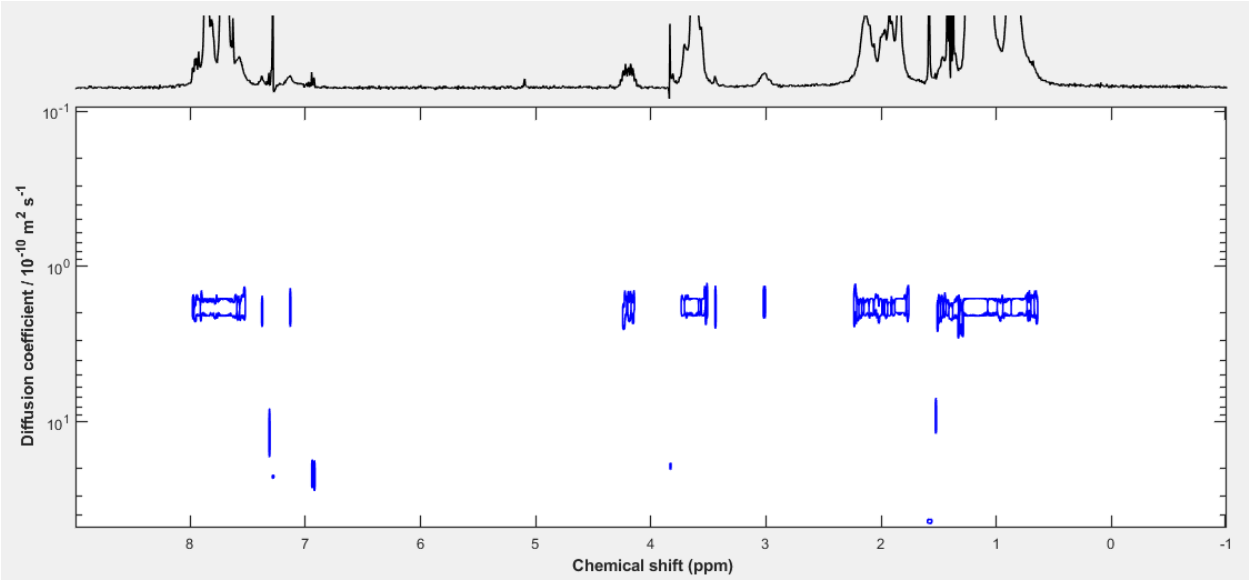

Figure 8.29. Exemplary DOSY NMR spectrum (400 MHz, $CDCl_3$, 300 K) of a Phos-PF8-Sty-*co*-PMMA comb polymer. Reprinted with permission from ref.[5] Copyright **2019** American Chemical Society.

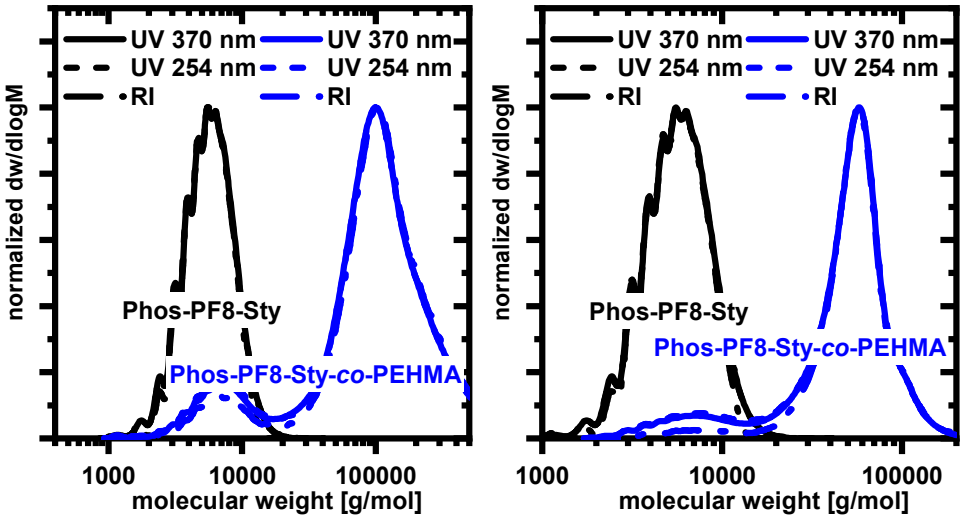

Figure 8.30. Molecular weight distribution (GPC) of random copolymers of Phos-PF8-Sty and EHMA. Left: Ratio of EHMA to Phos-PF8-Sty in the final comb polymer is 49/1 (**Table 4.3**, entry 8). Right: Ratio of EHMA to Phos-PF8-Sty in the final comb polymer is 16/1 (**Table 4.3**, entry 9). Reprinted with permission from ref.[5] Copyright **2019** American Chemical Society.

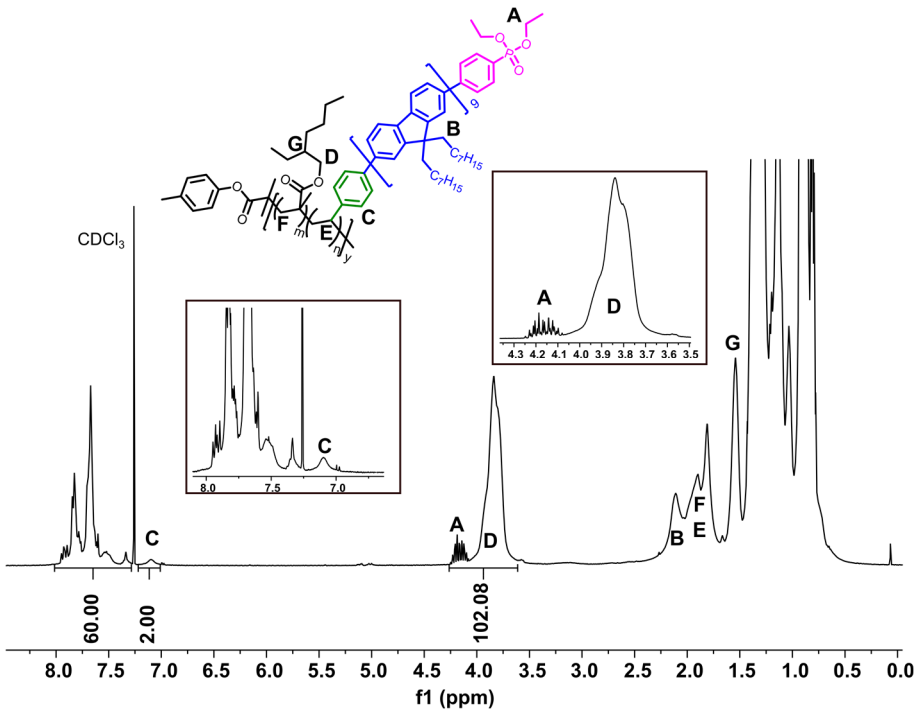

Figure 8.31. ^{1}H NMR spectrum (400 MHz, $CDCl_3$, 300 K) of the random copolymer Phos-PF8-Sty-*co*-PEHMA obtained in experiment 8 (**Table 4.3**). The ratio of EHMA units to Phos-PF8-Sty was calculated by setting the integral of the aromatic backbone to the same value as in the macroinitiator. The integral of protons D was obtained by subtraction of 4 from the combined integral of A and D and divided by 2 to yield the ratio of EHMA units to Phos-PF8 chains in the comb polymer. Reprinted with permission from ref.[5] Copyright **2019** American Chemical Society.

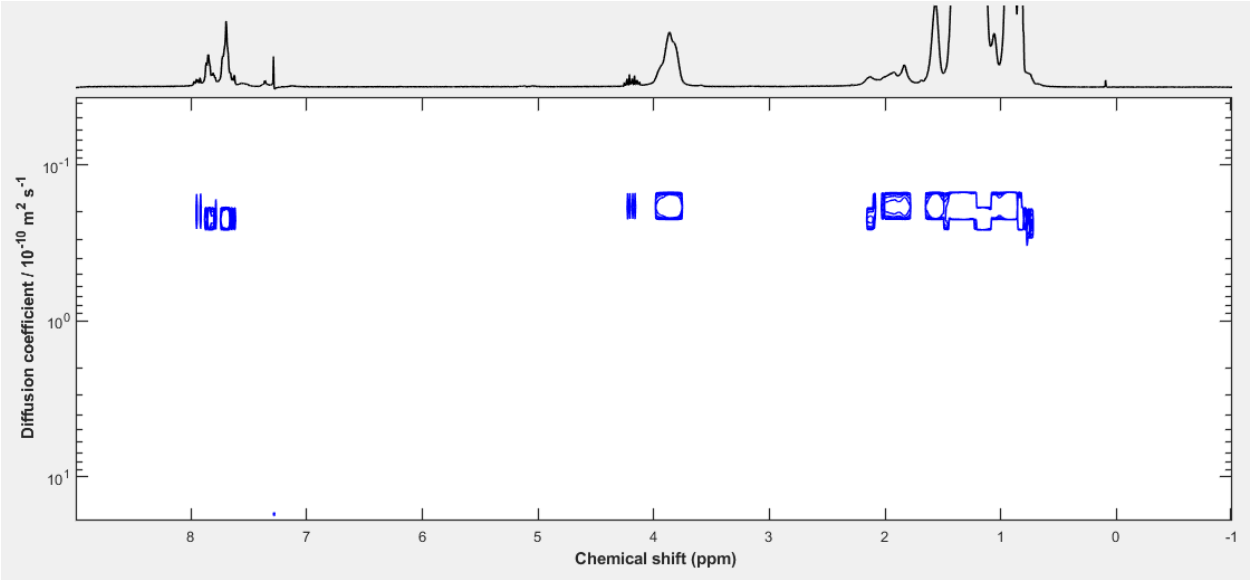

Figure 8.32. Exemplary DOSY NMR spectrum (400 MHz, $CDCl_3$, 300 K) of a Phos-PF8-Sty-*co*-PEHMA comb polymer. Reprinted with permission from ref.[5] Copyright **2019** American Chemical Society.

8.5 Hybrid Particles by a Direct Ligand Exchange: Additional Figures, Spectra, etc.

Scheme 8.1. Schematic energy levels of a PF8 CdSe/$Cd_xZn_{1-x}S$ hybrid particle. Energy levels are based on literature values.[23,24,25,281]

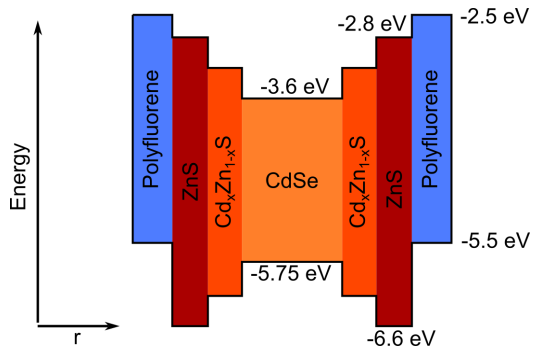

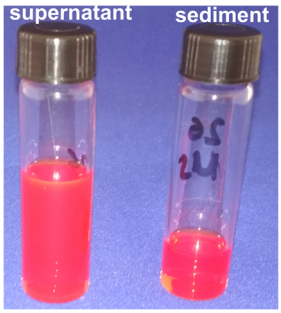

Figure 8.33. Photos of the dispersion (entry 1, **Table 5.1**) after preparative centrifugation. Left: Supernatant dispersion. Right: Sediment redispersed in toluene. As the supernatant is still deep red, indicating the presence of QDs, no quantitative separation of the (hybrid) QDs took place.

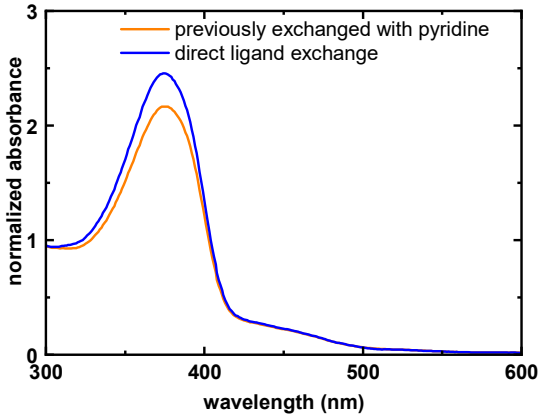

Figure 8.34. Absorption spectra of CdSe/CdS PF8 hybrid particles obtained a direct ligand exchange approach (entries 1–2, **Table 5.1**). For one sample (orange line), the native QD ligands had been exchanged with pyridine before the functionalization with PA-PF8-MA. After the ligand exchange reaction, the hybrid particles were separated from unbound PF8 by preparative centrifugation. Both spectra are normalized at a wavelength of 420 nm to the QD concentration. The PF8 is completely bound to the nanocrystals in both samples as proven by MW-AUC measurements.

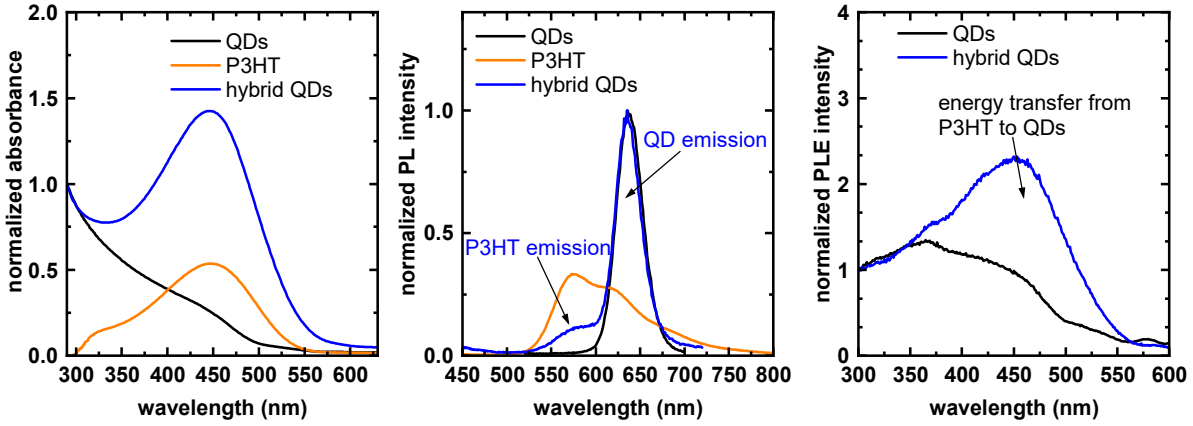

Figure 8.35. Absorption (left), photoluminescence ($\lambda_{exc.}$ = 380 nm; center) and photoluminescence excitation spectra ($\lambda_{det.}$ = 650 nm) of CdSe/CdS QDs, PA-P3HT and PA-P3HT CdSe/CdS hybrid QDs. The hybrid particles were synthesized by a direct ligand exchange reaction using 175 equiv. of P3HT vs. QDs. As the emission bands of P3HT and the QDs overlap, the hybrid QDs are not particularly suitable for high-resolution single-particle PL measurements.

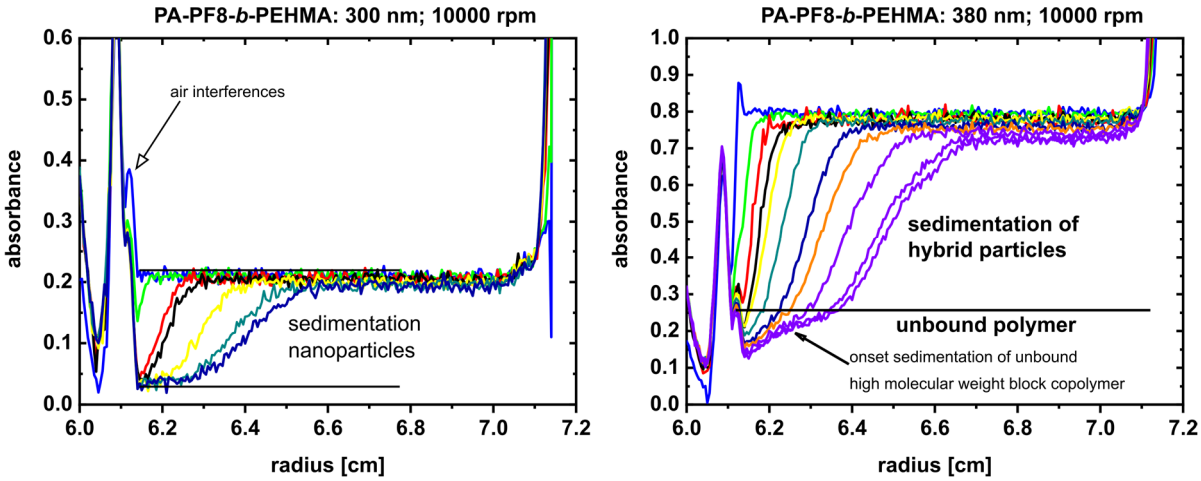

Figure 8.36. MW-AUC measurement data for the sedimentation of the PA-PF8-*b*-PEHMA hybrid particles obtained in experiment 2 (**Table 5.2**) tracked at 300 nm (left) and 380 nm (right).

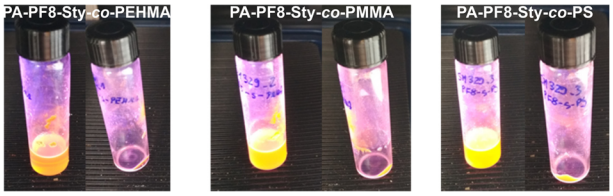

Figure 8.37. Photos under UV light illumination of the dispersion obtained in experiments 5–7, **Table 5.2**. In these experiments, the QDs were functionalized with conjugated nonconjugated comb copolymers by a direct ligand exchange reaction. In all three experiments a precipitate was formed (right photos) which could be separated from the supernatant dispersion (left) by centrifugation (5000 g).

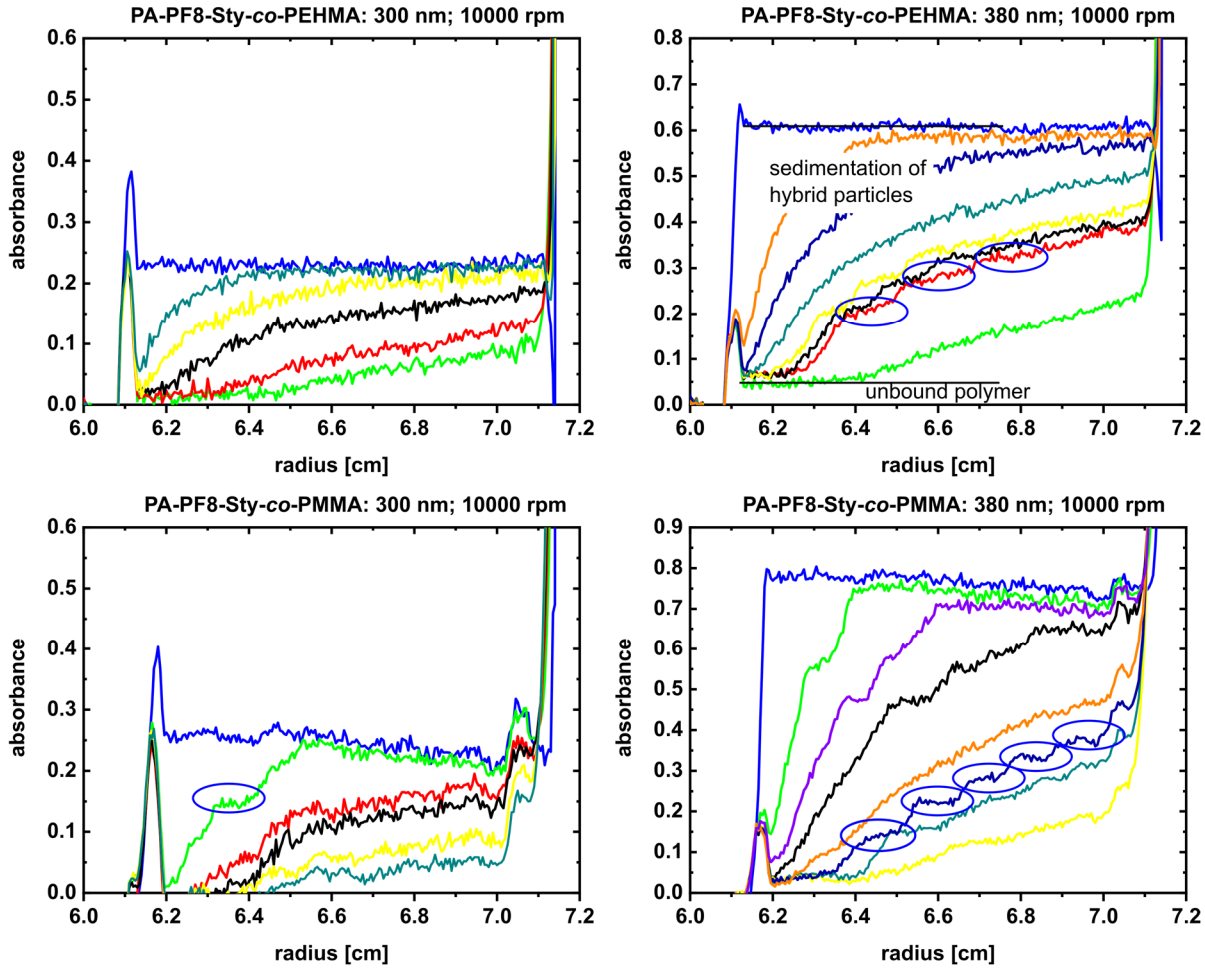

Figure 8.38. MW-AUC data for the sedimentation of the comb copolymer hybrid particles obtained in experiments 5–6 (**Table 5.2**) tracked at 300 nm (left) and 380 nm (right). The sedimenting hybrid particles consist of several species (marked with blue ovals).

8.6 Functionalization of CdSe/$(CdS)_2(ZnS)_2$ Quantum Dots by a Direct Approach: Additional Figures, Spectra, etc.

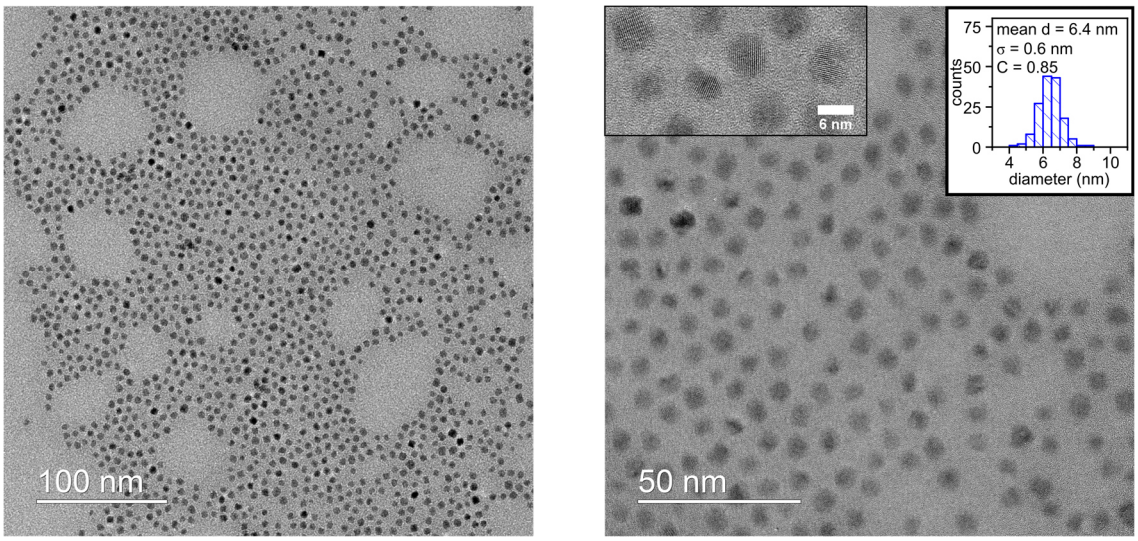

Figure 8.39. TEM images of PF8-functionalized CdSe/$(CdS)_2(ZnS)_2$ hybrid particles. Images show particles obtained in experiment 7, **Table 5.4**.

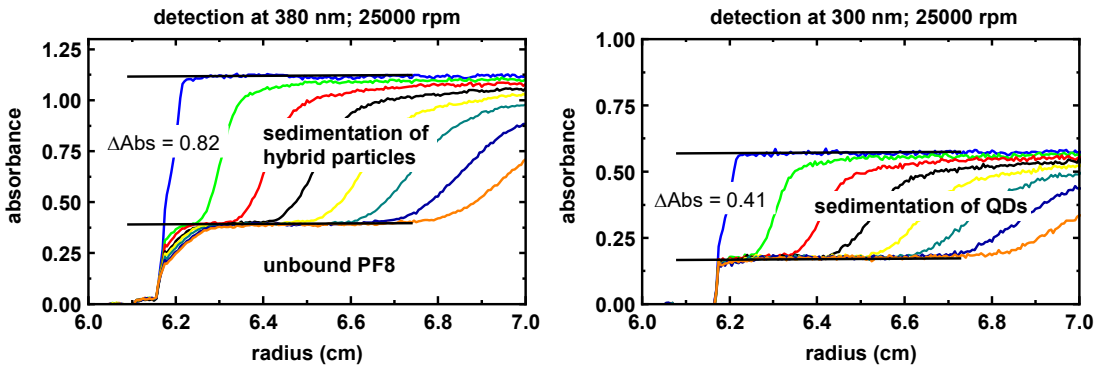

Figure 8.40. MW-AUC measurement data of the PF8 CdSe/$(CdS)_2(ZnS)_2$ hybrid QDs (75 chains PA-Ph-PF8) obtained in entry 2, **Table 5.4.** The sedimentation was tracked at λ = 300 nm where the absorption of the PF8 is negligible, and at λ = 380 nm where both NRs and PF8 absorb. The species causing the remaining absorption at 300 nm did not sediment even at 60000 rpm and is most probably a low molecular weight organic impurity. At λ = 380 nm, a complete sedimentation was observed at 60000 rpm.

8.7 Hybrid Particles Consisting of CdSe/CdS or CdSe/CdS/CdS Nanorods and PF8: Additional Spectra, Figures, etc.

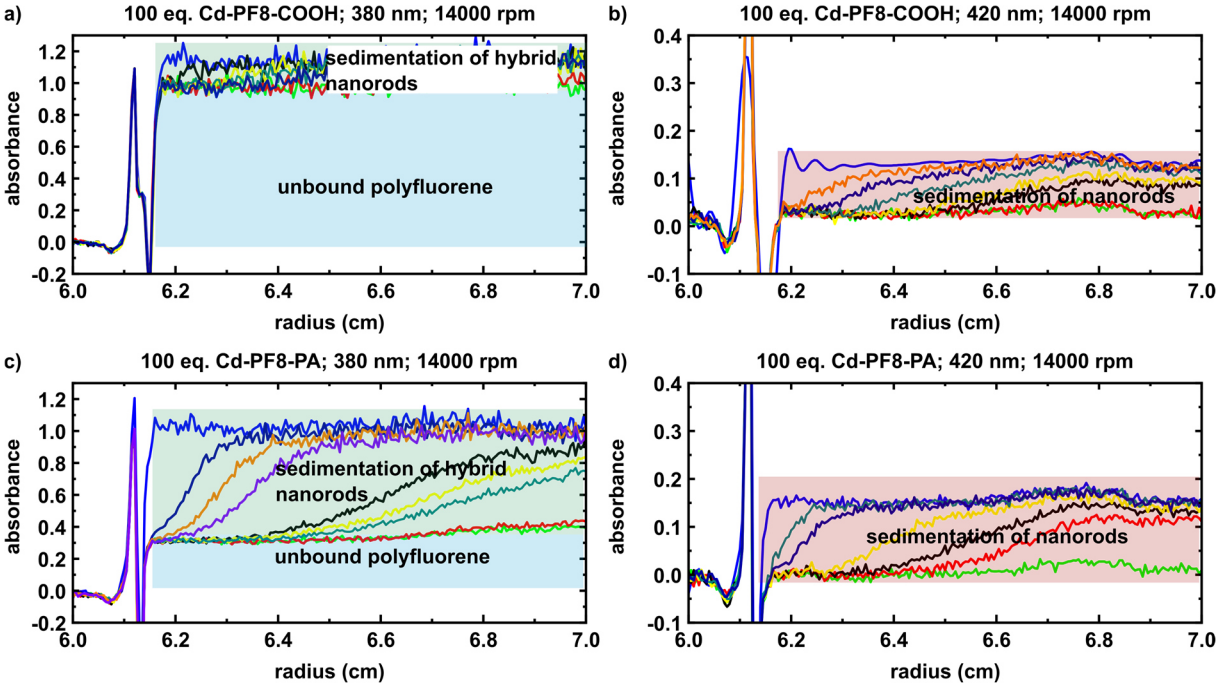

Figure 8.41. MW-AUC data for the dispersion obtained in experiments 3(a and b) and 6 (c and d), **Table 5.6**. The sedimentation of the "hybrid" particles was tracked at λ = 380 nm and the sedimentation of the NRs at λ = 420 nm.

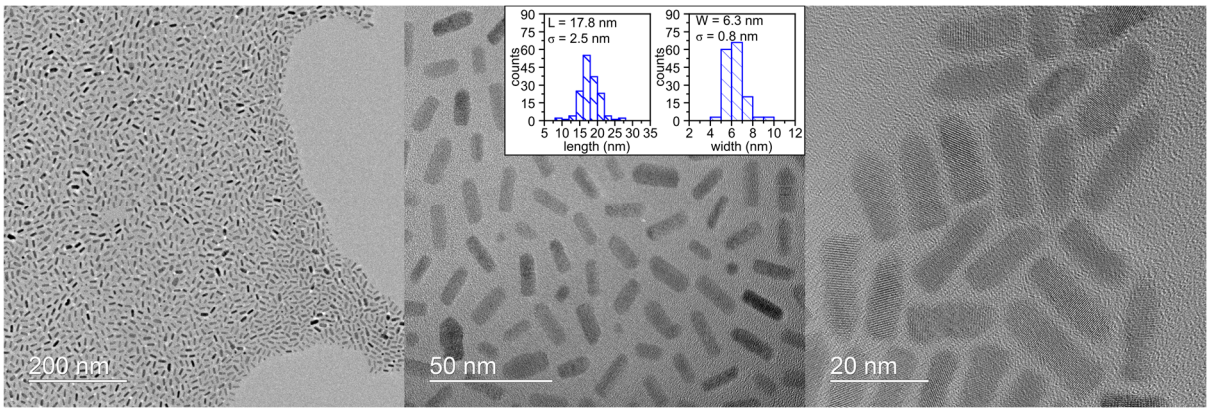

Figure 8.42. Exemplary TEM images of short PF8 CdSe/CdS/CdS hybrid nanorods.

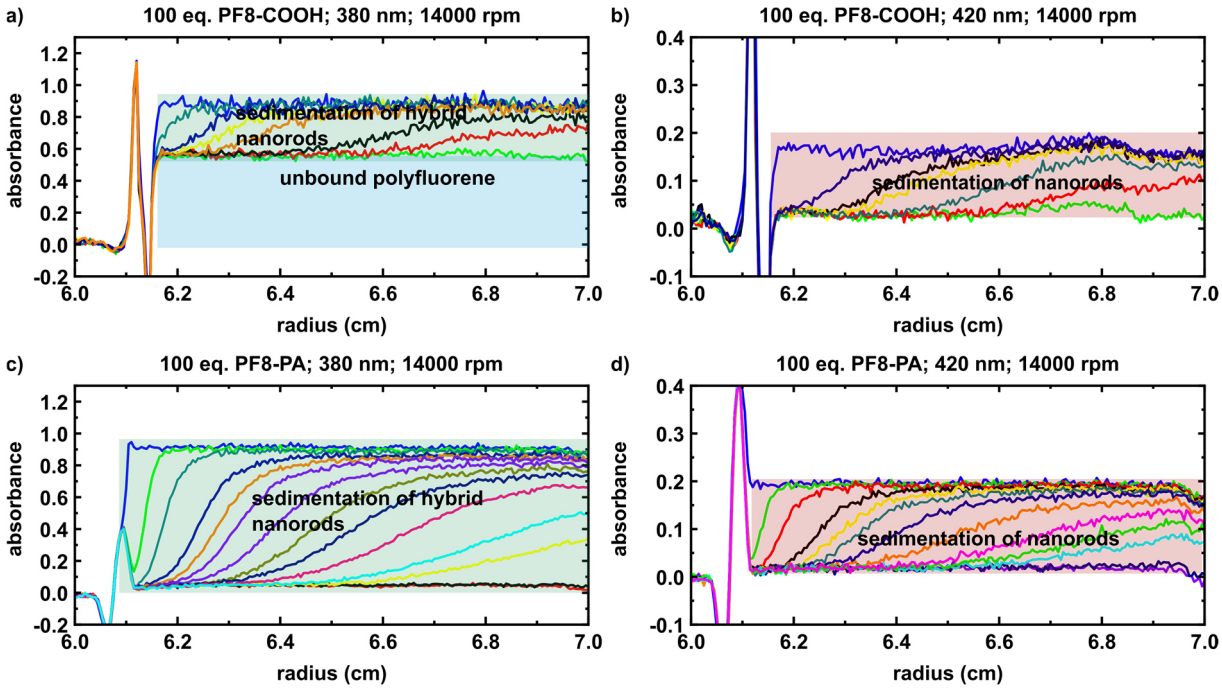

Figure 8.43. MW-AUC data for the dispersions obtained in experiments 9 (a and b) and 12 (c and d), **Table 5.6**. The sedimentation of the "hybrid" particles was tracked at λ = 380 nm and the sedimentation of the NRs at λ = 420 nm.

Quenching experiment:

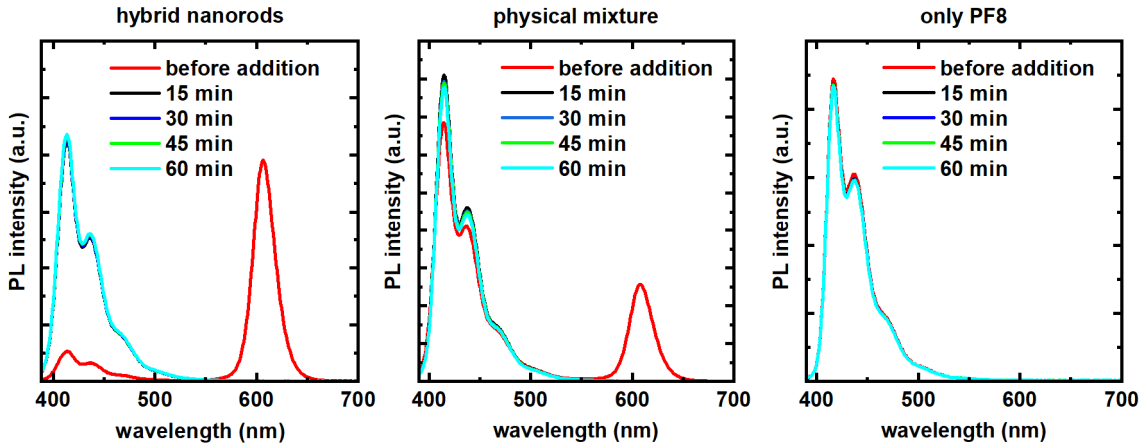

Figure 8.44. Photoluminescence spectra ($\lambda_{exc.}$ = 380 nm) of a hybrid particle dispersion (left), a physical mixture of CdSe/CdS/CdS NRs and unfunctionalized PF8 (center), and PF8 (right). TMS-Cl was added to the samples to remove all ligands from the nanocrystals' surface, and the PL intensity recorded over time.

Annotation: Trimethylsilylchloride can be used to detach all ligands from the surface of nanocrystals, thereby the PL of the nanocrystals was diminished and the integrated PL intensity of the formerly bound and quenched PF8 increased significantly (factor 8) in the case for hybrid NRs (**Figure 8.44** left). In a physical mixture of polymer and NRs (**Figure 8.44** center), the PL intensity of the polymer only increased minimally (5%),

whereas the PL intensity of pure PF8 in solution did not change after the addition of TMS-Cl (**Figure 8.44** right). This indicated that only the fluorescence of bound PF8 is strongly quenched by the semiconductor nanocrystals.

Table 8.1. Fluorescence lifetimes of PF8-functionalized CdSe/CdS/CdS hybrid nanorods. The fluorescence lifetimes belong to the PL decays shown in **Figure 5.18**. The decay of the nanocrystals was fitted by a biexponential decay function and the decay of the polymer by a mono exponential function using the FluoFit software package.

#	$\lambda_{exc.}$ [nm]	$\lambda_{emi.}$ [nm]	τ_1 [ns]	τ_2 [ns]	$<\tau_{intensity}>$ [ns]	χ^2
CdSe/CdS	405	590	38	12	17	1.01
CdSe/CdS/CdS	405	605	36	16	23	1.03
hybrid NRs	405	605	36	15	19	1.05
CdSe/CdS	485	590	38	12	17	1.03
CdSe/CdS/CdS	485	605	38	16	23	1.06
hybrid NRs	485	605	38	16	20	1.08
PF8-PA	405	414	0.39	-	0.39	1.05
PF8 in hybrid NRs	405	414	0.39	-	0.39	1.09

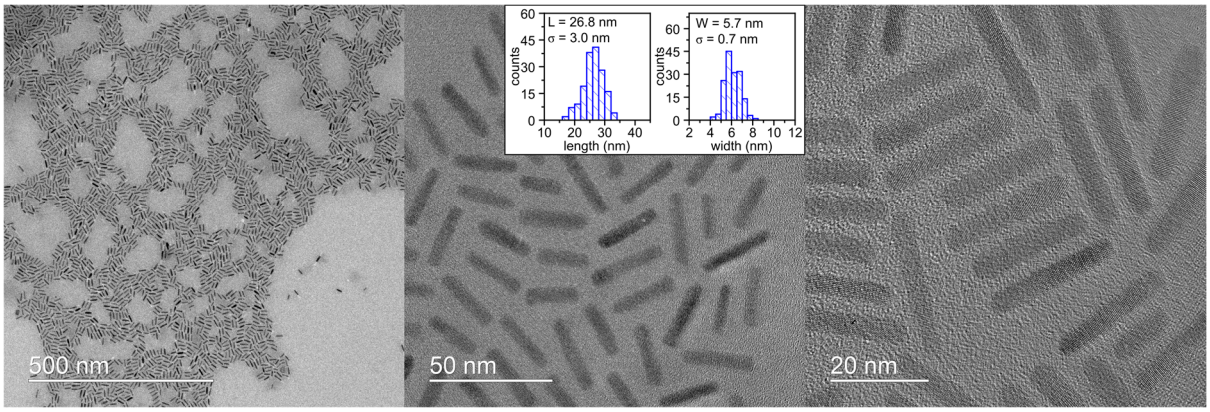

Figure 8.45. Exemplary TEM images of long (L = 27 nm) CdSe/CdS/CdS PF8-PA hybrid NRs.

8.8 Encapsulation of Nanoparticles and Single-Particle Spectroscopy: Additional Spectra, Images, Figures, etc.

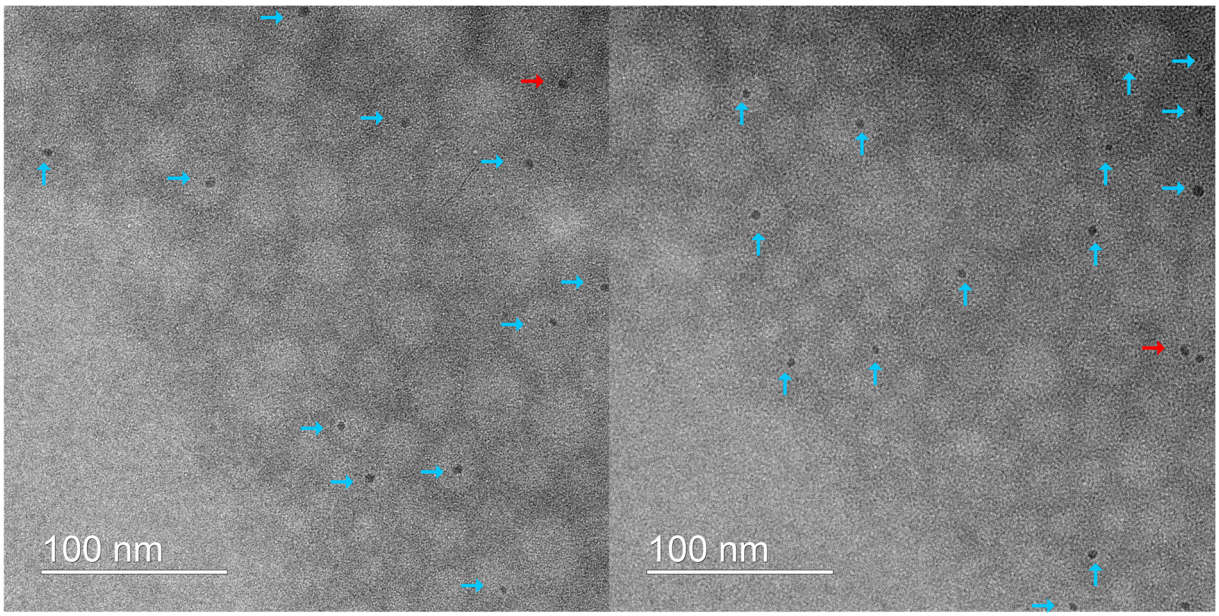

Figure 8.46. TEM images of CdSe/$(CdS)_4(ZnS)_4$ QDs encapsulated in cross-linked PMMA particles. The blue arrows indicate particles with one QD per polymer particle and the red arrows indicate particles containing several QDs.

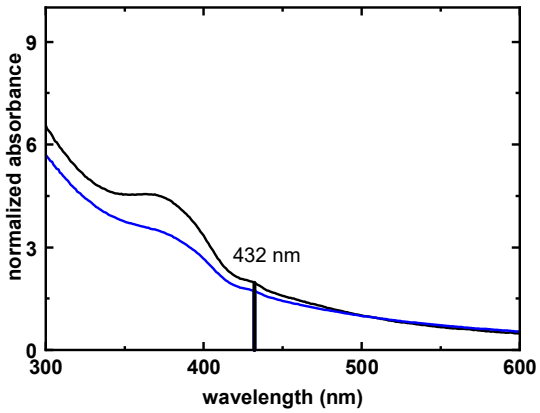

Figure 8.47. Absorption spectra of CdSe/$(CdS)_2(ZnS)_2$ polyfluorene hybrid particles embedded in PMMA-*co*-PEHMA polymer nanoparticles which were obtained in experiments 4 (blue) and 6 (black), **Table 6.2**.

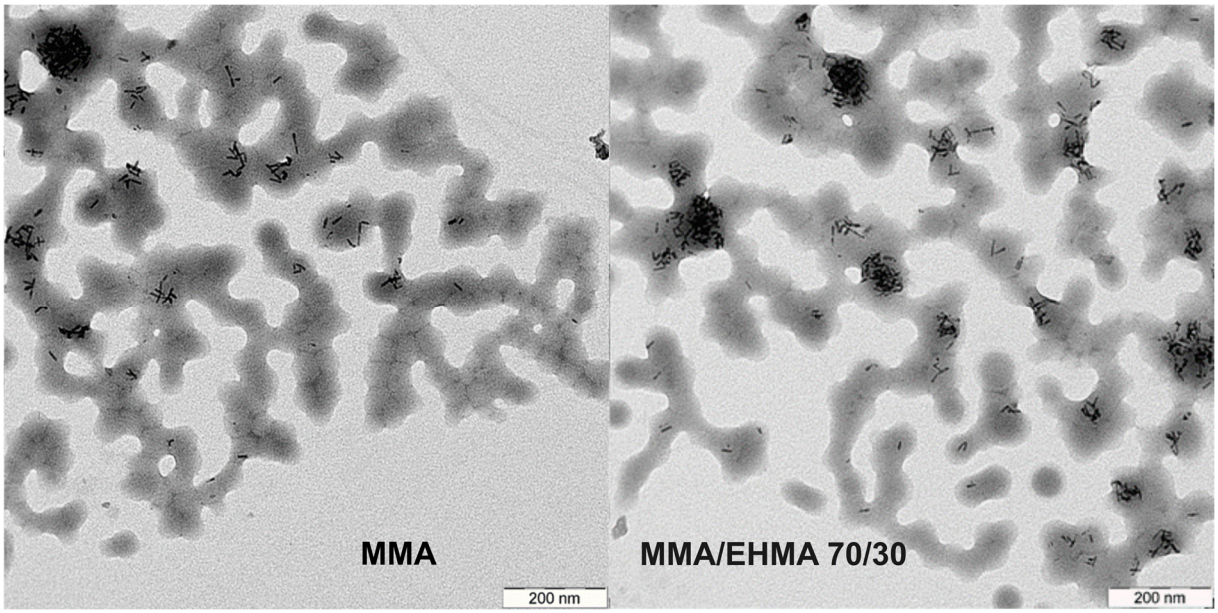

Figure 8.48. TEM images of the dried dispersions obtained in experiments 1–2, **Table 6.4**: CdSe/CdS NRs encapsulated into cross-linked PMMA particles (left) and embedded into cross-linked PMMA-*co*-PEHMA particles (right).

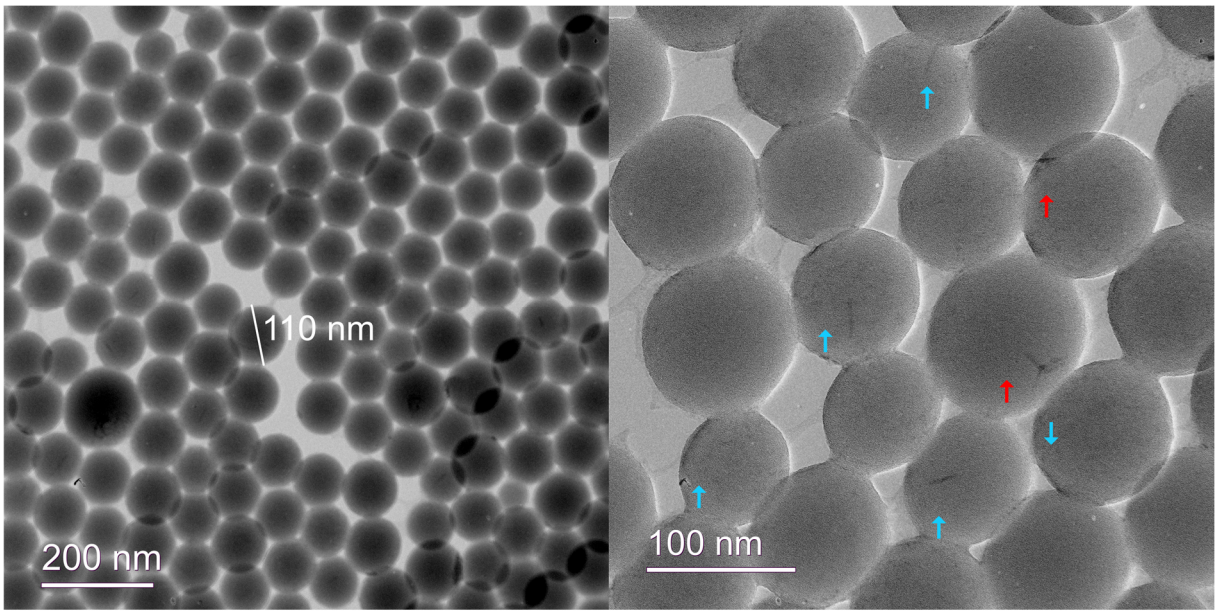

Figure 8.49. TEM images of the dried dispersion (CdSe/CdS NRs encapsulated in cross-linked PS particles) obtained in experiment 2, **Table 6.5**. The blue arrows indicate polymer particles with one NR and the red arrows indicate polymer particles containing several NRs.

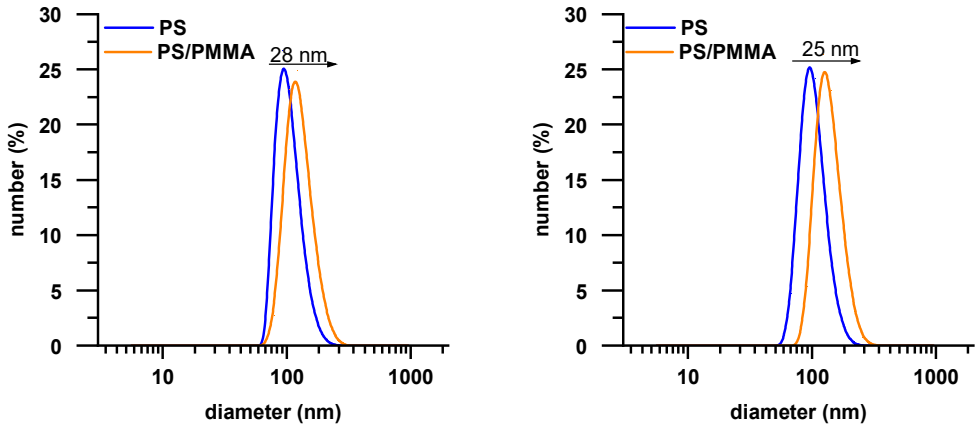

Figure 8.50. DLS traces (number based) of the dispersion obtained in experiments 3 (left) and 4 (right), **Table 6.5**, before (blue line) and after deposition of an additional PMMA shell (orange line).

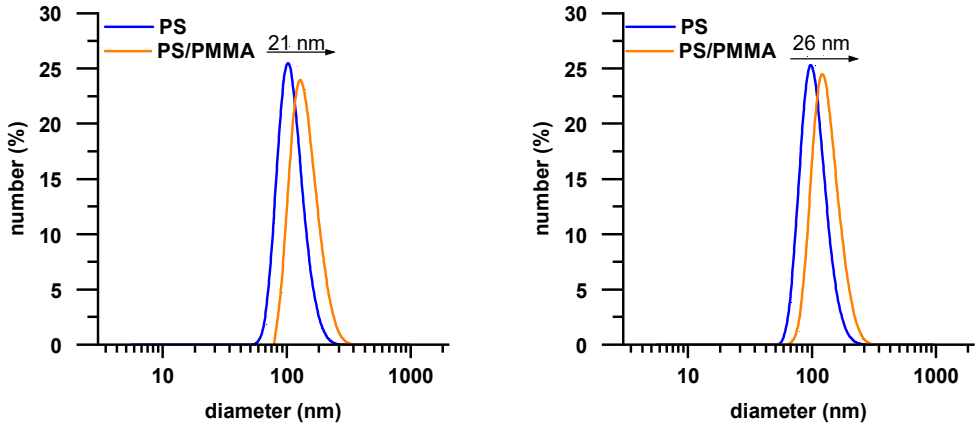

Figure 8.51. DLS traces (number based) of the dispersion obtained in experiments 2 (left) and 4 (right), **Table 6.6**, before (blue line) and after deposition of an additional PMMA shell (orange line).

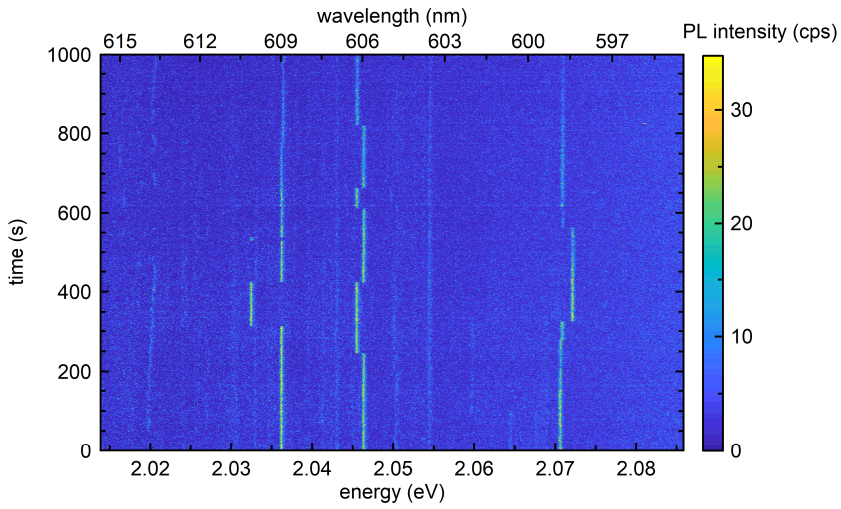

Figure 8.52. Highly resolved PL time trace of a cluster of encapsulated PF8 CdSe/CdS/CdS hybrid nanorods with clearly separated PL maxima. All of the rods were permanently charged and featured a very stable emission over a period of at least 1000 s (after 1000 s, a slight drift of the sample stage caused a decrease in intensity). The rods showed independent fluctuations in their emission wavelengths, indicating that they are locally separated and experiencing different local electric fields.

9 References

1. Boldt, K.; Kirkwood, N.; Beane, G. A.; Mulvaney, P., Synthesis of Highly Luminescent and Photo-Stable, Graded Shell CdSe/$Cd_xZn_{1-x}S$ Nanoparticles by In Situ Alloying. *Chem. Mater.* **2013,** *25*, 4731-4738.
2. Rabouw, F. T.; Lunnemann, P.; van Dijk-Moes, R. J. A.; Frimmer, M.; Pietra, F.; Koenderink, A. F.; Vanmaekelbergh, D., Reduced Auger Recombination in Single CdSe/CdS Nanorods by One-Dimensional Electron Delocalization. *Nano Lett.* **2013,** *13*, 4884-4892.
3. Pisanello, F.; Lemenager, G.; Martiradonna, L.; Carbone, L.; Vezzoli, S.; Desfonds, P.; Cozzoli, P. D.; Hermier, J. P.; Giacobino, E.; Cingolani, R.; De Vittorio, M.; Bramati, A., Non-blinking single-photon generation with anisotropic colloidal nanocrystals: towards room-temperature, efficient, colloidal quantum sources. *Adv. Mater.* **2013,** *25*, 1974-80.
4. Carbone, L.; Nobile, C.; De Giorgi, M.; Sala, F. D.; Morello, G.; Pompa, P.; Hytch, M.; Snoeck, E.; Fiore, A.; Franchini, I. R.; Nadasan, M.; Silvestre, A. F.; Chiodo, L.; Kudera, S.; Cingolani, R.; Krahne, R.; Manna, L., Synthesis and Micrometer-Scale Assembly of Colloidal CdSe/CdS Nanorods Prepared by a Seeded Growth Approach. *Nano Lett.* **2007,** *7*, 2942-2950.
5. Huber, S.; Mecking, S., Straightforward Synthesis of Conjugated Block Copolymers by Controlled Suzuki–Miyaura Cross-Coupling Polymerization Combined with ATRP. *Macromolecules* **2019,** *52*, 5917-5924.
6. Holder, E.; Tessler, N.; Rogach, A. L., Hybrid nanocomposite materials with organic and inorganic components for opto-electronic devices. *J. Mater. Chem.* **2008,** *18*, 1064-1078.
7. Reiss, P.; Couderc, E.; De Girolamo, J.; Pron, A., Conjugated polymers/semiconductor nanocrystals hybrid materials—preparation, electrical transport properties and applications. *Nanoscale* **2011,** *3*, 446-489.
8. Scheele, M.; Brütting, W.; Schreiber, F., Coupled organic–inorganic nanostructures (COIN). *Phys. Chem. Chem. Phys.* **2015,** *17*, 97-111.
9. Scheele, M., Bridging the Gap: Where Inorganic Quantum Dots and Organic Semiconductors Meet. *Bunsenmagazin* **2014,** *16*, 168-175.
10. He, M.; Qiu, F.; Lin, Z., Toward High-Performance Organic-Inorganic Hybrid Solar Cells: Bringing Conjugated Polymers and Inorganic Nanocrystals in Close Contact. *J. Phys. Chem. Lett.* **2013,** *4*, 1788-96.
11. Heinemann, M. D.; von Maydell, K.; Zutz, F.; Kolny-Olesiak, J.; Borchert, H.; Riedel, I.; Parisi, J., Photo-induced Charge Transfer and Relaxation of Persistent Charge Carriers in Polymer/Nanocrystal Composites for Applications in Hybrid Solar Cells. *Adv. Funct. Mater.* **2009,** *19*, 3788-3795.
12. Mubarok, M. A.; Aqoma, H.; Wibowo, F. T. A.; Lee, W.; Kim, H. M.; Ryu, D. Y.; Jeon, J.-W.; Jang, S.-Y., Quantum Dot Solar Cells: Molecular Engineering in Hole Transport

π-Conjugated Polymers to Enable High Efficiency Colloidal Quantum Dot Solar Cells. *Adv. Energy Mater.* **2020,** *10*, 2070035.
13. Huynh, W. U.; Dittmer, J. J.; Alivisatos, A. P., Hybrid Nanorod-Polymer Solar Cells. *Science* **2002,** *295*, 2425-2427.
14. Giovanella, U.; Pasini, M.; Lorenzon, M.; Galeotti, F.; Lucchi, C.; Meinardi, F.; Luzzati, S.; Dubertret, B.; Brovelli, S., Efficient Solution-Processed Nanoplatelet-Based Light-Emitting Diodes with High Operational Stability in Air. *Nano Lett.* **2018,** *18*, 3441-3448.
15. Colvin, V. L.; Schlamp, M. C.; Alivisatos, A. P., Light-emitting diodes made from cadmium selenide nanocrystals and a semiconducting polymer. *Nature* **1994,** *370*, 354-357.
16. Lee, J.; Sundar, V. C.; Heine, J. R.; Bawendi, M. G.; Jensen, K. F., Full Color Emission from II–VI Semiconductor Quantum Dot–Polymer Composites. *Adv. Mater.* **2000,** *12*, 1102-1105.
17. Zhao, L.; Zhou, Z.-L.; Guo, Z.; Gibson, G.; Brug, J. A.; Lam, S.; Pei, J.; Mao, S. S., Development of semi-interpenetrating polymer networks and quantum dots–polymer nanocomposites for low-cost, flexible OLED display application. *J. Mater. Res.* **2012,** *27*, 639-652.
18. Bao, B.; Li, M.; Li, Y.; Jiang, J.; Gu, Z.; Zhang, X.; Jiang, L.; Song, Y., Patterning Fluorescent Quantum Dot Nanocomposites by Reactive Inkjet Printing. *Small* **2015,** *11*, 1649-1654.
19. Xie, W.; Gomes, R.; Aubert, T.; Bisschop, S.; Zhu, Y.; Hens, Z.; Brainis, E.; Van Thourhout, D., Nanoscale and Single-Dot Patterning of Colloidal Quantum Dots. *Nano Lett.* **2015,** *15*, 7481-7487.
20. Park, J.-S.; Kyhm, J.; Kim, H. H.; Jeong, S.; Kang, J.; Lee, S.-e.; Lee, K.-T.; Park, K.; Barange, N.; Han, J.; Song, J. D.; Choi, W. K.; Han, I. K., Alternative Patterning Process for Realization of Large-Area, Full-Color, Active Quantum Dot Display. *Nano Lett.* **2016,** *16*, 6946-6953.
21. Michler, P.; Kiraz, A.; Becher, C.; Schoenfeld, W. V.; Petroff, P. M.; Zhang, L.; Hu, E.; Imamoglu, A., A Quantum Dot Single-Photon Turnstile Device. *Science* **2000,** *290*, 2282-2285.
22. Somaschi, N.; Giesz, V.; De Santis, L.; Loredo, J. C.; Almeida, M. P.; Hornecker, G.; Portalupi, S. L.; Grange, T.; Antón, C.; Demory, J.; Gómez, C.; Sagnes, I.; Lanzillotti-Kimura, N. D.; Lemaítre, A.; Auffeves, A.; White, A. G.; Lanco, L.; Senellart, P., Near-optimal single-photon sources in the solid state. *Nat. Photonics* **2016,** *10*, 340-345.
23. Guo, Z.-S.; Zhao, L.; Pei, J.; Zhou, Z.-L.; Gibson, G.; Brug, J.; Lam, S.; Mao, S. S., CdSe/ZnS Nanoparticle Composites with Amine-Functionalized Polyfluorene Derivatives for Polymeric Light-Emitting Diodes: Synthesis, Photophysical Properties, and the Electroluminescent Performance. *Macromolecules* **2010,** *43*, 1860-1866.
24. Querner, C.; Reiss, P.; Sadki, S.; Zagorska, M.; Pron, A., Size and ligand effects on the electrochemical and spectroelectrochemical responses of CdSe nanocrystals. *Phys. Chem. Chem. Phys.* **2005,** *7*, 3204-3209.
25. Steiner, D.; Dorfs, D.; Banin, U.; Della Sala, F.; Manna, L.; Millo, O., Determination of Band Offsets in Heterostructured Colloidal Nanorods Using Scanning Tunneling Spectroscopy. *Nano Lett.* **2008,** *8*, 2954-2958.
26. Efros, A. L.; Rosen, M.; Kuno, M.; Nirmal, M.; Norris, D. J.; Bawendi, M., Band-edge exciton in quantum dots of semiconductors with a degenerate valence band: Dark and bright exciton states. *Phys. Rev. B* **1996,** *54*, 4843-4856.

27. Biadala, L.; Louyer, Y.; Tamarat, P.; Lounis, B., Direct Observation of the Two Lowest Exciton Zero-Phonon Lines in Single CdSe/ZnS Nanocrystals. *Phys. Rev. Lett.* **2009,** *103*, 037404-1-037404-5.
28. Akimov, I. A.; Hundt, A.; Flissikowski, T.; Henneberger, F., Fine structure of the trion triplet state in a single self-assembled semiconductor quantum dot. *Appl. Phys. Lett.* **2002,** *81*, 4730-4732.
29. Kroutvar, M.; Ducommun, Y.; Heiss, D.; Bichler, M.; Schuh, D.; Abstreiter, G.; Finley, J. J., Optically programmable electron spin memory using semiconductor quantum dots. *Nature* **2004,** *432*, 81-84.
30. Negele, C.; Haase, J.; Budweg, A.; Leitenstorfer, A.; Mecking, S., Stable Single-Photon Emission by Quantum Dot/Polymer Hybrid Particles. *Macromol. Rapid Commun.* **2013,** *34*, 1145-1150.
31. De San Luis, A.; Bonnefond, A.; Barrado, M.; Guraya, T.; Iturrondobeitia, M.; Okariz, A.; Paulis, M.; Leiza, J. R., Toward the minimization of fluorescence loss in hybrid cross-linked core-shell PS/QD/PMMA nanoparticles: Effect of the shell thickness. *Chem. Eng. J.* **2017,** *313*, 261-269.
32. Nann, T.; Mulvaney, P., Single quantum dots in spherical silica particles. *Angew. Chem. Int. Ed.* **2004,** *43*, 5393-5396.
33. Selvan, S. T.; Tan, T. T.; Ying, J. Y., Robust, Non-Cytotoxic, Silica-Coated CdSe Quantum Dots with Efficient Photoluminescence. *Adv. Mater.* **2005,** *17*, 1620-1625.
34. Werschler, F.; Lindner, B.; Hinz, C.; Conradt, F.; Gumbsheimer, P.; Behovits, Y.; Negele, C.; de Roo, T.; Tzang, O.; Mecking, S.; Leitenstorfer, A.; Seletskiy, D. V., Efficient Emission Enhancement of Single CdSe/CdS/PMMA Quantum Dots through Controlled Near-Field Coupling to Plasmonic Bullseye Resonators. *Nano Lett.* **2018,** *18*, 5396-5400.
35. Kurtsiefer, C.; Zarda, P.; Halder, M.; Weinfurter, H.; Gorman, P. M.; Tapster, P. R.; Rarity, J. G., A step towards global key distribution. *Nature* **2002,** *419*, 450-450.
36. Parigi, V.; Zavatta, A.; Kim, M.; Bellini, M., Probing Quantum Commutation Rules by Addition and Subtraction of Single Photons to/from a Light Field. *Science* **2007,** *317*, 1890.
37. Brus, L. E., A simple model for the ionization potential, electron affinity, and aqueous redox potentials of small semiconductor crystallites. *J. Chem. Phys.* **1983,** *79*, 5566-5571.
38. Efros, A.; Efros, A., Interband Light Absorption in Semiconductor Spheres. *Sov. Phys. Semicond.* **1982,** *16*, 772-775.
39. Ekimov, A. I.; Onushchenko, A. A., Quantum size effect in three-dimensional microscopic semiconductor crystals. *JETP Lett.* **1981,** *34*, 345-349.
40. Dingle, R.; Wiegmann, W.; Henry, C. H., Quantum States of Confined Carriers in Very Thin $Al_xGa_{1-x}As$-GaAs-$Al_xGa_{1-x}As$ Heterostructures. *Phys. Rev. Lett.* **1974,** *33*, 827-830.
41. Brus, L. E., Electron–electron and electron-hole interactions in small semiconductor crystallites: The size dependence of the lowest excited electronic state. *J. Chem. Phys.* **1984,** *80*, 4403-4409.
42. Smith, A. M.; Nie, S., Semiconductor nanocrystals: structure, properties, and band gap engineering. *Acc. Chem. Res.* **2009,** *43*, 190-200.
43. Panfil, Y. E.; Oded, M.; Banin, U., Colloidal Quantum Nanostructures: Emerging Materials for Display Applications. *Angew. Chem. Int. Ed.* **2018,** *57*, 4274-4295.
44. Owen, J.; Brus, L., Chemical Synthesis and Luminescence Applications of Colloidal Semiconductor Quantum Dots. *J. Am. Chem. Soc.* **2017,** *139*, 10939-10943.

45. Kamat, P. V., Quantum Dot Solar Cells. Semiconductor Nanocrystals as Light Harvesters. *J. Phys. Chem. C* **2008,** *112*, 18737-18753.
46. Kramer, I. J.; Sargent, E. H., Colloidal Quantum Dot Photovoltaics: A Path Forward. *ACS Nano* **2011,** *5*, 8506-8514.
47. Li, Y.-F.; Feng, J.; Sun, H.-B., Perovskite quantum dots for light-emitting devices. *Nanoscale* **2019,** *11*, 19119-19139.
48. Shirasaki, Y.; Supran, G. J.; Bawendi, M. G.; Bulović, V., Emergence of colloidal quantum-dot light-emitting technologies. *Nat. Photonics* **2012,** *7*, 13.
49. Dai, X.; Deng, Y.; Peng, X.; Jin, Y., Quantum-Dot Light-Emitting Diodes for Large-Area Displays: Towards the Dawn of Commercialization. *Adv. Mater.* **2017,** *29*, 1607022.
50. Bourzac, K., Quantum dots go on display. *Nature* **2013,** *493*, 283-283.
51. Dubertret, B.; Skourides, P.; Norris, D. J.; Noireaux, V.; Brivanlou, A. H.; Libchaber, A., In Vivo Imaging of Quantum Dots Encapsulated in Phospholipid Micelles. *Science* **2002,** *298*, 1759-1762.
52. Alivisatos, A. P.; Gu, W.; Larabell, C., Quantum Dots as Cellular Probes. *Annu. Rev. Biomed. Eng.* **2005,** *7*, 55-76.
53. Ma, G., Background-Free In vivo Time Domain Optical Molecular Imaging Using Colloidal Quantum Dots. *ACS Appl. Mater. Interfaces* **2013,** *5*, 2835-2844.
54. Murray, C. B.; Norris, D. J.; Bawendi, M. G., Synthesis and characterization of nearly monodisperse CdE (E = sulfur, selenium, tellurium) semiconductor nanocrystallites. *J. Am. Chem. Soc.* **1993,** *115*, 8706-8715.
55. Brichkin, S. B.; Razumov, V. F., Colloidal quantum dots: synthesis, properties and applications. *Russ. Chem. Rev.* **2016,** *85*, 1297-1312.
56. Heuer-Jungemann, A.; Feliu, N.; Bakaimi, I.; Hamaly, M.; Alkilany, A.; Chakraborty, I.; Masood, A.; Casula, M. F.; Kostopoulou, A.; Oh, E.; Susumu, K.; Stewart, M. H.; Medintz, I. L.; Stratakis, E.; Parak, W. J.; Kanaras, A. G., The Role of Ligands in the Chemical Synthesis and Applications of Inorganic Nanoparticles. *Chem. Rev.* **2019,** *119*, 4819-4880.
57. Frederick, M. T.; Weiss, E. A., Relaxation of Exciton Confinement in CdSe Quantum Dots by Modification with a Conjugated Dithiocarbamate Ligand. *ACS Nano* **2010,** *4*, 3195-3200.
58. Hassinen, A.; Moreels, I.; De Nolf, K.; Smet, P. F.; Martins, J. C.; Hens, Z., Short-Chain Alcohols Strip X-Type Ligands and Quench the Luminescence of PbSe and CdSe Quantum Dots, Acetonitrile Does Not. *J. Am. Chem. Soc.* **2012,** *134*, 20705-20712.
59. Brown, P. R.; Kim, D.; Lunt, R. R.; Zhao, N.; Bawendi, M. G.; Grossman, J. C.; Bulović, V., Energy Level Modification in Lead Sulfide Quantum Dot Thin Films through Ligand Exchange. *ACS Nano* **2014,** *8*, 5863-5872.
60. Giansante, C.; Infante, I.; Fabiano, E.; Grisorio, R.; Suranna, G. P.; Gigli, G., "Darker-than-Black" PbS Quantum Dots: Enhancing Optical Absorption of Colloidal Semiconductor Nanocrystals via Short Conjugated Ligands. *J. Am. Chem. Soc.* **2015,** *137*, 1875-1886.
61. Anderson, N. C.; Hendricks, M. P.; Choi, J. J.; Owen, J. S., Ligand Exchange and the Stoichiometry of Metal Chalcogenide Nanocrystals: Spectroscopic Observation of Facile Metal-Carboxylate Displacement and Binding. *J. Am. Chem. Soc.* **2013,** *135*, 18536-18548.
62. Owen, J., The coordination chemistry of nanocrystal surfaces. *Science* **2015,** *347*, 615-616.
63. Houtepen, A. J.; Hens, Z.; Owen, J. S.; Infante, I., On the Origin of Surface Traps in Colloidal II–VI Semiconductor Nanocrystals. *Chem. Mater.* **2017,** *29*, 752-761.

64. Veamatahau, A.; Jiang, B.; Seifert, T.; Makuta, S.; Latham, K.; Kanehara, M.; Teranishi, T.; Tachibana, Y., Origin of surface trap states in CdS quantum dots: relationship between size dependent photoluminescence and sulfur vacancy trap states. *Phys. Chem. Chem. Phys.* **2015,** *17*, 2850-2858.
65. Boles, M. A.; Ling, D.; Hyeon, T.; Talapin, D. V., The surface science of nanocrystals. *Nat. Mater.* **2016,** *15*, 141-153.
66. Pang, Z.; Zhang, J.; Cao, W.; Kong, X.; Peng, X., Partitioning surface ligands on nanocrystals for maximal solubility. *Nat. Commun.* **2019,** *10*, 2454.
67. Green, M. L. H., A new approach to the formal classification of covalent compounds of the elements. *J. Organomet. Chem.* **1995,** *500*, 127-148.
68. Owen, J. S.; Park, J.; Trudeau, P.-E.; Alivisatos, A. P., Reaction Chemistry and Ligand Exchange at Cadmium−Selenide Nanocrystal Surfaces. *J. Am. Chem. Soc.* **2008,** *130*, 12279-12281.
69. Fritzinger, B.; Capek, R. K.; Lambert, K.; Martins, J. C.; Hens, Z., Utilizing Self-Exchange To Address the Binding of Carboxylic Acid Ligands to CdSe Quantum Dots. *J. Am. Chem. Soc.* **2010,** *132*, 10195-10201.
70. Gomes, R.; Hassinen, A.; Szczygiel, A.; Zhao, Q.; Vantomme, A.; Martins, J. C.; Hens, Z., Binding of Phosphonic Acids to CdSe Quantum Dots: A Solution NMR Study. *J. Phys. Chem. Lett.* **2011,** *2*, 145-152.
71. Ip, A. H.; Thon, S. M.; Hoogland, S.; Voznyy, O.; Zhitomirsky, D.; Debnath, R.; Levina, L.; Rollny, L. R.; Carey, G. H.; Fischer, A.; Kemp, K. W.; Kramer, I. J.; Ning, Z.; Labelle, A. J.; Chou, K. W.; Amassian, A.; Sargent, E. H., Hybrid passivated colloidal quantum dot solids. *Nat. Nanotechnol.* **2012,** *7*, 577-82.
72. Drijvers, E.; De Roo, J.; Martins, J. C.; Infante, I.; Hens, Z., Ligand Displacement Exposes Binding Site Heterogeneity on CdSe Nanocrystal Surfaces. *Chem. Mater.* **2018,** *30*, 1178-1186.
73. Kairdolf, B. A.; Smith, A. M.; Stokes, T. H.; Wang, M. D.; Young, A. N.; Nie, S., Semiconductor Quantum Dots for Bioimaging and Biodiagnostic Applications. *Annu. Rev. Anal. Chem.* **2013,** *6*, 143-162.
74. Kovalenko, M. V.; Scheele, M.; Talapin, D. V., Colloidal Nanocrystals with Molecular Metal Chalcogenide Surface Ligands. *Science* **2009,** *324*, 1417-1420.
75. Anderson, N. C.; Owen, J. S., Soluble, Chloride-Terminated CdSe Nanocrystals: Ligand Exchange Monitored by ^{1}H and ^{31}P NMR Spectroscopy. *Chem. Mater.* **2013,** *25*, 69-76.
76. Knauf, R. R.; Lennox, J. C.; Dempsey, J. L., Quantifying Ligand Exchange Reactions at CdSe Nanocrystal Surfaces. *Chem. Mater.* **2016,** *28*, 4762-4770.
77. Balan, A. D.; Olshansky, J. H.; Horowitz, Y.; Han, H.-L.; O'Brien, E. A.; Tang, L.; Somorjai, G. A.; Alivisatos, A. P., Unsaturated Ligands Seed an Order to Disorder Transition in Mixed Ligand Shells of CdSe/CdS Quantum Dots. *ACS Nano* **2019,** *13*, 13784-13796.
78. Chen, P. E.; Anderson, N. C.; Norman, Z. M.; Owen, J. S., Tight Binding of Carboxylate, Phosphonate, and Carbamate Anions to Stoichiometric CdSe Nanocrystals. *J. Am. Chem. Soc.* **2017,** *139*, 3227-3236.
79. Reiss, P.; Protiere, M.; Li, L., Core/Shell semiconductor nanocrystals. *Small* **2009,** *5*, 154-68.
80. Chaudhuri, R. G.; Paria, S., Core/Shell Nanoparticles: Classes, Properties, Synthesis Mechanisms, Characterization, and Applications. *Chem. Rev.* **2012,** *112*, 2373-2433.
81. Simi, N. J.; Vinayakan, R.; Ison, V. V., Photoinduced electron transfer in novel CdSe–Cu_2Se type II core–shell quantum dots. *RSC Adv.* **2019,** *9*, 15092-15098.

82. Jiao, S.; Shen, Q.; Mora-Seró, I.; Wang, J.; Pan, Z.; Zhao, K.; Kuga, Y.; Zhong, X.; Bisquert, J., Band Engineering in Core/Shell ZnTe/CdSe for Photovoltage and Efficiency Enhancement in Exciplex Quantum Dot Sensitized Solar Cells. *ACS Nano* **2015,** *9*, 908-915.
83. Wang, Y.; Wang, Q.; Zhan, X.; Wang, F.; Safdar, M.; He, J., Visible light driven type II heterostructures and their enhanced photocatalysis properties: a review. *Nanoscale* **2013,** *5*, 8326-8339.
84. Pandey, A.; Guyot-Sionnest, P., Intraband spectroscopy and band offsets of colloidal II-VI core/shell structures. *J. Chem. Phys.* **2007,** *127*, 104710.
85. Wu, K.; Rodríguez-Córdoba, W. E.; Liu, Z.; Zhu, H.; Lian, T., Beyond Band Alignment: Hole Localization Driven Formation of Three Spatially Separated Long-Lived Exciton States in CdSe/CdS Nanorods. *ACS Nano* **2013,** *7*, 7173-7185.
86. Mahler, B.; Spinicelli, P.; Buil, S.; Quelin, X.; Hermier, J.-P.; Dubertret, B., Towards non-blinking colloidal quantum dots. *Nat. Mater.* **2008,** *7*, 659-664.
87. Chen, O.; Zhao, J.; Chauhan, V. P.; Cui, J.; Wong, C.; Harris, D. K.; Wei, H.; Han, H.-S.; Fukumura, D.; Jain, R. K.; Bawendi, M. G., Compact high-quality CdSe–CdS core–shell nanocrystals with narrow emission linewidths and suppressed blinking. *Nat. Mater.* **2013,** *12*, 445-451.
88. Wang, L.; Nonaka, K.; Okuhata, T.; Katayama, T.; Tamai, N., Quasi-Type II Carrier Distribution in CdSe/CdS Core/Shell Quantum Dots with Type I Band Alignment. *J. Phys. Chem. C* **2018,** *122*, 12038-12046.
89. Barford, W., *Electronic and optical properties of conjugated polymers*. Oxford University Press: Oxford, **2013**; Vol. 159, p 278.
90. Wu, C.; Chiu, D. T., Highly fluorescent semiconducting polymer dots for biology and medicine. *Angew. Chem. Int. Ed.* **2013,** *52*, 3086-109.
91. Shirakawa, H.; Louis, E. J.; Macdiarmid, A. G.; Chiang, C. K.; Heeger, A. J., Synthesis of Electrically Conducting Organic Polymers - Halogen Derivatives of Polyacetylene, (Ch)x. *J.C.S. Chem. Comm.* **1977,** *16*, 578-580.
92. Friend, R. H.; Gymer, R. W.; Holmes, A. B.; Burroughes, J. H.; Marks, R. N.; Taliani, C.; Bradley, D. D. C.; Dos Santos, D. A.; Bredas, J. L.; Logdlund, M.; Salaneck, W. R., Electroluminescence in conjugated polymers. *Nature* **1999,** *397*, 121-128.
93. Ostroverkhova, O., Organic Optoelectronic Materials: Mechanisms and Applications. *Chem. Rev.* **2016,** *116*, 13279-13412.
94. White, M. S.; Kaltenbrunner, M.; Głowacki, E. D.; Gutnichenko, K.; Kettlgruber, G.; Graz, I.; Aazou, S.; Ulbricht, C.; Egbe, D. A. M.; Miron, M. C.; Major, Z.; Scharber, M. C.; Sekitani, T.; Someya, T.; Bauer, S.; Sariciftci, N. S., Ultrathin, highly flexible and stretchable PLEDs. *Nat. Photonics* **2013,** *7*, 811-816.
95. Cheng, Y.-J.; Yang, S.-H.; Hsu, C.-S., Synthesis of Conjugated Polymers for Organic Solar Cell Applications. *Chem. Rev.* **2009,** *109*, 5868-5923.
96. Hou, J. H.; Inganas, O.; Friend, R. H.; Gao, F., Organic solar cells based on non-fullerene acceptors. *Nat. Mater.* **2018,** *17*, 119-128.
97. Sirringhaus, H., 25th Anniversary Article: Organic Field-Effect Transistors: The Path Beyond Amorphous Silicon. *Adv. Mater.* **2014,** *26*, 1319-1335.
98. Facchetti, A., Semiconductors for organic transistors. *Mater. Today* **2007,** *10*, 28-37.
99. Sakamoto, J.; Rehahn, M.; Wegner, G.; Schlüter, A. D., Suzuki Polycondensation: Polyarylenes à la Carte. *Macromol. Rapid Commun.* **2009,** *30*, 653-687.
100. Yokozawa, T.; Ohta, Y., Chapter 1: Controlled Synthesis of Conjugated Polymers in Catalyst-transfer Condensation Polymerization: Monomers and Catalysts. In

Semiconducting Polymers: Controlled Synthesis and Microstructure, The Royal Society of Chemistry: Cambridge, **2017**; Vol. 21, pp 1-37.

101. Su, Y. W.; Lin, W. H.; Hsu, Y. J.; Wei, K. H., Conjugated polymer/nanocrystal nanocomposites for renewable energy applications in photovoltaics and photocatalysis. *Small* **2014,** *10*, 4427-42.
102. Park, Y.; Advincula, R. C., Hybrid Semiconductor Nanoparticles: π-Conjugated Ligands and Nanostructured Films. *Chem. Mater.* **2011,** *23*, 4273-4294.
103. Huynh, W. U.; Dittmer, J. J.; Libby, W. C.; Whiting, G. L.; Alivisatos, A. P., Controlling the Morphology of Nanocrystal–Polymer Composites for Solar Cells. *Adv. Funct. Mater.* **2003,** *13*, 73-79.
104. Greenham, N. C.; Peng, X.; Alivisatos, A. P., Charge separation and transport in conjugated-polymer/semiconductor-nanocrystal composites studied by photoluminescence quenching and photoconductivity. *Phys. Rev. B* **1996,** *54*, 17628-17637.
105. Mazzio, K. A.; Prasad, S. K. K.; Okamoto, K.; Hodgkiss, J. M.; Luscombe, C. K., End-Functionalized Semiconducting Polymers as Reagents in the Synthesis of Hybrid II-VI Nanoparticles. *Langmuir* **2018,** *34*, 9692-9700.
106. Webber, D. H.; Brutchey, R. L., Ligand Exchange on Colloidal CdSe Nanocrystals Using Thermally Labile tert-Butylthiol for Improved Photocurrent in Nanocrystal Films. *J. Am. Chem. Soc.* **2012,** *134*, 1085-1092.
107. Talapin, D. V.; Lee, J.-S.; Kovalenko, M. V.; Shevchenko, E. V., Prospects of Colloidal Nanocrystals for Electronic and Optoelectronic Applications. *Chem. Rev.* **2010,** *110*, 389-458.
108. Zhang, Q.; Russell, T. P.; Emrick, T., Synthesis and Characterization of CdSe Nanorods Functionalized with Regioregular Poly(3-hexylthiophene). *Chem. Mater.* **2007,** *19*, 3712-3716.
109. Jung, J.; Yoon, Y. J.; Lin, Z., Semiconducting organic-inorganic nanocomposites by intimately tethering conjugated polymers to inorganic tetrapods. *Nanoscale* **2016,** *8*, 8887-98.
110. Zhao, L.; Lin, Z., Crafting Semiconductor Organic–Inorganic Nanocomposites via Placing Conjugated Polymers in Intimate Contact with Nanocrystals for Hybrid Solar Cells. *Adv. Mater.* **2012,** *24*, 4353-4368.
111. Odoi, M. Y.; Hammer, N. I.; Sill, K.; Emrick, T.; Barnes, M. D., Observation of Enhanced Energy Transfer in Individual Quantum Dot–Oligophenylene Vinylene Nanostructures. *J. Am. Chem. Soc.* **2006,** *128*, 3506-3507.
112. Bousquet, A.; Awada, H.; Hiorns, R. C.; Dagron-Lartigau, C.; Billon, L., Conjugated-polymer grafting on inorganic and organic substrates: A new trend in organic electronic materials. *Prog. Polym. Sci.* **2014,** *39*, 1847-1877.
113. de Roo, T.; Haase, J.; Keller, J.; Hinz, C.; Schmid, M.; Seletskiy, D. V.; Cölfen, H.; Leitenstorfer, A.; Mecking, S., A Direct Approach to Organic/Inorganic Semiconductor Hybrid Particles via Functionalized Polyfluorene Ligands. *Adv. Funct. Mater.* **2014,** *24*, 2714-2719.
114. Jung, J.; Yoon, Y. J.; Lin, Z., Intimate organic-inorganic nanocomposites via rationally designed conjugated polymer-grafted precursors. *Nanoscale* **2016,** *8*, 16520-7.
115. Milliron, D. J.; Alivisatos, A. P.; Pitois, C.; Edder, C.; Fréchet, J. M. J., Electroactive Surfactant Designed to Mediate Electron Transfer Between CdSe Nanocrystals and Organic Semiconductors. *Adv. Mater.* **2003,** *15*, 58-61.
116. Liu, J.; Tanaka, T.; Sivula, K.; Alivisatos, A. P.; Fréchet, J. M. J., Employing End-Functional Polythiophene To Control the Morphology of Nanocrystal–Polymer Composites in Hybrid Solar Cells. *J. Am. Chem. Soc.* **2004,** *126*, 6550-6551.

117. Querner, C.; Benedetto, A.; Demadrille, R.; Rannou, P.; Reiss, P., Carbodithioate-Containing Oligo- and Polythiophenes for Nanocrystals' Surface Functionalization. *Chem. Mater.* **2006,** *18*, 4817-4826.
118. Xu, J.; Wang, J.; Mitchell, M.; Mukherjee, P.; Jeffries-El, M.; Petrich, J. W.; Lin, Z., Organic-inorganic nanocomposites via directly grafting conjugated polymers onto quantum dots. *J. Am. Chem. Soc.* **2007,** *129*, 12828-12833.
119. Hens, Z.; Martins, J. C., A Solution NMR Toolbox for Characterizing the Surface Chemistry of Colloidal Nanocrystals. *Chem. Mater.* **2013,** *25*, 1211-1221.
120. Kopping, J. T.; Patten, T. E., Identification of Acidic Phosphorus-Containing Ligands Involved in the Surface Chemistry of CdSe Nanoparticles Prepared in Tri-*N*-octylphosphine Oxide Solvents. *J. Am. Chem. Soc.* **2008,** *130*, 5689-5698.
121. Zhao, L.; Pang, X.; Adhikary, R.; Petrich, J. W.; Lin, Z., Semiconductor Anisotropic Nanocomposites Obtained by Directly Coupling Conjugated Polymers with Quantum Rods. *Angew. Chem.* **2011,** *123*, 4044-4048.
122. Zhao, L.; Pang, X.; Adhikary, R.; Petrich, J. W.; Jeffries-El, M.; Lin, Z., Organic–Inorganic Nanocomposites by Placing Conjugated Polymers in Intimate Contact with Quantum Rods. *Adv. Mater.* **2011,** *23*, 2844-2849.
123. Xu, Z.; Hine, C. R.; Maye, M. M.; Meng, Q.; Cotlet, M., Shell Thickness Dependent Photoinduced Hole Transfer in Hybrid Conjugated Polymer/Quantum Dot Nanocomposites: From Ensemble to Single Hybrid Level. *ACS Nano* **2012,** *6*, 4984-4992.
124. Zang, H.; Routh, P. K.; Alam, R.; Maye, M. M.; Cotlet, M., Core size dependent hole transfer from a photoexcited CdSe/ZnS quantum dot to a conductive polymer. *Chem. Commun.* **2014,** *50*, 5958-60.
125. Skaff, H.; Sill, K.; Emrick, T., Quantum Dots Tailored with Poly(para-phenylene vinylene). *J. Am. Chem. Soc.* **2004,** *126*, 11322-11325.
126. Kanelidis, I.; Vaneski, A.; Lenkeit, D.; Pelz, S.; Elsner, V.; Stewart, R. M.; Rodriguez-Fernandez, J.; Lutich, A. A.; Susha, A. S.; Theissmann, R.; Adamczyk, S.; Rogach, A. L.; Holder, E., Inorganic-organic nanocomposites of CdSe nanocrystals surface-modified with oligo- and poly(fluorene) moieties. *J. Mater. Chem.* **2011,** *21*, 2656-2662.
127. Zoppe, J. O.; Ataman, N. C.; Mocny, P.; Wang, J.; Moraes, J.; Klok, H. A., Surface-Initiated Controlled Radical Polymerization: State-of-the-Art, Opportunities, and Challenges in Surface and Interface Engineering with Polymer Brushes. *Chem. Rev.* **2017,** *117*, 1105-1318.
128. Sontag, S. K.; Marshall, N.; Locklin, J., Formation of conjugated polymer brushes by surface-initiated catalyst-transfer polycondensation. *Chem. Commun.* **2009,** *23*, 3354-6.
129. Marshall, N.; Sontag, S. K.; Locklin, J., Substituted Poly(p-phenylene) Thin Films via Surface-Initiated Kumada-Type Catalyst Transfer Polycondensation. *Macromolecules* **2010,** *43*, 2137-2144.
130. Sontag, S. K.; Sheppard, G. R.; Usselman, N. M.; Marshall, N.; Locklin, J., Surface-Confined Nickel Mediated Cross-Coupling Reactions: Characterization of Initiator Environment in Kumada Catalyst-Transfer Polycondensation. *Langmuir* **2011,** *27*, 12033-12041.
131. Khanduyeva, N.; Senkovskyy, V.; Beryozkina, T.; Bocharova, V.; Simon, F.; Nitschke, M.; Stamm, M.; Grötzschel, R.; Kiriy, A., Grafting of Poly(3-hexylthiophene) from Poly(4-bromostyrene) Films by Kumada Catalyst-Transfer Polycondensation: Revealing of the Composite Films Structure. *Macromolecules* **2008,** *41*, 7383-7389.

132. Beryozkina, T.; Boyko, K.; Khanduyeva, N.; Senkovskyy, V.; Horecha, M.; Oertel, U.; Simon, F.; Stamm, M.; Kiriy, A., Grafting of Polyfluorene by Surface-Initiated Suzuki Polycondensation. *Angew. Chem. Int. Ed.* **2009,** *48*, 2695-2698.
133. Senkovskyy, V.; Khanduyeva, N.; Komber, H.; Oertel, U.; Stamm, M.; Kuckling, D.; Kiriy, A., Conductive polymer brushes of regioregular head-to-tail poly (3-alkylthiophenes) via catalyst-transfer surface-initiated polycondensation. *J. Am. Chem. Soc.* **2007,** *129*, 6626-6632.
134. Huddleston, N. E.; Sontag, S. K.; Bilbrey, J. A.; Sheppard, G. R.; Locklin, J., Palladium-Mediated Surface-Initiated Kumada Catalyst Polycondensation: A Facile Route Towards Oriented Conjugated Polymers. *Macromol. Rapid Commun.* **2012,** *33*, 2115-2120.
135. Tkachov, R.; Senkovskyy, V.; Horecha, M.; Oertel, U.; Stamm, M.; Kiriy, A., Surface-initiated Kumada catalyst-transfer polycondensation of poly(9,9-dioctylfluorene) from organosilica particles: chain-confinement promoted beta-phase formation. *Chem. Commun.* **2010,** *46*, 1425-1427.
136. Tkachov, R.; Senkovskyy, V.; Oertel, U.; Synytska, A.; Horecha, M.; Kiriy, A., Microparticle-Supported Conjugated Polyelectrolyte Brushes Prepared by Surface-Initiated Kumada Catalyst Transfer Polycondensation for Sensor Applications. *Macromol. Rapid Commun.* **2010,** *31*, 2146-2150.
137. Senkovskyy, V.; Tkachov, R.; Beryozkina, T.; Komber, H.; Oertel, U.; Horecha, M.; Bocharova, V.; Stamm, M.; Gevorgyan, S. A.; Krebs, F. C.; Kiriy, A., "Hairy" Poly(3-hexylthiophene) Particles Prepared via Surface-Initiated Kumada Catalyst-Transfer Polycondensation. *J. Am. Chem. Soc.* **2009,** *131*, 16445-16453.
138. Chatterjee, S.; Karam, T. E.; Rosu, C.; Wang, C.-H.; Youm, S. G.; Li, X.; Do, C.; Losovyj, Y.; Russo, P. S.; Haber, L. H.; Nesterov, E. E., Silica–Conjugated Polymer Hybrid Fluorescent Nanoparticles: Preparation by Surface-Initiated Polymerization and Spectroscopic Studies. *J. Phys. Chem. C* **2018,** *122*, 6963-6975.
139. Islam, M. A.; Purkait, T. K.; Mobarok, M. H.; Hoehlein, I. M. D.; Sinelnikov, R.; Iqbal, M.; Azulay, D.; Balberg, I.; Millo, O.; Rieger, B.; Veinot, J. G. C., Grafting Poly(3-hexylthiophene) from Silicon Nanocrystal Surfaces: Synthesis and Properties of a Functional Hybrid Material with Direct Interfacial Contact. *Angew. Chem. Int. Ed.* **2016,** *55*, 7393-7397.
140. de Roo, T.; Huber, S.; Mecking, S., CdSe/CdS—Conjugated Polymer Core–Shell Hybrid Nanoparticles by a Grafting-From Approach. *ACS Macro Lett.* **2016,** *5*, 786-789.
141. van Sark, W. G. J. H. M.; Frederix, P. L. T. M.; Van den Heuvel, D. J.; Gerritsen, H. C.; Bol, A. A.; van Lingen, J. N. J.; de Mello Donegá, C.; Meijerink, A., Photooxidation and Photobleaching of Single CdSe/ZnS Quantum Dots Probed by Room-Temperature Time-Resolved Spectroscopy. *J. Phys. Chem. B* **2001,** *105*, 8281-8284.
142. Hu, Z.; Liu, S.; Qin, H.; Zhou, J.; Peng, X., Oxygen Stabilizes Photoluminescence of CdSe/CdS Core/Shell Quantum Dots via Deionization. *J. Am. Chem. Soc.* **2020,** *142*, 4254-4264.
143. Pechstedt, K.; Whittle, T.; Baumberg, J.; Melvin, T., Photoluminescence of Colloidal CdSe/ZnS Quantum Dots: The Critical Effect of Water Molecules. *J. Phys. Chem. C* **2010,** *114*, 12069-12077.
144. Tang, X.; Kroger, E.; Nielsen, A.; Strelow, C.; Mews, A.; Kipp, T., Ultrathin and Highly Passivating Silica Shells for Luminescent and Water-Soluble CdSe/CdS Nanorods. *Langmuir* **2017,** *33*, 5253-5260.
145. Hu, X.; Gao, X., Silica–Polymer Dual Layer-Encapsulated Quantum Dots with Remarkable Stability. *ACS Nano* **2010,** *4*, 6080-6086.

146. Rogach, A. L.; Nagesha, D.; Ostrander, J. W.; Giersig, M.; Kotov, N. A., "Raisin Bun"-Type Composite Spheres of Silica and Semiconductor Nanocrystals. *Chem. Mater.* **2000,** *12*, 2676-2685.
147. Joumaa, N.; Lansalot, M.; Théretz, A.; Elaissari, A.; Sukhanova, A.; Artemyev, M.; Nabiev, I.; Cohen, J. H. M., Synthesis of Quantum Dot-Tagged Submicrometer Polystyrene Particles by Miniemulsion Polymerization. *Langmuir* **2006,** *22*, 1810-1816.
148. Weiss, C. K.; Landfester, K., Miniemulsion Polymerization as a Means to Encapsulate Organic and Inorganic Materials. In *Hybrid Latex Particles: Preparation with (Mini)emulsion Polymerization*, van Herk, A. M.; Landfester, K., Eds. Springer Berlin Heidelberg: Berlin, Heidelberg, **2010**; pp 185-236.
149. Fleischhaker, F.; Zentel, R., Photonic Crystals from Core-Shell Colloids with Incorporated Highly Fluorescent Quantum Dots. *Chem. Mater.* **2005,** *17*, 1346-1351.
150. de Roo, T. Organic/ Inorganic Semiconductor Hybrid Nanoparticles from Controlled Polymerizations. Doctoral Thesis, University of Konstanz, Konstanz, Germany, **2017**.
151. Gao, Y.; Reischmann, S.; Huber, J.; Hanke, T.; Bratschitsch, R.; Leitenstorfer, A.; Mecking, S., Encapsulating of single quantum dots into polymer particles. *Colloid Polym. Sci.* **2008,** *286*, 1329-1334.
152. Gerion, D.; Pinaud, F.; Williams, S. C.; Parak, W. J.; Zanchet, D.; Weiss, S.; Alivisatos, A. P., Synthesis and Properties of Biocompatible Water-Soluble Silica-Coated CdSe/ZnS Semiconductor Quantum Dots. *J. Phys. Chem. B* **2001,** *105*, 8861-8871.
153. Qian, J.; Li, X.; Wei, M.; Gao, X.; Xu, Z.; He, S., Bio-molecule-conjugated fluorescent organically modified silica nanoparticles as optical probes for cancer cell imaging. *Opt. Express* **2008,** *16*, 19568-19578.
154. Darbandi, M.; Thomann, R.; Nann, T., Single Quantum Dots in Silica Spheres by Microemulsion Synthesis. *Chem. Mater.* **2005,** *17*, 5720-5725.
155. Stöber, W.; Fink, A.; Bohn, E., Controlled growth of monodisperse silica spheres in the micron size range. *J. Colloid Interface Sci.* **1968,** *26*, 62-69.
156. Smith, A. M.; Duan, H.; Rhyner, M. N.; Ruan, G.; Nie, S., A systematic examination of surface coatings on the optical and chemical properties of semiconductor quantum dots. *Phys. Chem. Chem. Phys.* **2006,** *8*, 3895-3903.
157. Koole, R.; van Schooneveld, M. M.; Hilhorst, J.; de Mello Donegá, C.; Hart, D. C. '.; van Blaaderen, A.; Vanmaekelbergh, D.; Meijerink, A., On the incorporation mechanism of hydrophobic quantum dots in silica spheres by a reverse microemulsion method. *Chem. Mater.* **2008,** *20*, 2503-2512.
158. Fu, X.; Huang, K.; Liu, S., A rapid and universal bacteria-counting approach using CdSe/ZnS/SiO_2 composite nanoparticles as fluorescence probe. *Anal. Bioanal. Chem.* **2010,** *396*, 1397-1404.
159. Pietra, F.; van Dijk - Moes, R. J. A.; Ke, X.; Bals, S.; Van Tendeloo, G.; de Mello Donega, C.; Vanmaekelbergh, D., Synthesis of Highly Luminescent Silica-Coated CdSe/CdS Nanorods. *Chem. Mater.* **2013,** *25*, 3427-3434.
160. Hutter, E. M.; Pietra, F.; van Dijk - Moes, R. J. A.; Mitoraj, D.; Meeldijk, J. D.; de Mello Donegá, C.; Vanmaekelbergh, D., Method To Incorporate Anisotropic Semiconductor Nanocrystals of All Shapes in an Ultrathin and Uniform Silica Shell. *Chem. Mater.* **2014,** *26*, 1905-1911.
161. Anderson, B. D.; Wu, W.-C.; Tracy, J. B., Silica Overcoating of CdSe/CdS Core/Shell Quantum Dot Nanorods with Controlled Morphologies. *Chem. Mater.* **2016,** *28*, 4945-4952.

162. Zwiller, V.; Blom, H.; Jonsson, P.; Panev, N.; Jeppesen, S.; Tsegaye, T.; Goobar, E.; Pistol, M.-E.; Samuelson, L.; Björk, G., Single quantum dots emit single photons at a time: Antibunching experiments. *Appl. Phys. Lett.* **2001,** *78*, 2476-2478.
163. Yuan, Z.; Kardynal, B. E.; Stevenson, R. M.; Shields, A. J.; Lobo, C. J.; Cooper, K.; Beattie, N. S.; Ritchie, D. A.; Pepper, M., Electrically Driven Single-Photon Source. *Science* **2002,** *295*, 102-105.
164. Peng, X.; Schlamp, M. C.; Kadavanich, A. V.; Alivisatos, A. P., Epitaxial Growth of Highly Luminescent CdSe/CdS Core/Shell Nanocrystals with Photostability and Electronic Accessibility. *J. Am. Chem. Soc.* **1997,** *119*, 7019-7029.
165. Zhou, J.; Zhu, M.; Meng, R.; Qin, H.; Peng, X., Ideal CdSe/CdS Core/Shell Nanocrystals Enabled by Entropic Ligands and Their Core Size-, Shell Thickness-, and Ligand-Dependent Photoluminescence Properties. *J. Am. Chem. Soc.* **2017,** *139*, 16556-16567.
166. Hanifi, D. A.; Bronstein, N. D.; Koscher, B. A.; Nett, Z.; Swabeck, J. K.; Takano, K.; Schwartzberg, A. M.; Maserati, L.; Vandewal, K.; van de Burgt, Y.; Salleo, A.; Alivisatos, A. P., Redefining near-unity luminescence in quantum dots with photothermal threshold quantum yield. *Science* **2019,** *363*, 1199-1202.
167. Tan, R.; Yuan, Y.; Nagaoka, Y.; Eggert, D.; Wang, X.; Thota, S.; Guo, P.; Yang, H.; Zhao, J.; Chen, O., Monodisperse Hexagonal Pyramidal and Bipyramidal Wurtzite CdSe-CdS Core–Shell Nanocrystals. *Chem. Mater.* **2017,** *29*, 4097-4108.
168. Werschler, F.; Hinz, C.; Froning, F.; Gumbsheimer, P.; Haase, J.; Negele, C.; de Roo, T.; Mecking, S.; Leitenstorfer, A.; Seletskiy, D. V., Coupling of Excitons and Discrete Acoustic Phonons in Vibrationally Isolated Quantum Emitters. *Nano Lett.* **2016,** *16*, 5861-5865.
169. Talapin, D. V.; Nelson, J. H.; Shevchenko, E. V.; Aloni, S.; Sadtler, B.; Alivisatos, A. P., Seeded Growth of Highly Luminescent CdSe/CdS Nanoheterostructures with Rod and Tetrapod Morphologies. *Nano Lett.* **2007,** *7*, 2951-2959.
170. Tenne, R.; Teitelboim, A.; Rukenstein, P.; Dyshel, M.; Mokari, T.; Oron, D., Studying Quantum Dot Blinking through the Addition of an Engineered Inorganic Hole Trap. *ACS Nano* **2013,** *7*, 5084-5090.
171. Pisanello, F.; Leménager, G.; Martiradonna, L.; Carbone, L.; Vezzoli, S.; Desfonds, P.; Cozzoli, P. D.; Hermier, J.-P.; Giacobino, E.; Cingolani, R.; De Vittorio, M.; Bramati, A., Non-Blinking Single-Photon Generation with Anisotropic Colloidal Nanocrystals: Towards Room-Temperature, Efficient, Colloidal Quantum Sources. *Adv. Mater.* **2013,** *25*, 1974-1980.
172. Li, L.-s.; Alivisatos, A. P., Origin and Scaling of the Permanent Dipole Moment in CdSe Nanorods. *Phys. Rev. Lett.* **2003,** *90*, 097402.
173. Hu, J.; Li, L.-s.; Yang, W.; Manna, L.; Wang, L.-w.; Alivisatos, A. P., Linearly Polarized Emission from Colloidal Semiconductor Quantum Rods. *Science* **2001,** *292*, 2060-2063.
174. Zavelani-Rossi, M.; Lupo, M. G.; Krahne, R.; Manna, L.; Lanzani, G., Lasing in self-assembled microcavities of CdSe/CdS core/shell colloidal quantum rods. *Nanoscale* **2010,** *2*, 931-935.
175. Krahne, R.; Morello, G.; Figuerola, A.; George, C.; Deka, S.; Manna, L., Physical properties of elongated inorganic nanoparticles. *Phys. Rep.* **2011,** *501*, 75-221.
176. Jasieniak, J.; Smith, L.; van Embden, J.; Mulvaney, P.; Califano, M., Re-examination of the Size-Dependent Absorption Properties of CdSe Quantum Dots. *J. Phys. Chem. C* **2009,** *113*, 19468-19474.
177. Kirkwood, N.; Boldt, K., Protic additives determine the pathway of CdSe nanocrystal growth. *Nanoscale* **2018,** *20*, 18238-18248.

178. Negele, C. Einbettung von kolloidalen Quantenpunkten in Polymerpartikel. Doctoral Thesis, University of Konstanz, Konstanz, Germany, **2018**.
179. Peng, Z. A.; Peng, X., Mechanisms of the Shape Evolution of CdSe Nanocrystals. *J. Am. Chem. Soc.* **2001,** *123*, 1389-1395.
180. Kim, D.; Lee, Y. K.; Lee, D.; Kim, W. D.; Bae, W. K.; Lee, D. C., Colloidal Dual-Diameter and Core-Position-Controlled Core/Shell Cadmium Chalcogenide Nanorods. *ACS Nano* **2017,** *11*, 12461-12472.
181. Coropceanu, I.; Rossinelli, A.; Caram, J. R.; Freyria, F. S.; Bawendi, M. G., Slow-Injection Growth of Seeded CdSe/CdS Nanorods with Unity Fluorescence Quantum Yield and Complete Shell to Core Energy Transfer. *ACS Nano* **2016,** *10*, 3295-3301.
182. Oh, N.; Shim, M., Metal Oleate Induced Etching and Growth of Semiconductor Nanocrystals, Nanorods, and Their Heterostructures. *J. Am. Chem. Soc.* **2016,** *138*, 10444-10451.
183. Neher, D., Polyfluorene Homopolymers: Conjugated Liquid-Crystalline Polymers for Bright Blue Emission and Polarized Electroluminescence. *Macromol. Rapid Commun.* **2001,** *22*, 1365-1385.
184. Pei, Q.; Yang, Efficient Photoluminescence and Electroluminescence from a Soluble Polyfluorene. *J. Am. Chem. Soc.* **1996,** *118*, 7416-7417.
185. Gong, X.; Iyer, P. K.; Moses, D.; Bazan, G. C.; Heeger, A. J.; Xiao, S. S., Stabilized Blue Emission from Polyfluorene-Based Light-Emitting Diodes: Elimination of Fluorenone Defects. *Adv. Funct. Mater.* **2003,** *13*, 325-330.
186. Yang, R.; Wu, H.; Cao, Y.; Bazan, G. C., Control of Cationic Conjugated Polymer Performance in Light Emitting Diodes by Choice of Counterion. *J. Am. Chem. Soc.* **2006,** *128*, 14422-14423.
187. Müllen, K.; Grimsdale, A. C.; Chen, S. H.; Winokur, M. J.; List, E. J. W.; Lupton, J. M.; Wallace, J. U.; Huang, C. W., Polyfluorenes. In *Adv. Polym. Sci.*, Scherf, U.; Neher, D., Eds. Springer Verlag Berlin Heidelberg: Heidelberg, **2008**; Vol. 212, pp 1-319.
188. Xie, L.-H.; Yin, C.-R.; Lai, W.-Y.; Fan, Q.-L.; Huang, W., Polyfluorene-based semiconductors combined with various periodic table elements for organic electronics. *Prog. Polym. Sci.* **2012,** *37*, 1192-1264.
189. Li, X.; Bird, M.; Mauro, G.; Asaoka, S.; Cook, A. R.; Chen, H.-C.; Miller, J. R., Transport of Triplet Excitons along Continuous 100 nm Polyfluorene Chains. *J. Phys. Chem. B* **2015,** *119*, 7210-7218.
190. Yokoyama, A.; Miyakoshi, R.; Yokozawa, T., Chain-Growth Polymerization for Poly(3-hexylthiophene) with a Defined Molecular Weight and a Low Polydispersity. *Macromolecules* **2004,** *37*, 1169-1171.
191. Sheina, E. E.; Liu, J.; Iovu, M. C.; Laird, D. W.; McCullough, R. D., Chain growth mechanism for regioregular nickel-initiated cross-coupling polymerizations. *Macromolecules* **2004,** *37*, 3526-3528.
192. Kiriy, A.; Senkovskyy, V.; Sommer, M., Kumada Catalyst-Transfer Polycondensation: Mechanism, Opportunities, and Challenges. *Macromol. Rapid Commun.* **2011,** *32*, 1503-1517.
193. Yokoyama, A.; Suzuki, H.; Kubota, Y.; Ohuchi, K.; Higashimura, H.; Yokozawa, T., Chain-Growth Polymerization for the Synthesis of Polyfluorene via Suzuki−Miyaura Coupling Reaction from an Externally Added Initiator Unit. *J. Am. Chem. Soc.* **2007,** *129*, 7236-7237.
194. Yokozawa, T.; Kohno, H.; Ohta, Y.; Yokoyama, A., Catalyst-Transfer Suzuki−Miyaura Coupling Polymerization for Precision Synthesis of Poly(p-phenylene). *Macromolecules* **2010,** *43*, 7095-7100.

195. Kosaka, K.; Uchida, T.; Mikami, K.; Ohta, Y.; Yokozawa, T., AmPhos Pd-Catalyzed Suzuki–Miyaura Catalyst-Transfer Condensation Polymerization: Narrower Dispersity by Mixing the Catalyst and Base Prior to Polymerization. *Macromolecules* **2018,** *51*, 364-369.
196. Verswyvel, M.; Hoebers, C.; De Winter, J.; Gerbaux, P.; Koeckelberghs, G., Study of the controlled chain-growth polymerization of poly(3,6-phenanthrene). *J. Polym. Sci. Part A: Polym. Chem.* **2013,** *51*, 5067-5074.
197. Elmalem, E.; Kiriy, A.; Huck, W. T. S., Chain-Growth Suzuki Polymerization of n-Type Fluorene Copolymers. *Macromolecules* **2011,** *44*, 9057-9061.
198. Fischer, C. S.; Jenewein, C.; Mecking, S., Conjugated Star Polymers from Multidirectional Suzuki–Miyaura Polymerization for Live Cell Imaging. *Macromolecules* **2015,** *48*, 483-491.
199. Tokita, Y.; Katoh, M.; Ohta, Y.; Yokozawa, T., Mechanistic Investigation of Catalyst-Transfer Suzuki-Miyaura Condensation Polymerization of Thiophene-Pyridine Biaryl Monomers with the Aid of Model Reactions. *Chem. Eur. J.* **2016**.
200. Fischer, C. S.; Baier, M. C.; Mecking, S., Enhanced Brightness Emission-Tuned Nanoparticles from Heterodifunctional Polyfluorene Building Blocks. *J. Am. Chem. Soc.* **2013,** *135*, 1148-1154.
201. Elmalem, E.; Kiriy, A.; Huck, W. T., Chain-growth suzuki polymerization of n-type fluorene copolymers. *Macromolecules* **2011,** *44*, 9057-9061.
202. Zhang, H.-H.; Peng, W.; Dong, J.; Hu, Q.-S., *t*-Bu_3P-Coordinated 2-Phenylaniline-Based Palladacycle Complex/ArBr as Robust Initiators for Controlled Pd(0)/*t*-Bu_3P-Catalyzed Suzuki Cross-Coupling Polymerization of AB-Type Monomers. *ACS Macro Lett.* **2016,** *5*, 656-660.
203. Zhang, H.-H.; Xing, C.-H.; Hu, Q.-S., Controlled Pd(0)/*t*-Bu_3P-Catalyzed Suzuki Cross-Coupling Polymerization of AB-Type Monomers with PhPd(*t*-Bu_3P)I or $Pd_2(dba)_3$/*t*-Bu_3P/ArI as the Initiator. *J. Am. Chem. Soc.* **2012,** *134*, 13156-13159.
204. Zhang, H.-H.; Xing, C.-H.; Hu, Q.-S.; Hong, K., Controlled Pd(0)/*t*-Bu_3P-Catalyzed Suzuki Cross-Coupling Polymerization of AB-Type Monomers with ArPd(*t*-Bu_3P)X or $Pd_2(dba)_3$/*t*-Bu_3P/ArX as the Initiator. *Macromolecules* **2015,** *48*, 967-978.
205. Miyakoshi, R.; Yokoyama, A.; Yokozawa, T., Development of catalyst-transfer condensation polymerization. Synthesis of π-conjugated polymers with controlled molecular weight and low polydispersity. *J. Polym. Sci. Part A: Polym. Chem.* **2008,** *46*, 753-765.
206. Zhang, H.-H.; Xing, C.-H.; Tsemo, G. B.; Hu, Q.-S., *t*-Bu_3P-Coordinated 2-Phenylaniline-Based Palladacycle Complex as a Precatalyst for the Suzuki Cross-Coupling Polymerization of Aryl Dibromides with Aryldiboronic Acids. *ACS Macro Lett.* **2013,** *2*, 10-13.
207. Shipp, D. A., Reversible-Deactivation Radical Polymerizations. *Polym. Rev.* **2011,** *51*, 99-103.
208. Jenkins Aubrey, D.; Jones Richard, G.; Moad, G., Terminology for reversible-deactivation radical polymerization previously called "controlled" radical or "living" radical polymerization (IUPAC Recommendations 2010). *Pure Appl. Chem.* **2009,** *82*, 483-491.
209. Braunecker, W. A.; Matyjaszewski, K., Controlled/living radical polymerization: Features, developments, and perspectives. *Prog. Polym. Sci.* **2007,** *32*, 93-146.
210. Matyjaszewski, K., Atom Transfer Radical Polymerization (ATRP): Current Status and Future Perspectives. *Macromolecules* **2012,** *45*, 4015-4039.

211. Jakubowski, W.; Matyjaszewski, K., Activators Regenerated by Electron Transfer for Atom-Transfer Radical Polymerization of (Meth)acrylates and Related Block Copolymers. *Angew. Chem.* **2006,** *118*, 4594-4598.
212. Jakubowski, W.; Min, K.; Matyjaszewski, K., Activators Regenerated by Electron Transfer for Atom Transfer Radical Polymerization of Styrene. *Macromolecules* **2006,** *39*, 39-45.
213. Matyjaszewski, K.; Jakubowski, W.; Min, K.; Tang, W.; Huang, J.; Braunecker, W. A.; Tsarevsky, N. V., Diminishing catalyst concentration in atom transfer radical polymerization with reducing agents. *Proc. Natl. Acad. Sci. USA* **2006,** *103*, 15309-15314.
214. Guillaneuf, Y.; Gigmes, D.; Marque, S. R. A.; Astolfi, P.; Greci, L.; Tordo, P.; Bertin, D., First Effective Nitroxide-Mediated Polymerization of Methyl Methacrylate. *Macromolecules* **2007,** *40*, 3108-3114.
215. Chen, P.; Yang, G.; Liu, T.; Li, T.; Wang, M.; Huang, W., Optimization of opto-electronic property and device efficiency of polyfluorenes by tuning structure and morphology. *Polym. Int.* **2006,** *55*, 473-490.
216. Jin, X.-H.; Price, M. B.; Finnegan, J. R.; Boott, C. E.; Richter, J. M.; Rao, A.; Menke, S. M.; Friend, R. H.; Whittell, G. R.; Manners, I., Long-range exciton transport in conjugated polymer nanofibers prepared by seeded growth. *Science* **2018,** *360*, 897-900.
217. de Cuendias, A.; Hiorns, R. C.; Cloutet, E.; Vignau, L.; Cramail, H., Conjugated rod–coil block copolymers and optoelectronic applications. *Polym. Int.* **2010,** *59*, 1452-1476.
218. McCullough, L. A.; Matyjaszewski, K., Conjugated Conducting Polymers as Components in Block Copolymer Systems. *Mol. Cryst. Liq. Cryst.* **2010,** *521*, 1-55.
219. Lee, E.; Hammer, B.; Kim, J.-K.; Page, Z.; Emrick, T.; Hayward, R. C., Hierarchical Helical Assembly of Conjugated Poly(3-hexylthiophene)-block-poly(3-triethylene glycol thiophene) Diblock Copolymers. *J. Am. Chem. Soc.* **2011,** *133*, 10390-10393.
220. Marsitzky, D.; Klapper, M.; Müllen, K., End-Functionalization of Poly(2,7-fluorene): A Key Step toward Novel Luminescent Rod−Coil Block Copolymers. *Macromolecules* **1999,** *32*, 8685-8688.
221. Kim, H. J.; Kim, H. S.; Kwon, Y. K., Synthesis of an Amphiphilic π-Conjugated Triblock Copolymer of Poly(9,9-didodecylfluorene-2,7-diyl) and Poly(hydroxyl ethyl methacrylate). *Macromol. Res.* **2005,** *13*, 529-532.
222. Lu, S.; Liu, T.; Ke, L.; Ma, D.-G.; Chua, S.-J.; Huang, W., Polyfluorene-Based Light-Emitting Rod−Coil Block Copolymers. *Macromolecules* **2005,** *38*, 8494-8502.
223. Lin, S.-T.; Fuchise, K.; Chen, Y.; Sakai, R.; Satoh, T.; Kakuchi, T.; Chen, W.-C., Synthesis, thermomorphic characteristics, and fluorescent properties of poly[2,7-(9,9-dihexylfluorene)]-block-poly(N-isopropylacrylamide)-block-poly(N-hydroxyethylacrylamide) rod-coil-coil triblock copolymers. *Soft Matter* **2009,** *5*, 3761.
224. Deng, C.; Jiang, P.; Shen, X.; Ling, J.; Hogen-Esch, T. E., White light emission of multi-chromophore photoluminescent nanoparticles using polyacrylate scaffold copolymers with pendent polyfluorene groups. *Polym. Chem.* **2014,** *5*.
225. Bronstein, H. A.; Luscombe, C. K., Externally Initiated Regioregular P3HT with Controlled Molecular Weight and Narrow Polydispersity. *J. Am. Chem. Soc.* **2009,** *131*, 12894-12895.
226. Stefan, M. C.; Bhatt, M. P.; Sista, P.; Magurudeniya, H. D., Grignard metathesis (GRIM) polymerization for the synthesis of conjugated block copolymers

containing regioregular poly(3-hexylthiophene). *Polym. Chem.* **2012,** *3*, 1693-1701.
227. Iovu, M. C.; Sheina, E. E.; Gil, R. R.; McCullough, R. D., Experimental Evidence for the Quasi-"Living" Nature of the Grignard Metathesis Method for the Synthesis of Regioregular Poly(3-alkylthiophenes). *Macromolecules* **2005,** *38*, 8649-8656.
228. Jeffries-EL, M.; Sauvé, G.; McCullough, R. D., In-Situ End-Group Functionalization of Regioregular Poly(3-alkylthiophene) Using the Grignard Metathesis Polymerization Method. *Adv. Mater.* **2004,** *16*, 1017-1019.
229. Jeffries-El, M.; Sauvé, G.; McCullough, R. D., Facile Synthesis of End-Functionalized Regioregular Poly(3-alkylthiophene)s via Modified Grignard Metathesis Reaction. *Macromolecules* **2005,** *38*, 10346-10352.
230. Iovu, M. C.; Zhang, R.; Cooper, J. R.; Smilgies, D. M.; Javier, A. E.; Sheina, E. E.; Kowalewski, T.; McCullough, R. D., Conducting Block Copolymers of Regioregular Poly(3-hexylthiophene) and Poly(methacrylates): Electronic Materials with Variable Conductivities and Degrees of Interfibrillar Order. *Macromol. Rapid Commun.* **2007,** *28*, 1816-1824.
231. Iovu, M. C.; Jeffries-El, M.; Sheina, E. E.; Cooper, J. R.; McCullough, R. D., Regioregular poly(3-alkylthiophene) conducting block copolymers. *Polymer* **2005,** *46*, 8582-8586.
232. Iovu, M. C.; Craley, C. R.; Jeffries-El, M.; Krankowski, A. B.; Zhang, R.; Kowalewski, T.; McCullough, R. D., Conducting Regioregular Polythiophene Block Copolymer Nanofibrils Synthesized by Reversible Addition Fragmentation Chain Transfer Polymerization (RAFT) and Nitroxide Mediated Polymerization (NMP). *Macromolecules* **2007,** *40*, 4733-4735.
233. Mougnier, S.-J.; Brochon, C.; Cloutet, E.; Magnet, S.; Navarro, C.; Hadziioannou, G., Facile and Versatile Synthesis of Rod-Coil Poly(3-hexylthiophene)-Based Block Copolymers by Nitroxide-Mediated Radical Polymerization. *J. Polym. Sci. Part A: Polym. Chem.* **2012,** *50*, 2463-2470.
234. Sommer, M.; Lang, A. S.; Thelakkat, M., Crystalline–Crystalline Donor–Acceptor Block Copolymers. *Angew. Chem. Int. Ed.* **2008,** *47*, 7901-7904.
235. Qian, J.; Li, X.; Lunn, D. J.; Gwyther, J.; Hudson, Z. M.; Kynaston, E.; Rupar, P. A.; Winnik, M. A.; Manners, I., Uniform, High Aspect Ratio Fiber-like Micelles and Block Co-micelles with a Crystalline π-Conjugated Polythiophene Core by Self-Seeding. *J. Am. Chem. Soc.* **2014,** *136*, 4121-4124.
236. Kim, Y.; Kim, H. J.; Kim, J.-S.; Yun, H.; Park, H.; Han, J.; Kim, B. J., Modulating Regioregularity of Poly(3-hexylthiophene)-based Amphiphilic Block Copolymers To Control Solution Assembly from Nanowires to Micelles. *Chem. Mater.* **2018,** *30*, 7912-7921.
237. Zeysing, B.; Gosch, C.; Terfort, A., Protecting Groups for Thiols Suitable for Suzuki Conditions. *Org. Lett.* **2000,** *2*, 1843-1845.
238. Itoh, T.; Mase, T., Practical Thiol Surrogates and Protective Groups for Arylthiols for Suzuki–Miyaura Conditions. *J. Org. Chem.* **2006,** *71*, 2203-2206.
239. Queffelec, C.; Petit, M.; Janvier, P.; Knight, D. A.; Bujoli, B., Surface modification using phosphonic acids and esters. *Chem. Rev.* **2012,** *112*, 3777-807.
240. McKenna, C. E.; Higa, M. T.; Cheung, N. H.; McKenna, M.-C., The facile dealkylation of phosphonic acid dialkyl esters by bromotrimethylsilane. *Tetrahedron Lett.* **1977,** *18*, 155-158.
241. Willemse, R. X. E.; van Herk, A. M., Copolymerization Kinetics of Methyl Methacrylate–Styrene Obtained by PLP-MALDI-ToF-MS. *J. Am. Chem. Soc.* **2006,** *128*, 4471-4480.

242. Castañar, L.; Poggetto, G. D.; Colbourne, A. A.; Morris, G. A.; Nilsson, M., The GNAT: A new tool for processing NMR data. *Magn. Reson. Chem.* **2018,** *56*, 546-558.
243. Lavanya Devi, C.; Yesudas, K.; Makarov, N. S.; Jayathirtha Rao, V.; Bhanuprakash, K.; Perry, J. W., Combined experimental and theoretical study of one- and two-photon absorption properties of D–π–A–π–D type bis(carbazolylfluorenylethynyl) arene derivatives: Influence of aromatic acceptor bridge. *Dyes Pigm.* **2015,** *113*, 682-691.
244. Suzuki, N.; Matsuda, T.; Nagai, T.; Yamazaki, K.; Fujiki, M., Investigation of the Intra-CH/π Interaction in Dibromo-9,9′-dialkylfluorenes. *Cryst. Growth Des.* **2016,** *16*, 6593-6599.
245. Zhang, X.; Tian, H.; Liu, Q.; Wang, L.; Geng, Y.; Wang, F., Synthesis of fluorene-based oligomeric organoboron reagents via kumada, heck, and stille cross-coupling reactions. *J. Org. Chem.* **2006,** *71*, 4332-4335.
246. Ehrenreich, P.; Groh, A.; Goodwin, H.; Huster, J.; Deschler, F.; Mecking, S.; Schmidt-Mende, L., Tailored Interface Energetics for Efficient Charge Separation in Metal Oxide-Polymer Solar Cells. *Sci. Rep.* **2019,** *9*, 74.
247. Kalek, M.; Jezowska, M.; Stawinski, J., Preparation of Arylphosphonates by Palladium(0)-Catalyzed Cross-Coupling in the Presence of Acetate Additives: Synthetic and Mechanistic Studies. *Adv. Synth. Catal.* **2009,** *351*, 3207-3216.
248. Dai, C.; Fu, G. C., The First General Method for Palladium-Catalyzed Negishi Cross-Coupling of Aryl and Vinyl Chlorides: Use of Commercially Available Pd(P(*t*-Bu)$_3$)$_2$ as a Catalyst. *J. Am. Chem. Soc.* **2001,** *123*, 2719-2724.
249. Baltus, C. B.; Chuckowree, I. S.; Press, N. J.; Day, I. J.; Coles, S. J.; Tizzard, G. J.; Spencer, J., Olefin cross-metathesis/Suzuki–Miyaura reactions on vinylphenylboronic acid pinacol esters. *Tetrahedron Lett.* **2013,** *54*, 1211-1217.
250. Liras, M.; Barawi, M.; de la Peña O'Shea, V. A., Hybrid materials based on conjugated polymers and inorganic semiconductors as photocatalysts: from environmental to energy applications. *Chem. Soc. Rev.* **2019,** *48*, 5454-5487.
251. Beane, G.; Boldt, K.; Kirkwood, N.; Mulvaney, P., Energy Transfer between Quantum Dots and Conjugated Dye Molecules. *J. Phys. Chem. C* **2014,** *118*, 18079-18086.
252. Zeng, B.; Palui, G.; Zhang, C.; Zhan, N.; Wang, W.; Ji, X.; Chen, B.; Mattoussi, H., Characterization of the Ligand Capping of Hydrophobic CdSe–ZnS Quantum Dots Using NMR Spectroscopy. *Chem. Mater.* **2017,** *30*, 225-238.
253. Locklin, J.; Patton, D.; Deng, S.; Baba, A.; Millan, M.; Advincula, R. C., Conjugated Oligothiophene-Dendron-Capped CdSe Nanoparticles: Synthesis and Energy Transfer. *Chem. Mater.* **2004,** *16*, 5187-5193.
254. Khlyabich, P.; Burkhart, B.; Rudenko, A.; Thompson, B., Optimization and Simplification of Polymer-Fullerene Solar Cells through Polymer and Active Layer Design. *Polymer* **2013,** *54*, 5267–5298.
255. Vokhmintcev, K. V.; Samokhvalov, P. S.; Nabiev, I., Charge transfer and separation in photoexcited quantum dot-based systems. *Nano Today* **2016,** *11*, 189-211.
256. Ansari, M. A.; Mohiuddin, S.; Kandemirli, F.; Malik, M. I., Synthesis and characterization of poly(3-hexylthiophene): improvement of regioregularity and energy band gap. *RSC Adv.* **2018,** *8*, 8319-8328.
257. Chen, Y.; Cordero, J. M.; Wang, H.; Franke, D.; Achorn, O. B.; Freyria, F. S.; Coropceanu, I.; Wei, H.; Chen, O.; Mooney, D. J.; Bawendi, M., A Ligand System for Flexible Functionalization of Quantum Dots via Click Chemistry. *Angew. Chem.* **2018,** *130*, 4741-4746.
258. Jha, P. P.; Guyot-Sionnest, P., Trion Decay in Colloidal Quantum Dots. *ACS Nano* **2009,** *3*, 1011-1015.

259. Klimov, V. I.; Mikhailovsky, A. A.; McBranch, D. W.; Leatherdale, C. A.; Bawendi, M. G., Quantization of Multiparticle Auger Rates in Semiconductor Quantum Dots. *Science* **2000,** *287*, 1011-1013.
260. Javaux, C.; Mahler, B.; Dubertret, B.; Shabaev, A.; Rodina, A. V.; Efros, A. L.; Yakovlev, D. R.; Liu, F.; Bayer, M.; Camps, G.; Biadala, L.; Buil, S.; Quelin, X.; Hermier, J. P., Thermal activation of non-radiative Auger recombination in charged colloidal nanocrystals. *Nat. Nanotechnol.* **2013,** *8*, 206-12.
261. Galland, C.; Ghosh, Y.; Steinbruck, A.; Hollingsworth, J. A.; Htoon, H.; Klimov, V. I., Lifetime blinking in nonblinking nanocrystal quantum dots. *Nat Commun* **2012,** *3*, 908.
262. Efros, A. L.; Nesbitt, D. J., Origin and control of blinking in quantum dots. *Nat. Nanotechnol.* **2016,** *11*, 661-671.
263. Baker, J. L.; Widmer-Cooper, A.; Toney, M. F.; Geissler, P. L.; Alivisatos, A. P., Device-scale perpendicular alignment of colloidal nanorods. *Nano Lett.* **2010,** *10*, 195-201.
264. Green, M., The nature of quantum dot capping ligands. *J. Mater. Chem.* **2010,** *20*, 5797.
265. Jeong, S.; Achermann, M.; Nanda, J.; Ivanov, S.; Klimov, V. I.; Hollingsworth, J. A., Effect of the Thiol−Thiolate Equilibrium on the Photophysical Properties of Aqueous CdSe/ZnS Nanocrystal Quantum Dots. *J. Am. Chem. Soc.* **2005,** *127*, 10126-10127.
266. Strauss, H. M.; Karabudak, E.; Bhattacharyya, S.; Kretzschmar, A.; Wohlleben, W.; Cölfen, H., Performance of a fast fiber based UV/Vis multiwavelength detector for the analytical ultracentrifuge. *Colloid Polym. Sci.* **2008,** *286*, 121-128.
267. Bhattacharyya, S. K.; Maciejewska, P.; Börger, L.; Stadler, M.; Gülsün, A. M.; Cicek, H. B.; Cölfen, H., Development of a Fast Fiber Based UV-Vis Multiwavelength Detector for an Ultracentrifuge. *Prog. Colloid Polym. Sci.* **2006,** *131*, 9-22.
268. Titov, A. V.; Král, P., Modeling the Self-Assembly of Colloidal Nanorod Superlattices. *Nano Lett.* **2008,** *8*, 3605-3612.
269. Ghezelbash, A.; Koo, B.; Korgel, B. A., Self-Assembled Stripe Patterns of CdS Nanorods. *Nano Lett.* **2006,** *6*, 1832-1836.
270. Negele, C.; Haase, J.; Leitenstorfer, A.; Mecking, S., Polyfluorene Nanoparticles and Quantum Dot Hybrids via Miniemulsion Polymerization. *ACS Macro Lett.* **2012,** *1*, 1343-1346.
271. Bomm, J.; Büchtemann, A.; Fiore, A.; Manna, L.; Nelson, J. H.; Hill, D.; van Sark, W. G. J. H. M., Fabrication and spectroscopic studies on highly luminescent CdSe/CdS nanorod polymer composites. *Beilstein. J. Nanotechnol.* **2010,** *1*, 94-100.
272. Chen, S.; Su, A.; Su, C.; Chen, S., Crystalline forms and emission behavior of poly (9, 9-di-*n*-octyl-2, 7-fluorene). *Macromolecules* **2005,** *38*, 379-385.
273. Pittman Jr., C. U.; Lee, H., Radical-initiated polymerization of β-methyl-α-methylene-γ-butyrolactone. *J. Polym. Sci. Pol. Chem.* **2003,** *41*, 1759-1777.
274. Qi, G.; Nolan, M.; Schork, F. J.; Jones, C. W., Emulsion and controlled miniemulsion polymerization of the renewable monomer γ-methyl-α-methylene-γ-butyrolactone. *J. Polym. Sci. Pol. Chem.* **2008,** *46*, 5929-5944.
275. Haase, J. Hybrid-Nanostrukturen mit einzelnen Halbleiter-Quantenpunkten für die Ultrakurzzeitphysik. Doctoral Thesis, University of Konstanz, Konstanz, **2014**.
276. Louyer, Y.; Biadala, L.; Tamarat, P.; Lounis, B., Spectroscopy of neutral and charged exciton states in single CdSe/ZnS nanocrystals. *Appl. Phys. Lett.* **2010,** *96*, 203111.
277. Patton, B.; Langbein, W.; Woggon, U., Trion, biexciton, and exciton dynamics in single self-assembled CdSe quantum dots. *Phys. Rev. B* **2003,** *68*, 9.

278. Fernée, M. J.; Littleton, B. N.; Rubinsztein-Dunlop, H., Detection of Bright Trion States Using the Fine Structure Emission of Single CdSe/ZnS Colloidal Quantum Dots. *ACS Nano* **2009,** *3*, 3762-3768.
279. Beyler, A. P.; Marshall, L. F.; Cui, J.; Brokmann, X.; Bawendi, M. G., Direct observation of rapid discrete spectral dynamics in single colloidal CdSe-CdS core-shell quantum dots. *Phys. Rev. Lett.* **2013,** *111*, 177401.
280. Conradt, F. Ultraschnelle Anrege-Abfrage-Spektroskopie an einzelnen kontrolliert geladenen Halbleiter-Polymer-Hybridquantenpunkten. Master Thesis, University of Konstanz, Konstanz, Germany, **2020**.
281. Zhu, H.; Song, N.; Lian, T., Controlling Charge Separation and Recombination Rates in CdSe/ZnS Type I Core−Shell Quantum Dots by Shell Thicknesses. *J. Am. Chem. Soc.* **2010,** *132*, 15038-15045.